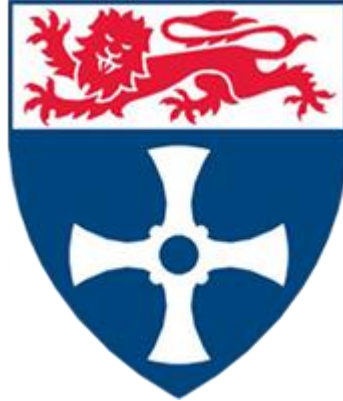


NEWCASTLE UNIVERSITY

SCHOOL OF MECHANICAL AND SYSTEMS ENGINEERING



**A thermodynamic and economic modelling study of
recovering heat from MSF desalination cogeneration plant**

By

Mohammed Abdullah Salem Al-Washahi

B.Sc., M.Sc.

A thesis submitted to the School of Mechanical and Systems Engineering

for the degree of

Doctor of Philosophy

In Mechanical Engineering

Supervised by

Dr. Sandy Anderson

Dr. Guohong Tian

February 2014

Abstract

This study focuses on an actual cogeneration power and MSF desalination plant and models it, analyses it, and proposes enhancements to MSF desalination at different, real operating scenarios. Based on actual data gathered from the plant for a full operating year, the study has identified the major operating scenarios of this cogeneration plant due to seasonal change to provide a real basis for assessing thermal, economic and environmental performance. It is difficult to standardize thermal evaluation of such systems because the net products, electrical power and water, are different in quality. Exergy analysis has achieved worldwide acceptance for thermal system assessment but no study was found in the literature that addressed the evaluation of power and MSF desalination together using exergy analysis. This thesis, therefore, makes an original contribution to this issue in three areas.

Firstly, as simulation is the only practical approach to investigate enhancements to complex plants, the simulation models developed for the power and water desalination plant have been validated against actual operating data to substantiate the credibility of this approach. For the power plant model, validation against actual plant data at the three operating scenarios gave differences between the model and actual data varying from 1.0% to 3.7%. The MSF desalination system was modelled and validated against vendor testing data with the highest difference of 3.9%.

Secondly, while previously both power production and desalination have been evaluated separately using the exergy approach, this study has applied it in a standardized approach to a specific cogeneration power and water desalination plant, including exergy analysis of the MSF desalination in detail that has not been found in the literature. It has been shown that the specific coupling of MSF desalination with a combined power plant is not a preferable option for thermal performance, which is contrary to the previous studies using Heat Utilization Factor as a performance indicator. The simulation was used to carry out a pioneer attempt of detailed energy and exergy analysis using the latest published thermodynamics properties, assuming that seawater solution is not an ideal solution (assumed in previous studies). Extraction of the hot distillate water from MSF up to stage 8 could enhance exergy efficiency to 14%. Extraction of hot distillate water from MSF stages was found to increase the unit water production up to 2%. Further, utilizing the hot water to heat up the make-up seawater flow through an Internal Heating (IH) caused an increase of brine recirculation temperature and reduced the powering steam by 5% and therefore reduces natural gas consumption and CO₂ emissions by 57000 tonnes. Implementation of this modification has a one-year payback period.

Thirdly, this study has, for the first time, studied the recovery of low-grade heat from MSF hot distillate water to enhance power or water production through the Absorption Chiller (AC), the Organic Rankine Cycle (ORC), and the Single Effect Desalination (SED). There appears to be no literature exploring MSF hot distillates to power AC to cool the gas turbine inlet by AC or dedicated SED (though previous studies have investigated steam powered MED).

The temperature of these hot distillate stages was between 65°C and 100°C, suitable for low-grade heat recovery technologies and it was confirmed that utilizing part of the heat up to 10°C temperature difference in the AC, ORC, and SED and reconnected back to IH had no adverse impact on the original MSF performance.

Utilizing the heat to produce cooling from a single effect H₂O/LiBr AC, the produced cooling load could be used to cool down the gas turbine inlet temperature to augment the electrical power generation. The AC was modelled and validated against manufacturer data. Reducing the GT inlet temperature by AC cooling increased the cogeneration plant electrical power production by 3.8% for every 5°C reduction, with CO₂ emissions reduced by 29000 tonnes and a 2.4 year payback period to implement such a modification.

An ORC unit was modelled and validated against an existing plant. From both energy and exergy aspects, it was found that R245fa performs better as a working fluid than R134a in this application. Annually this option could increase plant power generation by 9000 MWh and reduce CO₂ emissions by 13000 tonne. The economic assessment of this option showed the payback period was the highest at 5.2 years.

Powering of hot water SED from hot MSF distillate water was the fourth heat recovery option studied (for the first time). The SED was modelled and validated against manufacturer published data with a 3.2% difference. The SED was able to produce 240000 tonne/year of water. This hybridization saved 11000 tonnes/year in CO₂ emissions. The implementation of the modification has a 1.8 years payback period.

بِسْمِ اللَّهِ الرَّحْمَنِ الرَّحِيمِ

**IN THE NAME OF ALL ALLAH
THE MOST GRACIOUS AND THE MOST MERCIFUL**

أهدي هذا العمل الى أمي وأبي

I dedicate this work to my Mom and Dad

Acknowledgments

Thanks to Al-Mighty God, who gave me the ability and health to conduct this work. I would like to express my deepest gratitude and sincere thanks to Dr. Sandy Anderson for his constant support, advice and suggestion in conducting this work. Thanks also to Dr. Guohang Tian for his help and advices in following up my progress in the project.

Sincere thanks to Aqua power plant manager Mr. Salim Al-Hatmi and operation manager Mr. Hamoud Al-Amri for their continuous support and facilitate the data gathering.

Lastly, but not least, I would like to express my gratitude to my great wife and lovely children (Marwan, Reem, Hebah and Shazha) for their encouragement, patience and understanding during the course of this work.

List of publications derived from this Thesis

- [1] Al-Weshahi, M. A, Anderson, A, Tian, G. (2013) “Exergy efficiency enhancement of MSF desalination by heat recovery from hot distillate water stages”, *Applied Thermal Engineering*, 53, pp: 226-233.
- [2] Al-Weshahi, M. A, Anderson, A, Tian, G, Makhdoum, B. M. A. (2013) “Validation of simulation model for cogeneration power and water desalination plant”, *International Journal of Modelling and Optimization*, 3, pp: 46-51.
- [3] Al-Weshahi, M. A, Anderson, A, Tian, G. (2013) “Organic Rankine cycle recovering stage heat from MSF desalination distillate water”, *Applied Energy*, Paper under revision process.
- [4] Al-Weshahi, M. A, Anderson, A, Tian, G. (2011) “Exergy efficiency enhancement of MSF desalination by heat recovery from hot distillate water stages”, *Sustainable Thermal Energy Management in the Process Industries International Conference*, 25-26 October 2011, Newcastle Upon Tyne, UK.
- [5] Al-Weshahi, M. A, Anderson, A, Tian, G, Makhdoum, B. M. A. (2013) “Validation of simulation model for cogeneration power and water desalination plant”, *International Conference on System Modelling and Optimization (ICSMO 2013)*, 24-25 February 2013, Rome, Italy.
- [6] Al-Weshahi, M. A, Anderson, A, Tian, G. (2013) “Organic Rankine cycle recovering stage heat from MSF desalination distillate water”, *International Conference on Applied Energy (ICAE2013)*, 1-4 July 2013, Pretoria, South Africa.
- [7] Al-Weshahi, M. A, Anderson, A, Tian, G. (2014) “Performance enhancement of MSF desalination by recovering stage heat from distillate water using internal heat exchanger”, *International Conference on Applied Energy (ICAE2014)*, 30 May-2nd June 2014, Taipei, Taiwan. Paper submitted.

Table of Contents

Abstract	ii
Dedication	iv
Acknowledgments	v
List of publications derived from this Thesis	vi
Table of contents	vii
List of figures	xiii
List of tables	xix
Abbreviations	xxi
Nomenclatures	xxii

Chapter 1

Introduction	1
1.1 Power and water shortage crises in GCC countries	2
1.2 Objective of the thesis	5
1.3 Thesis layout	7

Chapter 2

Literature Review	9
2.1 Desalination technologies	10
2.1.1 MSF desalination	10
2.1.2 ME Desalination	11
2.1.3 VC Desalination	12
2.1.4 RO and ED Desalination	13
2.1.5 Comparison between different desalination techniques	14
2.2 Powering Desalination	16
2.2.1 Renewable Energy	16
2.2.2 Cogeneration Plant	16
2.3 Thermal plant performance and exergy analysis	18
2.3.1 Role of exergy analysis	18
2.3.2 Exergy analysis for cogeneration systems	20
2.3.2.1 Combined power plant thermal analysis	22
2.3.2.2 Desalination thermal analysis	24

2.4 Improving MSF desalination performance	25
2.4.1 MSF plant enhancements	25
2.4.2 Low-grade heat recovery technologies	29
2.4.2.1 Absorption Chiller (AC)	30
2.4.2.1.1 Working principle	30
2.4.2.1.2 Properties of absorption working fluids	31
2.4.2.1.3 LiBr/H ₂ O absorption chiller configuration	33
2.4.2.1.4 Thermal analysis studies of LiBr/H ₂ O single effect AC	33
2.4.2.1.5 GT inlet cooling using LiBr–H ₂ O AC	36
2.4.2.2 Organic Rankine Cycle (ORC)	38
2.4.2.2.1 Properties of working fluids	40
2.4.2.2.2 Thermal analysis studies of ORC	43
2.4.2.3 Multi Effect (ME) desalination	46
2.5 Closing remarks	47

Chapter 3

Actual Cogeneration Plant Operational Data Analysis	49
3.1 Motivation and objectives	50
3.2 Oman monthly power and water profile	50
3.3 Meteorology Data Analysis	51
3.3.1 Dry bulb temperature and relative humidity analysis	52
3.3.2 Seawater temperature (SWT) analysis	54
3.4 Power and MSF desalination cogeneration plant description	55
3.4.1 Power plant description	56
3.4.2 MSF desalination process description	58
3.5 Plant operation scenarios analysis	59
3.6 Closing Remarks	62

Chapter 4

Methodology	64
4.1 Energy and exergy analysis	65
4.1.1 Cogeneration plant	65
4.1.2 Desalination	69

4.1.3 Heat Recovery	72
4.1.3.1 LiBr–H ₂ O Absorption chiller	72
4.1.3.2 Organic Rankine Cycle (ORC)	76
4.1.4 Heat exchangers	78
4.2 CO ₂ Footprint estimation	80
4.3 Simulation and economics	80
4.3.1 Model Development Kit (MDK)	81
4.3.1.1 Advanced power plant library	81
4.3.1.2 Desalination process library	82
4.3.1.3 Refrigeration process library	82
4.3.2 Process Simulation Environment (PSE)	82
Chapter 5	
Power plant modelling and simulation: validation and parametric study	
5.1 Introduction	85
5.2 Power plant modelling	85
5.3 Power plant model validation	86
5.4 Power plant energy and exergy analyses	92
5.4.1 Power plant energy analysis	92
5.4.2 Power plant exergy analysis	96
5.5 Power plant parametric study	99
5.5.1 Ambient temperature	100
5.5.2 Relative humidity	104
5.5.3 Supplementary Firing (SF) flow	106
5.5.4 MSF load	109
5.6 Closing Remarks	111
Chapter 6	
MSF Desalination modelling and simulation: validation and parametric study	
6.1 Introduction	114
6.2 MSF modelling	114

6.3 MSF desalination models validation	115
6.4 MSF energy and exergy analysis	119
6.5 MSF exergy efficiency enhancement possibilities	127
6.6 MSF parametric analysis	129
6.6.1 MSF Unit load variations	129
6.6.2 Seawater feed temperature (T_1)	131
6.6.3 Seawater feed salinity ($w_{s,1}$)	132
6.6.4 Seawater feed flow (\dot{m}_1)	134
6.6.5 Brine recirculation flow (\dot{m}_{12})	135
6.6.6 Brine recirculation temperature (T_{12})	136
6.7 Closing Remarks	138

Chapter 7

Performance enhancement of MSF desalination using recovered heat from stages	140
7.1 MSF desalination unit with Internal Heating (IH)	141
7.2 MSF desalination unit with IH energy and exergy analyses	144
7.3 Impact of using IH in MSF on the cogeneration plant	146
7.4 Utilization of the extracted distillate heat in addition to IH	150
7.5 Closing Remarks	152

Chapter 8

Single-effect Absorption Chiller (AC) powered by hot distillate water from the MSF stages	154
8.1 Single-effect Absorption Chiller (AC) modelling and validation	155
8.1.1 Validation of single effect AC model	155
8.1.2 AC powered by MSF hot distillate	158
8.2 Analysis of single effect AC powered by MSF stages	159
8.2.1 Energy analysis	159
8.2.2 Exergy analysis	162
8.2.3 Single-effect AC parametric study	165
8.3 Gas turbine inlet temperature cooling using AC powered from MSF	168
8.4 Closing Remarks	174

Chapter 9

Organic Rankine Cycle (ORC) powered by hot distillate water from MSF stages	176
9.1 ORC modelling and validation	177
9.1.1 Validation of ORC model	177
9.1.2 ORC working fluids investigation	179
9.2 Analysis of ORC powered by MSF stages	181
9.2.1 ORC system energy analysis	182
9.2.2 ORC system exergy analysis	184
9.2.3 ORC parametric study	188
9.3 Impact on the cogeneration plant of powering ORC from MSF	194
9.4 Closing Remarks	198

Chapter 10

Single Effect Desalination (SED) powered by hot distillate water from MSF stages	199
10.1 Hot water SED modelling and validation	200
10.1.1 Validation of SED model	200
10.2 Analysis of SED powered by MSF hot distillate	201
10.2.1 Hot water SED system energy analysis	201
10.2.2 Hot water SED system exergy analysis	204
10.2.3 Hot water SED parametric studies	207
10.3 Impact of powering SED from MSF hot water on the cogeneration plant	212
10.4 Closing Remarks	215

Chapter 11

Economic assessment	217
11.1 Introduction	218
11.2 Estimation of initial and operation and maintenance costs	218
11.2.1 Heat Exchanger Option	218
11.2.2 Absorption Chiller	221
11.2.3 Organic Rankine Cycle	221

11.2.4 Single Effect Desalination	222
11.3 Revenue Estimation	223
11.4 Profitability Analysis	224

Chapter 12

Conclusions and future recommendations	227
12.1 Use of simulation models for cogeneration plant development	228
12.1.1 Identification of real plant operational requirements and conditions	228
12.1.2 Applicability of modelling software (e.g. IPSEpro)	228
12.2 Plant performance enhancement	229
12.3 Benefits from exergy analysis approach	231
References	234
Appendices	249

List of Figures

Chapter 1

Figure 1.1	GCC total electricity and energy consumption	2
Figure 1.2	Projected water demand in selected GCC countries	3
Figure 1.3	Total CO ₂ emissions of the GCC countries	4
Figure 1.4	Oman projected power and water demand from 2011–2018	4

Chapter 2

Figure 2.1	Common desalination technologies	10
Figure 2.2	Schematic drawing of MSF desalination	11
Figure 2.3	Schematic drawing of ME desalination	12
Figure 2.4	Schematic drawing of VC desalination. Left: TVC, right: MVC	13
Figure 2.5	RO desalination process diagram	14
Figure 2.6	ED desalination process	14
Figure 2.7	Growth in desalination technologies	16
Figure 2.8	Schematic of power and water cogeneration plant with SF	18
Figure 2.9	Distillate extraction MSF performance enhancement correction curve	26
Figure 2.10	Thermodynamics comparisons between extracting the distillate and normal MSF process	27
Figure 2.11	Schematic drawing of hybrid MSF/MED	28
Figure 2.12	PB power modified MSF process	29
Figure 2.13	Schematic drawing of basic AC	31
Figure 2.14	Schematic of general ORC cycle components	40
Figure 2.15	Typical T-s diagram for an ORC	40
Figure 2.16	ORC fluid classification: isentropic, dry, and wet in order	41

Chapter 3

Figure 3.1	An example of arid countries annual power/water demand profile	51
Figure 3.2	Daily average DBT distribution for Muscat city	52
Figure 3.3	Monthly min/max DBT variation	52
Figure 3.4	Cumulative frequency distribution of DBT	53
Figure 3.5	Daily average ARH distribution for Muscat city	54
Figure 3.6	Monthly min/max ARH variation	54
Figure 3.7	Annual average variation of SWT	55
Figure 3.8	Monthly minimum/maximum recorded SWT	55
Figure 3.9	Schematic drawing of studied MSF desalination unit	58
Figure 3.10	Cogeneration plant electrical power and water production profile	59
Figure 3.11	Typical Plant operating scenarios as percentage of normal operational	60
Figure 3.12	Schematic plant drawing for scenario II	61
Figure 3.13	Schematic plant drawing for scenario III	61

Chapter 4

Figure 4.1	MSF stage construction	72
Figure 4.2	Schematic drawing of single effect LiBr–H ₂ O AC	73
Figure 4.3	Snap shot from IPSEpro of the ORC cycle	77
Figure 4.4	Newton–Raphson method root estimation	83

Chapter 5

Figure 5.1	IPSEpro Power plant model at scenario I	86
Figure 5.2	Power plant validation: gas flow (kg/s)	90
Figure 5.3	Power plant validation: HRSG steam flow (t/h)	90
Figure 5.4	Power plant validation: ST load (MW)	91
Figure 5.5	Power plant validation: MSF flow (kg/s)	91

Figure 5.6	Power plant validation: ST condensate (kg/s)	92
Figure 5.7	Exergy efficiency of the cycle equipment (scenario I)	97
Figure 5.8	Comparison of exergy destruction ratios between the three operating scenarios	97
Figure 5.9	Influence of the ambient temperature on plant gross electrical power	100
Figure 5.10	Effect of the ambient temperature on power plant efficiency	101
Figure 5.11	Effect of the ambient temperature on power plant heat utilization factor	101
Figure 5.12	Effect of ambient temperature on plant overall exergy efficiency	102
Figure 5.13	Effect of ambient temperature on energy CO ₂ emissions	103
Figure 5.14	Effect of ambient temperature on exergy CO ₂ emissions	103
Figure 5.15	Effect of relative humidity on plant and steam turbine power	104
Figure 5.16	Effect of relative humidity on power plant efficiency and heat utilization factor	105
Figure 5.17	Effect of relative humidity on plant exergy efficiency	105
Figure 5.18	Effect of relative humidity on CO ₂ emissions	106
Figure 5.19	Effect of SF flow on gross and steam turbine power	107
Figure 5.20	Effect of SF flow on HRSG flow and efficiency	107
Figure 5.21	Effect of SF flow on power plant efficiency and heat UF	108
Figure 5.22	Effect of SF flow on overall plant exergy efficiency	108
Figure 5.23	Effect of SF flow on CO ₂ emissions	109
Figure 5.24	Effect of MSF load on gross and steam turbine power	109
Figure 5.25	Effect of MSF load on power plant efficiency and heat UF	110
Figure 5.26	Effect of MSF load on overall plant exergy efficiency	110
Figure 5.27	Effect of MSF load on CO ₂ emissions	112

Chapter 6

Figure 6.1	MSF unit IPSEpro model	115
Figure 6.2	Comparison between model and vendor data at 35°C SWT and 100% UL	117
Figure 6.3	Comparison between model and vendor data at 35°C SWT and 60% UL	117
Figure 6.4	Comparison between model and vendor data at 24°C SWT and 100% UL	118
Figure 6.5	Comparison between model and vendor data at 24°C SWT and 60% UL	118
Figure 6.6	Exergy Destruction (%) in MSF desalination components.	123
Figure 6.7	Exergy efficiency and exergy destruction of heat recovery stages	127
Figure 6.8	Exergy efficiency and exergy destruction of heat rejection stages	127
Figure 6.9	MSF exergy enhancement by recovering hot distillate water	128
Figure 6.10	Variation of unit variables as the UL changes	129
Figure 6.11	PR and SHC versus load variation	130
Figure 6.12	P/W ratio and EE versus load change	130
Figure 6.13	Effect of seawater feed temperature variation on distillate production and PR	131
Figure 6.14	Effect of seawater feed temperature variation on exergy efficiency and P/W ratio	132
Figure 6.15	Influence of seawater feed salinity change on steam consumption and PR	133
Figure 6.16	Influence of seawater feed salinity change on exergy efficiency and PC	133
Figure 6.17	Influence of seawater feed flow on steam consumption and PR	134
Figure 6.18	Influence of seawater feed flow on exergy efficiency and PC	135
Figure 6.19	Influence of brine recirculation flow on steam, distillate, rejected brine, and make up flow rates	135
Figure 6.20	Influence of brine recirculation flow on performance ration and specific heat consumption	136
Figure 6.21	Influence of brine recirculation flow on exergy efficiency and W_{\min}	136
Figure 6.22	Effect of brine recirculation temperature on steam flow and PR	137
Figure 6.23	Effect of brine recirculation temperature change on exergy efficiency and unit PC	138

Chapter 7

Figure 7.1	Extracted distillate mass flow rate and temperature at unit full load MSF and an average SWT of 27°C	142
Figure 7.2	Schematic drawing of MSF desalination with IH	143
Figure 7.3	Effect of increasing number of MSF power stages on heat exchanger UA and distillate mass flow rate	143
Figure 7.4	Effect of increasing number of MSF stages powering IH on unit production and steam flow	144
Figure 7.5	Reduction of seawater flow and seawater pump power consumption as MSF stages power increases	145
Figure 7.6	Exergy efficiency enhancement of the MSF desalination unit using IH powered by stage extracted hot distillate	146
Figure 7.7	Total exergy destruction reduction of the MSF desalination unit using IH powered by stage extracted hot distillate	146
Figure 7.8	Effect of increasing the amount of heat recovered from the MSF stages by IH on reducing the cogeneration plant natural gas consumption	147
Figure 7.9	Effect of increasing the heat recovered from the MSF stages by IH on enhancing the cogeneration plant energy efficiency	148
Figure 7.10	Effect of increasing the amount of heat recovered from MSF stages by IH on enhancing the cogeneration plant exergy efficiency	148
Figure 7.11	Effect of increasing the amount of heat recovered from MSF stages by IH on enhancing the cogeneration plant equivalent electrical energy saving	149
Figure 7.12	Effect of increasing the amount of heat recovered from MSF stages by IH on reducing cogeneration plant CO ₂ emissions	150
Figure 7.13	Effect of increasing amount of heat recovered from MSF stages by IH on annual CO ₂ emissions savings	150
Figure 7.14	IH heat absorption at different heat utilization levels before IH	151
Figure 7.15	MSF steam consumption at different levels of heat utilization from extracted distillates	152
Figure 7.16	MSF PR at different levels of heat utilization from extracted distillates	152

Chapter 8

Figure 8.1	Schematic drawing of LiBr–H ₂ O AC IPSEpro model	156
Figure 8.2	Single-effect AC (Table 8.1 and 8.2) on a Dühring chart	158
Figure 8.3	Single-effect AC powered by MSF hot distillate water (Stages 1 and 7) on Dühring chart	159
Figure 8.4	Effect of increase of MSF heat recovery stages on AC refrigeration capacity	160
Figure 8.5	Effect of the increase of MSF heat recovery stages on AC COP	160
Figure 8.6	Variation of cycle component heat transfer as the MSF recovery stages increase	161
Figure 8.7	Variation of chilled water flow and (m_{11}/m_{17}) ratio as the MSF recovery stage increases	161
Figure 8.8	Variation of cooling water flow as the MSF recovery stages increase	162
Figure 8.9	Standard chemical exergy and chemical exergy destruction due to dissolving of strong and weak solutions	163
Figure 8.10	Effect of the number of MSF recovery stages on the AC exergy efficiency and destruction	164
Figure 8.11	Exergy destruction ratio (%) of AC cycle components as the MSF recovery stage increases	165
Figure 8.12	MSF exergy enhancement resulting from powering a single-effect AC	165
Figure 8.13	Effect of the chilled water inlet temperature on the COP and capacity of a single-effect AC	166
Figure 8.14	Effect of the chilled water inlet temperature on the exergy efficiency of a single-effect AC	167

Figure 8.15	The effect of the cooling water temperature on the COP and capacity of a single-effect AC	168
Figure 8.16	The effect of the cooling water temperature on the exergy efficiency of a single-effect AC	168
Figure 8.17	Schematic drawing of GT air inlet cooling using a single-effect AC	169
Figure 8.18	Effect of the GT air inlet temperature cooling using AC powered by the MSF stages	170
Figure 8.19	Effect of AC GT cooling on power plant efficiency for the three operating scenarios	171
Figure 8.20	Effect of AC GT cooling on gas/power ratio at the three operating scenarios	171
Figure 8.21	Effect of AC GT cooling on plant exergy efficiency for the three operating scenarios	172
Figure 8.22	Equivalent electrical energy saved from the cooling of the GT inlet by a single-effect AC powered by the hot distillate from the MSF stages	173
Figure 8.23	Annual natural gas saving for the three scenarios resulting from coupling the MSF with the AC for GT inlet cooling	173
Figure 8.24	CO ₂ emissions reduction from cooling the GT inlet temperature by a single-effect AC powered by hot distillate from the MSF stages	174
Figure 8.25	Annual CO ₂ emissions saving from powering the AC by the hot distillate water from the MSF	174

Chapter 9

Figure 9.1	Schematic drawing of the IPSEpro ORC	178
Figure 9.2	p-h diagram of the Chena ORC unit using the R134a refrigerant	179
Figure 9.3	p-h diagram of the Chena ORC unit using R245fa refrigerant	181
Figure 9.4	ORC mass flow and evaporator heat transfer for R134a and R245fa for the MSF power stages	182
Figure 9.5	ORC evaporator and condenser UA for both refrigerants for the MSF power stages	183
Figure 9.6	ORC gross and net power produced for R134a and R245fa for the MSF power stages	183
Figure 9.7	Variation of thermal efficiency of both ORC refrigerants for the MSF power stages	184
Figure 9.8	ORC exergy efficiency for both refrigerants at different MSF power stages	185
Figure 9.9	Exergy efficiency for both refrigerants' evaporator and pump for the MSF power stages	186
Figure 9.10	The R134a ORC cycle component exergy destruction for different MSF power stages	187
Figure 9.11	R245fa ORC cycle component exergy destruction for different MSF power stages	187
Figure 9.12	Exergy efficiency enhancement of MSF with R134a and R245fa refrigerants as the MSF power stage increases	188
Figure 9.13	Influence of the evaporator temperature on gross and net power for both the R134a and R245fa ORC unit	189
Figure 9.14	Influence of the evaporator temperature on refrigerant pump power consumption and refrigerant mass flow rate for both the R134a and R245fa ORC units	189
Figure 9.15	Influence of the change in evaporator temperature on evaporator UA and NTU for both the R134a and R245fa ORC units	190
Figure 9.16	Influence of the evaporator temperature on ORC efficiency and cooling water flow for R134a and R245fa	190
Figure 9.17	Influence of the evaporator temperature on ORC exergy efficiency and exergy destruction for both ORC refrigerants	191
Figure 9.18	Influence of cooling water temperature on ORC gross and net power for both ORC refrigerants	192
Figure 9.19	Effect of cooling water temperature change on ORC pump power consumption and refrigerant mass flow rate for both refrigerants	192

Figure 9.20	Effect of cooling water temperature change on ORC condenser UA and NTU for both refrigerants	193
Figure 9.21	Influence of cooling water temperature on ORC thermal efficiency and refrigerant mass flow rate for both refrigerants	193
Figure 9.22	Effect of cooling water temperature change on ORC exergy efficiency and total exergy destruction for both refrigerants	194
Figure 9.23	Schematic drawing of cogeneration plant with ORC technology recovering the heat from MSF desalination	195
Figure 9.24	Operating scenarios' annual energy augmentation resulting from powering the ORC from the MSF	196
Figure 9.25	Operating scenarios' energy efficiency enhancement resulting from powering the ORC from the MSF	196
Figure 9.26	Operating scenarios' exergy efficiency enhancement resulting from powering the ORC from the MSF	197
Figure 9.27	Annual CO ₂ emissions saving from powering the ORC from the MSF desalination	197

Chapter 10

Figure 10.1	The IPSEpro model of SED	200
Figure 10.2	Comparison between the actual SED data and the model prediction	201
Figure 10.3	Influence of MSF powering stage on SED production and GOR	202
Figure 10.4	Influence of MSF powering stage on cooling and rejected seawater mass flow rate	202
Figure 10.5	Influence of MSF powering stage on SED condenser heat duty and UA	203
Figure 10.6	Influence of MSF powering stage on SED effect heat duty and UA	203
Figure 10.7	Influence of MSF powering stage on the pumps' total power consumption	204
Figure 10.8	Influence of MSF powering stage on SED exergy efficiency and destruction	205
Figure 10.9	Influence of MSF powering stage on the exergy destruction of SED components	206
Figure 10.10	Influence of MSF powering stage on the exergy destruction ratio of the SED components	206
Figure 10.11	Influence of MSF powering stage on the exergy efficiency enhancement of the MSF desalination.	207
Figure 10.12	Influence of cooling water temperature on SED water production and GOR	208
Figure 10.13	Influence of cooling water temperature on SED exergy destruction and exergy destruction ratio	208
Figure 10.14	IPSEpro model of the seven effects	209
Figure 10.15	Influence of number of effects on water production and GOR	209
Figure 10.16	Influence of number of effects on seawater cooling flow	210
Figure 10.17	Influence of number of effects on condenser duty and UA	210
Figure 10.18	Influence of the number of effects on exergy efficiency and destruction	211
Figure 10.19	Influence of number of effects on component exergy destruction	211
Figure 10.20	Influence of number of effects on component exergy destruction ratio	212
Figure 10.21	Cogeneration plant configuration showing the MSF powering the SED	212
Figure 10.22	Annual impact of powering the SED from the MSF stages on water production from the cogeneration plant operating scenarios.	213
Figure 10.23	Equivalent electrical energy saving result from powering the SED from the MSF	213
Figure 10.24	Impact of powering the SED from the MSF on the exergy efficiency enhancement of the cogeneration plant at the three operating scenarios	214
Figure 10.25	Impact of powering SED from MSF on the CO ₂ reduction of the cogeneration plant at the three operating scenarios	214
Figure 10.26	Impact of powering SED from the MSF on annual CO ₂ emissions saving	215

Chapter 11

Figure 11.1	MS Excel worksheet for the heat exchanger cost calculations	220
Figure 11.2	Payback period for four heat recovery technology implementations	225
Figure 11.3	Net present value for four heat recovery technology implementations	226
Figure 11.4	Average rate of return for four heat recovery technology implementations	226

List of Tables

Chapter 2

Table 2.1	Comparisons between different desalination technologies	15
Table 2.2	Energy versus exergy	20
Table 2.3	Trade-off between NH ₃ -H ₂ O and H ₂ O-LiBr absorption chiller working fluids	33
Table 2.4	AC configuration performance	33
Table 2.5	Non-exhaustive list of ORC manufacturers	39
Table 2.6	Most common refrigerants used ORC in industry	42
Table 2.7	Physical and environmental data for refrigerants R134a and R245fa	43

Chapter 3

Table 3.1	Summary of Oman water and power demand	51
Table 3.2	Plant main equipment characteristics	57
Table 3.3	Studied MSF unit specifications	59
Table 3.4	Plant annual operation scenarios	62

Chapter 4

Table 4.1	c and b constants for Gibbs function differentiation	71
Table 4.2	Feuerecker equation for LiBr enthalpy estimation	74
Table 4.3	Kaita correlation constants	74
Table 4.4	Constant for osmotic coefficient estimation	76

Chapter 5

Table 5.1	Set/Calculated values in power plant model	88
Table 5.2	Power plant input/output parameters	89
Table 5.3	Simulated results of the cycle streams thermodynamic properties in scenario I	93
Table 5.4	Performance indicators evaluation at the three operating scenarios	94
Table 5.5	Cycle equipment exergy efficiency and exergy destruction calculations	96

Chapter 6

Table 6.1	Set (input) and Calculated (output) values for MSF desalination model	119
Table 6.2	Model results for unit performance indicators	120
Table 6.3	Thermodynamic properties of the indicated streams	121
Table 6.4	MSF exergy analysis results	122
Table 6.5	Cooling water inlet/outlet stage parameters	124
Table 6.6	Distillate water inlet/outlet stage parameters	125
Table 6.7	Brine inlet/outlet stage parameters	126

Chapter 8

Table 8.1	Single-effect AC specifications	156
Table 8.2	Single-effect AC validation	157
Table 8.3	Exergy efficiency and destruction calculation of single-effect AC components	163

Chapter 9

Table 9.1	Specifications of the Chena Alaska ORC unit	177
Table 9.2	Validation of the ORC IPSEpro model	178
Table 9.3	Results of both the refrigerants modelled	181
Table 9.4	Exergy efficiency and exergy destruction calculation methods for the ORC	185

Chapter 10

Table 10.1	Exergy analysis method for hot water SED	205
------------	--	-----

Chapter 11

Table 11.1	Heat exchanger costs for the four enhancement options	221
Table 11.2	AC option initial and operation maintenance cost estimation	221
Table 11.3	ORC option initial and operation maintenance	222
Table 11.4	SED option initial and operation maintenance cost estimation	222
Table 11.5	Summary of heat recovery technology improvements	223
Table 11.6	Summary of heat recovery technology revenue estimation	224

Abbreviations

AC	Absorption chiller
BFP	Boiler feed pump
CCP	Condenser cooling pump
CHP	Combined heat and power
COP	Coefficient of performance
CP	Condensate pump
DSP	Desuperheater
ED	Electrolysis desalination
EES	Engineering equation solver
ERT	Energy recovery turbine
GCC	Gulf cooperation council
Geo	Geothermal
GOR	Gain output ratio
G/P	Gas/Power
GT	Gas turbine
HP/LP	High pressure/ low pressure
HPT	High pressure turbine
HR	Heat recovery
HRSG	Heat recovery steam generator
HUF	Heat utilization factor
IH	Internal Heating
ISO	International organization for standardization
LPT	Low pressure turbine
ME	Multi effect
MENA	Middle east and north Africa
MIGD	Million imperial gallon per day
MSF	Multi stage flash
NG	Natural gas
PE	Pressure exchange
PP	Power plant
PR	Performance ratio
ORC	Organic Rankine cycle
RO	Reverse osmosis
RS	Reduction station
SED	Single effect desalination
SF	Supplementary firing
SFB	Supplementary firing burner
SHC	Specific heat consumption
ST	Steam turbine
TBT	Top brine temperature
TPC	Total power consumption
VC	Vapour compression

Nomenclature

a	Activity	-
\dot{E}	Total exergy rate	kW
f	Circulation ratio	-
g	Gibbs function	kJ/kmol
h	Enthalpy	kJ/kg
LHV	Lower heating value	kJ/kg
\dot{m}	Mass flow rate	kg/s
m	Molecular weight	g/mol
NTU	Number of transfer unit	-
p	Pressure	Pa
\dot{Q}	Heat transfer rate	kW
R	Universal gas constant	kJ/(kmol.K)
s	Entropy	kJ/(kg.K)
T	Temperature	°C
U	Internal energy	kW
UA	Heat transfer conductance	kW/m ²
v	Velocity	m/s
V	Volume	m ³
w	Salinity	g/kg
\dot{W}	Electrical power	kW
y	Exergy destruction ratio	-
x	Concentration	%
z	Elevation	m

Greek Symbols

η	Efficiency
Δ	Difference
μ	Seawater chemical potential
ε	Effectiveness
δ	Differential
γ	Chemical potential
Φ	Osmotic coefficient
α	Natural gas CO ₂ emissions ratio

Subscripts

A	Absorber
B	Brine
BD	Blow down
BH	Brine heater
c	Cooling
C	Condenser

CH	Chemical
cv	Control volume
d	Destruction
e	Exit
E	Evaporator
FS	Feed seawater
G	Generator
gen	generated
GT	Gas turbine
HRC	Heat recovery
HRJ	Heat rejection
HX	Heat exchanger
i	Inlet
is	Isentropic
II	Exergetic efficiency
J	Stream number
k	Component
KE	Kinetic
LM	Logarithmic mean
min	Minimum
max	Maximum
net	Net amount
p	Product
PP	Pump
ORC	Organic Rankine Cycle
PH	Physical
PO	Potential
R	Refrigerant
s	Salt
SF	Supplementary firing
ST	Steam turbine
sw	Seawater
T	Total
Th	Throttling
w	water

Chapter 1

Introduction

1.1 Power and water shortage crises in GCC countries

Rapid population growth and the high rate of urbanization and industrialization in the Gulf Cooperation Council (GCC) countries (Saudi Arabia, Oman, Kuwait, United Arab Emirates (UAE), Qatar, and Bahrain) have created pressing demands for both fresh water and electrical energy. The electricity demand of these countries has nearly doubled in the last decades (Figure 1.1) and continues growing on average yearly by 6%, with the majority of this consumption for domestic purposes (mainly for air conditioning during the summer season) [1, 2].

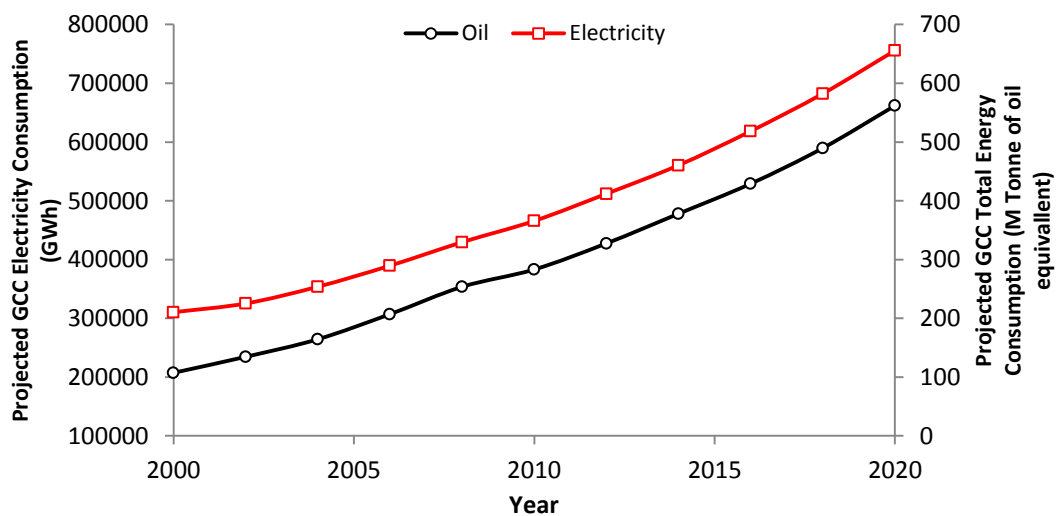


Figure 1.1: GCC total electricity and energy consumption [3]

(Values from 2000–2008 actual, 2008–2010 estimated, after 2010 forecast)

In one of the world's most arid regions, the GCC countries suffer from water resource shortage and are highly dependent on industrialized water technologies, such as desalination. Similar to electricity demand, water consumption rose drastically in the last decade to cope with mega projects in the region (Figure 1.2). Interestingly, from 1970 to 2005, water demand in the GCC countries increased 30% more than the regional population [3]. Most of this demand (on average 70%) was used in agriculture, adding only 1% to the income of the GCC economies [3].

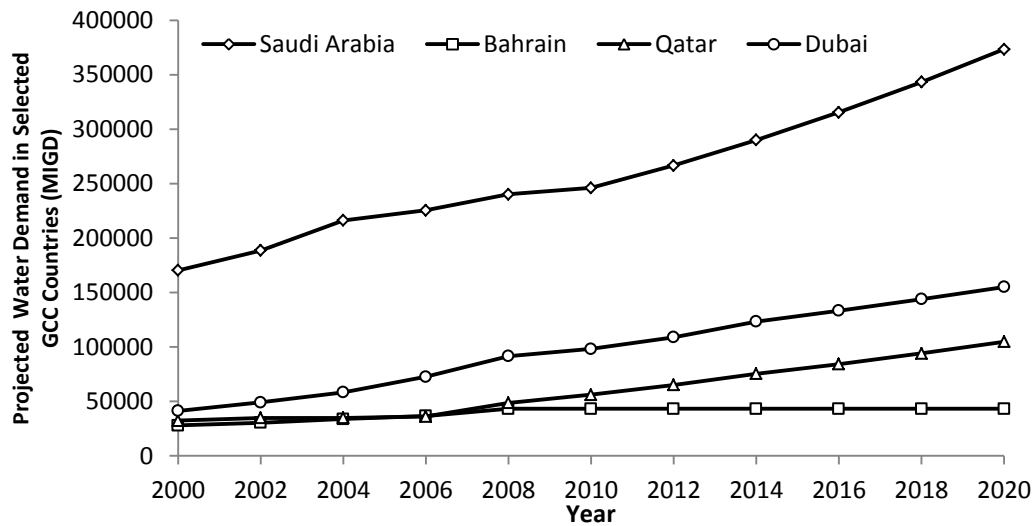


Figure 1.2: Projected water demand in selected GCC countries [4]

(Values from 2000–2008 actual, 2008–2010 estimated, after 2010 forecast)

In stark contrast to this water scarcity, the GCC countries control around 40% of the world's known oil reserves and 23% of proven natural gas reserves [4]. Despite the availability of oil and natural gas, consumption of these resources to generate electricity and fresh water reduces the national income percentage (considered more than 80% in the GCC countries). The GCC states, therefore, are trying to divert away from the high dependence on both the finite products of oil and gas [4]. The other driving force for the GCC countries to reduce their high dependence on oil and natural gas consumption is the high environmental impact produced from burning both products to produce water and electricity (Figure 1.3). The six GCC countries emitted approximately 45–50% of the cumulative Arab countries' CO₂ emissions [5].

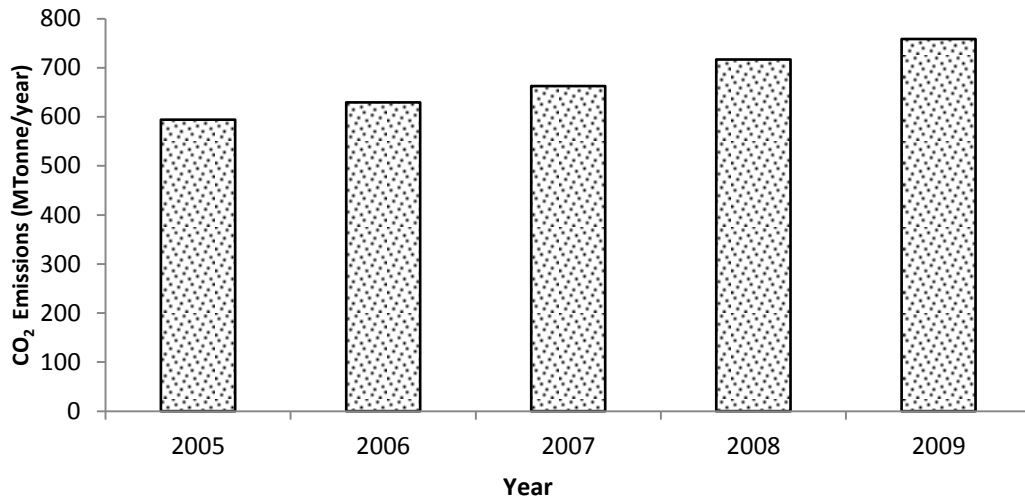


Figure 1.3: Total CO₂ emissions of the GCC countries [1]

This study will focus on one of these GCC countries, the Sultanate of Oman [6]. Similar to the other GCC states, Oman witnessed a rapid expansion, especially in petrochemical industries with a high demand for power and water. However, its oil production was one of the lowest compared with other GCC states. Figure 1.4 describes the projected average daily demand of electricity and fresh water in Oman from 2011 to 2018 [7, 8]. Therefore, the Oman government is thinking seriously about utilizing the waste resources from existing thermal systems, in addition to exploiting the geographical location and weather for renewable energies, such as wind and solar energy [9].

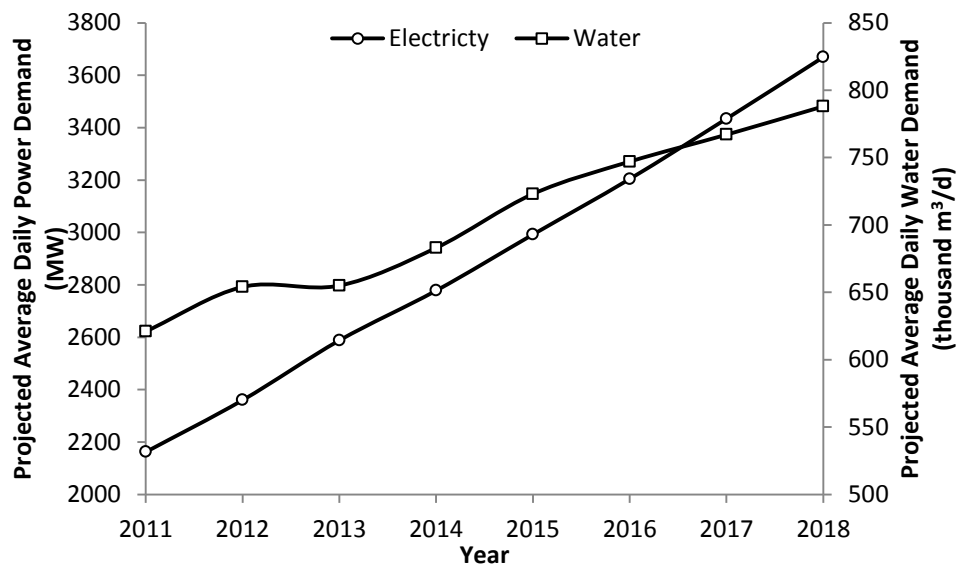


Figure 1.4: Oman projected power and water demand from 2011–2018

1.2 Objective of the thesis

Desalinated water represents a small percentage of worldwide water use. However, this percentage reaches close to 100% in some Arab cities, resulting in more than 50% of desalinated water being produced in the Middle East and North Africa area. Among the desalination technologies, Multi-Stage Flash (MSF) desalination is the most common type. Characterized by high reliability, easy operation, and low performance degradation with age, it is flawed by high steam and electrical power consumption. From the 1960s, when MSF desalination was commercialized until now, few modifications have been implemented on the unit design or for performance enhancement due to the excess availability of fossil fuels in the GCC. Now, with the increasing shortage of water resources and awareness of the negative impact of CO₂ emissions, there is more incentive to investigate making these units more sustainable with better efficiency.

As is typical in engineering practice, the development of both complex plant and plant performance analysis is evolutionary, building on previous developments. The aim of this study is to progress both of these aspects further with respect to a cogeneration MSF desalination plant. In terms of plant technology, the genesis of this study lies in the recent improvements by Leading Edge Technology (LET) [10, 11] in 2005 for the Layyah MSF desalination plant, UAE. This introduced the concept of extracting the hot distillate as it travels from one stage to a lower pressure stage as a means of enhancing unit production [12].

However, when discussing plant performance, the issue then arises as to which performance indicators are most appropriate. It has been recognized [13] that exergy analysis is a more rational basis for evaluating the overall performance and environmental impacts of combined product plant (e.g., CHP). Nevertheless, this approach has not been exploited fully with a cogeneration desalination plant. Due to the complexity of this type of plant and its operating requirements, the use of simulation modelling is the only practical recourse for such investigation, as it overcomes the time and cost barriers to experiments or actual unit testing. This practice is now commonplace, yet few published studies [14] validate such models against actual plant performance [15].

Against this background, the general aim of this study will be embodied in the following specific objectives:

Firstly, to explore the thermodynamic, environmental and economic aspects of improving the performance of a specific cogeneration power plant with MSF desalination (536 MW power and 3800 m³/h water production in Oman), by:

- a) Identifying its typical seasonal operational conditions and requirements from its operational history records.
- b) Developing the initial concept pioneered at Layyah in 2005 through investigation of an innovative concept for heat recovery from the MSF stages.
- c) Exploring the technical plant hybridization possibilities for utilizing this recovered heat for producing:
 - i. Either, more water product (either by internal heat recovery or by powering an additional Single Effect Desalination (SED) plant).
 - ii. Or, more power product (either by an additional Organic Rankine Cycle (ORC) or by powering an Absorption Chiller (AC) for the gas turbine (GT) intake to improve GT performance).

Secondly, to improve exergy analysis of a cogeneration MSF desalination plant, along with the additional heat recovery plant identified above, by:

- d) Implementation of a more rigorous and detailed approach to exergy sources and destruction than has been the case in the previous literature on these types of plant.
- e) Evaluation of whether conclusions on the plant thermal performance using exergy analysis may differ from those arrived at by traditional First Law performance criteria, such as the utilization factor (UF).

Thirdly, to provide greater confidence in the use of simulation software for the above purposes by validating the models against real plant actual performance data:

- f) Obtained in this study for the representative specific cogeneration MSF desalination plant to be investigated.
- g) Published for real low temperature heat recovery AC, ORC, and SED.

1.3 Thesis layout

To embody these objectives, the rest of this thesis is as follows:

- Chapter 2 presents a literature review covering the latest published work related to the study. This includes description and thermal analysis studies of the power plant, MSF desalination, AC, ORC, and SED.
- Chapter 3 is devoted to the analysis of the representative cogeneration plant historical operating data along with the analysis of plant location weather data to provide operation scenarios so the suggested plant improvements can be evaluated.
- Chapter 4 presents the thermal analysis methodology for cogeneration plant and heat recovery technologies. It includes a description of the modelling software and its components.
- Chapter 5 covers modelling and validation of the power side of the cogeneration plant at the identified operating scenarios. Moreover, the simulation results are used to perform energy and exergy analyses of the plant and a parametric study of the factors affecting the power plant performance.
- Chapter 6 covers modelling and validation of the MSF desalination of the plant, with detailed analysis using energy and exergy. It also includes a parametric study of the factors that influence MSF performance and proposes a plant modification to enhance MSF desalination exergy efficiency.
- Chapter 7 is devoted to the original concept of efficiency enhancement of the MSF desalination unit using internal heat exchange powered by extracted hot distillate from the MSF stages. The impact of this MSF enhancement on the driving cogeneration plant performance indicators is investigated, including the optimal utilization of part of the heat before coupling with other heat recovery technologies (AC, ORC, and SED).
- Chapter 8 presents a pioneering study on modelling, validation, and simulation of single effect lithium bromide–water (LiBr–H₂O) AC energized by part of the heat extracted from the hot distillate from the MSF stages. The simulation results are used for detailed energy and exergy analyses with consideration of the chemical exergy for the first time. This chapter then

investigates utilizing the cooling produced from AC to enhance cogeneration plant performance indicators through cooling the GT inlet temperature.

- Chapter 9 includes modelling, validation, and simulation of an ORC powered by hot water extracted from the MSF stages. It covers an assessment of R134a and R245fa as working fluids for an ORC using both energy and exergy approaches. A parametric study of the factors effecting ORC performance is included. The implications of powering this ORC on cogeneration plant performance indicators are investigated.
- Chapter 10 investigates recovering part of the heat from the extracted distillate water to produce additional water from SED. It covers modelling, validation, and simulation of the SED and energy and exergy analysis of the unit. The main parameters effecting performance of the SED are investigated, and the effect of powering this on the cogeneration plant is explained.
- Chapter 11 investigates the economic viability of the four heat recovery options.
- Chapter 12 presents the study findings and provides future study recommendations.

Chapter 2

Literature Review

2.1 Desalination technologies

Oman and other GCC countries started relying on seawater desalination to meet the water demand shortage from 1960 when the first seawater desalination plant was installed in Kuwait [16]. Desalination technologies are classified into two main categories based on their method of extracting the salts: thermal and separation (Figure 2.1). In thermal desalination, a heat source is used to evaporate the seawater as with MSF and Multi Effect (ME) desalination [17]. In separation desalination, either a pressure gradient as in reverse osmosis or electrical current as in electrolysis desalination, [17] are required.

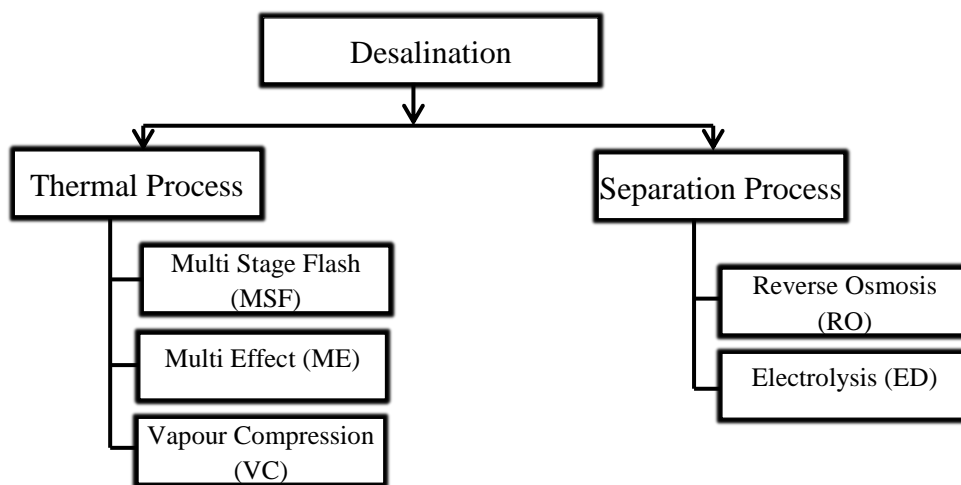


Figure 2.1: Common desalination technologies

2.1.1 MSF desalination

Weirs of Cathcart in Scotland invented MSF desalination in 1950 based on the principle of evaporating seawater under low pressure in a closed vessel [18]. MSF desalination currently produces more than 64% of total world's production of desalinated water, and this percentage reaches 80% in the GCC countries [19, 20]. Figure 2.2 describes the process of MSF desalination. The main sea water pump supplies the source seawater to heat the rejection stages. Most of this of this seawater will be rejected again to the sea, while part of it will pass as makeup to the deaerator, where oxygen is removed from the seawater to avoid tube corrosion of the heat recovery stages. A brine recycle pump transfers recycled brine (the sea water accumulated in the deaerator or last stage) to the tube side of the heat recovery stages, where the flashed brine at the condenser of each stage heats it gradually.

After exiting from stage 1, the brine is heated finally to its terminal temperature by the heating steam in the brine heater. It then flows to the first stage of the evaporator, where the initial flash evaporation occurs. As the brine would be still hot enough to boil again at slightly lower pressure, the flashing process is then repeated as it passes through the series of interconnected stage chambers. Flashed vapour is condensed by the cooling water in the tubes, then condensed distillate flows from each stage to a common distillate corridor, where the distillate pump extracts it. It is worthy to mention when the distillate moves from stage to stage, part of it transfers part of its heat to the brine recycle tubes and it re-flashes, since the next stage is maintained at a lower pressure. The re-flashing phenomenon in the distillate corridor increases as the accumulated distillate from stage to stage increases, mixing with the brine vapour and using part of the condensing heat transfer area. Antifoam and anti-scalant chemicals are injected in the MSF desalination to reduce seawater foaming and the scaling that can form at higher temperatures [21].

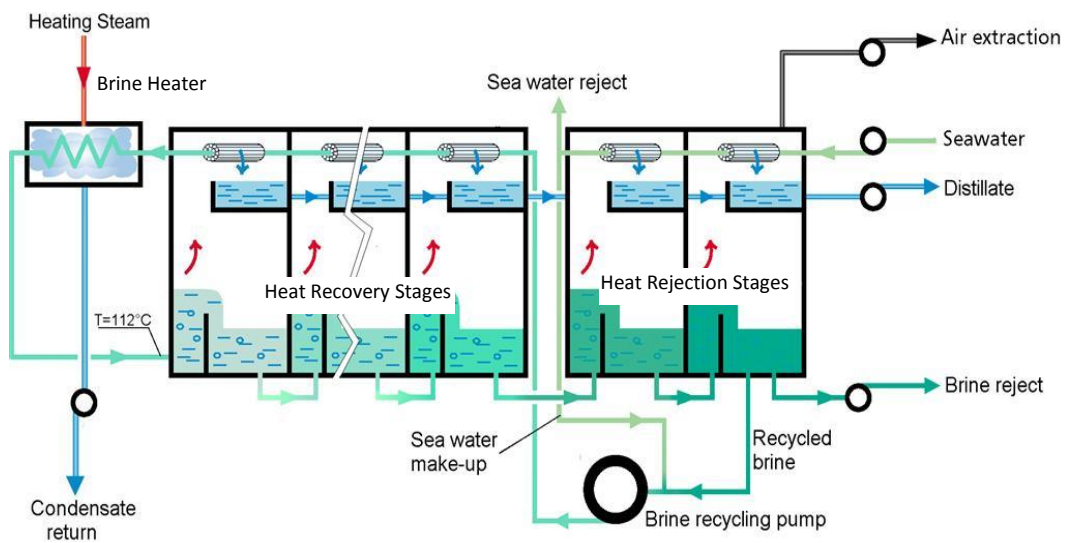


Figure 2.2: Schematic drawing of MSF desalination [22]

2.1.2 ME Desalination

ME desalination represents only 3.5% of the total world's desalinated water production, despite being the oldest large-scale desalination method [23]. Similar to MSF, ME desalination evaporation takes place in interconnected vessels, called "effects", maintained under vacuum conditions (Figure 2.3). Seawater is sprayed in to each effect over the hot tube bundles. In the first effect, low-pressure (LP) steam

(in the tubes) heats up the sprayed seawater to evaporation point. Distillate vapour from the first effect moves to the adjacent effect to function as a heat source instead of the steam in the first effect. The process is repeated until the last effect, where the accumulated distillate from the different effects gathered in a common channel is extracted by the distillate pump, while a brine pump rejects the concentrated brine. Similar chemicals to MSF are injected in ME desalination for the same reason.

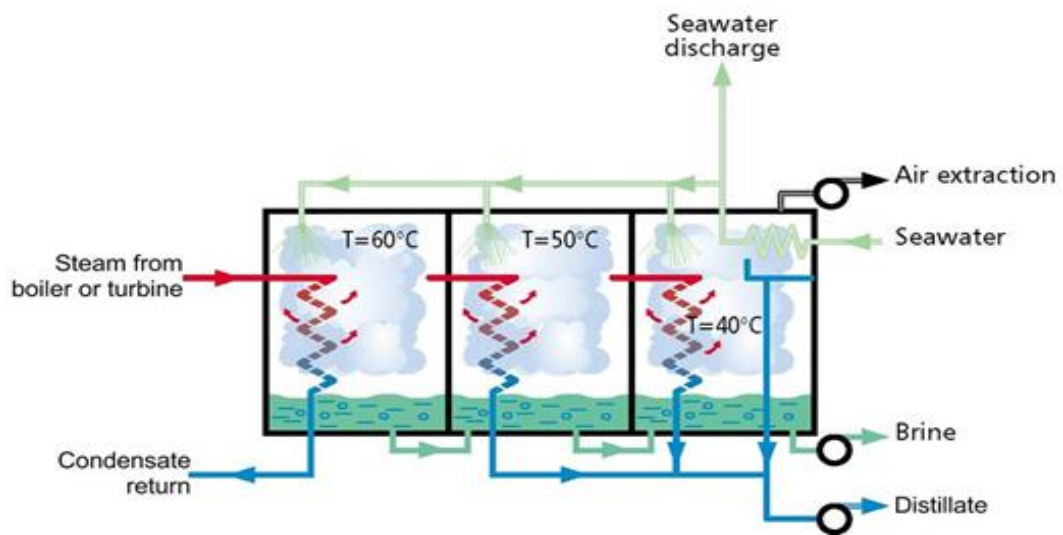


Figure 2.3: Schematic drawing of ME desalination [22]

2.1.3 VC Desalination

Vapour Compression (VC) desalination is a modified scheme of ME desalination (Figure 2.4). The heat required for evaporation of the seawater is obtained either by using a steam ejector to extract part of the generated distillate vapour (in this case, Thermal Vapour Compression, TVC) or by using an electrical driven Mechanical Compressor (MVC). By both methods, compressing the vapour increases its temperature, which heats up the seawater in the first effect, with the rest of the process continuing as for ME desalination.

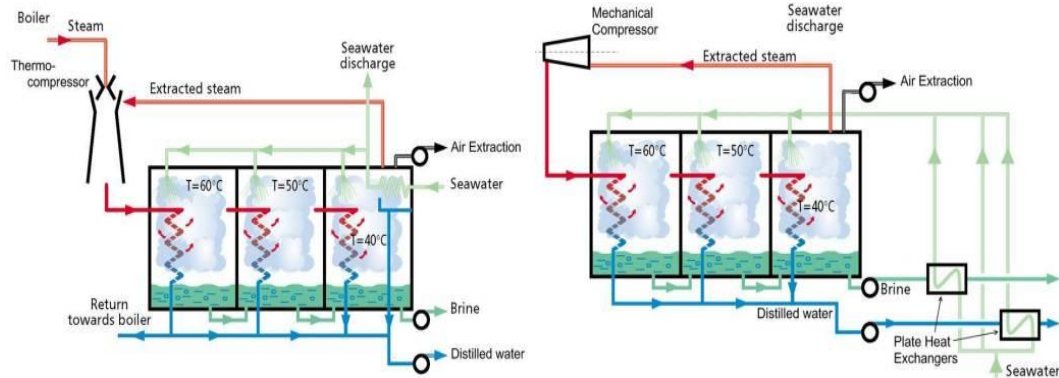


Figure 2.4: Schematic drawing of VC desalination. Left: TVC, right: MVC [22]

2.1.4 RO (Reverse Osmosis) and ED (Electrolysis Desalination)

RO desalination was commercialized in the 1970s. The working principle of RO desalination depends on separating the solvent (pure water) from the solute (seawater) by exploiting pressure to make the solvent flow in the opposite direction to the osmosis, leaving the solute on the HP side of the semi permeable membrane. Unlike, thermal desalination techniques, RO feed seawater should be passed through a pre-filtration system to remove suspended solids from the seawater before it reaches the membrane, which does not have mechanical filtration capabilities. The HP pump is used to increase the filtered seawater pressure up to 65 bar to facilitate the separation of salts from the seawater (Figure 2.5). The rejected concentrated seawater has a High Pressure (HP), leading to the main recent development in RO as recovering this HP energy through Energy Recovery Turbine (ERT) and Pressure Exchange (PE) mechanisms. Both technologies play a role in the reduction of the electrical energy consumption of the RO [24]. RO desalination consumes more chemicals compared with thermal desalination. Coagulants and fluctuants are injected before the pre-treatment, and anti-scalants (for scale protection), sodium bisulfite (protect from oxidation), and hydrochloric acid are added to adjust the pH level and to control hydrolysis [17, 25].

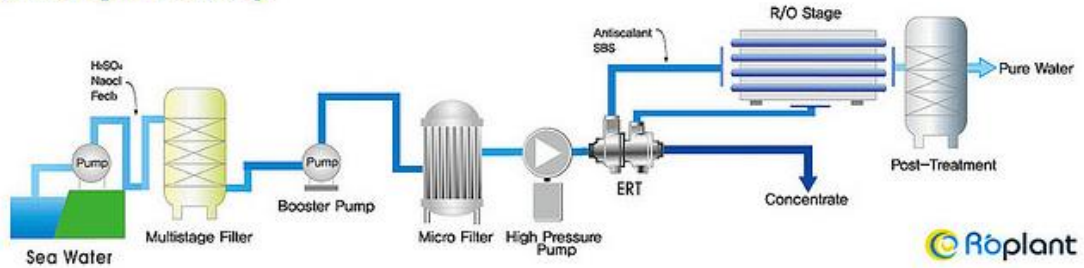


Figure 2.5: RO desalination process diagram

ED was commercialized before RO desalination in the early 1960s [26]. The working principle of ED depends on electrochemical separation. Most of the salts dissolved in water are charged, cationic (positively charged), or ionic (negatively charged), and they migrate to electrodes with an opposite electric charge (Figure 2.6). This technology has many other applications in the biomedical, environmental, and table salt industries [27].

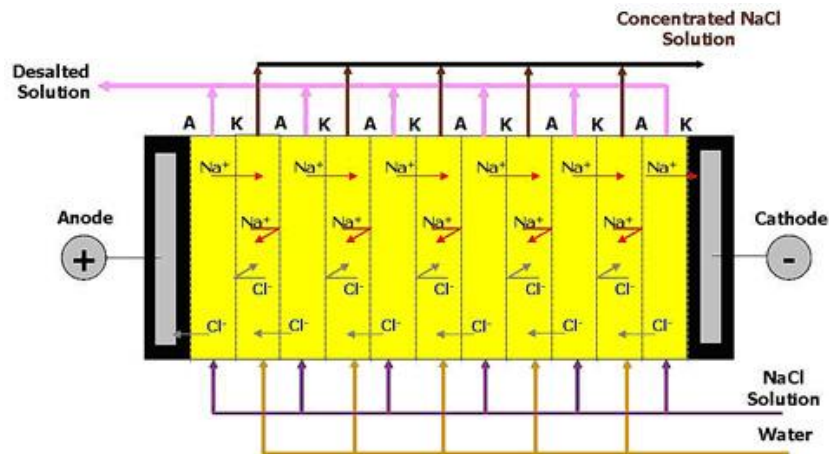


Figure 2.6: ED desalination process [26]

2.1.5 Comparison between different desalination techniques

Many studies have been published comparing different desalination technologies based on energy consumption, product cost, quality, and environmental impact. As can be seen from Table 2.1, membrane technology (specifically RO desalination) is the optimum based on combining both energy consumption and CO₂ emissions. However, the higher operation and maintenance cost makes the unit product cost closer to that from the thermal desalination technologies. On other hand, thermal desalination (specifically MSF) on a commercial scale achieves the highest product quality, reaching to 5 µs/cm, making the post-treatment process easier and cheaper

[28]. None of the comparative studies consider the post-treatment of produced distillate (re-mineralization).

	MSF	ME	MVC	TVC	RO	ED
Energy requirement (kW/m ³) [29]	250–300	150–220	–	220–240	–	–
Electrical consumption (kW/m ³) [29]	3.5–5	1.5–2.5	11–12	1.5–2	5–9	2.6–5.5
Total electric equivalent (kW/m ³) [29]	15–25	8–201	11–12	21.5–22	5–9	2.6–5.5
Maximum value of CO ₂ emissions (kg CO ₂ /m ³) [29]	24	19.2	11.5	21	8.6	5.3
Distillate quality (ppm) [29]	< 20	< 20	< 20	< 20	< 500	20–500
Unit product cost (US \$/m ³) [18]	0.52–1.75	0.52–1.01	2–2.6	0.827 [17]	0.52–0.56	n.a.

Table 2.1: Comparisons between different desalination technologies

RO desalination has been growing rapidly over the last decade in non-GCC countries due to improvements in membrane quality, but MSF remains the favourite desalination technology in GCC countries, as can be seen from Figure 2.7 [19]. MSF reliability, ease of control, low performance degradation over the year, stability, low maintenance, and high availability are the reasons behind the GCC countries selecting this technology [20]. Seawater conditions, such as turbidity and suspended solids, impact MSF desalination less. RO desalination has lower GCC market confidence through failing in achieving design capacity [19] and the influence of seawater conditions. In 2008, more than five RO desalination plants were shut down in UAE and Oman due to the red tide phenomenon (harmful algal blooms) clogging pre-treatment sand filters [30]. On other hand, RO desalination remains the best choice for small-scale applications where thermal energy (steam) is unavailable [19], and the technology will be able to compete with MSF if designers succeed in producing higher capacity units [19, 31].

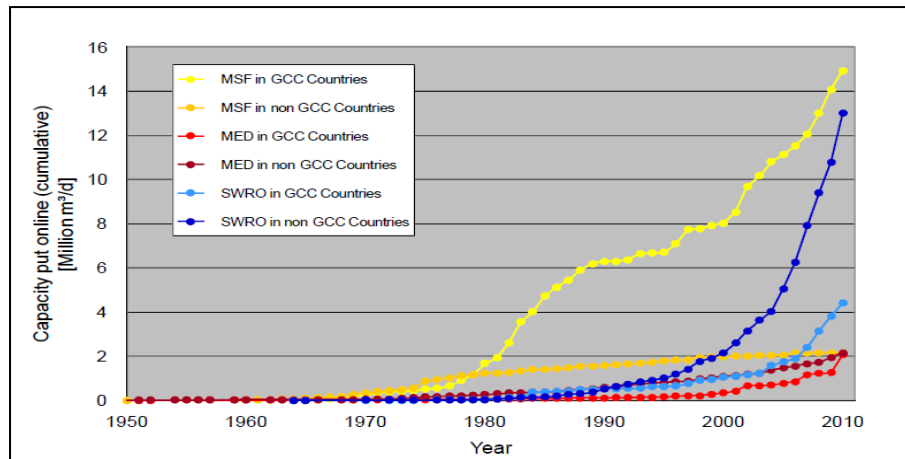


Figure 2.7: Growth in desalination technologies [19]

2.2 Powering Desalination

As discussed in previous sections, either electrical power or heat could power desalination. The source of this energy could be from a renewable source (e.g., wind, solar, and tidal energy) or from a heat supplying plant (e.g., cogeneration plant).

2.2.1 Renewable Energy

Coupling renewable energy resources (such as thermal solar thermal, photo-voltaic, wind, and geothermal) with desalination technologies is a promising solution to both water shortage and reducing global warming gases [23]. The breakdown of desalination technologies driven by renewable energy source is 10% MSF, 10% ME, 5% VC, 62% RO, 5% ED, and others 4%. Most of these are powered by solar photo-voltaic (43%), with 27% by solar thermal, 20% by wind, and 10% by hybridization technologies [29]. Many factors affect the selection of an appropriate renewable energy source and desalination technology: production, energy consumption, capital cost, suitability, operation and maintenance costs, and level of acceptance of communities [32]. Despite the environmental and natural resource saving, the product cost of renewable desalination (above 2 US\$/m³) is still high compared with conventional desalination plants (average 1 US\$/m³) due to the higher capital cost of renewable equipment, cost of maintenance, and lower availability factor [29, 33].

2.2.2 Cogeneration Plant

Cogeneration is the simultaneous generation of electrical power and process thermal energy in one plant. It has been used in many industrial applications, such as paper mills, the chemical industry, and desalination, where the cogeneration plant is used

to produce water besides electricity (sometimes called a dual purpose plant) [34, 35, 36]. Most power and water (particularly by MSF desalination) in the GCC countries and North Africa are produced using a cogeneration plant [18, 37]. A cogeneration plant has many advantages over separate stand-alone power plants and MSF desalination plants, that is, a higher thermal efficiency, less fuel consumption, flexible operation, lower CO₂ emissions, lower financial investment, and less manpower requirements. However, its main disadvantages are slightly lower availability and longer duration for commissioning and construction [34, 38, 39].

In a cogeneration plant (Figure 2.8), GTs are used to produce electrical power through a Brayton cycle, where the GT exhaust is utilized to produce High-Pressure (HP) steam through a Heat Recovery Steam Generator (HRSG). This HP steam generates additional electrical power from a steam turbine [38], while at the lower pressure stages, part of it is used to power a thermal desalination plant, such as MSF. For arid countries in general and Oman specifically, power demand varies significantly through the year, whereas water demand remains fairly constant [40]. Thus, a cogeneration plant should be designed to meet all possible scenarios resulting from power and water demand variations. Therefore, some cogeneration plants provide a Supplementary Firing (SF) facility to maintain water production from MSF desalination in case of a reduction of GT load or shut down [41]. In addition, for such a plant in winter season, where the power demand is low and the steam turbine is shut down, a pressure reduction station option is provided to supply the steam required for MSF desalination through reducing the HRSG steam pressure to the MSF powering steam pressure [42].

Two types of steam turbine can be used in such a scheme: condensing or extraction. In the condensing type, the steam exits the steam turbine at the condenser pressure, where part of the steam has been extracted from different pressure stages for different uses (heating, desalination, vacuum system, etc.). However, in back pressure steam turbines, steam exits the turbine at a pressure greater than or equal to the atmospheric pressure, the pressure depending on the needs of the thermal purpose [43]. The principle advantage of the condensing turbine over the backpressure is that it increases the amount of energy extracted per kg of steam and amount of power generated. Moreover, the condensate from the condensing turbine can be pumped back to the boiler, whereas in the back pressure steam turbine, new

fresh demineralized water should be injected to the boiler. This point is of importance, especially in countries where a shortage of pure water exists [44].

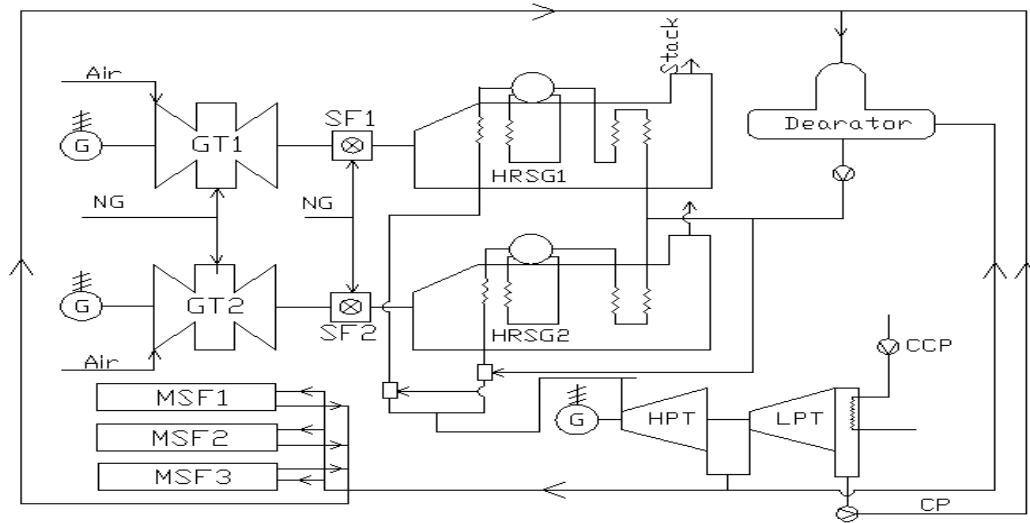


Figure 2.8: Schematic of power and water cogeneration plant with SF

2.3 Thermal plant performance and exergy analysis

2.3.1 Role of exergy analysis

Thermal systems consume large quantities of natural and economical resources and contribute clearly to the climate change problem. Therefore, these systems should be designed, constructed, and operated for effective working and reduction of environmental impacts. Proper thermal analysis tools should be used to maximize the benefits and to control the adverse effects. Energy and exergy analyses are the two main tools of analysing and evaluating proposals for the improvement and optimization of thermal systems [38, 45, 46]. Generally, thermal systems are analysed through energy. However, in recent decades, exergy analysis has gained increasing acceptance as a useful tool in thermal system design, evaluation, optimization, and improvement [47, 48, 49]. Using both energy and exergy analyses provides a complete picture and better understanding of the thermal system behaviour. Energy analysis depends on the First Law of Thermodynamics (which is simply the energy conservation principle) [38], whereas exergy analysis simultaneously takes account of the Second Law of Thermodynamics and is an instrumental measure of thermal system irreversibilities, focusing on both the quantity and quality of the energy [45]. The quality stands for the ability of an

energy source having a certain amount of energy to cause change or to produce useful work [50, 51].

The exergy of a stream is measured when a stream moves from a state with high disorder (low quality) to an equilibrium with minimal disorder (high quality), which is selected mostly at environment conditions (“dead state”) with specified ambient, temperature, and chemical concentration. During this process, part of the exergy is destroyed due to irreversibility, since all real thermodynamic processes are irreversible. The exergy destruction is the expression that refers to the loss of the maximum theoretical available energy due to the process entropy generation. The exergy destruction is a loss in a system or a process energy component, which is obtained by multiplying the absolute temperature of the environment by the entropy produced. Entropy could be either extensive or intensive property that is defined as heat absorbed by a substance at a certain absorbed temperature [52]. Therefore, energy is conserved and exergy is destroyed.

To measure the quality of performance of a thermodynamic system, not only the processes that occur in the system must be taken into account but also all other interactions with the surroundings. All types of irreversibility of the maximum theoretical work occurring in the system components should be evaluated. The lack of the ability of energy analysis to perform this (irreversibility determination) shows the importance of exergy analysis [53, 54]. Determining the exergy losses in a thermal system identifies the possibilities for enhancing it through reducing the irreversibilities in the system due to entropy generation by an economical modification of these processes [53, 54, 55]. Table 2.2 summarizes the comparison between energy and exergy analyses.

Energy	Exergy
Dependent on the matter and energy flow but independent of the environment parameters.	Dependent on matter and energy parameters and also on the environmental parameters.
Has a value different from zero.	Reach to zero if it is under equilibrium with environment (dead state).
Conserved in all process by the First Law of Thermodynamics.	Conserved for ideal reversible processes only and destroyed partially or completely as described by the Second Law of Thermodynamics.

Table 2.2: Energy versus exergy [13]

Thermal system efficiency is an important parameter used to indicate how well the energy conversion is accomplished. Thermal efficiency (energy efficiency) describes how much work output is extracted from the input energy, whereas exergy efficiency (Second Law efficiency) expresses how much actual work is obtained from the maximum possible theoretical available work. Exergy is linked strongly to sustainability and environmental impact since it is measured with respect to the environment [50, 56]. A thermal system approaching a 100% exergy efficiency means that all exergy is converted to useful work without internal or waste losses and the system has zero thermal emissions or impact on the environment [57].

2.3.2 Exergy analysis for cogeneration systems

The role of exergy analysis appears clearer when thermal systems are designed to produce two products different in nature (e.g., electricity and heat), despite both being types of energy. Unlike electrical energy, heat cannot be 100% converted to work, and the degree of conversion is dependent highly on its temperature. Therefore, for a thermal system producing both electrical power and heat, both products should be evaluated based on a unique quality, which is their ability to produce useful work or exergy [45,46,13].

Darwish et al [58] reported that the Kuwait Ministry of Energy measured the efficiency of cogeneration power and MSF desalination plant by:

$$efficiency = \frac{power\ output}{fuel\ energy\ consumed\ by\ cogeneration - thermal\ energy\ to\ MSF} \quad (2.1)$$

However, they believed this definition implicitly but erroneously assumed the MSF desalination is charged by fuel energy equal to the heat supplied to the desalination.

Darwish et al suggested using the exergy content of the MSF thermal energy to remove the confusion and standardise both power output and MSF thermal energy based on their exergies:

$$efficiency = \frac{power\ output + electrical\ energy\ loss\ as\ thermal\ energy\ input\ to\ MSF}{fuel\ energy\ consumed\ by\ cogeneration} \quad (2.2)$$

Fischer et al [59] found that energy and exergy efficiencies are similar in the case of a standalone power plant allocated for only electrical power generation [59, 60] while, if cogeneration is producing electrical power and heat, then the exergy approach should be used. The difference between energy and exergy efficiencies is more than double in cases when power and heat was considered. In addition, for cogeneration environmental impacts, such as CO₂ emissions, evaluation should be based on exergy since it standardizes both product (power and heat) based on their ability to produce useful power.

Saidur et al [61] studied the role of exergy analysis in pinpointing the equipment performance. The study focused on a conventional industrial boiler with energy efficiency at 72.5% while exergy efficiency was 24.9%. This energy efficiency suggested a limitation for further improvements, whereas the exergy figure encourages further enhancement. Based on exergy destruction analysis for industrial boiler components, Saidur et al suggested a modification using a variable speed fan could reduce exergy destruction with a promising one-year payback period.

An exergy rather than an energy analysis should be used to assess national resources, such as buildings, transportation, and utilities, where both electrical and heat energy are involved. Rosen [62] carried out a comparison between energy and exergy efficiencies of four sectors (residential, transportation, industrial, and utility) for Ontario (Canada), Turkey, and Saudi Arabia and found energy and exergy analyses gave similar results where there is no conversion of energy from electrical to heat (in the case of utility and transportation). However, a wide variation between energy and exergy efficiencies was noticed in the building and industrial sectors due to conversion of high quality energy (e.g., fossils fuel and electricity) to low temperature heat used in heating or cooling.

Koroneos et al [63] believed an investigation of a sustainable low carbon environment could be based on exergy as the main indicator. This study selected

Greece as a case study, outlining building exergetic profiles. Three-quarters of a building's exergy consumption during an 80 life years was caused by heating, cooling, and lighting, while only one-quarter was due its construction period (materials extraction, process, transport), in contrast to energy based analysis.

Kennedy et al [64] found the exergy method is the more precise technique to determine CO₂ allocation for power and water production because it utilizes a detailed physical model of a cogeneration plant to calculate the energy required for either the electricity or the water production. Kennedy et al claimed the exergy method is the accepted method for the most accurate assessment of capital, operation, and maintenance costs. However, it requires plant detail design features, such as ambient temperature, gas quality, and plant type.

Although a cogeneration power plant with MSF desalination is a common configuration, all literature focused on energy not exergy analysis. However, many authors discuss the exergy of combined power plant and limited researchers analyse the exergy of desalination alone. The reasons for this could be the lack of plant data, especially of desalination coupled with power plant, and the complexity of evaluating the exergy of the seawater stream. However, in both situations, the literature demonstrates clearly the difference between energy and exergy performance parameters.

2.3.2.1 Combined power plant thermal analysis

Ozkan et al [65] performed an exergy analysis of a cogeneration plant (55000 MWh/year and 75000 tonne/year saturated steam). The authors revealed that the major exergy destruction in the heat exchanger and in the GT combustion chamber was 44% and 30%, respectively. However, the steam boiler had the lowest exergy efficiency at 51%. Ozkan et al recommended improvement of the heat exchanger to enhance the overall system exergy efficiency.

Fellah et al [43] conducted an exergy analysis of GT14 GT power in Libya at three different plant operating loads: 85.0% (full operating load), 60.0%, and 40.0%. The exergy efficiency increased from 20.5% at 40.0% load to 29.1% at full operating load. The ratio of total exergy destruction to the fuel input exergy decreased from 61.0% at 40.0% to 48.6% at full operating load. At all three operation loads, the combustion chamber was the main contributor of exergy destruction.

Modesto and Nebra [66] performed an exergy analysis on a 201 MW steam power plant for a Brazilian steel mill. The plant exergy efficiency, on average, was 32.0%, with the HP boiler the main contributor of exergy destruction, with 78.3% from the plant's total exergy destruction. The highest exergy of efficiency was for the attemperator followed by the deaerator at 98.4% and 92.2 % respectively.

Shi and Che [67] evaluated the exergy efficiency of a conventional combined power plant using liquefied natural gas as the powering fuel. The plant exergy efficiency was 52.0%, with the combustion chamber having the highest share in plant exergy destruction (59.0%), followed by the GT (22.0%). The authors proposed increasing the fuel temperature by recovering waste heat from the HRSG stack, resulting in an increase of exergy efficiency by 2.80%.

Cihan et al [68] performed a 250 MW combined power plant (2 GT + 1 ST) energy and exergy analysis. The results showed plant energy and exergy efficiencies of 46.0% and 45.0%, respectively. However, within this energy analysis, stack losses were 53.0% of the total plant energy losses, while this figure represented only 4.00% by exergy analysis. Furthermore, exergy analysis confirmed 63.0% of the total exergy destruction was lost in the GT combustion chambers. The authors suggested depending on exergy analysis for plant improvement and optimization since energy analysis lacks determination of the energy quality.

Ameri et al [69] carried out an energy and exergy analysis of a 420 MW plant (1 GT + 1 ST + SF). The results showed a decrease of both energy and exergy efficiency from 47.0% and 45.5% to 46.0% and 44.0% as a result of using the SF. However, the combined cycle power plant electrical power output increased by 7.38% when the SF was used. In both cases, the combustion chamber caused the majority of exergy destruction, with the SF burner the second cause of exergy destruction.

Khaliq and Dincer [70] conducted an analysis of cogeneration plant (GT + process heating) with compressor inlet absorption cooling and evaporative after cooling. Plant energy and exergy efficiencies were 75.0% and 49.0%, respectively. The authors observed that the exergy destruction of the combustion chamber was 75.0% of the total plant exergy destruction.

2.3.2.1 Desalination thermal analysis

Kempton et al [71] analysed exergy in three types of desalination: RO, MED, and MSF. They found that the typical exergy efficiencies were 30.1%, 14.3%, and 7.73% for RO, MED, and MSF, respectively. In addition, Kempton et al estimated CO₂ emissions for these technologies as 2.91 kg CO₂/m³ and 5.22 kg CO₂/m³ for RO and MED, whereas MSF was mentioned as generating three to four times these figures. However, the authors treated MSF as an overall system without mentioning the reasons behind the exergy destruction in the MSF evaporator, which accounts for 75.0% from the total unit exergy destruction.

Kahraman and Cengel [72] analysed the exergy of a 22-stage MSF desalination plant in Saudi Arabia coupled with a power plant producing 272 kg/s of distillate water. Kahraman and Cengel assumed seawater was an ideal mixture of two components (NaCl and H₂O) to enable them to calculate the chemical exergy of the seawater, as suggested initially by Cerci [73]. They found that the exergy efficiency of the unit was only 4.20% and that the exergy input is destroyed by 77.8%, 5.30%, and 8.30% in the MSF evaporator, pump motors, and brine heater, respectively. The authors concluded that low MSF exergy efficiency represented the large amount of energy used and therefore, suggested using the power plant condenser, as a MSF brine heater could save exergy destruction and improve cogeneration plant performance.

Sharqawy et al [74] analysed the same MSF plant using the latest published thermodynamics properties of seawater [75]. The authors claimed the aqueous sodium chloride solution and seawater contains strong electrolytes and cannot be represented by an ideal mixture, as this leads to negative values for seawater exergy streams. The authors compared results with the previous study findings and the differences reached 570% for some streams while the calculated exergy efficiency differed by 83.0%. The MSF unit exergy efficiency was found to be 7.65%, and the majority of the input exergy was lost in the evaporator, brine heater, and pump motors, by 75.5%, 10.5%, and 5.58%, respectively.

Mabrouk et al [76] performed a thermoeconomic comparison study between MSF, TVC, MVC, and RO desalination producing 5000 m³/day. The study revealed that the exergy efficiencies of these technologies are 1.87%, 2.10%, 5.75%, and 15.7%, respectively, whereas the product cost was at level of 2.64 \$/m³, 3.32 \$/m³, 1.67

$\$/\text{m}^3$, and $1.34 \$/\text{m}^3$ for the technologies. As far as MSF is concerned, Mabrouk et al recommended further improvement of the MSF distiller train to reduce the exergy destruction. Mistry et al [77] studied different desalination technologies: MSF, MED, RO, MVC, direct contact membrane, and humidification-dehumidification. They found the exergy efficiency of these technologies to be typically 2.9%, 5.9%, 31.9%, 8.5%, 1%, and 2.4%, respectively. The authors suggested using exergy analysis for evaluating thermal systems in general and for desalination specifically, to determine the potential for further improvements, because it standardizes all forms of energy on their ability to produce useful work.

In most of these previous studies, the MSF desalination system was analysed as a whole unit, without detailed exergy analysis of the internal components to specify the exact locations of exergy destruction. Nafey et al [78] conducted a detailed exergy analysis of a $5000 \text{ m}^3/\text{day}$ MSF desalination plant and found that the exergy efficiency was only 1.83%, which was considered too low. Exergy efficiency of the evaporator stages and first stage were found to have highest exergy destruction.

2.4 Improving MSF desalination performance

As mentioned previously, MSF desalination is the dominant desalination technology in GCC countries but the literature reveals it has the lowest exergy efficiency. Therefore, it is worth investigating the cause of the poor MSF desalination exergy efficiency to propose enhancement possibilities.

2.4.1 MSF plant enhancements

Limited studies discuss methods to improve MSF desalination. This may be due to the lack of detailed operational data necessary for the further analysis. In addition, MSF desalination performance is typically measured by the gain output ratio (GOR), which represents simply the amount of distillate per amount of steam consumed. However, this kind of indicator lacks the capabilities to identify the ideal MSF case. Exergy efficiency estimation removes this GOR limitation and enables estimation actual performance compared with an ideal MSF.

In an early study, Tanios [79] performed a practical test on Shuwaikh MSF (Kuwait) to investigate the capabilities to increase or decrease the distillate production. He found variation of top brine temperature (TBT) to 16.6°C greater than the design value at 94% of brine flow rate resulted in increasing the distillate production by

20%. In the same study, he recommended adjusting the distillate header orifice between the stages to reduce the flashing portion of the distillate (in the distillate corridor) when the distillate moves from one stage to another, since each stage was maintained at a lower pressure than the previous one.

Sommariva et al [12] discussed performance enhancement of MSF desalination by overcoming the distillate re-flashing phenomenon in distillate corridor. The study proved experimentally and theoretically that extracting the distillate from the stage just after condensation prevents it from moving from one stage to the next and will improve the stage efficiencies and increase production. The authors suggested a correction line for the MSF water production based on extracting the distillate from the first stage (Figure 2.9). Moreover, they suggested that using available sensible heat in the collected distillate through heat exchange to increase the brine recycle temperature could save the available heat and increase the production. This conclusion was in agreement with other published works by Mussati et al [80, 81].

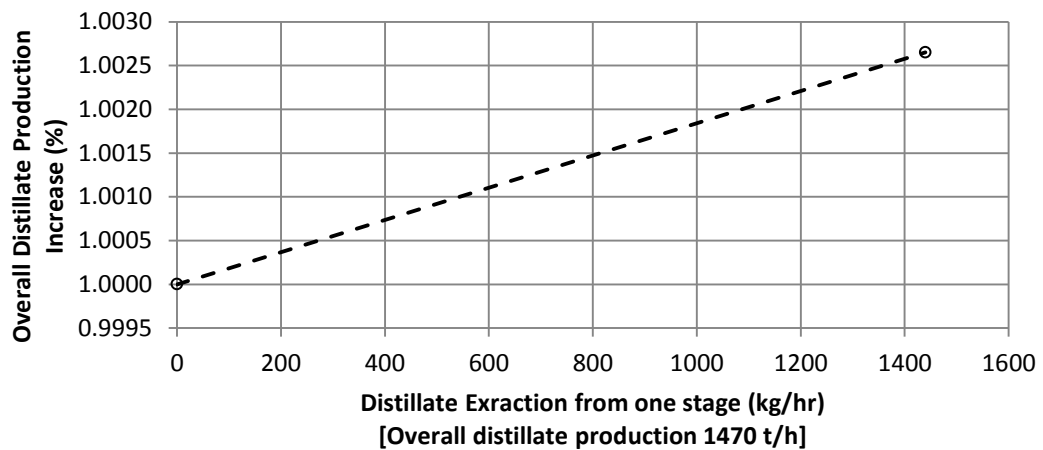


Figure 2.9: Distillate extraction MSF performance enhancement correction curve (as cited in [12])

Thermodynamically, Sommariva et al [12] compared two different scenarios on the T-s diagram (Figure 2.10). The thick line represents the process when the distillate is extracted outside the evaporator and not allowed to move to the adjacent stage. The thin line shows the normal process in a MSF distiller. The area on the diagram shows the heat transfer magnitude, which was greater in the case of extracting the distillate.

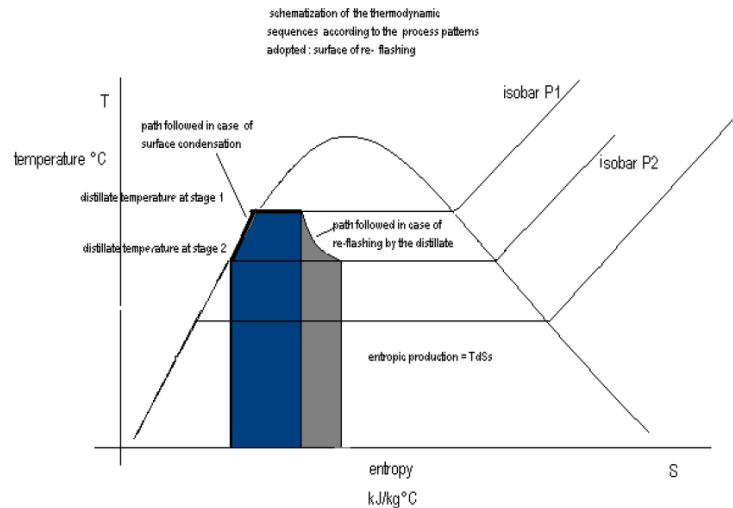


Figure 2.10: Thermodynamics comparisons between extracting the distillate and normal MSF process (as cited in [12])

The most important modification seen on MSF to date is the upgrading of Sharjah Layyah MSF desalination unit 9 in the UAE by LET [82]. This modification was based originally on the patent of Leon Awerbush (GB 2443802) consisting of [83]:

1. Using nano-filtration technology to remove bivalent scale forming ions to enable increased TBT and increased brine recirculation flow.
2. Increasing the brine recycle flow through increasing the makeup flow, which guaranteed a lower salinity in brine recycle flow and increased the efficiency, since the makeup temperature is higher than the brine recycle temperature.
3. Diversion of distillate stream from heat recovery section to avoid re-flashing and re-condensation in the heat rejection section and utilizing its enthalpy in a low-grade heat application, such as MED (Figure 2.11). This modification was based on the patent of Awerbuch and Sommariva (EP1781390 B1) [10].

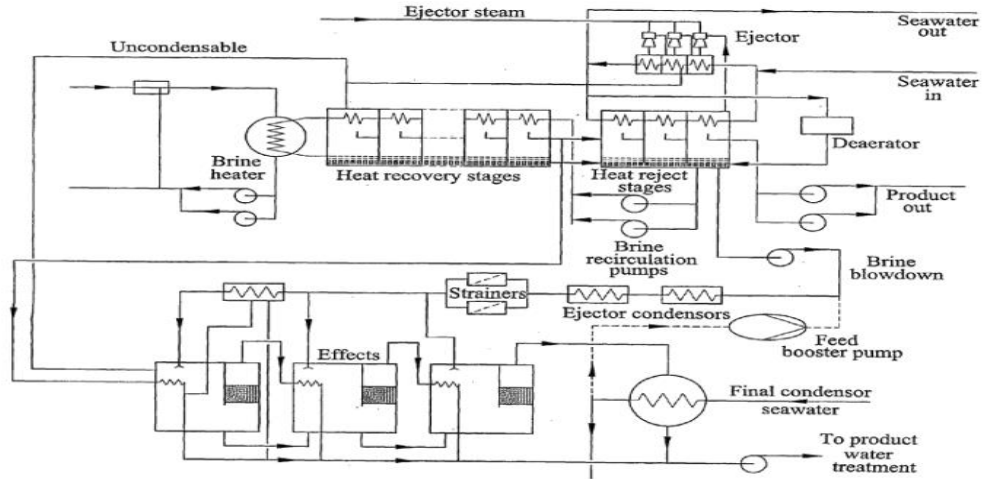


Figure 2.11: Schematic drawing of hybrid MSF/MED [10]

This combination of concepts increased distillate production by 45% from 5 MIGD to 7.5 MIGD and improved distillate purity. This modification was achieved without building new seawater intake and saved land space. Financially, the saving in investment cost was around 47% compared with installing a new RO desalination system. LET succeeded to extract the distillate from heat recovery section and cool it down using a heat exchanger prior to further modification to hybridize it with MED through the flashing tank (Figure 2.11), which will add approximately another 5 MIGD [11].

Helal et al [82] performed a simulation study of the above modifications for a MSF desalination plant in Umm Al Nar East 4-6, Abu Dhabi. The results showed good agreement with the actual enhancement on the Layyah MSF. The authors found extracting the distillate alone raised the distillate production by only 2% compared with a conventional plant. Therefore, this study revealed the necessity of utilizing the enthalpy of the extracted distillate in low-grade heat applications, as this can add revenue to the project and save additional heat exchanger costs to cool it down.

In 2000, PB Power developed a modified MSF process that enhanced a cogeneration power and water plant [84]. The modification suggested extracting part of the distillate stream of the product and heating it by condensate return to the power plant. This would be done through a plate heat exchanger for linking it to the product collection tray to warm up the brine recycled in the tubes (Figure 2.12). Moreover, a reduction in condensate temperature could be compensated by recovering heat from

the HRSG exhaust through a heat exchanger or economizer. Thermodynamically, this modification, increasing the brine heater inlet temperature, and reduced the brine heater steam consumption drastically at a constant TBT. On other hand, it reduced the plant production by 0.5%, which proved Sommoriva et al's [12] idea of a higher amount of distillate corridor increasing the re-flashing and reducing the production. The modification was implemented at Shuwaihat cogeneration plant in Abu Dhabi for six MSF distillers. It decreased steam consumption by 6% with a modification cost of less than 0.1% of distiller cost and CO₂ reduction of 80,000 t/year. However, the study did not include the additional economizer cost to increase the condensate temperature again in the HRSG.

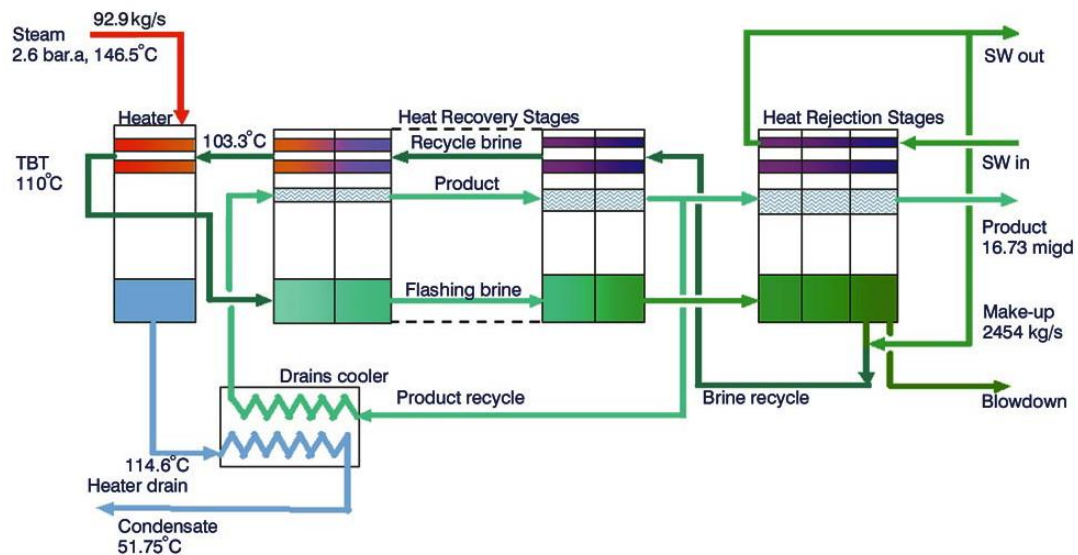


Figure 2.12: PB power modified MSF process [84]

Junjie et al [85] proposed a modification of the MSF desalination evaporator to enhance the distillate production through utilizing the MED desalination concept and reusing cooling water as feed to the MSF. The authors suggested extracting part of the distillate vapour from each stage and using its latent heat to warm up the brine of the next stage through heat exchange. The simulation results showed an increase of GOR by 74.1%, a reduction of capital cost by 21.8%, and a decrease of the product cost by 10.7%.

2.4.2 Low-grade heat recovery technologies

An aim of this study is to enhance actual MSF desalination unit performance since it has low exergy efficiency. The previous studies showed extracting the distillate from

MSF desalination has two main advantages: increasing unit production and providing a low-grade sensible heat source that could be recovered through heat recovery technologies. The extracted distillate temperature depends on the TBT and varies based on location of extraction. In this study, this temperature is in the range of 65°C to 100°C (from the first eight stages). Therefore, the study will focus on recovering this heat through heat recovery technologies to enhance the MSF unit performance, which then reflects on the performance of the cogeneration plant performance.

The selection of the suitable heat recovery technology should meet the available temperature range and provide a new source of the most wanted products in arid countries: power or water. From literature survey, it was found the AC, ORC, IH, and MED were the most suitable technologies.

2.4.2.1 Absorption Chiller (AC)

In 1850, Edmond Carré developed the first AC using sulphuric acid as working fluid, and then in 1873, his brother Ferdinand Carré patented a commercial ammonia/water refrigerator. Serious development started only after the 1960s, when single effect lithium bromide–water (LiBr–H₂O) was used [86]. The AC technologies succeed in converting low-grade heat to a cooling effect. The heat source can be supplied directly through the burning of fossils fuels, such as natural gas, or using LP steam and hot water indirectly, but the main advantage of the AC is the ability to recover and utilize waste heat streams rejected from industrial applications or available through renewable energy, such as solar [87].

2.4.2.1.1 Working principle

To describe the working principle of the AC, it is useful to start with explaining the more familiar VC cycle because there are two differences. The first difference is that AC is a heat driven cycle while the electrical compressor drives VC mechanically. Secondly, in VC, the working fluid is the refrigerant only. However in AC, the working fluid consists of a combination of two working fluids: the refrigerant and an absorbent, which can absorb the refrigerant [88]. A pump with generator, absorber, heat exchanger, and throttling valve replaces the compressor in the VC cycle. Figure 2.13 shows the basic scheme of AC.

The recovered heat (\dot{Q}_G) is utilized to heat up the diluted solution in the generator, which releases the refrigerant (H_2O) superheated vapour. This moves to the condenser while the concentrated solution of LiBr in the saturated liquid condition flows towards the heat exchanger. In the condenser, the refrigerant superheated vapour condenses due to heat absorption by cooling water (\dot{Q}_C) and changes to the saturated liquid state. It then flows through an expansion valve where the phase changes to vapour since it is maintained at a lower pressure (vacuum) downstream of the expansion valve. At the evaporator, heat is absorbed to create external chilling (\dot{Q}_E). In the absorber, the concentrated solution (vapour liquid state) is dispersed on the absorber tubes and the vapour coming from the evaporator is absorbed into the concentrated solution. The rejected heat from this absorption process is removed by cooling water (\dot{Q}_A) to dilute the concentrated solution and change it to a sub-cooled state. The solution pump (\dot{W}_{PP}) increases the pressure of the sub-cooled diluted solution, moving it to the heat exchanger to absorb heat (\dot{Q}_{HX}) from the concentrated solution from the generator.

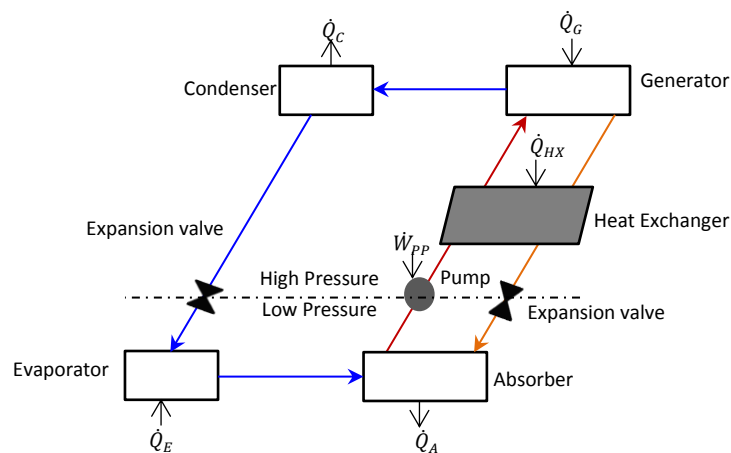


Figure 2.13: Schematic drawing of basic AC

2.4.2.1.2 Properties of absorption working fluids

The performance of the absorption system is correlated directly to the thermo-physical, chemical, and thermodynamic properties of the working fluid. ASHRAE fundamentals [89] summarize the main characteristics of the suitable absorbents and refrigerants for the absorption system:

- The refrigerant should have a high latent heat to reduce the circulation rate of the absorbent and refrigerant.

- b. The refrigerant should have a low freezing temperature to achieve better cooling and more volatility to separate it easily from the absorbent.
- c. The absorbent should have a strong affinity for the refrigerant to promote dilution.
- d. Both absorbent and refrigerant should be away from solidification point during system operation.
- e. The mixture should be with low viscosity to reduce pumping power.
- f. Refrigerant, absorbent and their mixture should be safe and non-toxic in order to reduce environmental impact.

Many studies have discussed different working fluids for AC applications [89, 90, 91]. These include water/sodium hydroxide, water/sulphuric acid, ammonia/sodium thiocyanate, and many other mixtures. However, it has been concluded that $\text{NH}_3\text{-H}_2\text{O}$ and $\text{LiBr-H}_2\text{O}$ are the most appropriate fluids compared with other working fluids and conventionally have been used in most ACs [90, 92, 93]

Table 2.3 illustrates the trade-off, where these conventional working fluids are ranked according to the various desirable properties [93]. For instance, for the AC with $\text{NH}_3\text{-H}_2\text{O}$ as working fluid, the heat source temperature should be between $125\text{--}170^\circ\text{C}$ with air cooled and between $95\text{--}125^\circ\text{C}$ when water cooled. On the other hand, the $\text{LiBr-H}_2\text{O}$ AC can be operated with heat source temperature in range of $70\text{--}95^\circ\text{C}$ water cooled [94]. Furthermore, at the same cooling capacity and evaporator temperature, the $\text{LiBr-H}_2\text{O}$ AC Coefficient of Performance (COP) is slightly higher than that for $\text{NH}_3\text{-H}_2\text{O}$ [92]. The $\text{LiBr-H}_2\text{O}$ AC suffers from certain problems, such as a limited application range due to the crystallization phenomena (changing to solid phase), which starts to appear at certain LiBr concentrations and temperatures. In addition, the LiBr chilled water temperature normally has to be above 5°C since water is the refrigerant in this cycle [94].

In this study, LiBr and water were selected as the best working fluids, meeting the range of MSF hot distillate temperature, which is $65\text{--}100^\circ\text{C}$. Furthermore, the chilled water temperature is lower than the minimum ambient temperature in Oman; therefore, it can be used to cool down the GT inlet temperature in hot countries [95].

Property	NH ₃ -H ₂ O	H ₂ O/LiBr
Refrigerant		
High latent heat	Good	Excellent
Moderate vapour pressure	Too high	Too low
Low freezing temperature	Excellent	Limited application
Low viscosity	Good	Good
Absorbent		
Low vapour pressure	Poor	Excellent
Low viscosity	Good	Good
Mixture		
No solid phase	Excellent	Limited applications
Low toxicity	Poor	Good
High affinity between refrigerant and absorbent	Good	Good

Table 2.3: Trade-off between NH₃-H₂O and H₂O-LiBr absorption chiller working fluids [92, 93]

2.4.2.1.3 LiBr/H₂O absorption chiller configuration

The heating source temperature is considered the index to decide the configuration of the AC [96]. Single effect and double effect are the most common industrial AC configurations, although triple and half effect have started to be manufactured for certain heat source levels [96]. Figure 2.18 describes the configuration of the single effect AC. The double effect AC has two sets of generators, condensers, heat exchangers, and throttling valves. Table 2.4 presents typical performance data for different configurations of AC. This study will include the single effect AC, which meets the specification of the recovered heat from desalination

AC type	Heating source temperature (°C) [97, 98]	COP [96]
Half effect	60–54 [90]	≈ 0.38
Single effect	60–140	≈ 0.70
Double effect	120–180	≈ 1.3
Triple effect	200–250	≈ 1.7

Table 2.4: AC configuration performance

2.4.2.1.4 Thermal analysis studies of LiBr/H₂O single effect AC

A number of researchers have analysed single and double effect ACs using the energy approach. However, this approach is lacking in determination of the absorption system irreversibility. Exergy analysis succeeds in overcoming this limitation, which has encouraged a limited number of researchers to investigate sources of irreversibility (exergy destruction) in absorption systems [99].

Talbi and Agnew [100] carried out an energy and exergy analysis study of H₂O–LiBr single effect AC powered by 500°C waste heat from diesel engine exhaust at 35°C ambient cooling temperature. The calculated COP and exergy efficiency of the system were found to be 0.67 and 2.8%, respectively. The absorber contributed 59% of the total system exergy destruction. However, the study ignored the influence of chemical exergy for all components.

Kaushik and Arora [99] developed the Engineering Equation Solver (EES) computer program code to perform energy and exergy analyses of a series of cooled single and double effect ACs. They confirmed the COP of single effect AC lies in the range of 0.60–0.75 with 1.0–1.3 for the double effect. However, both systems had a similar range of exergy efficiency of between 6.0% and 20%. The study covered the influence of generator inlet temperature on both COP and exergy efficiency at an evaporator temperature of 7.2°C and different absorber temperatures, while the condenser temperature was kept equal to absorber temperature. It was observed that the COP increases initially with an increase in generator inlet temperature and then tends to level off rather than continue to increase. Moreover, the exergetic efficiency of both systems increased at a lower temperature and then declined as the generator temperature rose. The absorber had the highest exergy destruction for both systems.

Gomri [101] conducted a comparative study between single and double effect ACs at the same output. When the evaporator temperature changed from 4°C to 10°C and the generator temperature varied from 60–190°C at constant condenser and absorber cooling temperature (33°C), the COP was in the range of 0.73–0.79 for single effect and 1.22–1.42 for double effect. For similar COP, exergy efficiency was in the range of 12.5–23.2% for single effect and from 14.3– 25.1% for double effect ACs. In addition, the COP of both cycles rises with increasing generator inlet temperature and evaporator temperature but decreases with rising condenser temperature. For each condenser and evaporator temperature, there is an optimum generator temperature to achieve the highest COP and exergy efficiency, which is in agreement with another study by Shahata et al [102].

Using the EES computer code, Zedeh and Bozorgan [103] performed energy and exergy analysis of steam single effect absorption. The study found single effect AC has a high COP but low exergy efficiency than the double effect AC. The generator

and absorber are major contributors to the system exergy destruction. Consequently, the authors suggested operating the AC system at a lower temperature to overcome the high exergy destruction at the higher generator inlet temperature. Furthermore, the authors recommended exergy analysis for pinpointing sources of irreversibility (exergy destruction) in thermal systems.

Mehrabian and Shahbeik [104] developed a computer program to analyse single effect H₂O–LiBr ACs by using energy and exergy approaches. The authors observed increasing the evaporator and generator temperature or decreasing the condenser and generator temperature could lead to enhance system exergy efficiency. Temperatures of the hot water, cooling water, and chilled water, respectively, at inlet to the generator, evaporator, and condenser have a great effect on COP.

Al-Zahrani [105] developed an IPSEpro model for a 9304 kW single effect H₂O–LiBr using 97°C heat source temperature for the energy and exergy analysis of the proposed system. The study found system COP and exergy efficiency at 0.79 and 6.91%, respectively, and the generator destroyed 28% of input exergy, whereas the absorber destroyed 23%. A parametric study of the influence of the generator inlet temperature and evaporator temperature suggested that 88°C was the optimal heating source temperature leading to the best exergy efficiency and COP with increasing evaporator inlet temperature, causing a decrease of system exergy efficiency.

All these previous exergy analysis studies ignored the chemical exergy part of LiBr and considered the physical exergy only. However, this assumption is correct only where the solution concentration of the inlets and outlets of the components are the same (e.g., condenser and evaporator) [47–49], and in the case of single effect AC generator and absorber components, mixtures are maintained at different concentrations. Misra et al [106] performed one of the early studies on the exergy analysis of a steam powered single effect AC with chemical exergy based on Bejan et al's [46] standard LiBr exergy, which assumes a LiBr solution is an ideal solution [46]. The results showed the system exergy efficiency was 11%, whereas 45% of the exergy was destroyed in the evaporator assembly, which consists of condenser, evaporator, and absorber.

Palacios-Bereche et al [107] carried out a recent comprehensive exergy analysis of single effect AC. In this study, the researchers succeeded in calculating the chemical

exergy part of the LiBr solution with the estimation of exergy destruction due to dissolution of both solution elements to overcome the limitations of the ideal solution assumption. They implemented their procedure for the exergy analysis of the single effect AC powered by two different methods: direct fired and hot water. The exergy efficiency was 2.65% and 14.3% for direct fired and hot water, respectively, while in both cases; the generator and absorber were the main contributors to exergy destruction.

2.4.2.1.5 GT inlet cooling using LiBr–H₂O AC

With increasing demand for electrical power and restrictions on thermal system pollutants, researchers have been encouraged to investigate the performance enhancement of power generation systems. The ambient conditions, specifically the air ambient temperature, affect cogeneration plants highly, resulting in a shortage of electrical power to supply the GTs in hot countries [108, 109]. This is because at higher ambient temperatures, the air density decreases and consequently, the air mass flow rate reduces, causing a reduction in GT output [108, 109, 110]. Due to this GT output variation at different ambient conditions, the standard ISO (International Organization of Standards) condition is used for comparative purposes. GT manufacturers have used the standard to standardise GT output at 15°C, 1.013 bar, and 60% relative humidity [111].

A good example of the influence of GT inlet temperature is that the Alstom GT13E2 GT produces net power of 180 MW at ISO conditions, which reduces sharply to 135 MW at 50°C (possible temperature at summer of hot countries) [108]. Therefore, a reduction of GT inlet temperature improves GT and cogeneration plant output and efficiency. Technologies, such as fogging systems, evaporative cooling, mechanical vapour compression, and ACs, have been used widely to reduce GT inlet temperatures [112]. The chiller technologies are unlike evaporative coolers and fogging systems, which are limited by wet bulb temperature and affected highly by the ambient relative humidity [113]. The only disadvantage of absorption technology is the fuel cost if it is also operated by fossil fuel or electrical energy. However, it becomes more attractive when powered by waste heat “free energy” [112], the case in the current study.

Kakaras et al [114] carried out an investigation for selection of the best GT inlet temperature cooling technologies among evaporative cooler, compression chiller, AC, and fan for air recompression using ENBIPRO simulation software. The cooling technologies were investigated for two sites in Greece, with Lavario IV, Lavario V, ABB GT10, and LM2500+ GTs for one full year. The highest electricity generation was achieved by the AC, followed by the compression chiller, evaporative cooler, and air recompression in that order. From the economical side, the evaporative cooler is better than the other technologies in term of payback period, yet the AC yields more than double the gain in power capacity augmentation. The researchers mentioned that the waste heat from the GT exhaust did not power the AC fully. Additional steam was used to compensate for the reduction of the flue gas exhaust, which could explain the higher operation costs and longer payback period.

Ehyaie et al [115] studied the use of a single effect H₂O–LiBr AC powered by GT exhaust to reduce GT inlet temperature at two Iranian cities, Tabas and Bushehr. The researchers developed a FORTRAN program for both GTs, which are operating on open cycle using GT type SIEMENS V94.2 with 159 MW at the ISO conditions. The results showed using the AC enhanced the output power by 11.5 and 10.3% and increased the annual average energy efficiency by 24% and 34% for Tabas and Bushehr, respectively. Moreover, the absorption cooling increased the exergy efficiency for both cities, while the cost of electricity production reduced by 5.04% and 2.97%.

Ameri and Hajazi [116] studied the Chabahar GT (GE frame 5) enhancement using an AC powered by steam extracted from the HRSG to cool down the GT inlet temperature. The study revealed that using the AC increased the GT output by 11.3% and improved thermal efficiency slightly. Inlet GT cooling reduced electricity costs from 2.5 cents/kWh to 1.45 cents/kWh. The economic analysis showed that the payback period was 4.2 years, with an internal rate of return of 23.4%. However, the study included installation of a new HRSG with its components just to supply 9 bar saturated steam for the AC, and this increased the project capital investment. Instead a flue gas AC can be installed directly to recover GT exhaust as was studied by Al-Zahrani [105].

Boonnasa et al [117] studied the efficiency improvement of 127 MW combined power plant (2 GTs + 1 ST) in Thailand, through cooling of a GT inlet temperature using a single effect AC operated by extracted steam from the HRSG. The authors found using AC cooling could increase the GT and combined cycle power by 10.6% and 6.24%, respectively. However, the steam turbine power reduced by 2.43%, resulting from utilizing part of the steam consumption to power AC. The economic analysis showed promising figures of a 3.81 years payback period with a 40% internal rate of return.

2.4.2.2 Organic Rankine Cycle (ORC)

A high amount of low-grade heat is emitted either naturally (e.g., solar, biomass, geothermal) or industrially, such as waste heat from power and desalination plants. The low temperature of this was the main challenging factor for heat recovery. The ORC is one technology that could utilize heat from as low as 70°C up to 500°C and more to produce electrical power [94]. The working fluids in ORC chemically belong to the CFCs, HFCs, and HCFs. The ORC is similar to the steam Rankine cycle but their main feature is the low boiling points of the working fluids [118]. In addition, ORC units are low maintenance cost, require few operation staff, have a long unit life, less erosion in turbines, do not require demineralized water, and have simple start up procedures and easy control features [119]. Today, many ORC plants are available, varying in capacity from kW to MWs and powered by different heat resources. Since the 1980s, manufacturers have been available in the market providing ORC units powered by different heat sources in various temperature ranges. The three main ORC suppliers are Turboden (45% of worldwide installed units), Ormat (24% of worldwide installed units), and Maxxtec (23% of worldwide installed units) [120, 121]. Table 2.5 shows a sample of available ORC unit providers with the power sources and temperatures.

Manufacturer	Applications	Power range (kW)	Heat source temperature (°C)	Technology
Ormat, US	Geo., WHR, solar	200–70000	150–300	n-pentane and others
Turboden, Italy	Biomass-CHP, WHR, Geo.	200–2000	100–300	OMTS, Solkatherm
Adoratec/Maxxtec Germany	Biomass-CHP	315–1600	300	OMTS
Opcon, Sweden	Geo., WHR	350–800	< 120	Ammonia
GMK, Germany	Biomass-CHP, WHR, Geo.	50–5000	120-350	n/a
Bosch KWK, Germany	WHR	65–325	120–150	R245fa
Turboden	Geo., WHR	280	91–149	R245fa
PureCycle, US	WHR	125	> 121	R245fa
GE CleanCycle	WHR	n/a	100–400	R134a, R245fa
Cryostar, France	Geo., WHR	n/a	100–400	R134a, R245fa
Tri-o-gen, Netherland	WHR	160	> 350	Toluene
Electratherm, US	WHR, solar	50	> 93	R245fa
Infinity Turbine	WHR	250	> 80	R134a
UTC power	Geo.	250	73	R134a

Table 2.5: Non-exhaustive list of ORC manufacturers [121]

Conceptually, the ORC consists of similar components to the steam Rankine Cycle: evaporator, turbine, condenser, and refrigerant pump (Figure 2.14 with T-s diagram in Figure 2.15). In the evaporator, heat addition (pre-heating and evaporation: process in T-s diagram: 4 to 5 to 1) from the heating source takes place, which changes the sub-cooled state to slightly superheated vapour. Then, the expansion process converts thermal energy to mechanical power (process in T-s diagram: 1 to 2). The condenser is cooled by either cooled air or water, which removes the heat from the refrigerant to change it to the sub-cooled condition again (process in T-s diagram: 2 to 3). After that, the pump increases the refrigerant pressure and pumps it to the evaporator (process in T-s diagram: 3 to 4).

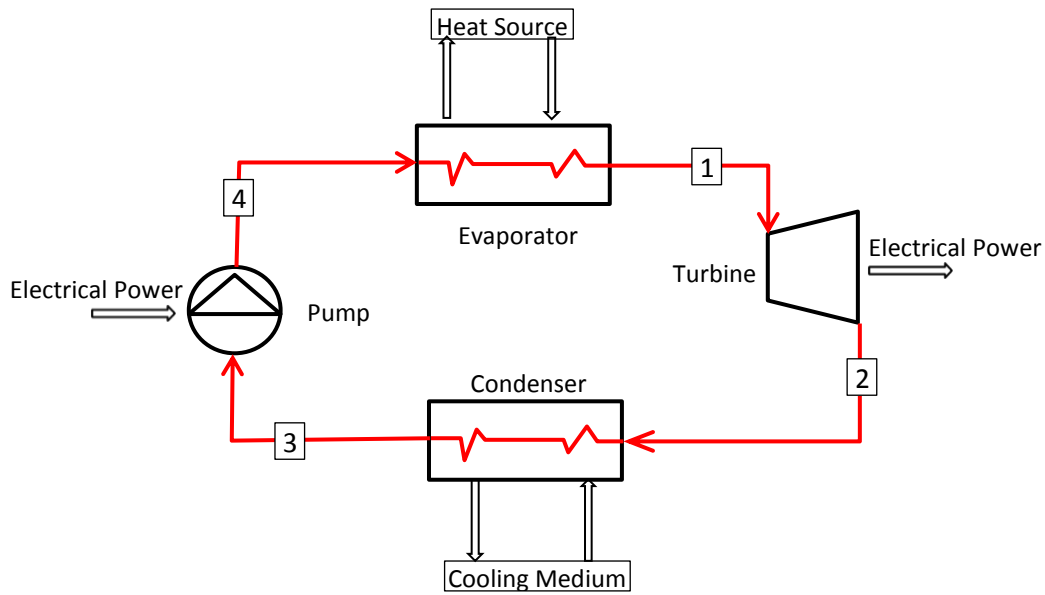


Figure 2.14: Schematic of general ORC cycle components

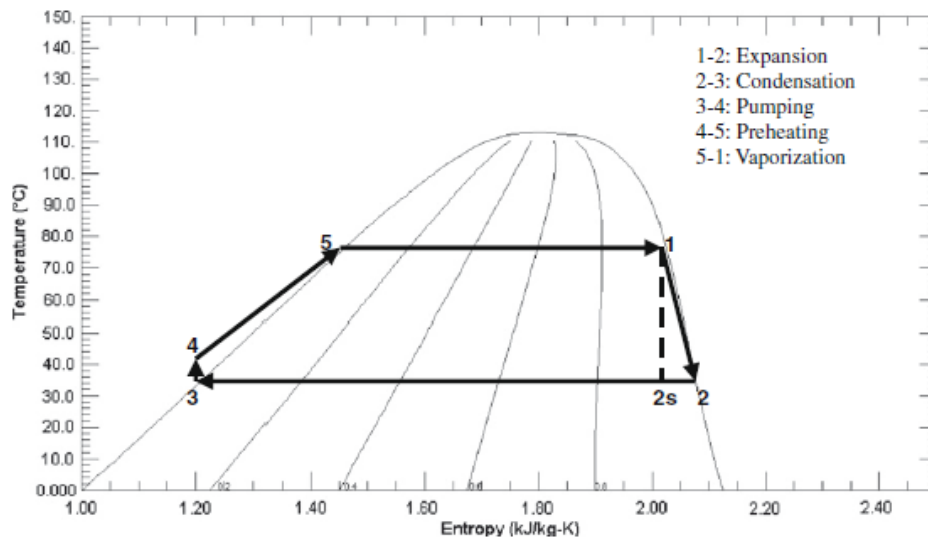


Figure 2.15: Typical T-s diagram for an ORC [122]

2.4.2.2.1 Properties of working fluids

The selection of the ORC working fluid has a key role in achieving higher ORC performance and output. ORC working fluids can be classified into three main categories based on their saturation vapour curve: isentropic, dry, and wet (Figure 2.16). The evaluation line identifies the refrigerant phases at the inlet to the outlet from the ORC turbine. All the three categories enter the turbine at the slightly superheated condition, but the outlet condition differs: with wet fluids, it lies in the vapour-liquid mixture region (vapour quality < 1); with isentropic fluids, it is located

on the saturated vapour line (vapour quality ≈ 1); and with dry, it is in the superheated region (single phase).

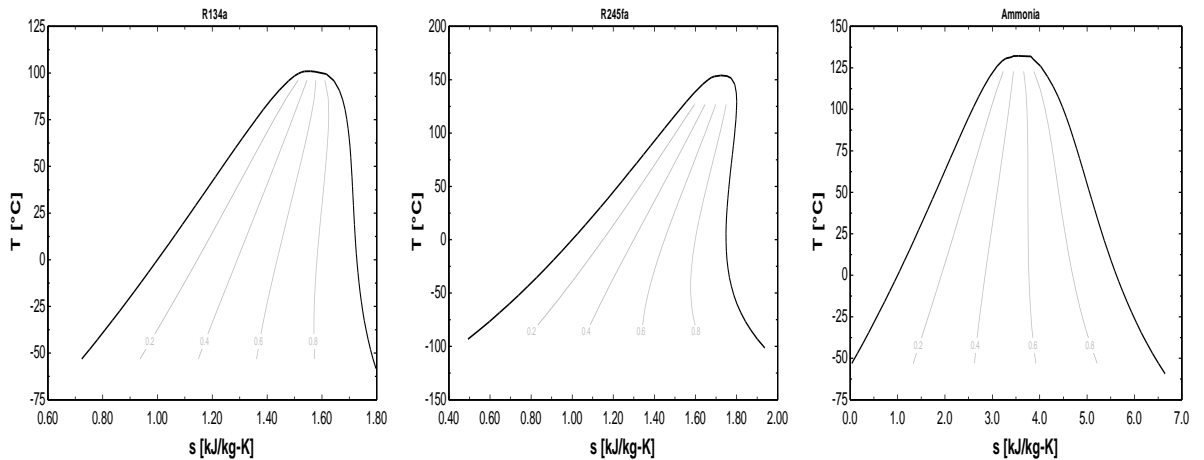


Figure 2.16: ORC fluid classification: isentropic, dry, and wet in order [120]

Many researchers have investigated selection of the best working fluid candidates for certain applications and temperatures [122–127]. The selection criteria used can be summarized as follows [120, 122–128]:

- a. Thermodynamic performance reflected in higher ORC electrical power output. The ORC performance depends on interdependent thermodynamic properties, such as specific heat capacity, density, critical pressure, and critical temperature. Thus, it is difficult to refer higher performance to any one property.
- b. Fluid should belong to isentropic or dry working fluids categories (Figure 2.21) because usage of wet fluids causes liquid droplets at lower pressures stages of the turbine, which results in erosion and vibration.
- c. Higher vapour density is very important in determining the component sizes, because low density causes higher volumetric flow rate and thus larger component sizes.
- d. Lower viscosity working fluid gain from higher heat transfer and reduced pressure drops.
- e. Higher thermal conductivity results in higher heat transfer coefficient in heat exchangers.
- f. Acceptable evaporating pressure, because higher pressures lead to increasing investment cost but lower pressures to reduced thermal efficiency.

- g. Positive gauge turbine outlet pressure (higher than atmospheric) prevents air ingress. However, it should be not far above atmospheric to avoid efficiency reduction.
- h. Working fluid condensing temperature should be higher than highest ambient temperature (for either water or air cooling) so it can be cooled.
- i. High safety level as classified by the ASHRAE Standard [89], so each working fluid candidate can be evaluated accordingly.
- j. Most refrigerant working fluids have low Ozone Depleting Potential (ODP) of null or very close to zero.
- k. Low Greenhouse Warming Potential (GWP), which is a measure over a specific time interval, commonly 20, 100, or 500 years with respect to CO₂ GWP, which is taken to be unity.
- l. The working fluid should have good availability in the market with competitive price for cost effectiveness.

Although, the studies covered a broad range of working fluids candidates only a few of them are used in the industry. Table 2.6 shows the common working fluids and their uses [120].

HFC-R134a	For very low temperature source applications, mainly used in geothermal power plant
HFC-R245fa	For low temperature applications, mainly used in waste heat recovery
n-pentane	For medium temperature applications, used only in commercial solar ORC power plant in Nevada
Solkatherm	For medium temperature applications, used in waste heat recovery applications
OMTS	For medium temperature applications, used in Bio-mass-CHP power plants
Toluene	For high temperature applications, used in waste heat recovery

Table 2.6: Most common refrigerants used ORC in industry [120]

As it can be seen from Table 2.6, R134a and R245fa are used widely, especially in low-grade heat source applications. Consequently, only R134a and R245fa will be considered in this study because the available heat source temperature from MSF desalination is between 65°C and 100°C. In addition, they also have good thermodynamic properties, low ODP, and low GWP (Table 2.7).

Physical properties	R134a	R245fa
Molecular weight (g/mol)	102.03	134.05
Critical pressure (bar)	40.59	36.40
Critical temperature (°C)	101.06	154.60
Vaporization heat at 1 atm (kJ/kg)	217.2	197.5
Boiling temperature at 1 atm (°C)	- 26.4	14.6
Environmental data	R134a	R245fa
Atmospheric lifetime	14	7.6
ASHRAE level of safety	A1	B1
Ozone Depleting Potential (ODP)	≈ 0	≈ 0
Greenhouse Warming Potential (GWP) 100 year	1320	1020

Table 2.7: Physical and environmental data for refrigerants R134a and R245fa [94]

2.4.2.2.2 Thermal analysis studies of ORC

As the focus of this thesis is not the evaluation of the working fluids, this section will focus on ORCs using R134a and R245fa as working fluids, either to evaluate the performance of each one separately or to compare between them. Furthermore, focus will be given where both energy and exergy evaluations were involved.

Kosmadakis et al performed a study to select the best ORC fluids among 33 candidates for a two-stage ORC: an upper cycle with 137°C and a lower cycle with 77°C to power RO desalination pumps and auxiliaries [124]. The upper cycle gains heat from a solar collector while the lower cycle evaporator works as the condenser for the upper one. The authors discussed the upper cycle fluid selection and found R245fa the most appropriate (although it was not the most efficient, it was safe and performed quite well). R134a was discarded from the upper cycle comparisons because of critical temperature lower than 137°C but was selected for the lower cycle [129].

Guo et al [126] carried out screening of several working fluids to find the best candidates for a low-grade heat geothermal application using both energy and exergy approaches. The study concluded R245fa followed by R134a are the most appropriate ORC working fluids for low-grade geothermal temperatures between 80°C and 100°C. At a geothermal source temperature of 90°C and with optimal evaporator temperature, ORC thermal efficiency was 4.87% and 5.27% for R134a and R245fa, respectively, whereas exergy efficiency was 47.2% for R134a and 48.4% for R245fa.

Lakew and Bolland [130] investigated ORC refrigerants, including R134a and R245fa, for low-grade heat source applications using net power, exergy efficiency, and heat exchanger size as evaluation criteria. The results showed at a 80°C heat source temperature, both refrigerants' net power increases when the turbine inlet pressure rises (or corresponding turbine inlet temperature), reaching an optimal value and then dropping. However, this behaviour changes when the heat source temperature is 200°C and here, the trend is rising continuously. In general, R245fa produces slightly more electrical power than R134a, although the researchers did not justify why R134a performed better than R245fa at 120°C and 160°C. R245fa was found to have slightly higher exergy efficiency than R134a when the turbine inlet pressure was varied for different heat source temperatures. Strangely, the authors revealed the exergy efficiency for all refrigerants dropped as heat source temperature increased at various turbine inlet pressures despite rising net electrical power produced.

An ORC system providing electrical power and heat using a combined solar system and geothermal heat was analysed for different working fluids: R245fa, R134a, and R236fa [131]. The results showed the better performance of R245fa compared with R134a: 13% and 25% for energy and exergy efficiency, respectively, for R245fa, while these figures were only 9.1% and 22.7% for R134a. In addition, R134a refrigerant pump power consumption and flow rate were higher than for R245fa by 33% and 42%, respectively. Nevertheless, the study observed that the evaporator was the main contributor of exergy destruction within the system for the different working fluids.

Aghahosseini and Dincer [132] conducted a comparative performance analysis of low temperature ORC using pure (R123, R245fa, R600a, R134a) and zeotropic (R407C [52% R134a + 23% R32 + 25% R125], and R404a [52% R143a + 44% R125 + 4% R134a]) working fluids. For R134a and R245fa, the thermal efficiency appeared to increase with the turbine inlet pressure (or corresponding temperature), and similar behaviour was noted for the exergy efficiency. The authors suggested using refrigerant at the turbine inlet at the saturated vapour condition rather than superheated because it was found superheating the vapour caused no change in thermal efficiency but a drop in exergy efficiency. Moreover, they also pinpointed that exergy efficiency of the ORC increased as ambient temperature rose due to

irreversibility reduction within the cycle. This finding means that exergy efficiency will be higher in hot countries, in contrast to energy efficiency, which is lower as a result of increasing turbine outlet pressure.

Schuster and Karl [133] developed an IPSEpro model to investigate an ORC unit powered by solar energy to supply electrical power for RO desalination pump. Four working fluids (R134a, R227ea, R236fa and R245fa) were investigated. The results showed R134a performed better than R245fa at lower turbine inlet temperature; however, R245fa takes the credits at higher ones. It is very important to emphasize that this study was carried out at different turbine outlet temperatures, which could lead to improper comparisons.

Energy and exergy analyses was performed to investigate seven working fluids (R134a, R113, R245ca, R245fa, R123, isobutene, and propane) with boiling points between -43°C and 48°C [134] by a parametric analysis of turbine inlet temperature, turbine inlet pressure, and condenser outlet temperature. It revealed that at an evaporator pressure 1.5 MPa, condenser temperature 25°C , and over the possible turbine inlet temperatures than thermal efficiency was higher for refrigerants with higher boiling temperature. For example R134a (boiling temperature -26.1°C) thermal efficiency was around 6.5% whereas R245fa (boiling temperature 14.9°C) was 14% (although a reduction of exergy efficiency was observed when turbine inlet temperature increased, from 35% to 28% for R134a and from 42% to 38% for R245fa). Increasing the turbine inlet temperature increased the thermal efficiency and reduced the exergy efficiency drastically. The authors concluded increasing the condenser outlet temperature reduces both energy and exergy efficiencies for all seven refrigerants.

Masheiti et al [135] discussed R134a and R245fa as working fluids for a low temperature 73°C geothermal ORC unit. The ORC with R134a produced more gross power compared with R245fa. However, due to high R134a refrigerant pumping power consumption, R245fa took the credit for net cycle electrical power. Power consumption for R134a was 9.5% of total gross power while this figure was only 2% for R245fa. Moreover, the ORC with R245fa exhibited lower pressure and temperature at turbine inlet, which reduced the overall heat transfer conductance

(UA) for both evaporator and condenser, making this refrigerant the more economical option.

2.4.2.3 Multi Effect (ME) desalination

The capability of ME desalination to be powered by low temperature sources has encouraged the study of utilizing heat energy from different alternatives, such as solar, geothermal, and waste heat recovery [29]. Most of the ME desalination is operated by LP steam gained by burning fossil fuels, but ME desalination with low capacity can be run by hot water with a similar operation principle. Therefore, this section will discuss other heat recovery technology alternatives to recover the low temperature heat from MSF hot distillate water to produce additional water through ME desalination.

A limited number of studies have presented hot water ME desalination. Karytsas [136] mentioned ME desalination at Milos Island, Greece driven by a hot geothermal stream with temperature of 70°C to 90 °C. The study showed the unit production was 600–800 m³/day and reduced CO₂ emissions due to the low-grade heat utilization.

Hughes et al [137] discussed a six effects' ME desalination unit driven by 90°C hot water and 65°C top brine temperature. The hot water consumption was 215 m³/h with 318 m³/h cooling water, utilized to produce 812 m³/day of distillate water.

A pilot geothermal two effects hot water ME desalination plant manufactured by Alfa Laval was tested at Kimolos Island, Greece [138]. The unit was able to recover heat from 80 m³/h geothermal hot water at 60°C to produce 80 m³/day of distillate water. The produce cost of this unit was estimated around 1.6 €/m³, taking only the annual operating cost into account.

Wang et al [139] developed a steady state model using mass and energy balance and heat transfer equations for SED driven by hot water. The model was validated against manufacturer experimental data and showed a relative error less than 5%. The number of the effects affected highly the water production of the ME desalination. It suggested boosting usage of the powering geothermal stream by recovering balance heat after discharge from the first effect to reuse it within the system. This increased the production by 25–60%.

2.5 Closing remarks

In the context of the objectives of the thesis, this literature review showed firstly the high dependence of the GCC countries on fossil fuels to produce power and water, resulting in consuming natural resources and causing environmental impact. MSF desalination is the dominant desalination type in the GCC countries and is integrated commonly with a combined power plant, motivating the necessity for enhancing cogeneration power and water plant performance. The literature also found the exergy analysis approach the most suitable to evaluate thermal systems that produce products different in quality, such as electrical power and water by desalination. However, no study was found that had evaluated a combined cogeneration power and water plant using the exergy approach simultaneously.

Secondly, in the literature, exergy efficiency of MSF was found to be the lowest among all desalination technologies, at around only 5%. However, only a limited number of studies investigated the reason behind that, probably due to lack of operational data of these systems and the difficulty in estimating the chemical exergy of the seawater solution. Thus, a detailed analysis of the MSF system internally is essential to understand better the sources of exergy destruction to propose system performance enhancements. Some studies have suggested the distillate re-flashing phenomenon within the distillate corridor reduces MSF water production and performance; therefore, recovering part of this could increase the efficiency of desalination and provide thermal energy for low-grade heat recovery technologies. However, few studies were conducted recommending utilizing sensible heat from extracted distillate.

Thirdly, the heat recovered from MSF distillate could be utilized by heat recovery technologies for different purposes. No attempts were found in the literature to address this point. AC is able to harvest low-grade heat to produce cooling capacity, which enables reduction of the high GT inlet temperatures in hot countries to augment the electrical power production. ORC units have been used to produce electrical power through utilizing low-grade heat down to 65°C. Alternatively, the low-grade heat could be used to increase water production either through regeneration within the existing unit or through coupling with low temperature desalination like ME. These four technologies could increase either electrical power

or water, which are the required products for the GCC countries. Despite that, no study was found that addressed hybridization of MSF desalination with these technologies, except for ME desalination.

Chapter 3

Actual Cogeneration Plant Operational Data Analysis

3.1 Motivation and objectives

The existing literature tends to investigate plant performance at a specific condition or conditions, for example, plant rated capacity. However, a real plant rarely operates at its rated capacity, with demand less than 100%, primarily in response to fluctuating demands. Even with “base load” operation, the loading will fluctuate according to at least seasonal variations in demand. This is likely to be accentuated in the case of a cogeneration desalination plant supplying two entirely different products: electrical power and water. The design of such a plant needs to take account of such variations (e.g., the provision of SF, as discussed in Section 3.5). Similarly, any attempt at plant performance analysis needs to be made for true representative plant operating conditions if it is to have real practical value.

As it is clearly impractical to analyse every conceivable plant operating condition, it is necessary to identify a much more limited set of typical plant operation scenarios that will be truly representative of the bulk of its annual operation. This can only be done for a particular plant in a particular system, but such a process can be illustrative of a general approach to this. As this does not appear to have been done previously for cogeneration desalination plant but is necessary for progression to the objectives of the study, the methodology will be illustrated for a specific plant at a specific location (Barka plant in Oman).

This chapter will explain the characteristics of monthly variations in electrical power generation and water production for Oman with a statistical analysis of the three main meteorological factors effecting cogeneration plant: dry bulb temperature, average relative humidity, and seawater temperature. Then, a detailed description of the cogeneration plant to be studied will be presented. Actual data from the plant will be analysed to classify typical annual plant operating scenarios to facilitate the modelling later on.

3.2 Oman monthly power and water profile

Seasonal variation of the power and water demand is a feature of arid countries, since the summer is characterised by hot temperature, where the air-conditioning load is maximum and the winter is cold, where the electrical power consumption is low [8]. In both seasons, the water demand remains almost the same (Figure 3.1), thus the variation in power production should not affect the water production [7].

Statistically, power and water demand can be classified into three main categories based on the power variation, since the water demand is almost stable the whole year (Table 3.1).

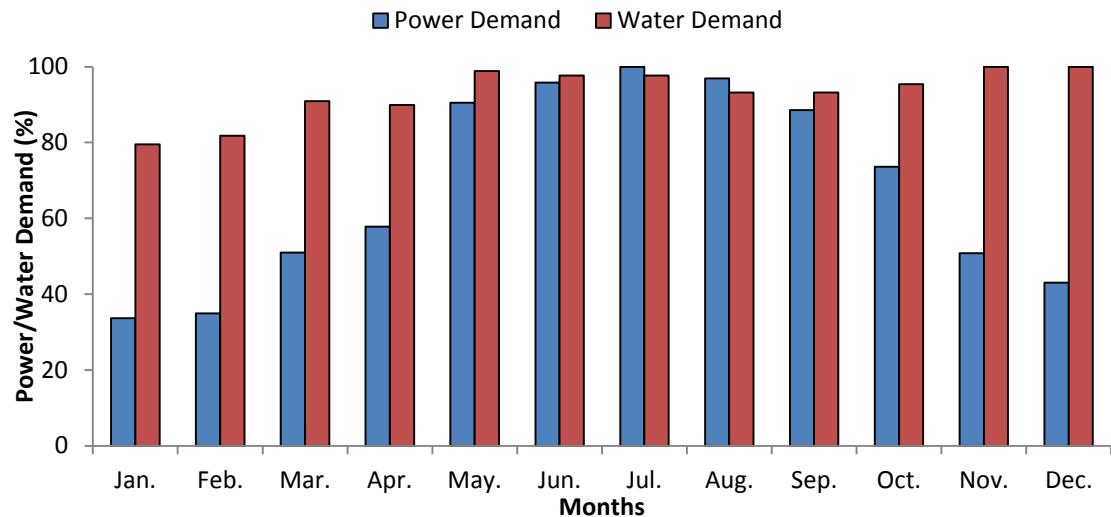


Figure 3.1: An example of arid countries annual power/water demand profile [8]

Number of Months	Avg. power demand (%)	Avg. water demand (%)	Months
3	35	90	December to February
5	90	97	May to September
4	60	92	March to April and November to October

Table 3.1: Summary of Oman water and power demand [8]

3.3 Meteorology Data Analysis

Graphical representation is used normally to analyse and interpret meteorological data. The proper analysis of meteorological factors, such as Dry Bulb Temperature (DBT), Average Relative Humidity (ARH), and Seawater Temperature (SWT) build an actual start point for engineering thermal system design, such as building load calculations, heating loads, ventilation, and air conditioning systems. Before assessing any design implications, it is important to specify summer and winter months [89]. A general approach is to select the four highest long-term monthly average DBTs as a summer period and the lowest three months for an average DBT as winter months [89]. However, it is important to mention that this approach depends on the climate zone.

3.3.1: Dry bulb temperature and relative humidity analysis

Meteorological data of the DBT and ARH were collected from Muscat (Capital of Oman) Meteorological Centre on a daily average basis. This city is classified meteorologically as in a humid-arid zone area. Figure 3.2 represents the daily mean DBT data distribution for the whole year. It can be seen from Figure 3.3 that May is the hottest month whereas December is the coldest. The highest, average, and lowest DBTs were 46.5°C, 29°C, and 14.1°C, respectively. Although, the lowest and the highest values can be identified, these values are not accepted to represent the outdoor design temperature.

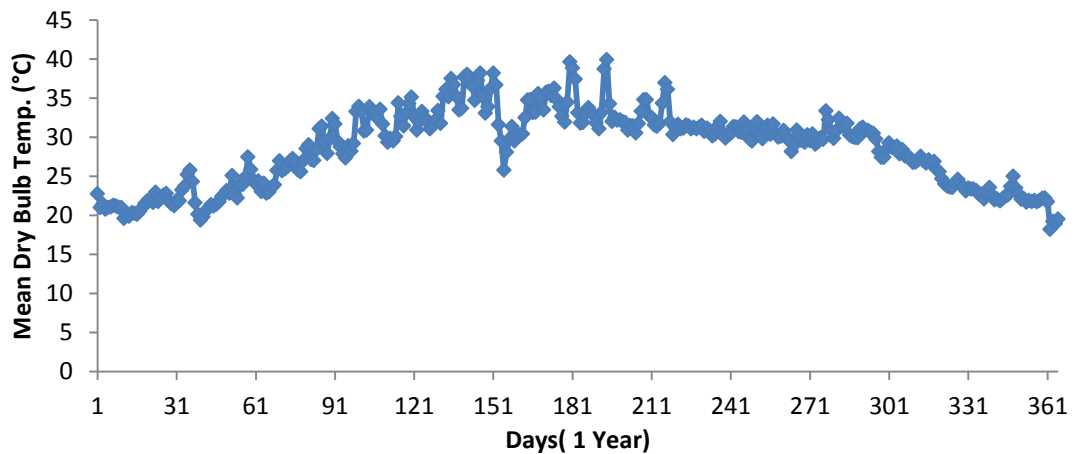


Figure 3.2: Daily average DBT distribution for Muscat city

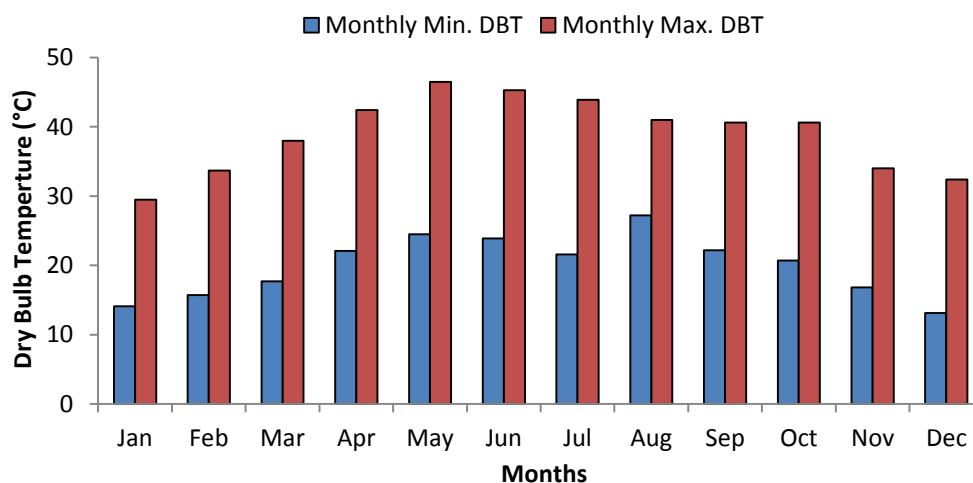


Figure 3.3: Monthly min/max DBT variation

During the design stage of a thermal system (such as an HVAC system and heat transfer plant equipment sizing), selection of the outdoor design temperature is necessary [140]. The outdoor design temperature is an indicator of the extreme conditions for thermal system load calculations. The ASHRAE handbook [89] suggested five different cumulative levels at which design outdoor temperatures are specified: 0.4%, 1%, 2%, 99%, and 99.6%. In thermal design conditions, the usual practice is the selection of 1% and 99% of cumulative frequency for summer cooling and winter heating, respectively. Figure 3.4 shows the accumulative frequency of a full year's meteorological data. Therefore, the corresponding outdoor design temperatures corresponding to 1% and 99% cumulative frequency are 18.5°C and 37.5°C.

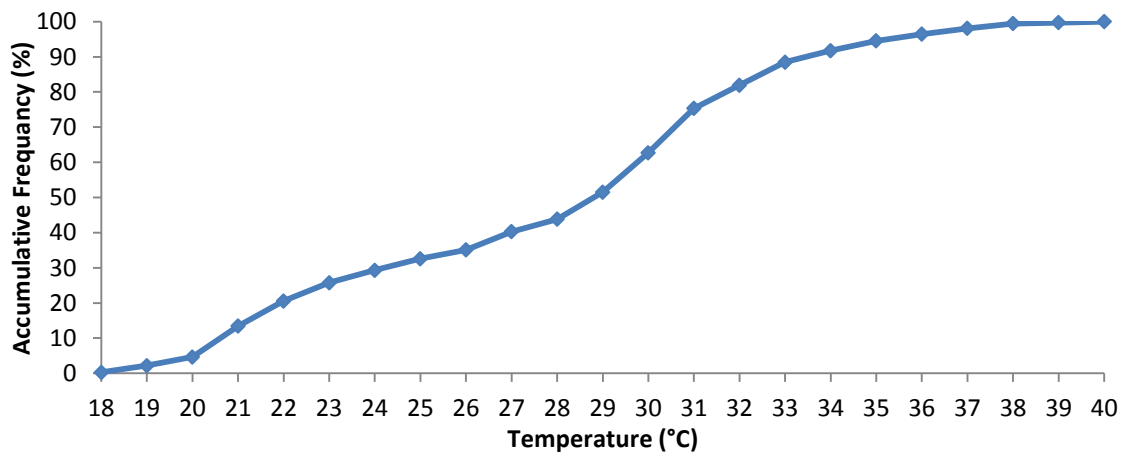


Figure 3.4: Cumulative frequency distribution of DBT

The daily average ARH for Muscat city for the year 2010 year is shown in Figure 3.5. The highest and lowest ARH in this year were 98% and 7%, respectively. The ARH for most of the year has a similar characteristic: high humidity at night and dry during the day time (Figure 3.6). Appendix 3-A shows daily ARH of hourly measurements.

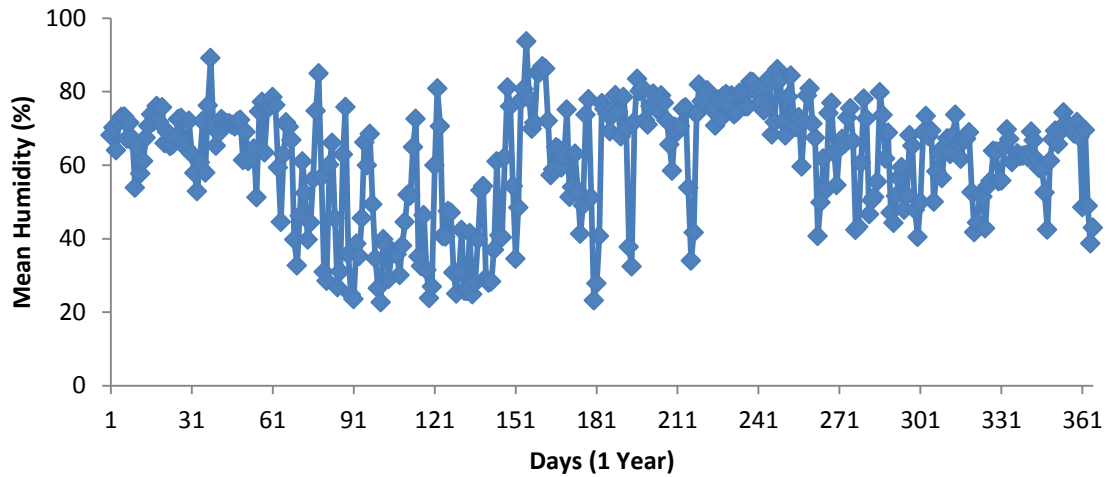


Figure 3.5: Daily average ARH distribution for Muscat city

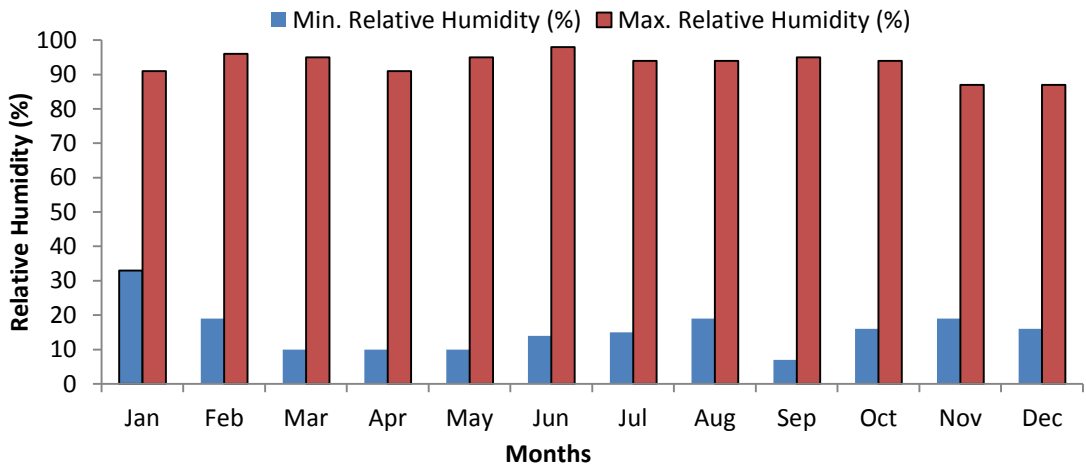


Figure 3.6: Monthly min/max ARH variation

3.3.2 Seawater temperature (SWT) analysis

SWT is an important factor for plant sensitivity analysis and design improvement since seawater, as was mentioned before, is used in this plant as MSF distiller feed and for equipment cooling. In addition, SWT affects the performance of MSF desalination significantly [105, 141]. Figure 3.7 shows the annual variation of the average SWT for Oman. Appendix 3-A shows daily SWT of hourly measurements.

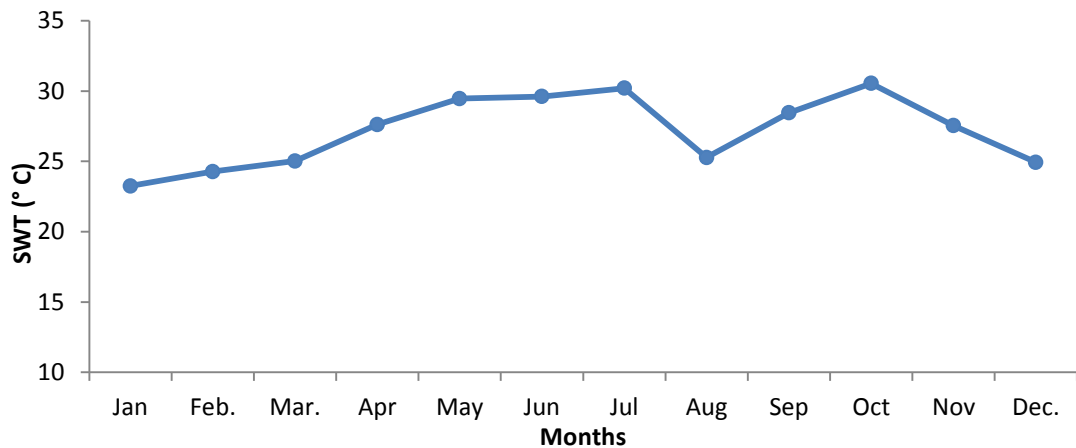


Figure 3.7: Annual average variation of SWT

It was observed that the maximum SWT recorded is for May and June months at 33°C and the minimum was measured at January at 22°C, with the annual average SWT as 27.2°C. Figure 3.8 describes monthly minimum and maximum recorded SWT.

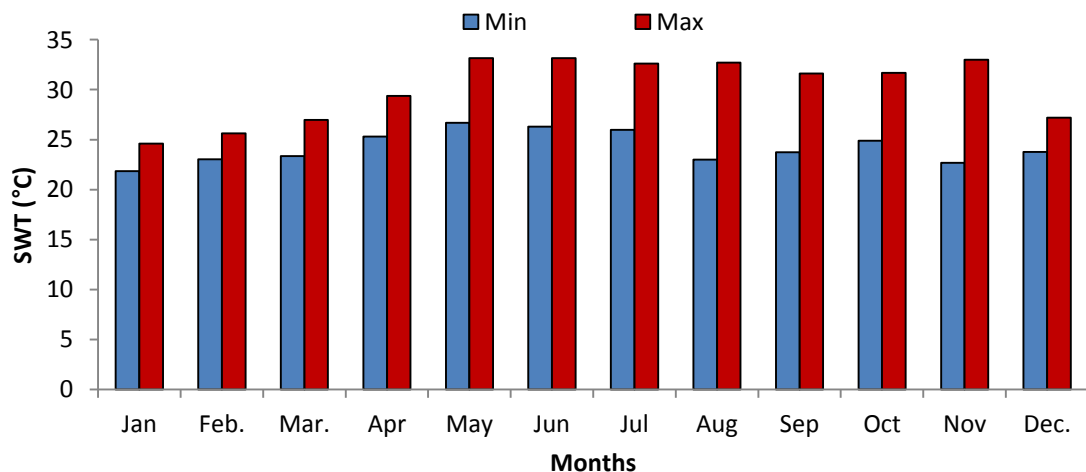


Figure 3.8: Monthly minimum/maximum recorded SWT

3.4 Power and MSF desalination cogeneration plant description

The cogeneration plant studied is located in Barka, a city adjacent to Muscat, the capital of Oman. This cogeneration plant was constructed in 2001 and commissioned successfully in 2003. It is designed to provide 536 MW electrical power through two GTs and one steam turbine and 3800 m³/h drinking water at ISO conditions from three identical MSF distillers. The cooling water and distiller feed water is seawater extracted by four parallel pipelines [15].

3.4.1 Power plant description

Figure 2.13 is a schematic for the power and MSF desalination plant studied. It has a gross power production of 536 MW from two GTs, each of them producing 158 MW and one steam turbine generating 220 MW at ISO conditions. Part of the steam produced from the power plant is used to produce 3800 m³/h of potable water through three MSF distillers. Natural gas is the normal fuel for this plant. After producing electrical power from the GT, the GT exhaust is directed to the HRSG, which produces HP steam (50 to 86 bar) for the HP turbine (HPT) to produce further electrical power. As the steam then moves to the LP turbine (LPT) (2 to 1.5 bar), the major part of this steam is extracted to the MSF distiller. The pressure of the MSF desalination steam is maintained through a steam turbine crossover valve, which dumps excess LP steam to the LP turbine. MSF LP steam is used to heat the seawater in the MSF brine heater it then returns it back to the power plant deaerator after mixing with condensate from the LP steam turbine condenser. Seawater is used as a cooling medium for the steam turbine condenser and other cycle auxiliaries. Furthermore, to maintain water production in case of lower power demand when the GT load is reduced, causing less production of steam from the HRSG, SF is started for both boilers to increase steam production to the desalination units through the steam turbine. Table 3.2 shows the design characteristics of the main components of the plant studied.

Unit	Quantity	Characteristics				
		parameter	unit	value		
GT	2	Model	–	V94.2		
		Fuel	–	Natural gas		
		Fuel Lower heat value	kJ/kg	50056		
		Generator power output	MW	158.9		
		Fuel mass flow	kg/s	9.2		
		Inlet air mass flow	kg/s	510		
		Turbine exhaust flow	kg/s	519.2		
		Turbine exhaust temperature	°C	519.2		
		GT system overall efficiency	%	34.47		
		Generator efficiency	%	98.44		
		Above specifications were at ISO condition [138]				
		HRSG	2	Model	–	Vertical tubes
Fuel	–			GT exhaust and supplementary firing		
Steam production without firing	t/h			248		
Steam production with firing	t/h			436		
Maximum/minimum operating pressure	bar			50/86		
Above characteristics at 50°C & 100% RH for HRSG and ST						
ST	1			Model	–	Double cylinder
		Maximum power production	MW	220		
		Mechanical efficiency	%	87		
		HP turbine outlet pressure	bar	80		
		LP turbine maximum/minimum flow	t/h	392/50		
		Condenser pressure	bar A	0.1		

Table 3.2: Plant main equipment characteristics [15]

3.4.2 MSF desalination process description

The main seawater pump supplies cleaned and hypochlorite disinfected seawater to heat rejection stages 19, 18, and 17 (Figure 3.3). Most of the seawater supplied will be rejected again to the sea, while part will pass to the deaerator as makeup. Inside the deaerator, oxygen is removed from the seawater to avoid corrosion of the tubes of the heat recovery stages 1 to 16 (Figure 3.9). Recycled brine (the sea water accumulated in the deaerator or last stage 19) flows in the tube side of the heat recovery section, where the flashed brine at the condenser of each stage gradually heats it. After exiting from stage 1, the brine is heated finally to its terminal temperature by the heating steam in the brine heater. It then returns to stage 1 of the evaporator where the initial flash evaporation occurs. As the brine would be still hot enough to boil again at slightly lower pressure, the flashing process is then repeated as it passes through a series of interconnected stage chambers 1–19. Flashed vapour is condensed by cooling brine in the tubes, and then this condensed distillate is removed from each stage to a common distillate channel, which is pumped finally by the distillate pump. Table 3.3 gives specifications of the MSF unit studied.

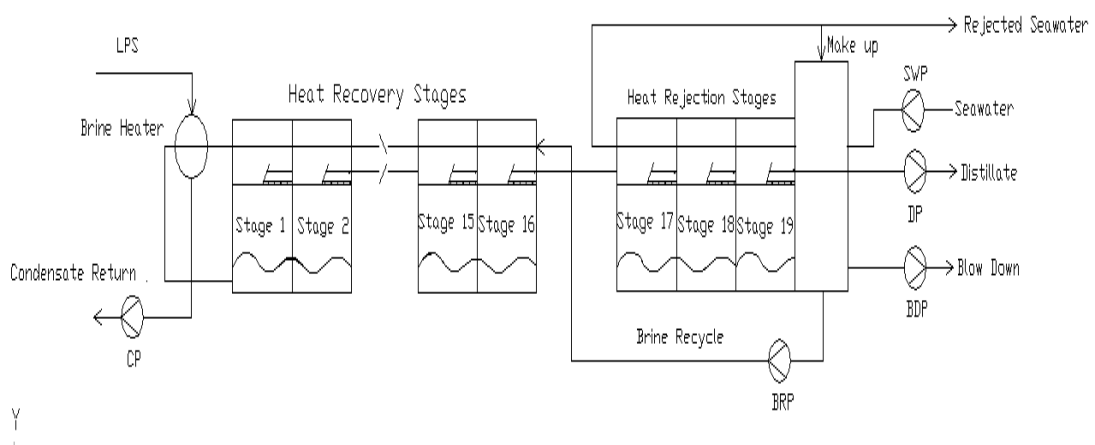


Figure 3.9: Schematic drawing of studied MSF desalination unit

Parameter	Unit	Value
Type of MSF	–	MSF, Recirculating type
Number of units	–	3 identical
Number of stages	–	19 stages (16 heat recovery and 3 heat rejection).
Capacity	m ³ /h	1270
Seawater feed flow	m ³ /h	10555
Seawater salinity	ppm	40000
Seawater operating range (maximum/minimum)	°C	35/24
Average steam consumption	kg/s	45.41
Brine recirculating flow	kg/s	3588
Vacuum system	–	Steam ejectors type
Unit entire pressure stage 1/stage 19	barG	0/- 0.96
Heat transfer in brine heater	MW	101.5

Table 3.3: Studied MSF unit specifications [15]

3.5 Plant operation scenarios analysis

Before modelling this plant, it is important to assess its typical standard operating regimes. The plant has a strong data history system, recording all instrumentation measurements every second. The operation and maintenance staff have been used continuously to evaluate plant performance or perform root cause analyses for certain failures. Actual data were recalled from the plant history every hour over a year. Around 4400 filtered readings were obtained after excluding plant shutdowns, plant trips, and instrumentation malfunctioning. The cogeneration plant net electrical power generation and water production are shown in Figure 3.10.

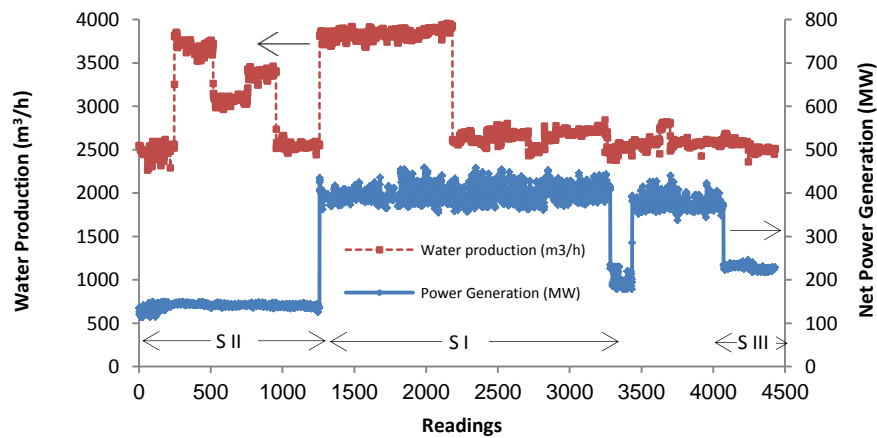


Figure 3.10: Cogeneration plant electrical power and water production profile

After statistical analysis of the filtered data, typical plant operational scenarios can be classified into three main scenarios as presented in Figure 3.11 according to the equipment necessary during power and water production.

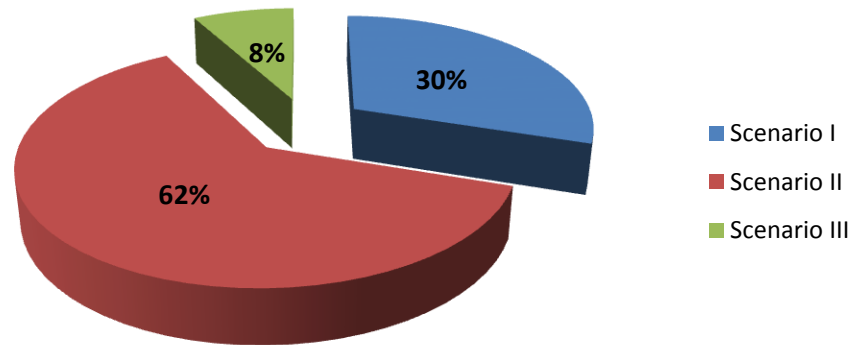


Figure 3.11: Typical Plant operating scenarios as percentage of normal operational time

Scenario I: 2 GT+ 2 HRSG+ 1 ST+ MSF

Scenario II: 1 GT+ 1 HRSG+ MSF

Scenario III: 1 GT+ 1 HRSG+ 1 ST+ MSF

Scenario I (Figure 3.11) is in operation for power and water production 62% of the year, and is as shown in Figure 2.13. Scenario I is a typical operating scenario of cogeneration plant in arid zone countries where the ambient temperature in summer reaches a maximum of 46°C and does not reduce below 27°C. Scenario II represents the winter season, where the requirement for power is less but the demand for water remains almost the same. Scenario III represents the transition period from summer to winter, where power demand starts reducing while maintaining the supply of water. In spite of the changes in power generation in these different seasonal scenarios, the average water production was around 3008 t/h on average over the year.

Figure 3.12 and 3.13 describe schematic drawings for scenarios II and III, respectively. At scenario II, the steam turbine is shut down (the lowest power demand) and LP steam for the MSF distillers is maintained using the HP/LP reduction station (reducing the HRSG high pressure to low pressure through control valve pressure control and change in pipe area) and an attemperator is used after that reduction station to adjust LP steam temperature.

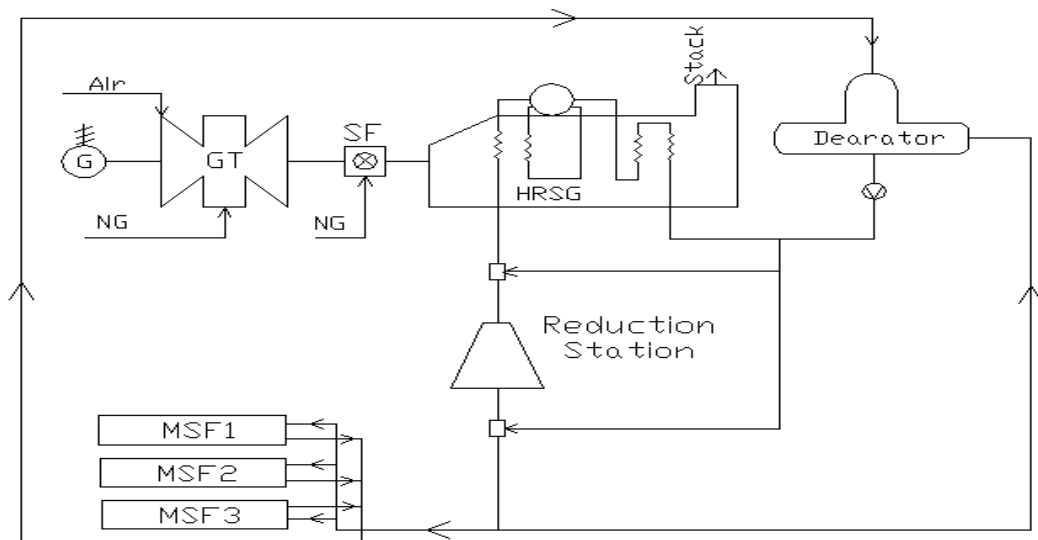


Figure 3.12: Schematic plant drawing for scenario II

For scenario III, a single GT and HRSG is kept at the rated design with maximum SF to maintain the steam requirements for the MSF distiller and steam turbine. The lower power production during this season allows time for plant equipment maintenance to meet the maximum demand for a hot summer season. Table 3.4 presents the studied plant operating characteristics for each typical scenario with maximum, minimum, and average values for the water production, power generation, ambient temperature, and relative humidity.

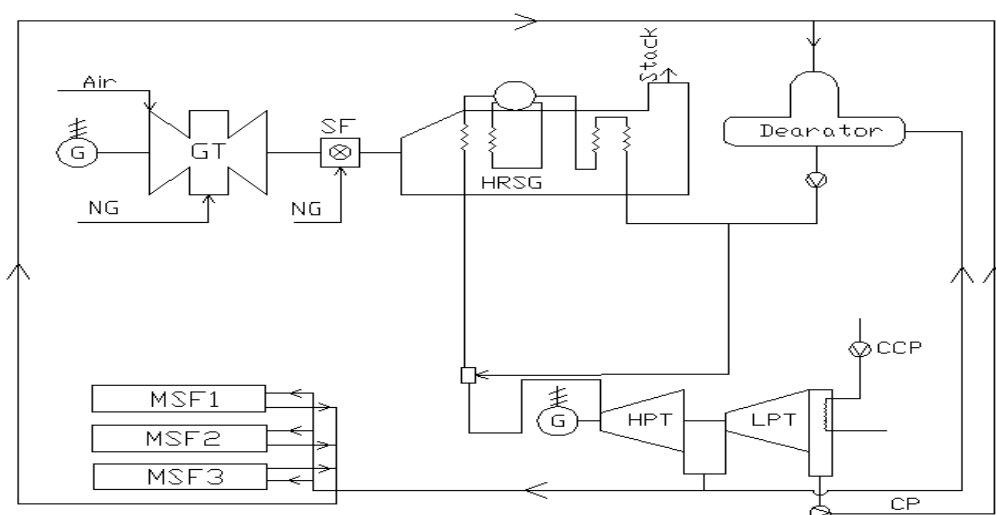


Figure 3.13: Schematic plant drawing for scenario III

Operating Scenario	Water Production (t/h)			Power Generation (MW)			Ambient Temperature (°C)			Humidity (%)		
	Max.	Min.	Avg.	Max.	Min.	Avg.	Max.	Min.	Avg.	Max.	Min.	Avg.
I	3800	2516	3066	436	357	398	46	27	33	100	7	59
II	3800	2266	3018	150	114	141	37	18	26	100	9	56
III	2688	2363	2548	247	217	228	34	21	27	91	24	59

Table 3.4: Plant annual operation scenarios

3.6 Closing Remarks

The purpose of the Chapter 3 has been to establish a basic data framework for the main research objectives in the following Chapters of this Thesis, so it is useful here to summarize what has been achieved.

Firstly, while it is important that subsequent performance modelling and analysis in chapters 5-6 is informed by the actual plant operational control methods, it is equally important that any plant operation scenarios modelled are informed by actual power and water demands satisfied by the plant. From the actual plant records for the power generation and water production it has been realised that typical operation can be characterised into only three seasonal normal operation scenarios, involving different configurations of the plant use. It will be necessary, therefore, to base further investigations on all these three scenarios:

Scenario I (summer): 2 GT+ 2 HRSG+1 ST+ MSF

Scenario II (winter): 1 GT+ 1 HRSG+ RS+ MSF

Scenario III (summer to winter transition): 1 GT+ 1 HRSG+1 ST+ MSF

Secondly, going beyond the basic issue of the plant thermodynamic performance, the intended economic (Chapter 11) and environmental (Section 4.2) evaluations required a typical annual plant profile of plant operation based on the actual operation to date. It has been shown that the three seasonal scenarios represent 62%, 30% and 8%, respectively, of the annual normal operation scheme.

Thirdly, all evaluations need to take into account the impact of natural climate variation on the key environmental (and uncontrollable) parameters: air temperature

(DBT) and humidity (ARH) plus seawater temperature (SWT). Based on analysis of the meteorological records a DBT of 29.0 °C, ARH of 60% and average SWT of 27.2 °C are used during simulations in this study.

Chapter 4

Methodology

As the cogeneration plant operational description was addressed in the previous chapter, the study of thermal analysis methodology will be presented in this chapter. This analysis will cover energy (First Law of Thermodynamics) and exergy analysis (Second Law of Thermodynamics) of the systems and subsystems for the studied cogeneration plant at the different classified operational scenarios. Moreover, the AC, ORC, IHE, and SED that are the selected heat recovery technologies in this study will be analysed using the same method. Furthermore, the study will emphasise the benefits recovered from each enhancement technology on the reduction of CO₂ emissions. Input values for these analyses will be extracted from the validated IPSEpro models of these cycles.

4.1 Energy and exergy analysis

4.1.1 Cogeneration plant

In steady state, control volume systems, the modelled components in the studied cogeneration plant, mass balance can be expressed with multiple inlet (i) and outlet (e) as [38]:

$$\sum \dot{m}_i = \sum \dot{m}_e \quad (4 - 1)$$

During the steady state condition, the total energy of a control volume remains constant ($\Delta \dot{B}_{CV} = 0$). Therefore, the amount of energy (B) entering must be equal to the amount of energy leaving and that can be obtained by:

$$\dot{B}_{in} = \dot{B}_{out} \quad (4 - 2)$$

The energy can be transferred in the control volume system by the mass, work, and heat. Equation 4.2 can be rewritten as:

$$\dot{Q}_{in} + \dot{W}_{in} + \sum \dot{m}_i \left(h_i + \frac{v_i^2}{2} + gz_i \right) = \dot{Q}_{out} + \dot{W}_{out} + \sum \dot{m}_e \left(h_e + \frac{v_e^2}{2} + gz_e \right) \quad (4 - 3)$$

This study assumed the fluid experienced negligible change in its kinetic (steady state) and potential (same elevation) energies [46]. Therefore, Equation 4.3 can be reduced to:

$$\dot{Q}_{in} + \dot{W}_{in} + \sum \dot{H}_i = \dot{Q}_{out} + \dot{W}_{out} + \sum \dot{H}_e \quad (4 - 4)$$

The thermal efficiency (η_I) of the power plant overall and its components were calculated based on the latest ASME standards [142, 143]. The thermal efficiencies of the GT and steam turbine (ST) can be expressed as:

$$\eta_{I,GT}(\%) = \frac{\dot{W}_{net,GT}}{\dot{m}_{GT,fuel} \times LHV} \times 100 \quad (4 - 5)$$

$$\eta_{I,ST}(\%) = \frac{\dot{W}_{net,ST}}{\dot{m}_i (\dot{h}_e - \dot{h}_i)} \times 100 \quad (4 - 6)$$

Thermal efficiency of the HRSG can be evaluated as the division of HRSG output, which is HP steam, by the inputs, the fuel energy from the GT exhaust (e), and SF and can be expressed as following [142, 143]:

$$\eta_{I,HRSG}(\%) = \frac{\dot{m}_i (\dot{h}_e - \dot{h}_i)}{(\dot{m}_{GT,e} \times h_{GT,e}) + (\dot{m}_{SF,fuel} \times LHV)} \times 100 \quad (4 - 7)$$

The overall power plant thermal efficiency is obtained by:

$$\eta_{I,Overall}(\%) = \frac{\dot{W}_{net,ST} + \dot{W}_{net,GT} - \dot{W}_{PP}}{(\dot{m}_{GT,fuel} \times LHV) + (\dot{m}_{SF,fuel} \times LHV)} \times 100 \quad (4 - 8)$$

In case of the cogeneration plant (producing both power and potable water), the heat utilization factor (HUF) can be expressed by [58, 144]:

$$HUF(\%) = \frac{\dot{W}_{net,ST} + \dot{W}_{net,GT} + [\dot{m}_{LPS,BH} \times (h_i - h_e)_{BH}]_{MSF} - \dot{W}_{PP}}{(\dot{m}_{GT,fuel} \times LHV) + (\dot{m}_{SF,fuel} \times LHV)} \times 100 \quad (4 - 9)$$

The overall cogeneration plant heat rate (HR) is defined as a ratio of heat consumed from the fuel to the net power generation [142, 143], thus:

$$HR_{Overall} = \frac{3600}{\eta_{I,Overall}} \quad (4 - 10)$$

The closed system entropy balance when the system moves from state 1 to state 2 can be expressed as following [46]:

$$(S_2 - S_1) = T_0 \int_1^2 \left[\frac{\delta Q}{T} \right]_b - T_0 S_{gen} \quad (4 - 11)$$

where T_0 and S_{gen} are the surrounding temperature and entropy generation, respectively.

Combining both the First and Second Law of Thermodynamics results in [46]:

$$(U_2 - U_1) + (KE_2 - KE_1) + (PE_2 - PE_1) - T_0(S_2 - S_1) = \int_1^2 \delta Q - T_0 \int_1^2 \left[\frac{\delta Q}{T} \right]_b - W - T_0 S_{gen} \quad (4 - 12)$$

Rearranging, the closed system balance can be written as:

$$(E_2 - E_1) = \int_1^2 \left[1 - \frac{T_0}{T_b} \right] \delta Q - [W - p_0(V_2 - V_1)] - T_0 S_{gen} \quad (4 - 13)$$

Equation (4.13) can be reduced to:

$$\Delta E = E_q + E_w - E_D \quad (4 - 14)$$

where:

$\Delta E = (E_2 - E_1)$ is the exergy change of the control volume system it represents. Each E describes the maximum reversible work that can be obtained from the system.

$E_q = \int_1^2 \left[1 - \frac{T_0}{T_b} \right] \delta Q$ is the exergy transfer, which is associated with heat transfer of the energy by the heat and crossing system boundary. This term is represented by the symbol and diminishes in the adiabatic system exergy analysis.

$E_w = [W - p_0(V_2 - V_1)]$ is the net useful work and it can be interpreted as the exergy transfer with the transfer of energy by work.

$E_D = T_0 S_{gen}$ is the destruction of exergy due to the irreversibility within the system. It is also commonly referred to the availability destruction and known also as Gouy–Stodola theorem [38].

The exergy balance of the closed system can be expressed in the time rate of change of exergy form as [46]:

$$\frac{dE}{dt} = \int_1^2 \left[1 - \frac{T_0}{T_b} \right] \delta \dot{Q} - \left[\dot{W} - p_0 \frac{dV}{dt} \right] - \dot{E}_D \quad (4 - 15)$$

Like the mass, energy, and entropy, the exergy is an extensive property that can be transferred to and out of the system, since most of the engineering systems in the industry are considered as control volume systems. Equation (4.15) can be rearranged to describe the control volume:

$$\frac{dE_{cv}}{dt} = \sum_j \left[1 - \frac{T_0}{T_b} \right] \delta \dot{Q}_j - \left[\dot{W}_{cv} - p_0 \frac{dV}{dt} \right] + \sum_i \dot{m}_i e_i - \sum_e \dot{m}_e e_e - \dot{E}_D \quad (4 - 16)$$

At the steady state condition, the two terms $\frac{dE_{cv}}{dt}$ and $\frac{dV}{dt} = 0$, and the above equation is reduced to:

$$0 = \sum_j \left[1 - \frac{T_0}{T_b} \right] \delta \dot{Q}_j - \dot{W}_{cv} + \sum_i \dot{m}_i e_i - \sum_e \dot{m}_e e_e - \dot{E}_D \quad (4 - 17)$$

This can be expressed as:

$$0 = \sum_j \dot{E}_{q,j} - \dot{W}_{cv} + \sum_i \dot{E}_i - \sum_e \dot{E}_e - \dot{E}_D \quad (4 - 18)$$

The total inlet exergy (E_i) and exit exergy (E_e) of any system or subsystem can be evaluated as a sum of physical exergy E_{PH} , chemical exergy E_{CH} , potential exergy E_{PO} , and kinetic exergy E_{KE} in the absence of the magnetic, electrical, and nuclear exergies.

Thus,

$$\dot{E} = \dot{E}_{PH} + \dot{E}_{CH} + \dot{E}_{PO} + \dot{E}_{KE} \quad (4 - 19)$$

\dot{E}_{PH} : Represents the total physical exergy rate of moving the stream from its state to the dead state, and it is the same term that was derived previously. The specific physical exergy for the (i) stream can be written as:

$$e_{ph} = (h_i - h_0) - T_0(s_i - s_0) \quad (4 - 20)$$

where T_0, h_0, s_0 are dead states: temperature, enthalpy, and entropy, respectively.

\dot{E}_{PO} : Expresses the total potential exergy rate due to the elevation change of the stream from the environment elevation, and most literature ignores this term by assuming the environment and the stream are at the same elevation [46–50].

\dot{E}_{KE} : Total kinetic exergy rate, which is a measure of a velocity difference between the stream inlet and outlet. It diminishes in most exergy publications by assuming no velocity gradient in the process [46–50].

\dot{E}_{CH} : Total stream chemical exergy rate due to the variation of the composition from the stream state to the dead state. The specific chemical exergy of the stream can be obtained by:

$$e_{ch} = \sum x_k e_{k,ch0} + RT_0 \sum x_k \ln \gamma x_k \quad (4 - 21)$$

where x_k stands for the components concentration, $e_{k,ch0}$ is standard chemical exergy of component k , and γ is component chemical potential coefficient that is equal to one for the ideal mixture [40]. It is necessary to emphasise that this term could vanish if no change in the fluid composition occurs [50–51].

The exergy efficiency can be defined as a ratio of the net work output to the fuel exergy to thermal system:

$$\eta_{II} = \frac{W_{net,out}}{\dot{E}_{in}} \quad (4 - 22)$$

In the case of the cogeneration system, where useful heat beside the net work can be used in other process, exergy efficiency is obtained by [46]:

$$\eta_{II} = \frac{W_{net,out} + \dot{E}_{useful}}{\dot{E}_{in}} \quad (4 - 23)$$

Exergy destruction rate can be evaluated by two ways, either with respect to the total input exergy of the fuel y_D or with respect to total exergy rate y_D^* , as can be seen from (4.23) and (4.24).

$$y_D = \frac{\dot{E}_D}{\dot{E}_{fuel,tot}} \quad (4 - 24)$$

$$y_D^* = \frac{\dot{E}_D}{\dot{E}_{D,tot}} \quad (4 - 25)$$

4.1.2 Desalination

For MSF desalination, the performance indicators are the gain out ratio (GOR) and the concentration ratio (CR). The GOR is defined as the amount of distillate produced per the amount of the pressure steam consumed [58, 85].

$$GOR = \frac{\dot{m}_{distillate}}{\dot{m}_{steam}} \quad (4 - 26)$$

The CR is expressed as a ratio of blow down salts concentration (C_{BD}) and feed seawater salts concentration (C_{FS}).

$$CR = \frac{C_{BD}}{C_{FS}} \quad (4 - 27)$$

The exergy analysis of the MSF desalination unit will be performed based on the latest thermodynamics properties of the seawater, which are obtained experimentally

[74, 75]. This method includes the chemical exergy of the seawater as a real mixture, not as an ideal mixture as was addressed in literature review in Chapter 2.

Equation (4.20) is used to calculate the physical exergy of the seawater stream. For the water and seawater, the enthalpy of seawater is obtained by [74, 75]:

$$h_{sw} = h_w - w_s [b_1 + b_2 w_s + b_3 w_s^2 + b_4 w_s^3 + b_5 T + b_6 T^2 + b_7 T^3 + b_8 w_s T + b_9 w_s^2 T + b_{10} w_s T^2] \quad (4 - 28)$$

where the water enthalpy is [74, 75]:

$$h_w = 141.355 + 4202.070 \times T - 0.535 \times T^2 + 0.004 \times T^3 \quad (4 - 29)$$

The effect of the stream pressure on the enthalpy of the stream is then added:

$$h_{sw}(T, p, w_s) = h_{sw}(T, p_0, w_s) + v(p - p_0) \quad (4 - 30)$$

The entropy of the seawater stream and pure water is given by:

$$s_{sw} = s_w - w_s [c_1 + c w_s + c_3 w_s^2 + c_4 w_s^3 + c_5 T + c_6 T^2 + c_7 T^3 + c_8 w_s T + c_9 w_s^2 T + c_{10} w_s T^2] \quad (4 - 31)$$

The pure water entropy is equal to:

$$s_w = 0.1543 + 15.383 \times T - 2.996 \times 10^{-2} \times T^2 + 8.193 \times 10^{-5} \times T^3 - 1.370 \times 10^{-7} \times T^4 \quad (4 - 32)$$

The chemical exergy of pure water and seawater stream is produced when the stream has a salt concentration different from the dead state concentration. The chemical exergy is obtained by [74]:

$$e_{ch} = \sum_{i=1}^n w_s (\mu_i^* - \mu_i^0) \quad (4 - 33)$$

where the μ_i^* and μ_i^0 are chemical potential of the (i) component at (T_0, p_0, w_s^*) and (T_0, p_0, w_{s0}) , respectively.

In case of seawater that consists of pure water and salt, the chemical potential can be obtained by the results from differentiating the Gibbs function as follows [74, 75]:

$$\mu_w = \frac{\partial G_{sw}}{\partial m_w} = g_{sw} - w_s \frac{\partial g_{sw}}{\partial w_s} \quad (4 - 34)$$

$$\mu_s = \frac{\partial G_{sw}}{\partial m_s} = g_{sw} + (1 - w_s) \frac{\partial g_{sw}}{\partial w_s} \quad (4 - 35)$$

where g_{sw} is the specific Gibbs function at T (°C) and can be obtained by [74, 75]:

$$g_{sw} = h_{sw} - (T + 273.15)s_{sw} \quad (4 - 36)$$

The differentiation of the Gibbs function is [74, 75]:

$$\frac{\partial g_{sw}}{\partial w_s} = \frac{\partial h_{sw}}{\partial w_s} - (T + 273.15) \frac{\partial s_{sw}}{\partial w_s} \quad (4 - 37)$$

The differentiation of the enthalpy and the entropy with respect to the salt concentration is obtained by using following correlation:

$$-\frac{\partial h_{sw}}{\partial w_s} = b_1 + 2b_2w_s + 3b_3w_s^2 + 4b_4w_s^3 + b_5T + b_6T^2 + b_7T^3 + 2b_8w_sT + 3b_9w_s^2T + 2b_{10}w_sT^2 \quad (4 - 38)$$

$$-\frac{\partial s_{sw}}{\partial w_s} = c_1 + 2c_2w_s + 3c_3w_s^2 + 4c_4w_s^3 + c_5T + c_6T^2 + c_7T^3 + 2c_8w_sT + 3c_9w_s^2T + 2c_{10}w_sT^2 \quad (4 - 39)$$

All the c and b constants are listed in Table 4.1.

$b_1 = -2.348 \times 10^4$	$b_6 = -4.417 \times 10^1$	$c_1 = -4.231 \times 10^2$	$c_6 = -1.443 \times 10^{-1}$
$b_2 = 3.152 \times 10^5$	$b_7 = 2.139 \times 10^{-1}$	$c_2 = 1.463 \times 10^4$	$c_7 = 5.879 \times 10^{-4}$
$b_3 = 2.803 \times 10^6$	$b_8 = -1.991 \times 10^4$	$c_3 = -9.880 \times 10^4$	$c_8 = -6.111 \times 10^1$
$b_4 = -1.446 \times 10^7$	$b_9 = 2.778 \times 10^4$	$c_4 = 3.095 \times 10^5$	$c_9 = 8.041 \times 10^1$
$b_5 = 7.826 \times 10^3$	$b_{10} = 9.728 \times 10^1$	$c_5 = 2.562 \times 10^1$	$c_{10} = 3.035 \times 10^{-1}$

Table 4.1: c and b constants for Gibbs function differentiation [74, 75]

The above correlations' working range does not cover heating the steam. Nevertheless, the heating steam enthalpy and entropy can be extracted from the steam table.

The MSF overall exergy efficiency is defined as the ratio of the minimum separation work W_{min} required to the total input exergy (E_{input}), which is the LP steam from the power plant.

$$\eta_{II,MSF} = \frac{W_{min}}{E_{input}} \quad (4 - 40)$$

Understating the internal construction of the MSF stage is an important factor that leads to calculate the stage exergy efficiency (stage process description was

explained in the previous chapter). This calculation is a pioneer in this field and has not been performed previously due to unavailability of the stream's inlet and outlet parameters. Consequently, Figure (4.1) shows the internal construction of the stage.

Thus, stage exergy efficiency is obtained by:

$$\eta_{II(stage)} = \frac{(E_{out}-E_{in})_{Cooling} + (E_{in}-E_{out})_{Distillate}}{(E_{in}-E_{out})_{Brine}} \quad (4 - 41)$$

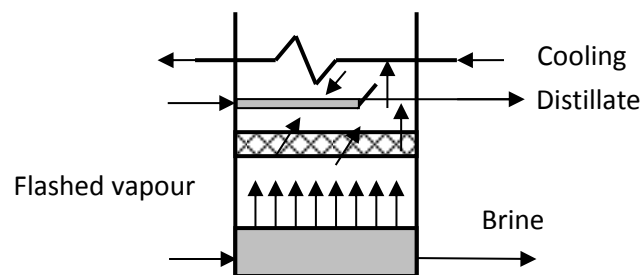


Figure 4.1: MSF stage construction

4.1.3 Heat Recovery

4.1.3.1 LiBr–H₂O Absorption chiller

The study will cover utilization of the waste heat from the MSF stages' distillate water to power a single effect LiBr–H₂O AC. This part of the chapter discusses the energy and exergy analysis of the AC. A schematic of such a cycle is shown in Figure 4.2, where the major cycle components are labelled and the streams are numbers for later state analysis.

At steady state, the net mass flow into each component is equal to zero and controlled by overall mass balance as per Equation 4.1 and component mass balance. In this cycle, there are two components: the refrigerant is water and the absorbent is LiBr–H₂O, so (*j*) components mass balance used to describe the process [92]:

For pure water component:

$$\sum_{j=1} (\dot{m}_j x_j)_i = \sum_{j=1} (\dot{m}_j x_j)_e \quad (4 - 42)$$

For LiBr components, the component balance can be written as:

$$\sum_{j=1} (\dot{m}_j(1 - x_j))_i = \sum_{j=1} (\dot{m}_j(1 - x_j))_e \quad (4 - 43)$$

Another mass flow parameter is important to describe the ratio of the strong solution flow to the refrigerant flow: the mass circulation ratio (f) and can be expressed as [104]:

$$f = \frac{\dot{m}_3}{\dot{m}_7} \quad (4 - 44)$$

The components' energy balance on each component is an important step to ensure the model output is correct and meaningful.

An energy balance of the evaporator can be written as:

$$\dot{Q}_E = \dot{m}_{10}h_{10} - \dot{m}_9h_9 \quad (4 - 45)$$

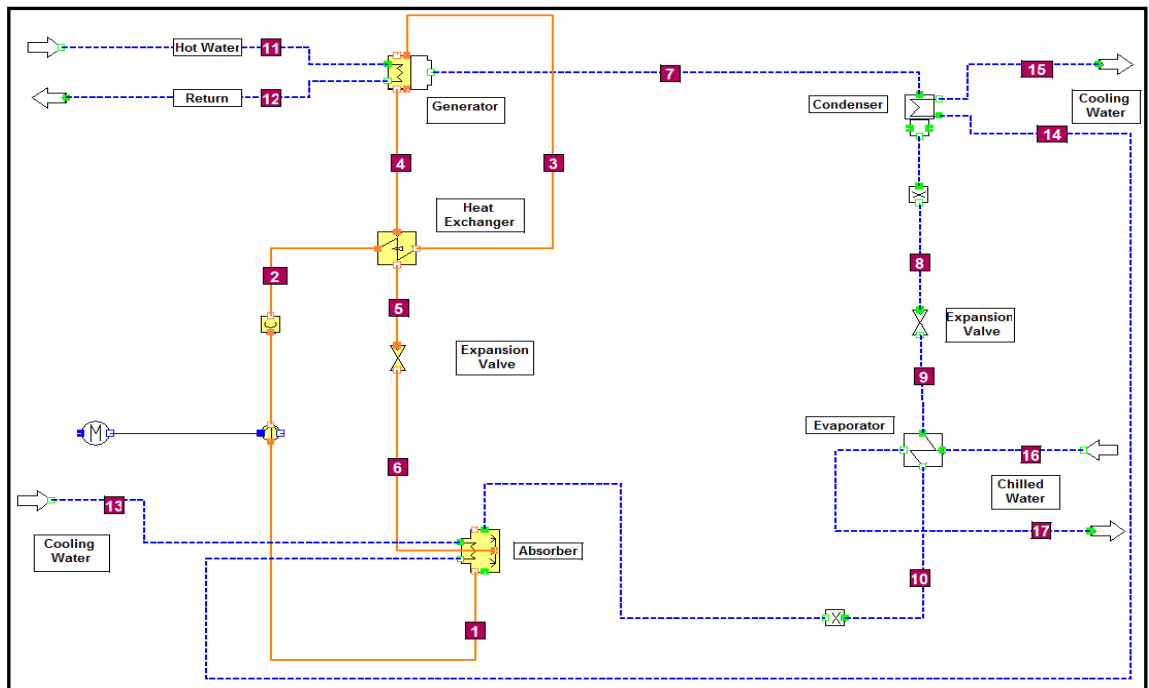


Figure 4.2: Schematic drawing of single effect LiBr-H₂O AC

Similarly for the condenser:

$$\dot{Q}_C = \dot{m}_7h_7 - \dot{m}_8h_8 \quad (4 - 46)$$

The generator energy balance can be obtained by:

$$\dot{Q}_G = \dot{m}_7h_7 + \dot{m}_4h_4 - \dot{m}_3h_3 \quad (4 - 47)$$

And similarly for the absorber:

$$\dot{Q}_A = \dot{m}_{10}h_{10} + \dot{m}_6h_6 - \dot{m}_1h_1 \quad (4 - 48)$$

An energy balance of the solution heat exchanger can be evaluated from the hot or cold side as it ends in same result:

$$\dot{Q}_{HX} = \dot{m}_4h_4 - \dot{m}_5h_5 = \dot{m}_3h_3 - \dot{m}_2h_2 \quad (4 - 50)$$

The solution pump work can be calculated by:

$$\dot{W}_{SP} = \dot{m}_2h_2 - \dot{m}_1h_1 \quad (4 - 51)$$

Water enthalpy and entropy can be extracted from the steam table, whereas the enthalpy and entropy of LiBr at different concentrations and temperatures (x, T) can be obtained as a result of an experimental correlation by Feuerecker et al [145].

$$h(T, x) = \sum_{n=0}^4 a_n x^n + T \sum_{n=0}^3 b_n x^n + T^2 \sum_{n=0}^2 c_n x^n + T^3 d_0 \quad (4 - 52)$$

The above correlation constants are listed in Table 4.2:

n	a_n	b_n	c_n	d_n
0	-945.8	-0.3293	7.4285E-3	-2.269E-6
1	47.7739E+1	4.076E-2	-1.5144E-4	
2	-1.59235	-1.36E-5	1.3555E-6	
3	2.09422E-2	-7.1366E-6		
4	-7.689E-5			

Table 4.2: Feuerecker equation for LiBr enthalpy estimation [145]

The LiBr solution entropy is calculated from the following equation, which is validated by Kaita [146] for: $40 \leq X$ (wt.%) ≤ 65 , and $0 \leq T$ (°C) ≤ 210 .

$$S = \sum_{i=0}^3 \sum_{j=0}^3 B_{ij} X^j T^i \quad (4 - 53)$$

Equation (4-53) constants are shown in Table 4.3.

i	B_{i0}	B_{i1}	B_{i2}	B_{i3}
0	5.127558E-01	-1.393954E-02	2.924145E-05	9.035697E-07
1	1.226780E-02	-9.156820E-05	1.820453E-08	-7.991806E-10
2	-1.364895E-05	1.068904E-07	-1.381109E-09	1.529784E-11
3	1.021501E-08	0	0	0

Table 4.3: Kaita correlation constants [146]

AC performance is measured by evaluating the COP, which refers to ratio of absorbed heat by evaporator to released heat by generator [92].

$$COP = \frac{\dot{Q}_E}{\dot{Q}_G} \quad (4 - 54)$$

The exergy of the LiBr solution can be calculated by the sum of the physical and chemical exergy since the potential and kinetic exergy has a negligible effect in rest. Physical exergy is obtained by using Equation (4-20), whereas the enthalpy and entropy are calculated as discussed in the previous part.

Equation (4-21) is used to determine the chemical exergy of the LiBr–H₂O solution at different concentrations. This term was either neglected in previous studies or it was assumed as ideal solution. However, in this study, the chemical exergy of the LiBr–H₂O as the sum in the ideal solution (standard chemical exergy) and the chemical exergy destruction is due to the dissolution of the LiBr and H₂O. Many researchers have calculated the standard chemical exergy of LiBr–H₂O at different concentrations [48,49,147]:

$$e_{H_2O/LiBr_0}^{ch} = \frac{1}{M} (y_{H_2O} e_{H_2O,0}^{ch} + y_{LiBr} e_{LiBr,0}^{ch}) \quad (4 - 55)$$

where M is molecular weight and (y) is the mole fraction. $e_{H_2O,0}^{ch}$, $e_{LiBr,0}^{ch}$ are the standard chemical exergy for water and LiBr and equal to 0.9 kJ/mol and 101.6 kJ/mol, respectively [48,49,147].

In Equation (4-21), the right hand side term is called the exergy destruction due to dissolution that can be reduced to:

$$RT_0 \sum x_k \ln \gamma x_k = RT_0 \sum x_k (a_{H_2O/LiBr}) \quad (4 - 56)$$

where $(a_{H_2O/LiBr})$ is called the LiBr–H₂O activity.

In molar fraction forms, the equation can be rearranged to:

$$e_{dis}^{ch} = \frac{RT_0}{M_{H_2O/LiBr}} (y_{H_2O} \ln(a_{H_2O}) + y_{LiBr} \ln(a_{LiBr})) \quad (4 - 57)$$

where is:

$$\ln(a_{H_2O}) = -\Phi \cdot v \cdot m \cdot M_{H_2O} \quad (4 - 58)$$

where Φ is expressed as the osmotic coefficient as derived by Kim and Infante Ferrira [107,148].

$$\Phi = 1 + \sum_{i=1}^6 a_i \cdot m^{i/2} + \frac{p}{2 \cdot v} \sum_{i=1}^2 i \cdot b_i \cdot m^{i/2} \quad (4 - 59)$$

where a_i and b_i are obtained from:

$$a_i = \sum_{j=0}^2 a_{ij} \cdot T^{-j} \quad (4 - 60)$$

$$b_i = \sum_{j=0}^2 b_{ij} \cdot T^{-j} \quad (4 - 61)$$

a_{ij} and b_{ij} are listed in Table 4-4.

	$j = 0$	$j = 1$	$j = 2$
a_{1j}	-2.196316×10^1	4.937232×10^3	-6.5548406×10^5
a_{2j}	-3.810475×10^3	2.611535×10^6	-3.669991×10^8
a_{3j}	1.228085×10^5	-7.718792×10^7	1.039856×10^{10}
a_{4j}	-1.41674×10^6	9.195285×10^8	-1.189450×10^{11}
a_{5j}	7.765821×10^6	-4.937567×10^9	6.317555×10^{11}
a_{6j}	-1.511892×10^7	9.839974×10^9	-1.27379×10^{12}
b_{0j}	-4.417865×10^{-5}	3.114900×10^{-2}	-4.36112260
b_{1j}	3.07410×10^{-4}	-1.86321×10^{-1}	2.738714×10^1
b_{2j}	-4.080794×10^{-4}	2.160810×10^{-1}	-2.5175971×10^1

Table 4.4: Constant for osmotic coefficient estimation [107,148]

m is the molality, which is defined as the number of moles of solute per kilogram of solvent and is calculated from:

$$m = \frac{x_{LiBr}}{(1 - x_{LiBr}) \cdot M_{LiBr}} \quad (4 - 62)$$

The chemical activity for the LiBr compound can be obtained by:

$$\ln(a_{LiBr}) = -v \cdot \left[\ln(m) + \sum_{i=1}^6 \frac{(i+2)}{i} \cdot \left(a_i + i \cdot \frac{p \cdot b_i}{2 \cdot v} \right) \cdot (m)^{i/2} \right]_m^{m_{sat}} \quad (4- 63)$$

4.1.3.2 Organic Rankine Cycle (ORC)

As was mentioned in Chapter 2, the ORC is similar to the steam turbine cycle except the working fluids in the ORC are the refrigerants. Figure 4.3 shows a snap shot

from the ORC cycle in IPSEpro, where each number in the cycle represents the state of the stream.

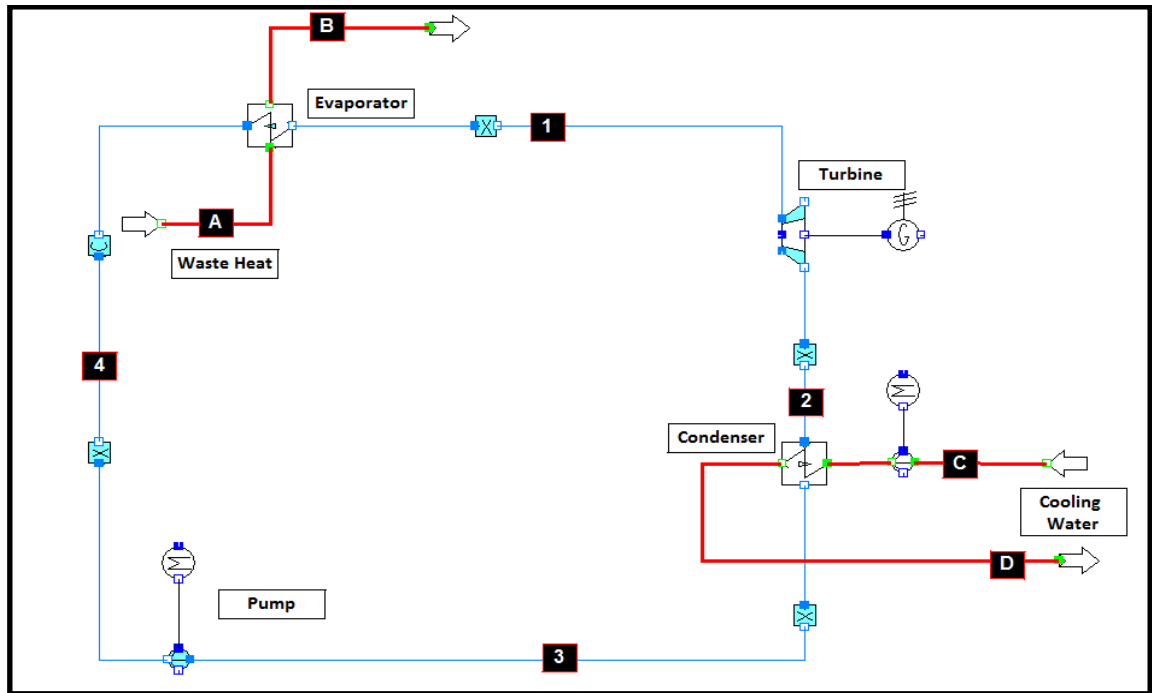


Figure 4.3: Snap shot from IPSEpro of the ORC cycle

The ORC turbine work (\dot{W}_{ORC}) resulting from the expansion process of the refrigerant mass is (\dot{m}_R) obtained by:

$$\dot{W}_{ORC} = \dot{m}_R \times (h_1 - h_2) \times \eta_s \times \eta_m \quad (4 - 64)$$

where η_s and η_m are isentropic and mechanical efficiencies of the ORC turbine, respectively.

Heat absorbed by the evaporator from hot distillate and heat rejected from the condenser to the seawater cooling are:

$$\dot{Q}_E = \dot{m}_R \times (h_1 - h_4) \quad (4 - 65)$$

$$\dot{Q}_C = \dot{m}_R \times (h_2 - h_3) \quad (4 - 66)$$

Work performed by the refrigerant circulated pump is:

$$\dot{W}_{PP} = \dot{m}_R \times (h_4 - h_3) \times \eta_m \quad (4 - 67)$$

Therefore, the net power production of the ORC can be estimated as subtraction of the power generated from the ORC turbine from power consumed by the refrigerant pump and the condenser cooling pump:

$$\dot{W}_{net} = \dot{W}_{ORC} - \dot{W}_{PP} - \dot{W}_{CP} \quad (4 - 68)$$

Thus, the ORC cycle efficiency is obtained by:

$$\eta_{ORC}(\%) = \frac{W_{net}}{Q_E} \times 100 \quad (4 - 69)$$

The exergy analysis of the ORC will be similar to the power plant in the cogeneration system that was explained before.

4.1.4 Heat exchangers

The cogeneration plant and heat recovery technologies consist of many of heat exchangers, such as boilers, condensers, evaporators, and brine heaters. Heat gained by the heat exchanger can be defined as a product of the overall heat transfer coefficient U , the heat exchanger area A , and the logarithmic mean temperature ΔT_{LM} :

$$Q_{absorbed \text{ or released}} = U * A * \Delta T_{LM} \quad (4 - 70)$$

IPSEpro adopted the same method using an iterative procedure to calculate the inlet and outlet stream properties to calculate a convergent solution for absorbed or released heat [149–151].

where:

$$\Delta T_{LM} = \frac{(T_{hot,in} - T_{cold,in}) - (T_{hot,out} - T_{cold,out})}{\ln \left[\frac{T_{hot,in} - T_{cold,out}}{T_{hot,out} - T_{cold,in}} \right]} \quad (4 - 71)$$

The Effectiveness and Number of Transfer Unit (ϵ -NTU) method is used to validate the modelled heat exchangers, consulted from [149–151], and was used throughout this study. It depends on the calculation of the heat exchanger effectiveness and the NTU, which are defined as:

Effectiveness (ϵ): the ratio of the actual heat transfer rate for a heat exchanger to the maximum possible heat transfer rate, can be defined as [149–151]:

$$\epsilon = \frac{\dot{Q}_{actual}}{\dot{Q}_{max}} \quad (4 - 72)$$

The actual heat transfer rate can be determined from the expression:

$$\dot{Q} = \epsilon * C_{min}(T_{hot,in} - T_{cold,in}) \quad (4 - 73)$$

For any heat exchanger [149–151]:

$$\varepsilon = f \left[NTU, \frac{C_{min}}{C_{max}} \right] \quad (4 - 74)$$

where:

C_{min}/C_{max} is known as the heat capacity ratio (C_r) and equal to C_{cold}/C_{hot} or C_{hot}/C_{cold} , depending on the relative magnitude of the hot and cold fluid heat capacity rates.

The NTU is a dimensionless parameter used widely for heat exchanger analysis [149–151] and is equal to:

$$NTU = \frac{UA}{C_{min}} \quad (4 - 75)$$

It is more convenient to work with ε -NTU relations of the form:

$$NTU = f \left[\varepsilon, \frac{C_{min}}{C_{max}} \right] \quad (4 - 76)$$

C_{min} equals smaller $(\dot{m}c_p)_{smaller}$, thus:

$$C_{min} = \frac{\dot{Q}_{actual}}{\Delta T_{larger}} \quad (6 - 77)$$

For the cross flow, when both fluids are unmixed, the effectiveness can be calculated from [94]:

$$\varepsilon = 1 - \exp \left[\left(\frac{1}{C_r} \right) (NTU)^{0.22} \{ \exp[-C_r (NTU)^{0.78}] - 1 \} \right] \quad (4 - 78)$$

For other heat exchangers, with all flow arrangements, such as evaporators and condensers, and when $C_r \approx 0$, the effectiveness and number of transfer units can be calculated from [94]:

$$\varepsilon = 1 - \exp(-NTU) \quad (4 - 79)$$

or

$$NTU = -\ln(1 - \varepsilon) \quad (4 - 80)$$

4.2 CO₂ Footprint estimation

Many researchers have evaluated the role of CO₂ in the global warming phenomena. Estimation of the CO₂ footprints from the current studied dual cogeneration plant is an important task since it is one of the evaluation criteria for the comparisons between the four different heat recovery technologies. In this study, CO₂ is calculated by two methods: the first one depends on energy calculation, and second one on exergy. The difference between these two methods was discussed in Chapter 2.

The CO₂ emissions' energy base for a natural gas fired cogeneration plant can be obtained by [105]:

$$CO_2 \text{ Emissions} \left(\frac{g}{kWh} \right)_{\text{energy base}} = \frac{3600 * \alpha * \dot{m}_{\text{Natural Gas}}}{(\dot{W}_{\text{net}} + \dot{Q}_{\text{useful}})} \quad (4 - 81)$$

where α is 3124 kg CO₂ per tonne of natural gas and \dot{Q}_{useful} is heat recovered from the process, which can be used as useful source for other thermal applications, such as powering AC, heating the ORC cycle, or domestic heating. It is necessary to mention \dot{Q}_{useful} cannot be converted completely to any type work (Second Law of Thermodynamics). Moreover, the conversion value will depend on the temperature of useful heat; the conversion is less at low temperatures.

The CO₂ emissions exergy base is:

$$CO_2 \text{ Emissions} \left(\frac{g}{kWh} \right)_{\text{exergy base}} = \frac{3600 * \alpha * \dot{m}_{\text{Natural Gas}}}{(\dot{W}_{\text{net}} + \dot{E}_{\text{useful}})} \quad (4 - 82)$$

where, \dot{E}_{useful} is the maximum useful exergy that can converted to real work, and it is measured logically by $\left(\frac{g}{kWh} \right)$, where the unit in the dominator represents real electrical power, which is not the case in the energy base calculation.

4.3 Simulation and economics

Computational modelling and simulation has become a key stone in many studies and in the design and testing of the equipment. The advantage of the modelling and simulation is that it saves time, is flexible, and various process scenarios can be performed [105]. The IPSEpro software was used in this study; it is a set of software

modules that can create, analyse, optimize, and even study the process from economic aspects. IPSEpro is highly flexible and comprehensive for modelling and analysing processes in engineering, chemical engineering, and many other related areas [152].

IPSEpro is characterised by its short calculation time, allowing you to change existing or even build components, which can then be integrated into the software. IPSEpro is COM-based software, and this increases its potential to interact with other software [152]. Moreover, it shows extreme flexibility in modelling the mass and heat balances and simulating the studied process. It has gained credit in the industry and with research companies, such as Rolls-Royce. IPSEpro simulated output results have been validated in many studies by comparison with actual process data and show good agreement [94, 105, 141]. In addition, the IPSEpro calculates the thermodynamics properties for any stream within the process, enabling the researcher to perform many related calculations, such as the energy and exergy analyses. On other hand, the disadvantage of the IPSEpro is it is not easy to find the exact error in the process modelling from error log file.

Process model creation in IPSEpro passes through two level: the first level in which the model is represented mathematically and graphically using the Model Development Kit (MDK). The IPSEpro calculation and results generation are performed by the second level, the process simulation environment (PSE) [105].

4.3.1 Model Development Kit (MDK)

SimTech built different libraries in the MDK that cover a wide range of different processes. In this study, libraries are used to develop models of the cogeneration plant at different operational scenarios and with heat recovery technologies: single stage LiBr–H₂O AC, the ORC, and the IHE.

4.3.1.1 Advanced power plant library

The advanced power plant library contains 49 units representing most of the equipment available in the power plant, for example turbine, compressor, boiler, and pump. Flexibility of the IPSEpro allows development of the equipment not available in the MDK library. The library provides the researcher the data base of the physical

and chemical properties of common liquids used in this process, such as water, steam, gas, and combustion [153]. In this study, this library is used to model the different scenarios for the power plant.

4.3.1.2 Desalination process library

The desalination library contains all necessary equipment that represents both types of desalination plant thermals and membranes. The desalination library covers different desalination technologies, such as MSF, MED, TVC, MVC, and RO. The library includes most of the equipment used in the desalination, such as heat exchanger, membranes, flashing stages, pumps, compressor, and ejectors. Moreover, the library includes the physical properties of most fluids in the desalination plants, for example, distillate water, seawater, and vapour [154]. However, this study focuses on MSF desalination only.

4.3.1.3 Refrigeration process library

The refrigeration process library is a component model library that enables its user to calculate the thermodynamic properties of more than 50 refrigerants. The library enables researchers and designers to model a number of advanced thermal compression processes and to evaluate environmental refrigerants. The library includes the physical properties database that covers a wide range of refrigerants and refrigerant mixtures for both compression and absorption [105]. This library is utilized to build and simulate the model of the single stage LiBr–H₂O AC and ORC cycle.

4.3.2 Process Simulation Environment (PSE)

The Process Simulation Environment (PSE) provides a series of MDK models to set up different process. The user selects the required components from the library menu and arranges them in a series form that represents realistic plant configuration. The user enters all process parameters directly to the system, and after executing, PSE generates output protocols automatically at the end of the simulation step.

The PSE uses an equation-oriented approach, and optimized mathematical methods guarantee fast and accurate calculations. To solve a system of equations, the PSE adopts a two-phase approach: analyzing and a numerical solution. In the analysis phase, the PSE first checks the model for errors in the process specifications; if the

specifications are correct, it determines the optimum solution method. In the numerical solution phase, the PSE solves the equations with the numerical methods; specifically, it uses the Newton–Raphson method for finding the iterative root solution [152]. This method is easy, rapidly convergent, and the best known method for finding good approximation to the value of x using the iterative equation. Figure 4.4 shows the Newton–Raphson method, whereas following equations are used to find the solution:

$$x_{n+1} = x_n - \frac{f(x)_n}{f'(x)_n} \quad (4 - 83)$$

where n is the number of the iteration, and $f'(x)$ is a derivative of the function.

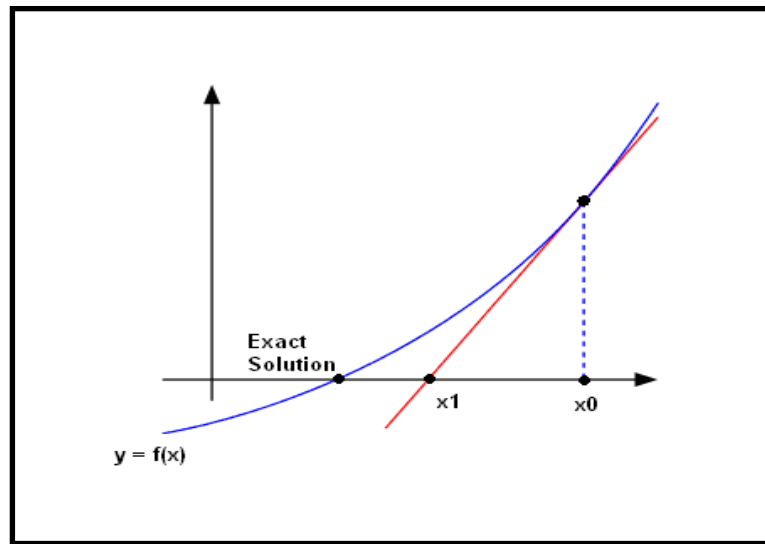


Figure 4.4: Newton–Raphson method root estimation

The PSE is a part of the IPSEpro software package used for economic evaluation of the engineering project [94]. This analysis is an important task to decide whether to accept the project implementation or to reject it. It enables the user to enter the project capital cost project investment, taxes, discount rate, revenues, and life of the project. It uses financial formulae to calculate a project’s detailed annual net present value, payback period, cost-benefit ratio, and average rate of return. Any change in project costs or revenues reflects on the results of project profitability analysis.

Chapter 5

Power plant modelling and simulation: validation and parametric study

5.1 Introduction

This Chapter discusses the IPSEpro modelling for the actual power plant operating scenarios that were analysed in Chapter 3. The models developed are validated against actual measured power plant data before their simulated results are utilized for detailed thermal evaluation using energy and exergy analyses (Chapter 4). The aims of these analyses are:

Firstly, to assess the impact of operational scenario change on both plant equipment efficiency and system overall performance indicators.

Secondly, to standardize combined power plant and MSF desalination thermal evaluation. Additionally, to use the exergy approach to locate the exergy destruction of all cycle components to realize the actual system thermal status and pinpoint the equipment which requires impact on this.

Finally, this chapter includes a parametric study of the influences of both the uncontrollable external factors (i.e., ambient temperature and relative humidity) and the controllable operational factors (i.e., SF flow, MSF load) on the power plant performance indicators and environmental impact.

5.2 Power plant modelling

The power plant operations were classified into three main scenarios in Chapter 3. The IPSEpro advanced power plant library was used to develop a separate model for each operating scenario. Figure 5.1 shows the IPSEpro model for scenario I, where all the equipment is in service, whereas the other two models are shown in Appendix 5-A. In IPSEpro, the model equipment is linked by connectors that represent the working fluids moving from one component to another. All streams are numbered and include the thermodynamic properties of the moving fluid. During the modelling phase, the equipment specifications listed in Chapter 3 are uploaded to the model, described as set values. Table 5.1 presents the composition and thermodynamic properties of all numbered streams, either “set” values (model inputs) by the user or “calculated” values (model outputs by the model). These values are used for the further energy and exergy analysis.

For validation, comparisons should take place between the same parameters as either inputs or outputs. As well as environmental parameters (ambient humidity, ambient

temperature, and ambient pressure), the input and output parameters of the IPSEpro model [155, 156] have been based on the real plant control room operator interfering with the actual plant. Consequently, the model input variables for the power plant are the same parameters that the control operator changes and the outputs were the results of the plant responding to these changes. For the power plant model, Table 5.2 describes the model inputs (extracted from the measured plant data) and the outputs (used for validation parameters between the measured data and model results).

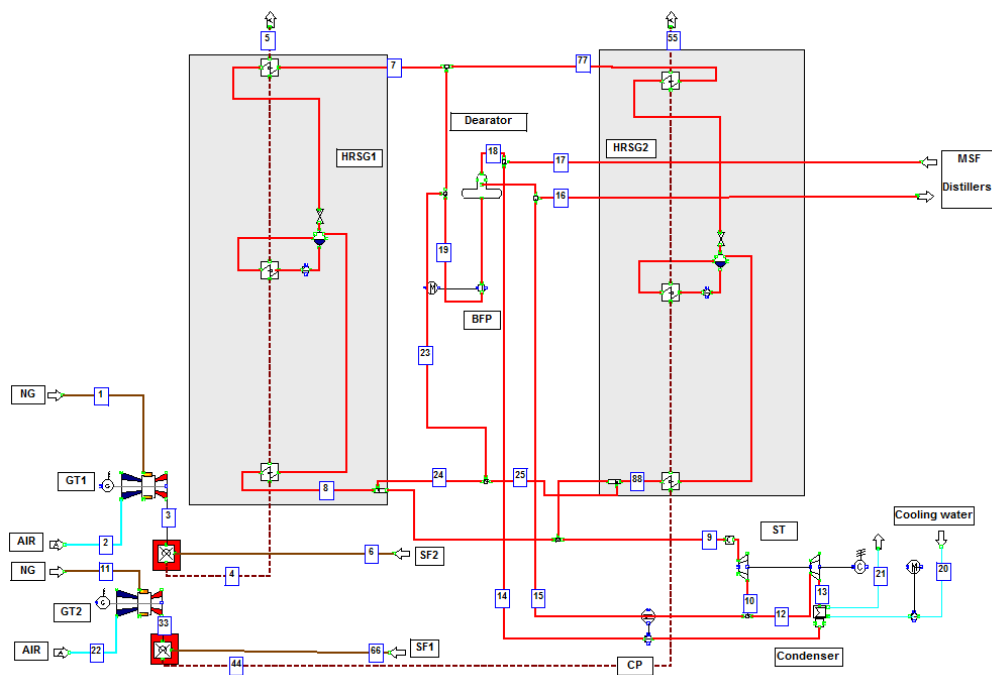


Figure 5.1: IPSEpro Power plant model at scenario I

5.3 Power plant model validation

To ensure representative comparisons for the three scenarios to reflect the model confidence level, the data are sorted based on the ambient temperature and relative humidity. Three data sets were selected from each 1°C range of the ambient temperature: minimum, median, and maximum. The total numbers of data sets used in this validation were 40, 48, and 32 readings for scenarios I, II, and III, respectively. Appendix 5-B presents the detailed comparisons between measured data and model results for the three scenarios.

The model confidence level was assessed by the calculation of relative difference between measured (X_i) and model (Y_j) data combined for each of the three scenarios [157]:

$$e = \sqrt{\frac{\sum(e_i)^2}{N}} \text{ where } e_i = \left[\frac{X_i - Y_i}{X_i} \right] \times 100 \text{ (\%)} \quad (5 - 1)$$

Figures 5.2–5.6 compare model results with the corresponding measured power plant data. For the power plant validation, the model gas flow for all three scenarios is predicted closely with differences in the range 1.1% to 1.5% (Figure 5.2). This is an expected result since all three scenarios use the same GT plant. These differences in gas flow probably represent the best that can be expected from such a comparison, taking into account the precision of the site measurement devices; the model assumption of constant lower heating value (in reality, there is a slight variation due to gas composition variations that affect gas flow at certain loads); and the model's inability to represent physical plant layout features that are not described in the model.

Stream No.	Composition	Flow	Temperature	Pressure	Entropy	Enthalpy	Specific volume
1, 11	Natural Gas	Cal	Set	Set	Cal	Cal	Cal
2, 22	Air	Cal	Set	Set	Cal	Cal	Cal
3, 33	GT exhaust	Cal	Cal	Cal	Cal	Cal	Cal
4, 44	GT exhaust after SF	Cal	Cal	Cal	Cal	Cal	Cal
5, 55	HRSG exhaust	Cal	Cal	Cal	Cal	Cal	Cal
6, 66	Natural Gas	Set	Set	Set	Cal	Cal	Cal
7, 77	Water	Cal	Cal	Cal	Cal	Cal	Cal
8, 88	HP steam	Cal	Set	Set	Cal	Cal	Cal
9	HP steam	Cal	Set	Set	Cal	Cal	Cal
10	LP steam	Cal	Cal	Set	Cal	Cal	Cal
12	LP steam	Cal	Cal	Cal	Cal	Cal	Cal
13	LP steam	Cal	Cal	Set	Cal	Cal	Cal
14	LP steam	Cal	Cal	Cal	Cal	Cal	Cal
15	LP steam	Cal	Cal	Cal	Cal	Cal	Cal
16	LP steam	Set	Cal	Cal	Cal	Cal	Cal
17	Condensate	Set	Set	Set	Cal	Cal	Cal
18	Condensate	Cal	Cal	Cal	Cal	Cal	Cal
19	Water	Cal	Cal	Cal	Cal	Cal	Cal
20	Water	Cal	Set	Set	Cal	Cal	Cal
21	Water	Cal	Set	Cal	Cal	Cal	Cal
23	Water	Cal	Cal	Cal	Cal	Cal	Cal
24	Water	Cal	Cal	Cal	Cal	Cal	Cal
25	Water	Cal	Cal	Cal	Cal	Cal	Cal

Table 5.1: Set/Calculated values in power plant model

Model inputs		Model outputs	
Ambient temperature	°C	GT gas flow	kg/s
GT load	MW	HRSG steam flow	t/h
SF gas flow	kg/s	ST load	MW
Steam pressure	bar	Condensate flow	kg/s
Steam temperature	°C	MSF unit load	kg/s

Table 5.2: Power plant input/output parameters

The differences in HRSG steam flow measurements (Figure 5.3) could be the result of measured data measurement uncertainty (from measurement device precision and location, etc.), model error, or both. The model HRSG flow could be affected by other related model parameters (such as steam pressure, steam temperature, or even calculated GT exhaust mass flow rate and exhaust temperature), as well as external (unmodelled) factors, such as flange leakage. One of the HRSG flows reads higher than the other by almost 15–20 t/h, when both of them are, in principle, identical and at the same operating conditions. This difference was observed only at low ambient temperature and the difference starts reducing with increase in ambient temperature.

The steam turbine load validation took place only for two scenarios (Figure 5.4), since this is the shut down for scenario II. Measurement device uncertainty is not likely to be significant for the steam turbine load because these are payment dependent devices and have to be checked and certified for billing purposes. The differences between model results and measured data are 1.4% for scenario I and 3.7% for scenario III. The trend of the model data suggests that the higher scenario III steam turbine load difference may be due to the assumption of constant mechanical efficiency in the model because the differences are almost the same for all comparisons.

Understanding the plant operation is important in analysing the patterns for MSF flow and ST condensate flow (Figures 5.5–5.6). Reduction of the MSF flow results in steam passing to the LP turbine and increasing the ST condensate. This relationship can be observed by noticing the improvement for the scenario II validation where there is no condensate flow.

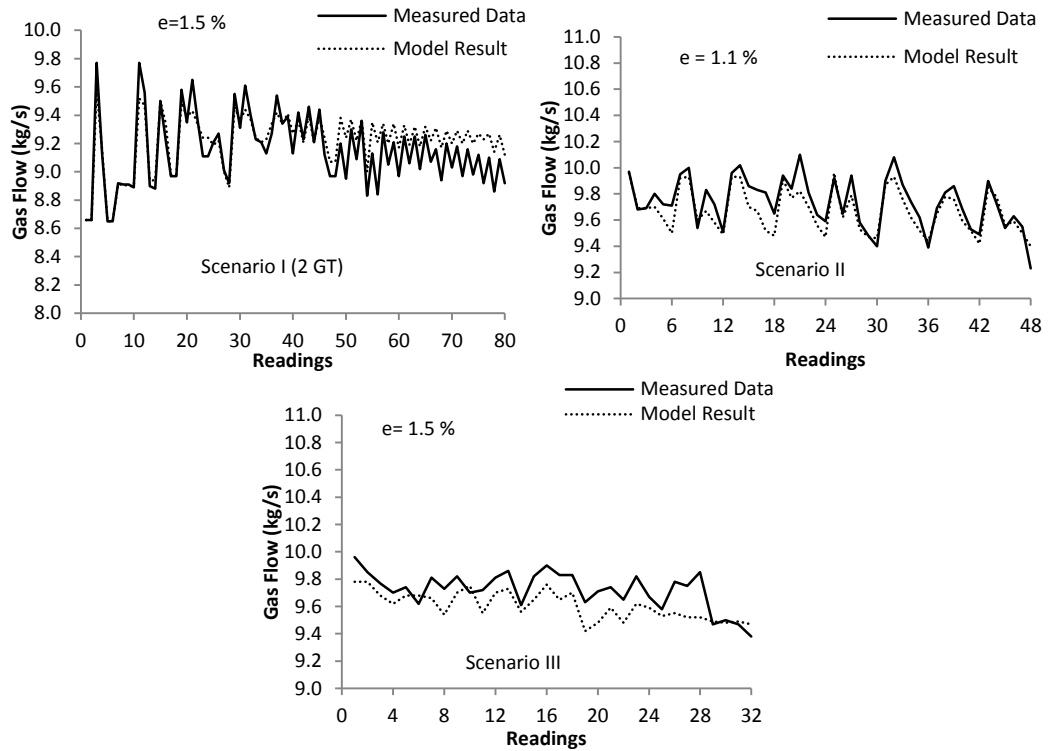


Figure 5.2: Power plant validation: gas flow (kg/s)

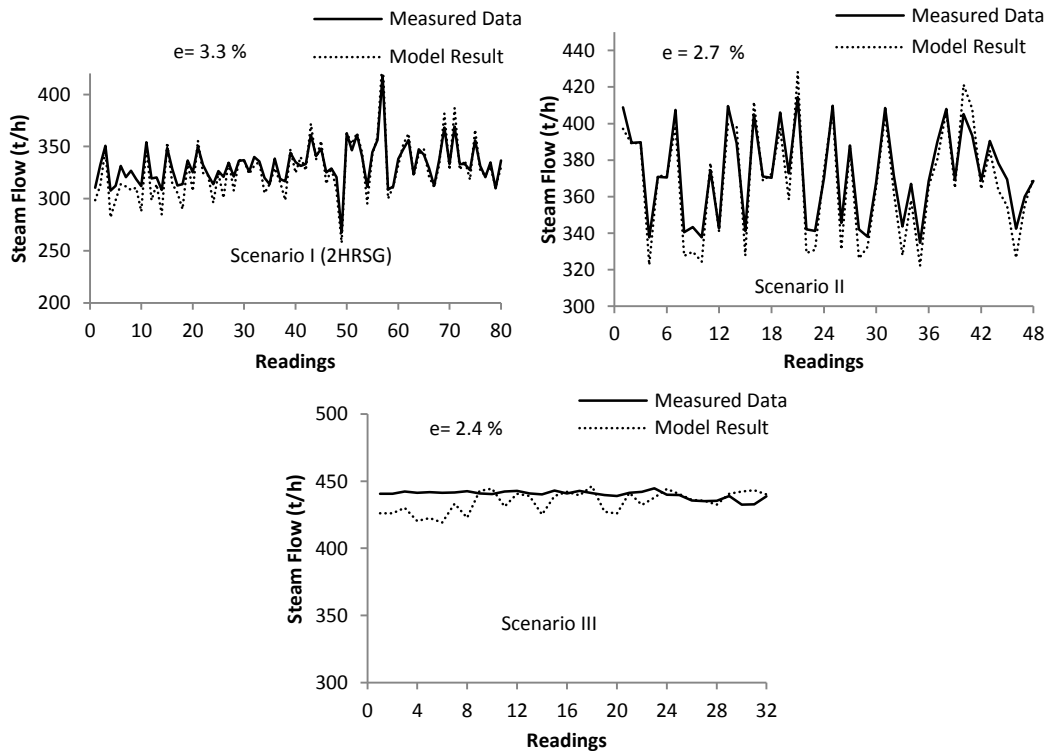


Figure 5.3: Power plant validation: HRSG steam flow (t/h)

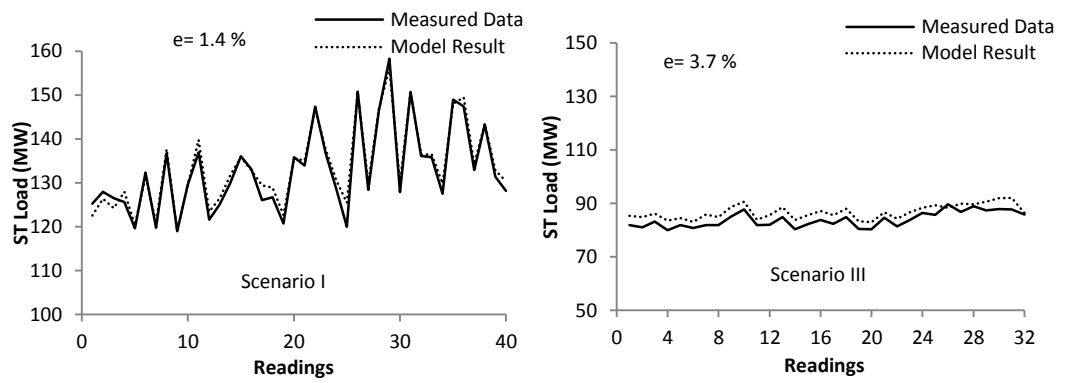


Figure 5.4: Power plant validation: ST load (MW)

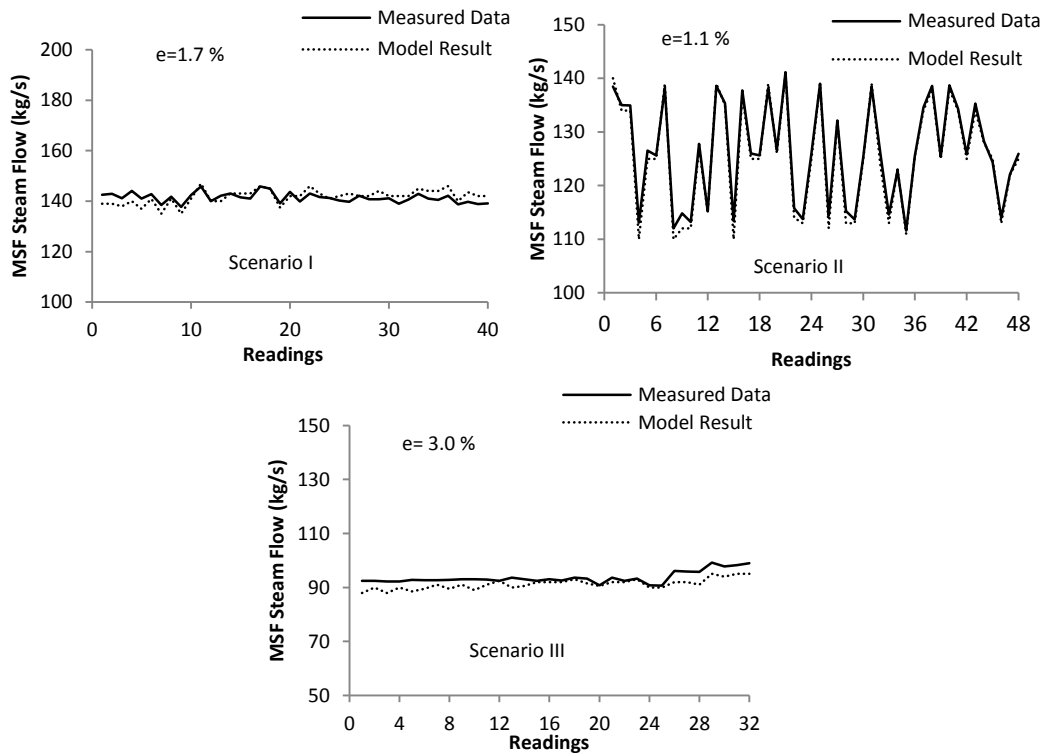


Figure 5.5: Power plant validation: MSF flow (kg/s)

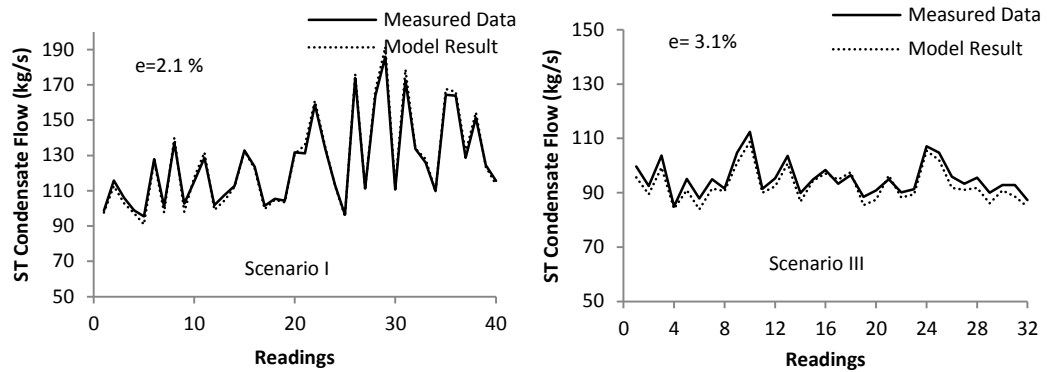


Figure 5.6: Power plant validation: ST condensate (kg/s)

5.4 Power plant energy and exergy analyses

To assess the power plant performance for the three operating scenarios, energy and exergy analysis methods are used (Chapter 4). The energy analysis determines the losses in the system by focusing on the quantity of the energy in each process streams without any information about the energy content degradation, whereas the exergy analysis indicates clearly the location of energy degradation by focusing on energy quality, as well as quantity [13]. Both studies are carried out at full load plant condition and annual average DBT of 29°C. The data required for these analyses are obtained from the validated model. Table 5.3 presents scenario I stream's thermodynamics properties, which are necessary to perform energy and exergy analyses, whereas the thermodynamics properties of scenario II and scenario III's streams are shown in Appendix 5-C.

5.4.1 Power plant energy analysis

Energy analysis results consist of individual cycle components performance assessment and overall plant performance indicators for three operating scenarios (Table 5.4). Cycle component assessment includes GT generated power, GT fuel consumption, GT efficiency, ST generated power, HRSG efficiency, steam production, and SF fuel consumption. Plant overall performance indicators are the gross power, auxiliary power consumption, plant thermal efficiency, gas/power (G/P) ratio, plant heat rate, and UF. Moreover, Table 5.4 includes the environmental impact of each operating scenario represented by CO₂ emissions estimation using both energy and exergy.

Stream No.	\dot{m} (kg/s)	T (°C)	P (bar)	h (kJ/kg)	s (kJ/(kg.K))	\dot{E}_{ph} (MW)	\dot{E}_{ch} (MW)	\dot{E}_T (MW)
1, 11	9.58	25.0	18.0	52.1	9.75	4.26	492	497
2, 22	480	29.0	1.01	29.2	6.90	0	0	0
3, 33	489	556	1.02	607	8.14	123	1.93	125
4, 44	492	799	1.01	907	8.50	224	1.94	226
5, 55	492	142	1.01	151	7.42	9.60	1.94	11.5
6, 66	3.16	25.0	1.11	52.1	11.1	1.41	162	164
7, 77	107	109	104	465	1.40	5.59	0.270	5.86
8,88	107	724	83.0	3937	7.32	189	0.270	189
9	246	540	83.0	3494	6.83	360	0.610	360
10	246	111	1.50	2637	7.08	131	0.610	131
12	93.6	111	1.50	2637	7.08	49.8	0.230	50.0
13	93.6	45.8	0.100	2282	7.20	13.0	0.230	13.3
14	93.6	42.8	1.30	179	0.610	0.210	0.230	0.440
15	152	111	1.50	2637	7.08	81.0	0.380	81.4
16	140	111	1.50	2637	7.08	74.4	0.350	74.8
17	140	104	10.0	437	1.35	5.38	0.350	5.73
18	234	79.6	1.30	333	1.07	4.40	0.580	4.98
19	246	109	104	465	1.40	12.8	0.610	13.4
20	6772	25.0	1.01	105	0.370	1.38	16.9	18.3
21	6772	32.0	2.00	134	0.460	3.08	16.9	19.9
23	31.4	109	104	465	1.40	1.63	0.080	1.71

Table 5.3: Simulated results of the cycle streams thermodynamic properties in scenario I (for stream identification refers back to Figure 5.1)

Performance Indicator	Unit	Scenario I	Scenario II	Scenario III
GT Power	MW	140 x 2	140	140
ST Load	MW	205	–	87
Gross power	MW	485	140	227
Auxiliaries power consumption	MW	24.4	18.7	18.18
Net Power	MW	461	121	209
MSF Load	%	100	100	80
GT efficiency	%	33.3	33.3	33.3
HRSG efficiency	%	83.4	83.4	83.4
GT gas flow	kg/s	9.58 × 2	9.58	9.58
SF gas flow	kg/s	3.16 × 2	3.16	3.16
Steam production	t/h	440 × 2	440	440
LP steam turbine flow	t/h	337	–	34.0
Overall power plant efficiency	%	41.9	21.7	37.3
Heat utilization factor	%	69.4	78.1	81.3
Heat rate	kJ/kW	5189	4609	4394
G/P ratio	kg/kW	0.185	0.327	0.220
G/S ratio	–	4.00	4.00	4.00
CO _{2,I} emissions	(g/kWh)	371	329	314
CO _{2,II} emissions	(g/kWh)	535	748	542

Table 5.4: Performance indicators evaluation at the three operating scenarios

Power generation is highest at scenario I, because both GTs and ST are in service, whereas ST is shut down at scenario II and partially operated at scenario III due to shortage of the steam production as a result of only one HRSG running. It is necessary to mention that at scenario III, to keep ST in service, the MSF load was reduced to maintain the minimum design flow through the LP steam turbine. Technically, less than this flow can increase the LP steam turbine last stage temperature, which causes excessive vibration and consequently, the ST trip mechanism is linked with a last stage temperature higher than 200°C.

Plant auxiliary power consumption is the lowest at scenario III, although the gross generated power was less at scenario II. This is because at scenario III, the MSF load

is 80% only and the auxiliary power consumption of the three MSF distillers is around 15.5 MW and only 5.5 MW for the power plant. Therefore, reduction of the MSF load has a more significant effect on auxiliary power consumption compared with power plant load.

Both GT and HRSG efficiency remained same for the three scenarios because they are at same operating condition: full load in GTs and full SF in HRSG. Scenario I has better power plant efficiency than the other two scenarios, which can be justified from the G/P ratio trend, where the G/P ratio is lowest at scenario I because both GTs and ST are in service to generate the electrical power.

Scenario I has highest power plant efficiency (41.9%) followed by scenario III due to the lower G/P ratio for both of them. This result matches with other studies [67, 69, 158], with the consideration that the plant outputs in this study are allocated for two products (power and water). On the other hand, scenario II power plant efficiency is the lowest, because the energy used to produce the HP steam was mostly lost at the HP/LP reduction station to meet LP steam criteria to power the MSF desalination.

From an energy analysis angle, the overall cogeneration plant (power and MSF desalination) performance can be judged easily using the heat UF and heat rate since these combine the energy outputs as power produced from the power plant and heat used to power the MSF distillers [58]. At full load, the steam turbine produces 205 MW whereas the MSF distillers consume 308 MW heat. Therefore, scenario III has the highest UF since most of the produced steam above 92% is used in the MSF distillers. The produced steam in scenario II was utilized to produce only one product water only, since the ST is in shut down condition. Thus, the heat rate of the cogeneration plant behaves opposite to the UF. Consequently, scenario I has the highest heat rate. Although, these indicators can be used to evaluate cogeneration plant performance, it is important to mention that they are indicators for the heat usage more than for overall plant performance evaluation. This challenge is raised because the MSF desalination output is not in the form of energy, but simply the amount of distillate water [13].

As a result of burning less fuel to produce the power and heat (heat rate) in scenario III, environmentally the CO_{2,I} emissions are the lowest compared with the other two scenarios. However, based on exergy, the CO₂ emissions are lowest with scenario I

because the net exergy forwarded to the MSF distiller is less compared with that for the real power produced from the steam turbine.

5.4.2 Power plant exergy analysis

The exergy analysis was carried out at an Oman average ambient air temperature of 29°C (Chapter 3), 1.013 bar pressure, and stream natural chemical composition. The stream properties required to perform this analysis were extracted from the simulated model data presented in Table 5.3 for scenario I (Appendix 5-C for the other operating scenarios). Definitions of the cycle components' exergy efficiencies and exergy destruction are presented in Table 5.5, leading to the results summarized in Figures 5.7 and 5.8. In spite of the exergy efficiency defining the utilization percentage or the output from the input exergy, the amount of exergy destruction is necessary in thermal system enhancement and improvement. A good example of that is that the exergy efficiency of the MSF was low at 5.7%, which represents a low use of the input exergy; however, a distinguished conclusion for the improvement and optimization cannot be made unless the amount of exergy destruction is known. Therefore, Figure 5.8 describes the exergy destruction ratio comparisons of the power plant input exergy (natural gas) between the three operating scenarios.

Equipment	Exergy Efficiency (%)	Exergy Destruction (MW)
GT1	$\frac{W_{out}}{(E_1 + E_2 - E_3)}$	$E_1 + E_2 - E_3 - W_{out}$
GT2	$\frac{W_{out}}{(E_{11} + E_{22} - E_{33})}$	$E_{11} + E_{22} - E_{33} - W_{out}$
SFB1	$\frac{E_4}{(E_3 + E_6)}$	$E_3 + E_6 - E_4$
SFB2	$\frac{E_{44}}{(E_{33} + E_{66})}$	$E_{33} + E_{66} - E_{44}$
HRSG 1	$\frac{(E_8 - E_7)}{(E_4 - E_5)}$	$E_4 + E_7 - E_8 - E_5$
HRSG 2	$\frac{E_{88} - E_{77}}{(E_{44} - E_{55})}$	$E_{44} + E_{77} - E_{88} - E_{55}$
HPT	$\frac{W_{out}}{(E_9 - E_{10})}$	$E_9 - E_{10} - W_{out}$
LPT	$\frac{W_{out}}{(E_{12} - E_{13})}$	$E_{12} - E_{13} - W_{out}$
Deaerator	$\frac{E_{19}}{(E_{18} + (E_{15} - E_{16}) + W_{BFP})}$	$E_{18} + (E_{15} - E_{16}) + W_{BFP} - E_{19}$
Desuperheater	$\frac{E_9}{(E_8 + E_{88} + E_{23})}$	$E_8 + E_{88} + E_{23} - E_9$

Table 5.5: Cycle equipment exergy efficiency and exergy destruction calculations

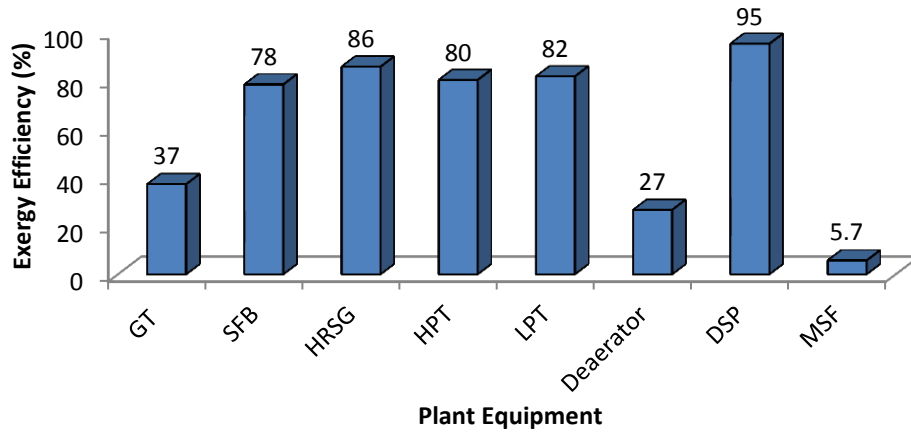


Figure 5.7: Exergy efficiency of the cycle equipment (scenario I)

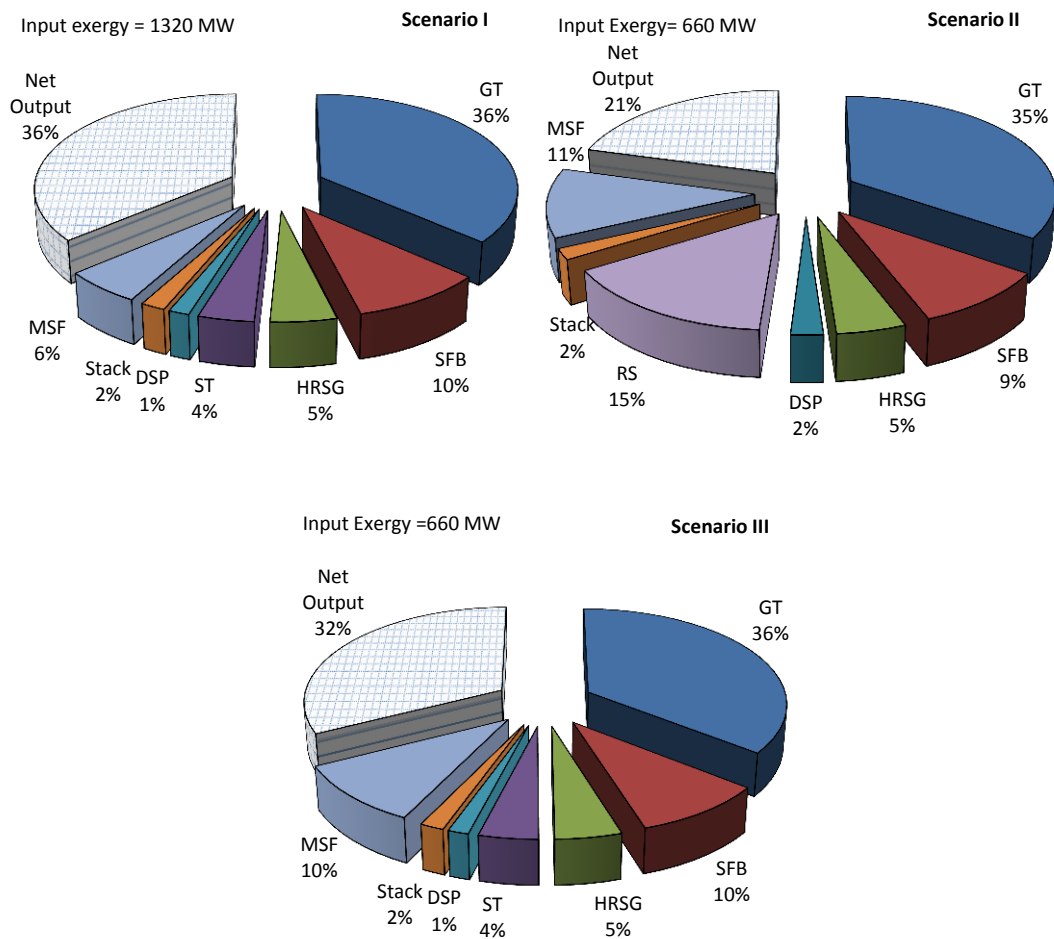


Figure 5.8: Comparison of exergy destruction ratios between the three operating scenarios

As can be seen from Figure 5.8, the input fuel exergy is 1320 MW for scenario I due to the operation of both GTs and SFBs, while only 660 MW for the other two scenarios since only a single GT and SFB were in service. Nevertheless, the exergy efficiency is highest at scenario I at 36%, whereas, it is only 21% and 32% for scenarios II and III, respectively. The benefits of the exergy methods can be seen clearly by explaining the reasons behind the lower exergy efficiency at scenario II, where the seasonal variation of power demand forced steam turbine shut down and MSF demand depends on the reduction station. Almost 100 MW (equivalent to electrical power) was lost as a result of reducing the HP steam from the HRSG to LP steam for MSF desalination at the reduction station. Compared with this, in scenario III, extracting the LP steam from the steam turbine enhanced the exergy efficiency by 50% (used to generate electrical power at HP turbine instead of losing the work at the reduction station).

In spite of scenario I having higher input fuel exergy than the other two scenarios, for all three scenarios, the GT was the dominant exergy destruction component with 36% exergy destruction from the input fuel exergy. This agrees with most published research in this field relating to high exergy destruction in fuel burning at the combustion chamber [70, 159, 160]. Similarly, the SFB consumes 10% from the input exergy supporting the conclusion of high exergy destruction reported in combustion chambers.

The study showed 5% from the input exergy was destroyed in the HRSG and 2% from it was rejected to the atmosphere through the stack for the three studied scenarios. In addition, the steam turbine system (HP turbine, LP turbine, and condenser) was noticed consuming 4% and 5% from the fuel exergy for scenarios I and scenario III, respectively.

The study found also the MSF distillers annihilated 6 %, 11%, and 10% from the overall cogeneration plant input exergy at scenarios I, II, and III, respectively. This is mainly due to the low exergy efficiency of this type of thermal desalination, as was reported in previous studies [71, 74, 77]. However, these studies did not explain the location of the exergy destruction in the sophisticated structure of these units in detail.

5.5 Power plant parametric study

Throughout their operation, two types of factors affect power plant performance: operational factors (i.e., SF flow and MSF load) and external factors (e.g., ambient temperature and relative humidity). Therefore, a parametric study of variations in ambient temperature, relative humidity, SF flow, and MSF load has been conducted using the validated IPSEpro model, studying their impact on the performance outputs: gross power generation, steam turbine power production, power plant efficiency, UF, overall exergy efficiency, CO₂ emissions (energy base), and CO₂ emissions (exergy base).

The operational factors (SF flow and MSF load) play the main role in changing the plant configuration, with four different configurations used to investigate their impact on the plant performance indicators:

- Power Plant (PP) standalone: describes the power plant running in combined cycle configuration without the coupling of MSF desalination or using any source of additional energy input like supplementary firing.
- PP with MSF desalination (PP + MSF): refers to the combined power plant running coupled with MSF desalination cogeneration plant. To maintain the minimum flow through the LP steam turbine in this case, the MSF distiller load is reduced to 85%.
- PP with SF (PP + SF): the aim in choosing this configuration is to realize the influence of using the SF in the HRSG on power plant overall performance indicators.
- PP with SF coupled with MSF desalination (PP + SF + MSF): the cogeneration plant configuration that produces high power and water demand due to the use of supplementary firing.

Of the two external factors, the influence of the relative humidity was not found to depend significantly on the plant operational configuration.

5.5.1 Ambient temperature

The electrical power generation is characterized by high power demand in summer and relatively low load in winter, mainly due to the change in the ambient temperature [106]. Figure 5.9 shows the impact of changing the ambient temperature from 10°C to 50°C on the power plant at full load condition in all four configurations. As would be expected, the PP + SF configuration produces the highest electrical power (because both GT and ST were at maximum rated capacity) whereas PP + MSF produces the lowest (since most of the LP steam was directed to the MSF distiller for water production). At all four configurations, the gross generated electrical power reduces by 5.5% averagely for every 10°C rise in ambient temperature, although each configuration has its own gross electrical generation value. This finding is in agreement with previous published work [69, 108, 109, 115].

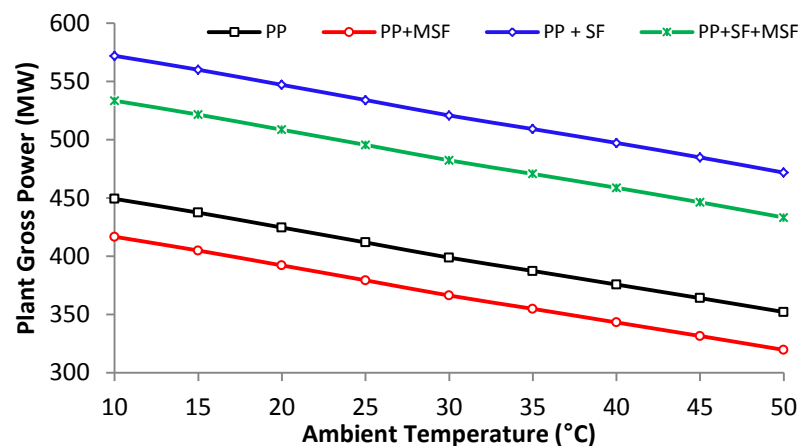


Figure 5.9: Influence of the ambient temperature on plant gross electrical power

Figure 5.10 shows the increase in ambient temperature reduced power plant efficiency for every 10°C increase by 0.16% (PP) to 0.23% (PP + SF) but 0.54% (PP + MSF) to 0.49% (PP + SF + MSF). The decreasing trend can be explained by the impact of increasing ambient temperature reducing GT efficiency and the impact of the MSF load on the steam turbine load (Appendix 5-D), so the configurations with MSF exhibit a higher rate of decrease in thermal efficiency as shown in Figure 5.10. On other hand, the configurations with MSF show higher heat utilization factors (Figure 5.11) since this performance index counts the steam energy consumed in the MSF desalination equally with generated power.

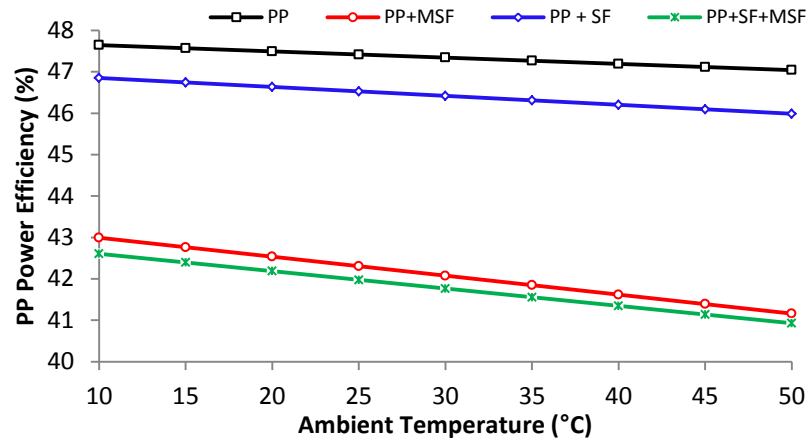


Figure 5.10: Effect of the ambient temperature on power plant efficiency

Interestingly, Figure 5.11 shows the rise in ambient temperature reducing the heat UF for the configurations without MSF, whereas enhancing the UF for the configurations with MSF desalination. This is because the influence of MSF being in service is to increase the G/P ratio.

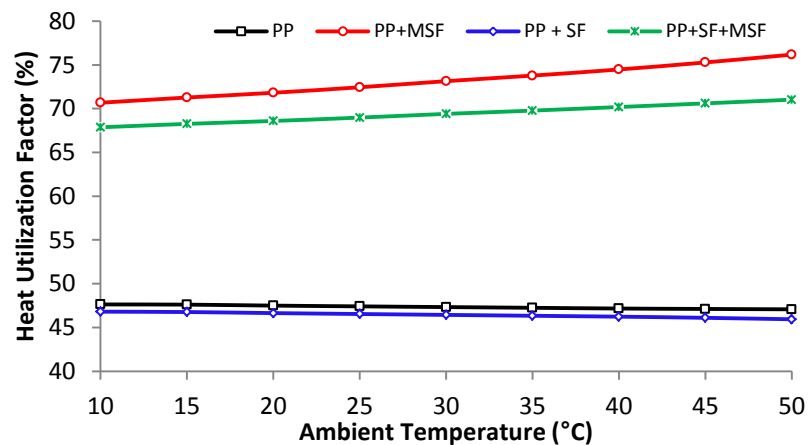


Figure 5.11: Effect of the ambient temperature on power plant heat utilization factor

By contrast with Figure 5.10, Figure 5.12 shows that an increase in ambient temperature reduces the exergy destruction at the GT significantly (main contributor of the cycle exergy destruction as was explained previously) and therefore, enhances the exergy efficiency for all four configurations. However, the rate of increase is negligible to only 0.8% for power only configurations but doubles when using MSF.

An interesting finding from Figure 5.12 showed that coupling the power plant with MSF degrades the overall exergy efficiency by up to 7%, which is explained by the high exergy destruction of this type of thermal desalination, in contrast to SF, which

has no significant effect on exergy efficiency. This conclusion opposes directly the approach of representing the overall cogeneration plant performance by the heat utilization factor, which shows coupling MSF with power plant enhancing performance (Figure 5.11). The influence of the ambient temperature on cycle equipment exergy efficiency and exergy destruction the four configurations was listed in appendix 5-D. Another noteworthy comparison between energy efficiency (Figure 5.10) and exergy efficiency (Figure 5.12) is that increasing the ambient temperature increases (not decreases) exergy efficiency.

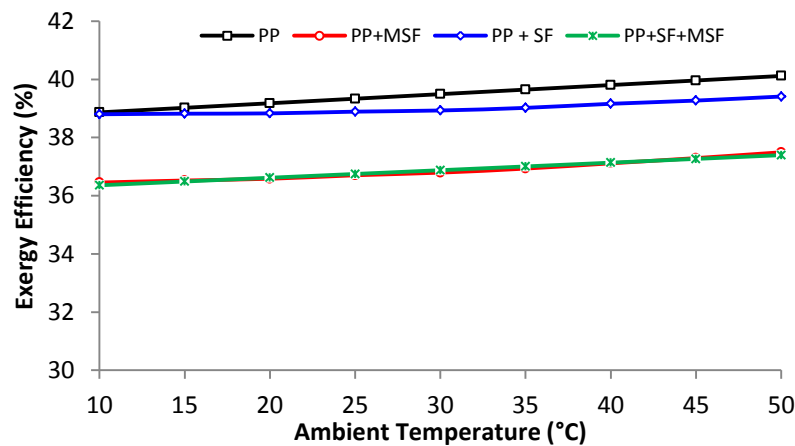


Figure 5.12: Effect of ambient temperature on plant overall exergy efficiency

Environmentally, the influence of the ambient temperature variation has been analysed using the both energy and exergy base methods. Based on the energy method (Figure 5.13), a 10°C rise of ambient temperature increases the CO₂ emissions by around 0.5% for the configurations where the MSF is not in operation. However, operating the MSF decreased the CO₂ emissions by almost 1.0%. By contrast, CO₂ emissions based on exergy do not differ from energy base for the configurations where the MSF distillers are not in operation, with the PP + MSF and PP + SF + MSF configurations' CO₂ emissions' exergy base shows a 40% difference from the energy method of estimation. In the energy base MSF, consumed heat is included, whereas in the exergy base, the exergy feed to MSF was used in the calculation. Moreover, the influence of the ambient temperature had the same trend for all four configurations: CO₂ emissions increased as the ambient temperature rose (Figure 5.14). This contrast credits using the exergy based method in the emission estimation since it represents useful work [13].

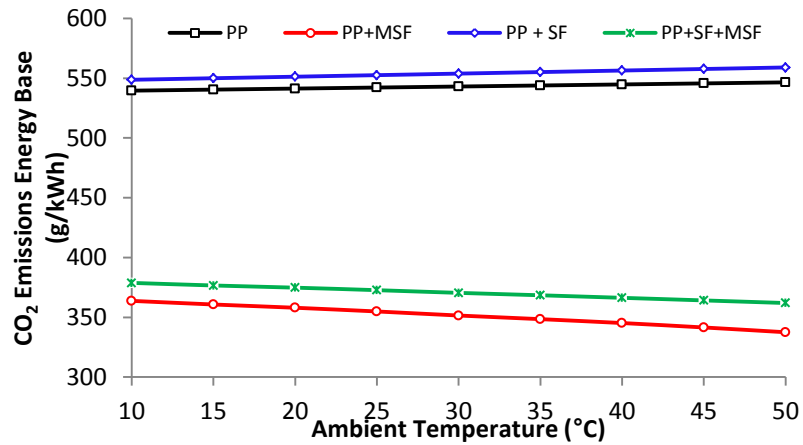


Figure 5.13: Effect of ambient temperature on energy CO₂ emissions

Moreover, the influence of the ambient temperature had the same trend for the four configurations: CO₂ emissions increased as the ambient temperature rose by the same trend, as it can be seen from Figure 5.14. This result raised the credit of using the exergy in the analysis since it represents useful work [13].

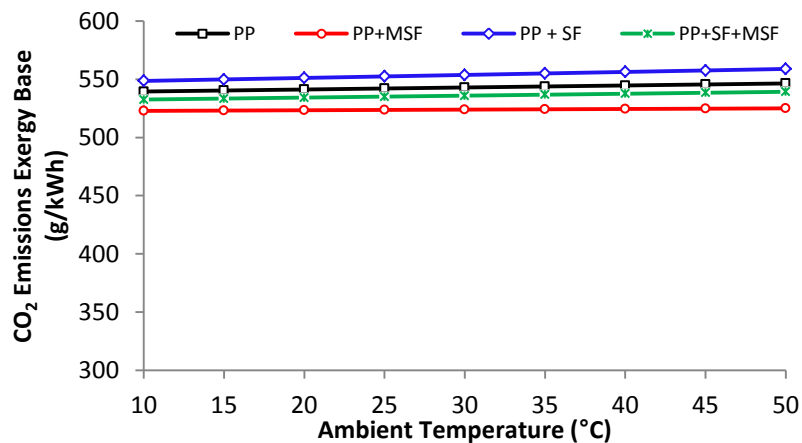


Figure 5.14: Effect of ambient temperature on exergy CO₂ emissions

Finally, ambient temperature is found strongly to affect the performance of all the different plant configurations since the GT is the common equipment in all configurations. This suggests controlling GT inlet temperature through cooling technologies may result in clear enhancement of plant performance and hence reduce the CO₂ emissions significantly.

5.5.2 Relative humidity

The arid countries (e.g., Oman) are characterized by a high variation of the relative humidity (Section 3.3.1); therefore, the effect of relative humidity changes on cogeneration power plant performance indicators should be investigated. This effect was studied with relative humidity varying from 0% to 100% at full load PP + SF + MSF configuration and 15°C ambient temperature. A 10% change in the relative humidity, gives a slight rise (only 0.02%) of the gross electrical power due to increase in the GT exhaust density [65]. Consequently, the steam production was in the HRSG, which in turn, produces more electrical power from the steam turbine (Figure 5.15), in agreement with previous studies [69, 70]. Moreover, the rise of the gross power plant at the same natural gas consumption enhances the power plant efficiency and heat UF by the same percentage (Figure 5.16).

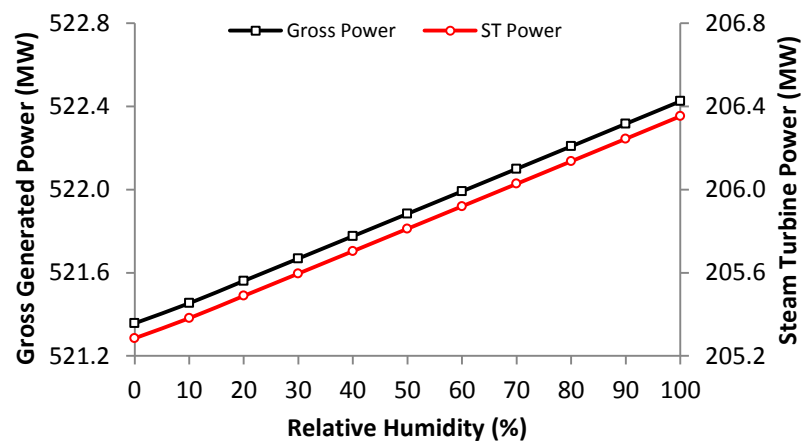


Figure 5.15: Effect of relative humidity on plant and steam turbine power

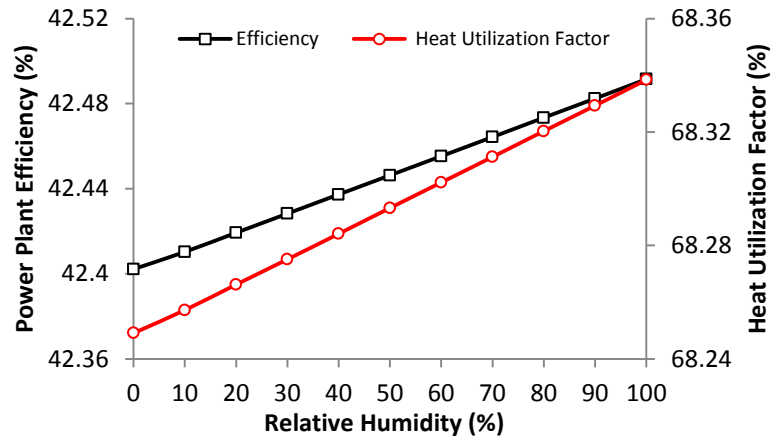


Figure 5.16: Effect of relative humidity on power plant efficiency and heat utilization factor

For a similar reason, for a 10% rise in relative humidity, there is a 0.3% increase in exergy efficiency (Figure 5.17). This can be explained by the enhancement of steam turbine power while the fuel feed exergy remains the same.

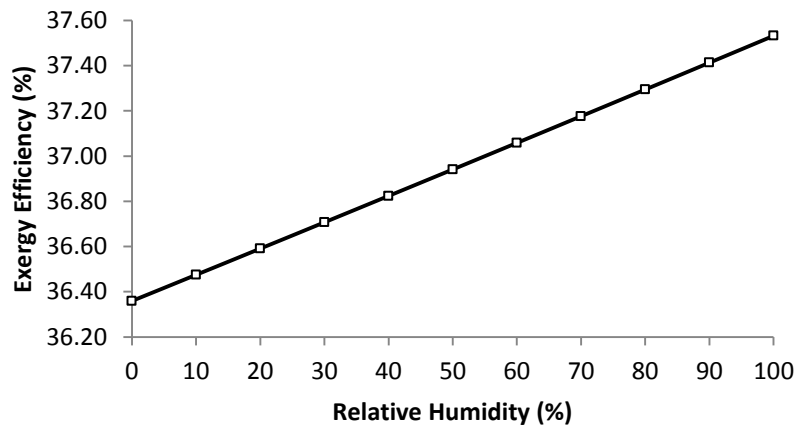


Figure 5.17: Effect of relative humidity on plant exergy efficiency

An increase in relative humidity reduces the CO₂ emissions for both energy and exergy methods by similar trends (Figure 5.18). Even though the decrease is not much at 0.02%, it can be considered as a significant effect when this value is estimated annually for high production cogeneration plants (like the one in this study).

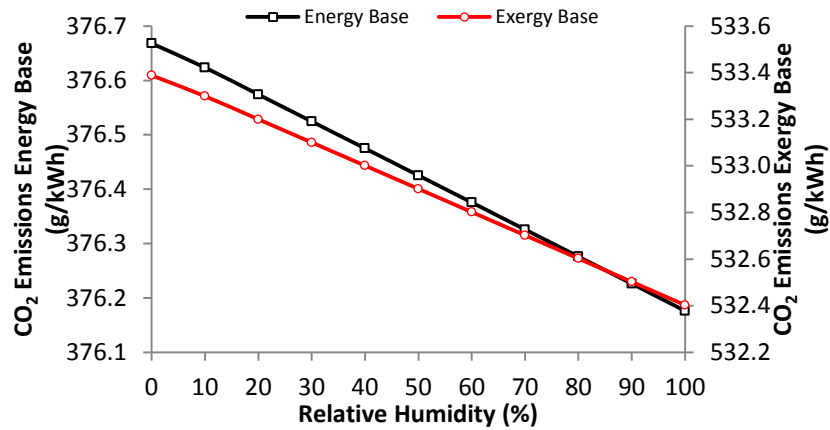


Figure 5.18: Effect of relative humidity on CO₂ emissions

5.5.3 Supplementary Firing (SF) flow

To investigate the impact of SF on plant performance, this section focuses on variation of the SF flow (transition configuration from full load PP + MSF to PP + SF + MSF). The study changed the flow from 0% (0 kg/s natural gas SF flow) to 100% (3.16 kg/s SF flow) at ISO conditions and full MSF load (Figure 5.19). A 10% change in SF flow causes an increase in steam turbine power by 14.5%, which is reflected by 3.1% on gross power production. This enhancement in steam turbine power results from increase of the steam production from the HRSG, which is directed to the HP and LP steam turbine, since the MSF desalination is at constant load. Interestingly, the HRSG efficiency (Figure 5.20) is affected positively by a rise in SF flow compared with a conventional boiler. This can be explained because it increases the turbine exhaust temperature unlike a conventional boiler [161]. This finding agrees with limited published work on this type of HRSG [161, 162].

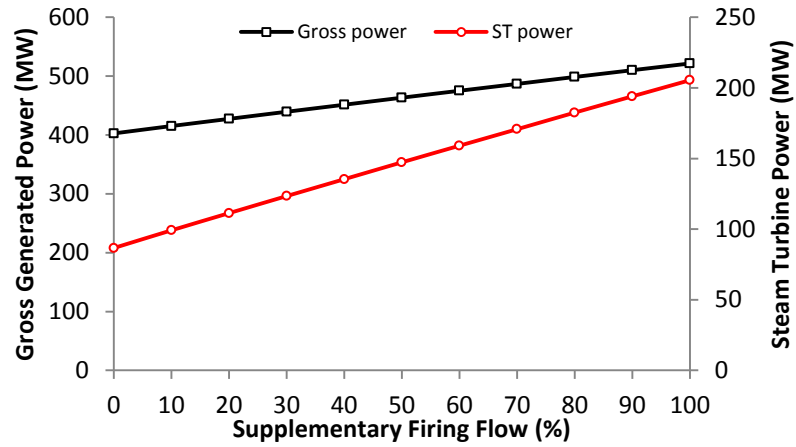


Figure 5.19: Effect of SF flow on gross and steam turbine power

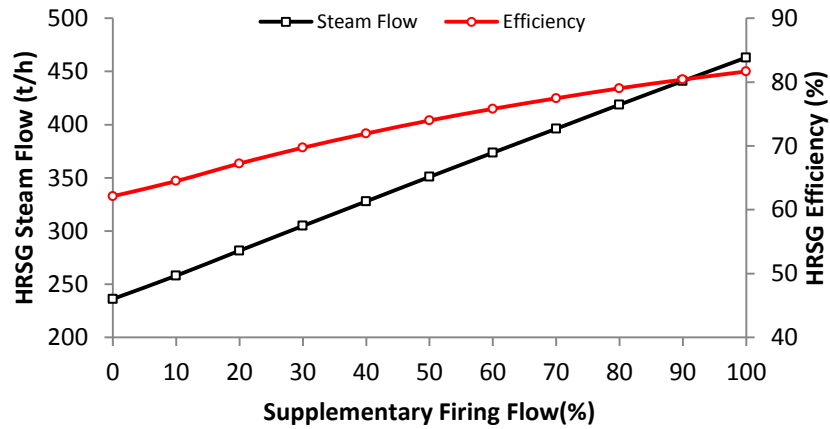


Figure 5.20: Effect of SF flow on HRSG flow and efficiency

Figure 5.21 shows an increase of SF flow by 10% causes a slight insignificant drop in power plant efficiency due to usage of this flow to produce the HP steam to power a high mechanical efficiency steam turbine. On the other hand, this change in SF flow leads to a more than 1.0% reduction in heat UF because the produced steam was utilized in a steam turbine at a constant MSF load. Figure 5.21 shows the impact of the SF change on power plant efficiency and heat utilization factor.

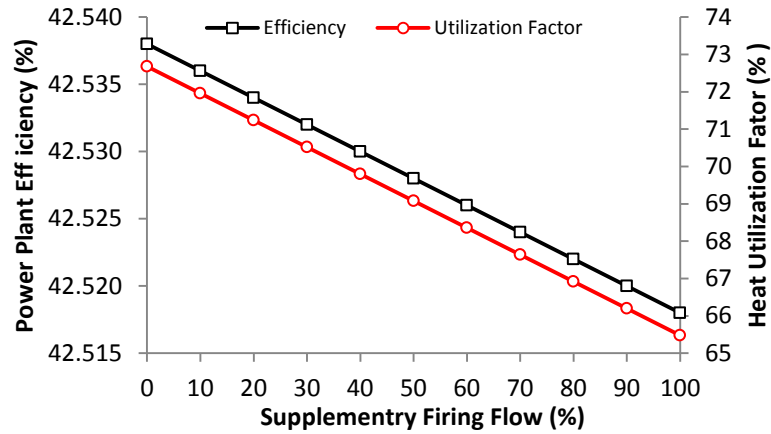


Figure 5.21: Effect of SF flow on power plant efficiency and heat UF

Moreover, an increase in SF flow reduces the overall plant exergy efficiency unremarkably, less than 0.1% for every 10% change (Figure 5.22). This trend is a result of most of the natural gas input exergy being converted to electrical power since the MSF distillers are kept at constant load. Details of the impact of SF flow on plant equipment exergy efficiency, exergy destruction, and exergy destruction ratio are in Appendix 5-E.

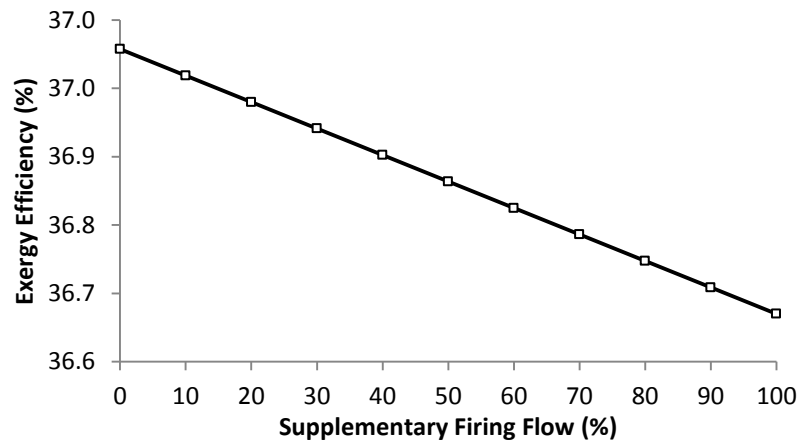


Figure 5.22: Effect of SF flow on overall plant exergy efficiency

Environmentally, CO₂ emissions (Figure 5.23) rose linearly with an increase in SF due to the increase of natural gas consumption compared with gained output. However, this increase was 1% for energy base and only 0.3% for the exergy base for every 10% rise in the SF flow.

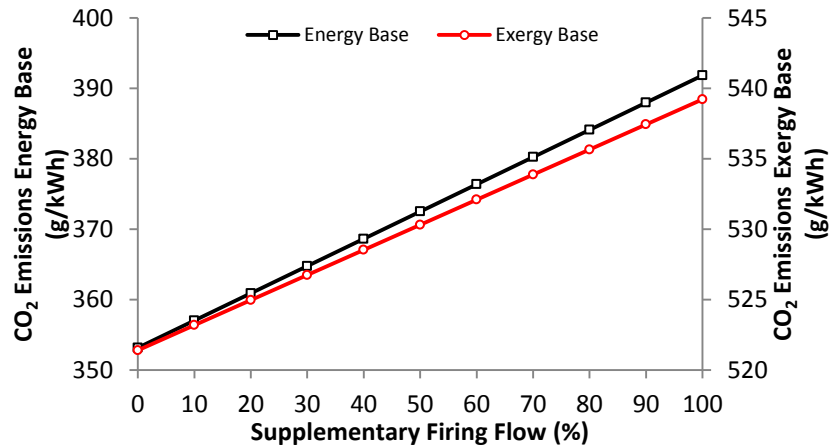


Figure 5.23: Effect of SF flow on CO₂ emissions

5.5.4 MSF load

The MSF load can be varied from 0% load to 100% load (as a transition configuration from PP + SF to PP + SF + MSF) to investigate the effect of the hybridization of the combined power plant with MSF thermal desalination. The gross power plant generation drops linearly by 0.7% for every 10% increase in MSF load, as a result of reduction of the steam turbine power generation by 1.6% (Figure 5.24) because part of the LP steam that is used to produce power from LP turbine was extracted to raise the MSF load. Consequently, there is a drop in power plant efficiency due to the rise in MSF load and a reduction of the gross power (Figure 5.25). In contrast, the heat UF increases sharply, from 46% with no MSF in operation to 68% with full load MSF due to the high steam utilization in MSF desalination.

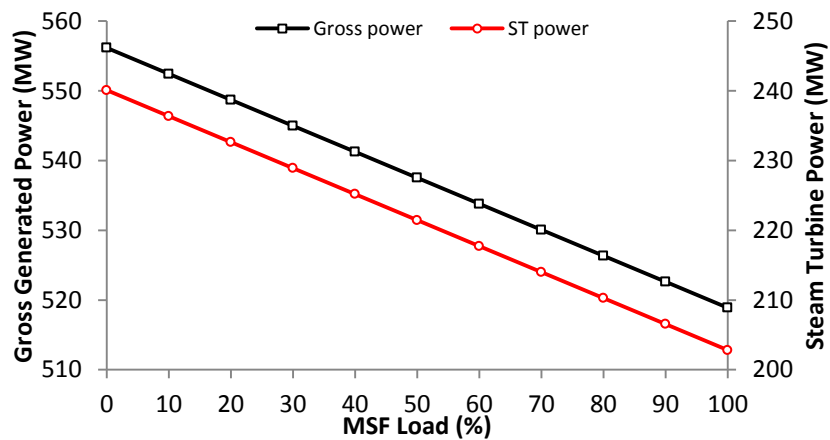


Figure 5.24: Effect of MSF load on gross and steam turbine power

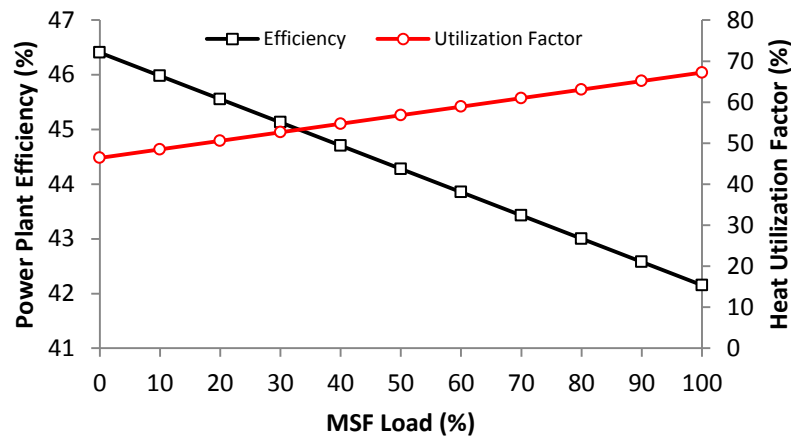


Figure 5.25: Effect of MSF load on power plant efficiency and heat UF

However, an original observation (Figure 5.26) is that coupling the combined cycle power plant with MSF desalination decreases the overall exergy efficiency even though it enhances the heat UF. A 10% rise in MSF load reduces plant exergy efficiency by 0.6% (Figure 5.26). This change in MSF load has no impact on the power plant equipment, which is running at full load condition except for the LP steam turbine and condenser and consequently, has no impact on their exergy efficiency and exergy destruction status.

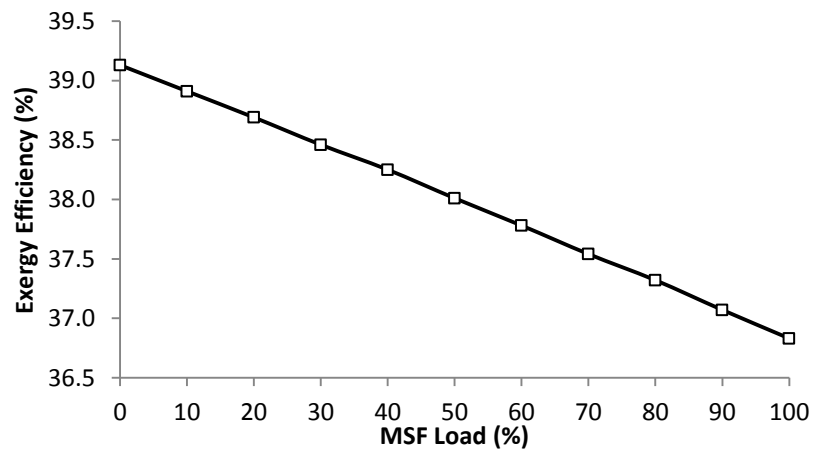


Figure 5.26: Effect of MSF load on overall plant exergy efficiency

CO₂ emissions reduce as MSF load is increased (Figure 5.27). However, the drop using the energy base (4.3% for every 10% increase in MSF load) is sharper than using the exergy base (only 0.6%). This can be explained by low exergy input to the MSF unit even with a high amount of LP steam flow (LP steam with low temperature has low quality, therefore, it is carrying low exergy at 26 MW full load

for each distiller); whereas the energy base method depends on total steam flow and not on steam quality (energy supplied, around 308 MW for each distiller).

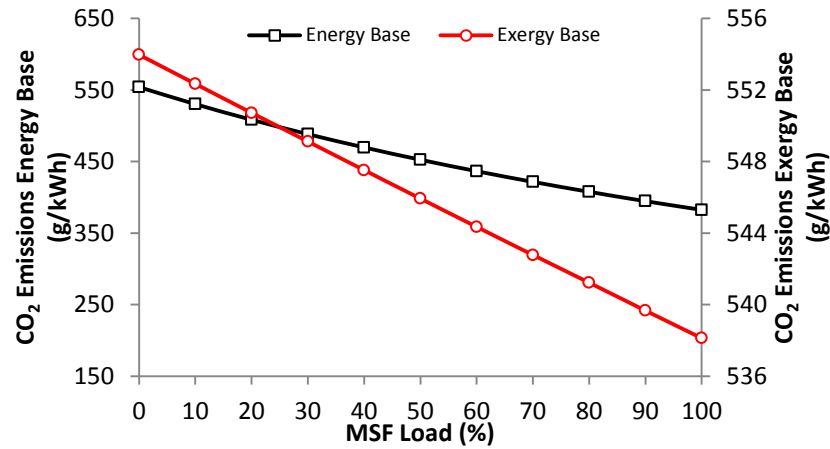


Figure 5.27: Effect of MSF load on CO₂ emissions

5.6 Closing Remarks

Prior to any use of software (IPSEpro in this study) plant simulation models, it is mandatory to validate such models. For the purposes of this study, this has been divided into power production plant (using available actual plant operational data) in this Chapter 5 and the water production plant (against vendor data) subsequently in Chapter 6. The actual power plant was modelled for three different operating scenarios. These scenario models were validated against plant measured data and the relative differences between them were found to vary from only 1.1% to 3.7%. These differences could be attributed to either various modelling assumptions or to input data uncertainties, as well as measured plant performance uncertainties due to measurement devices precision and effects of external factors. It is suggested that these results should give confidence in the subsequent use of these models (Chapters 7-10) for suggesting improvements to the plant.

With the simulation models validated, it was credible to move forward to the performance analysis aims outlined in the Introduction to Chapter 5. Analysis of the simulation results showed that scenario I had the highest power plant efficiency (42%) while scenario II was the lowest (21%). However the Heat Utilization Factor showed the opposite since it took into account the heat delivered to the MSF, but this study suggests that it is more useful to represent cogeneration plant with different products (e.g. power and water) using exergy efficiency rather than Heat Utilization

Factor. The exergy efficiency was highest at scenario I (36%) and again lowest at scenario II (21%), with the GT system the main contributor of exergy destruction, representing 36% from input exergy for all operating scenarios. In addition, shutting down the steam turbine (scenario II) and using the HP/LP reduction station instead caused 15% destruction of input exergy.

The parametric study revealed that the power plant was highly affected by the ambient temperature with relatively insignificant impact of relative humidity. It also found using the supplementary firing had less impact on plant performance indicators compared with coupling the power plant with MSF desalination due to the low exergy efficiency of MSF desalination (to be confirmed in Chapter 6). Consequently, controlling the GT inlet temperature (Chapter 8) and finding possibilities to increase MSF exergy efficiency (Chapter 7) could improve performance in all operating scenarios.

Chapter 6

MSF Desalination modelling and simulation: validation and parametric study

6.1 Introduction

This chapter will focus on the modelling and model validation of the MSF unit. Model input parameters are selected from unit specification and vendor testing data. The validation of model results will be by comparisons with vendor testing data at different SWTs (seawater temperature) and unit loads. Results from the validate models are then utilized to perform energy and exergy analyses at average annual SWT of 27°C and the normal unit load of 100%.

This validated model makes an original MSF individual stages exergy analysis possible that investigates the sources of exergy destruction, which result in the low unit exergy efficiency. Furthermore, such an investigation indicates the potential for novel exergy efficiency enhancement through heat recovery from the stages produced distillate.

Finally, this validated model can also be used for a parametric study to investigate the influence of unit load, SWT, feed seawater flow, feed seawater salinity, and brine recirculation flow and temperature on MSF unit energy and exergy related performance indicators.

6.2 MSF modelling

The IPSEpro desalination library was used to develop the model of the MSF desalination units. Only one model was built for this purpose since the three units are identical (as described in Chapter 3). Figure 6.1 shows the IPSEpro MSF model with numbered streams. Each number identifies the composition of the stream and six thermodynamic properties (flow, temperature, pressure, specific volume, enthalpy, and either salinity in the case of seawater or entropy for any other stream). These values can be utilized in energy and exergy analysis calculations.

To validate this MSF unit model, in principle detailed measured data of temperature, pressure, and salinity for the inlet and outlet streams of all the individual stages should be provided (in this study, 16 heat recovery + 3 heat rejection). However, this requires many measuring instruments that would have increased the unit price considerably. In fact, measuring devices were installed only at the inlet and outlet streams of the unit. However, the vendor supplied all these data as unit guaranteed heat and mass balance values. Therefore, the vendor testing data were gathered from

the plant owner. These data cover properties at minimum and maximum operating SWT and Unit Load (UL) for each stream:

- 35°C SWT and 100% UL
- 35°C SWT and 60% UL
- 24°C SWT and 100% UL
- 24°C SWT and 60% UL

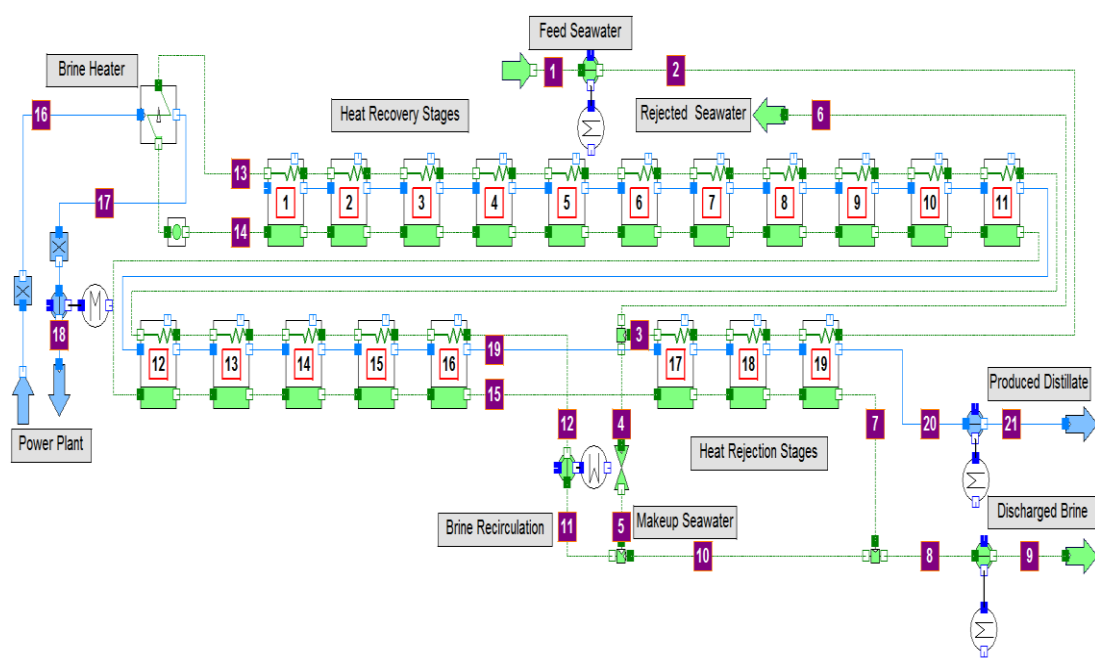


Figure 6.1: MSF unit IPSEpro model

Table 6.1 indicates model input (Set) and the model outputs (Cal), and model inputs are either unit specifications or set values extracted from the vendor data.

6.3 MSF desalination models validation

The MSF unit model validation was performed through comparison between the model data and vendor testing data. To ensure the validity of the model, detailed comparisons between vendor testing data and model results at all the individual stages, as well as at the main unit input/output properties were made for all four vendor conditions (Figures 6.2 to 6.5). The relative difference between the two compared values was estimated by Equation (5-1) for all the validation curves.

The relative difference varies only from 0.7% to 3.6% over all the vendor conditions (Figures 6.2 to 6.5). The differences between the vendor data and model results can be justified by two main reasons. Firstly, measurement uncertainty in vendor measuring devices and, secondly, model assumptions, such as having exact equal layout dimensions whereas in reality, there are slight layout differences over the three nominally identical MSF units. These model results show better agreement than the recent published study conducted by Abdul-Wahab et al [14] for the same unit. Details for this validation are presented in Appendix 6-A. This validation of the model provides a confidence level for further thermal analysis.

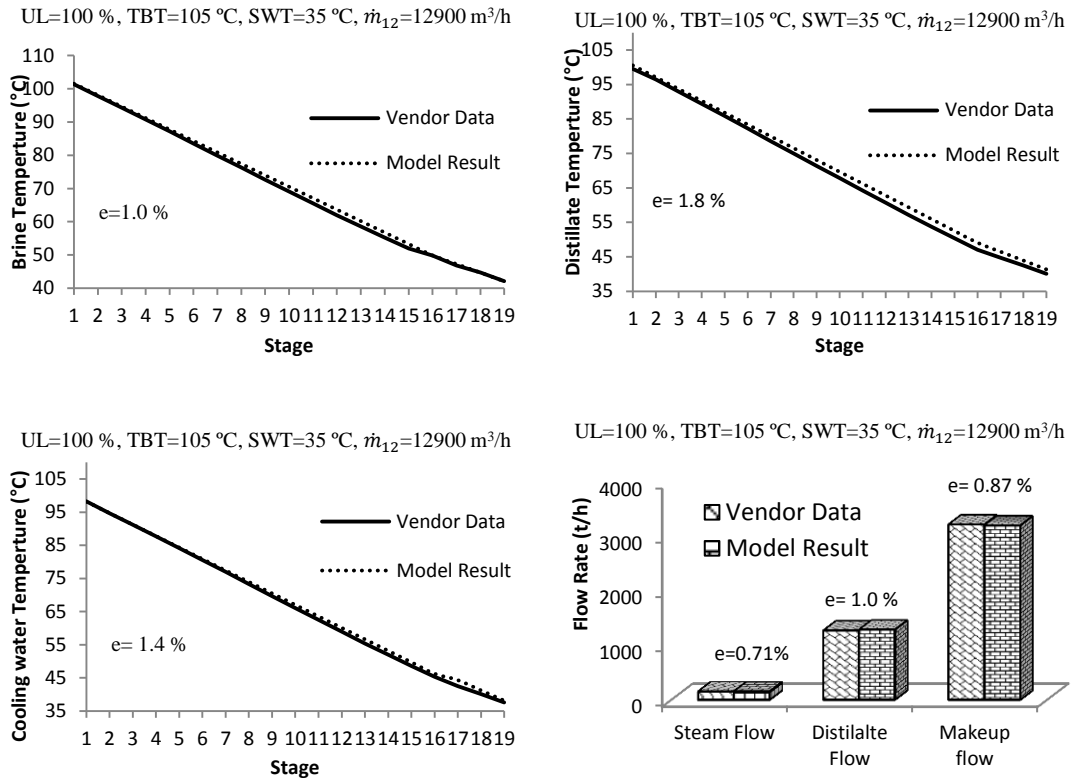


Figure 6.2: Comparison between model and vendor data at 35°C SWT and 100% UL

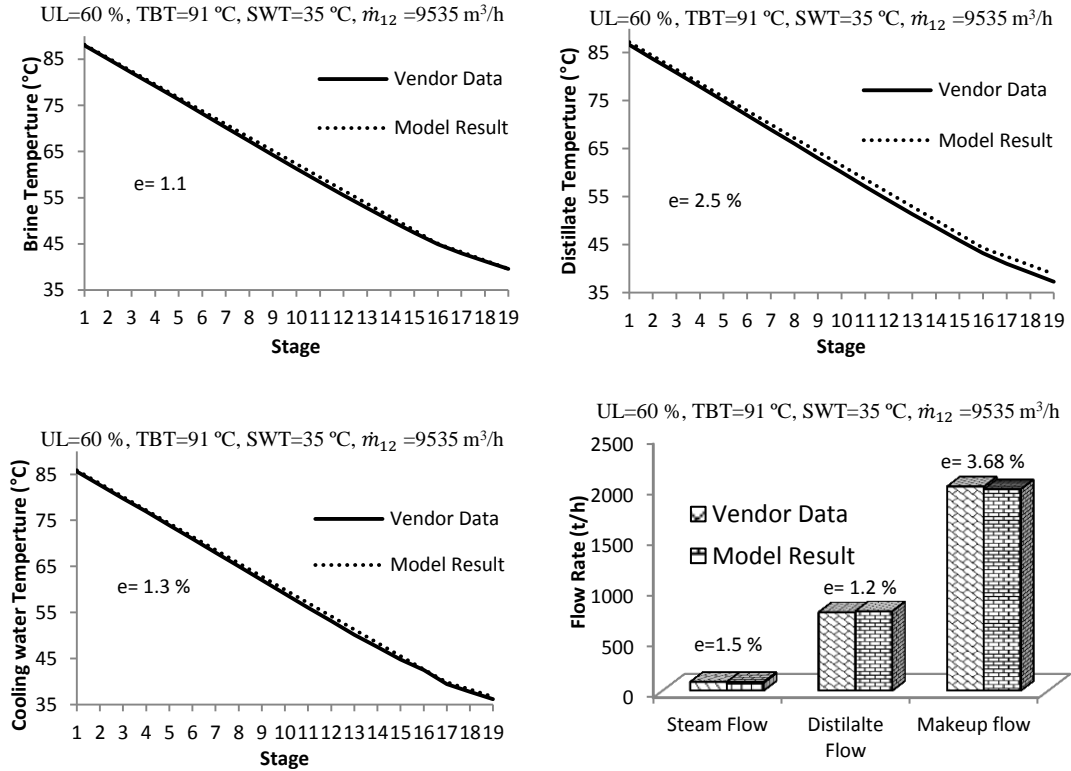


Figure 6.3: Comparison between model and vendor data at 35°C SWT and 60% UL

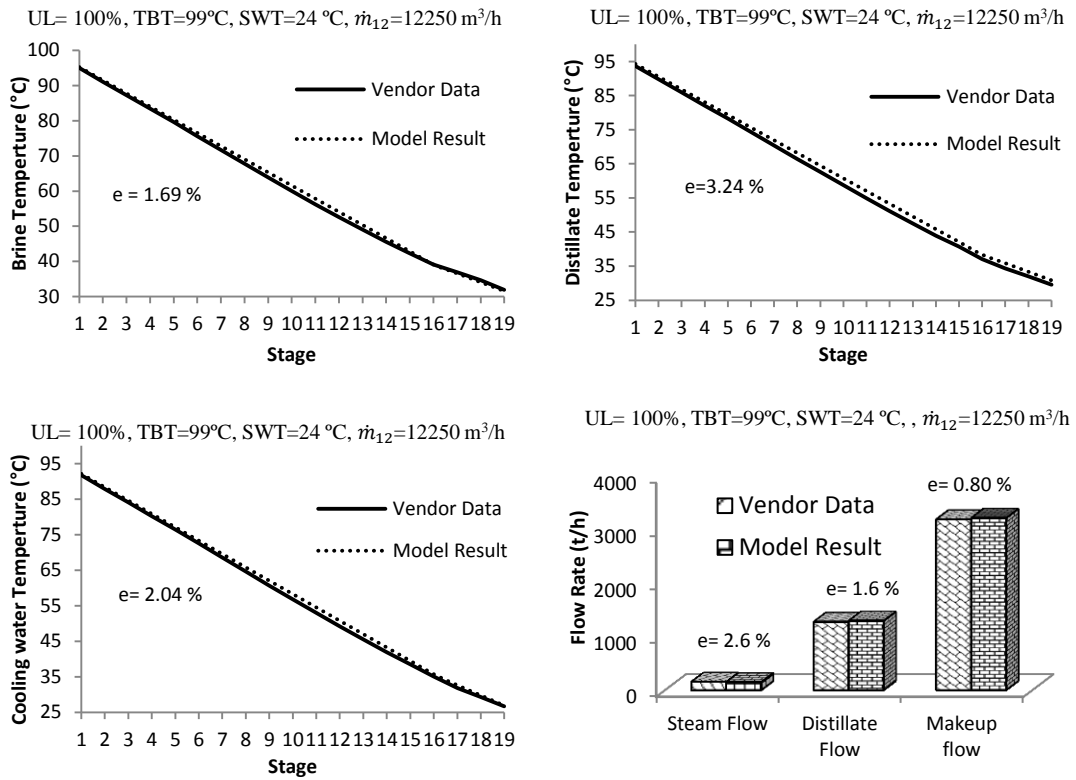


Figure 6.4: Comparison between model and vendor data at 24°C SWT and 100% UL

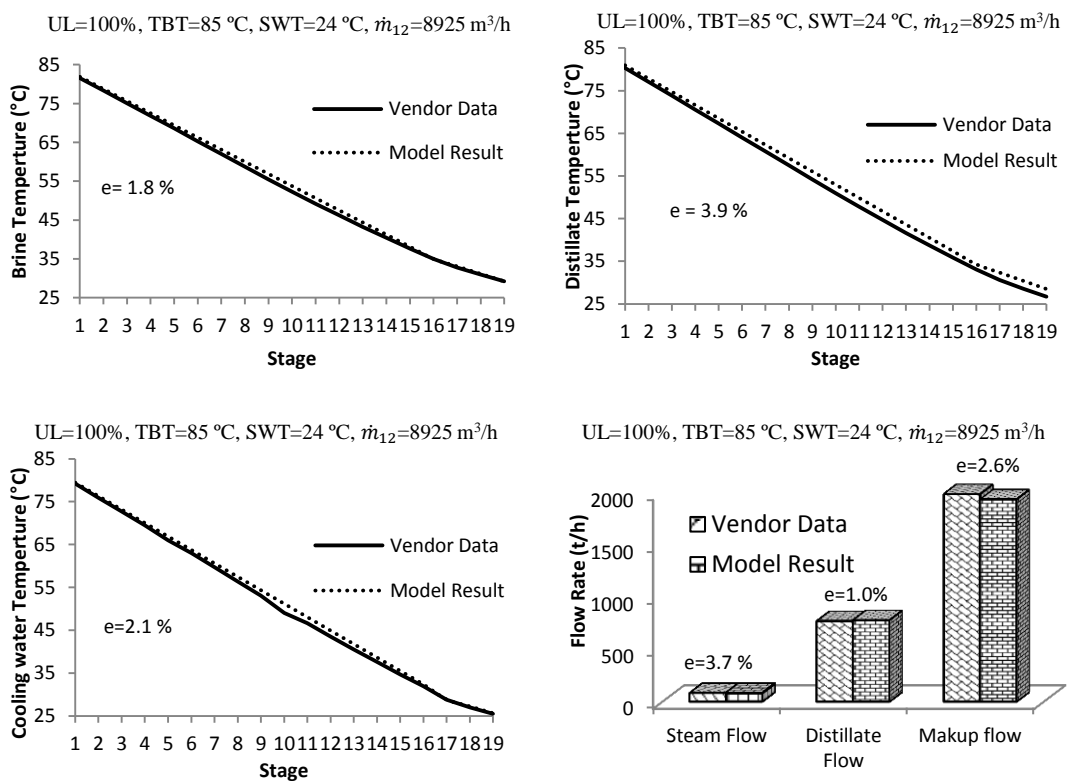


Figure 6.5: Comparison between model and vendor data at 24°C SWT and 60% UL

Stream No. (Figure 6.1)	Composition	Flow	Temperature	Pressure	Salinity	Enthalpy	Entropy	Specific volume
1	Seawater	Set	Set	Set	Set	Cal.	-	Cal.
2	Seawater	Cal.	Cal.	Cal.	Cal.	Cal.	-	Cal.
3	Seawater	Cal.	Cal.	Cal.	Cal.	Cal.	-	Cal.
4	Seawater	Cal.	Cal.	Cal.	Cal.	Cal.	-	Cal.
5	Seawater	Cal.	Cal.	Cal.	Cal.	Cal.	-	Cal.
6	Seawater	Cal.	Cal.	Cal.	Cal.	Cal.	-	Cal.
7	Seawater	Cal.	Cal.	Cal.	Cal.	Cal.	-	Cal.
8	Seawater	Cal.	Cal.	Cal.	Cal.	Cal.	-	Cal.
9	Seawater	Cal.	Cal.	Set	Set	Cal.	-	Cal.
10	Seawater	Cal.	Cal.	Cal.	Cal.	Cal.	-	Cal.
11	Seawater	Cal.	Cal.	Cal.	Cal.	Cal.	-	Cal.
12	Seawater	Set	Cal.	Cal.	Cal.	Cal.	-	Cal.
13	Seawater	Cal.	Cal.	Cal.	Cal.	Cal.	-	Cal.
14	Seawater	Cal.	Set	Cal.	Cal.	Cal.	-	Cal.
15	Seawater	Cal.	Cal.	Cal.	Cal.	Cal.	-	Cal.
16	Water	Cal.	Set	Cal.	-	Cal.	Cal.	Cal.
17	Water	Cal.	Cal.	Cal.	-	Cal.	Cal.	Cal.
18	Water	Cal.	Cal.	Set	-	Cal.	Cal.	Cal.
19	Water	Cal.	Cal.	Cal.	-	Cal.	Cal.	Cal.
20	Water	Cal.	Cal.	Cal.	-	Cal.	Cal.	Cal.
21	Water	Cal.	Cal.	Set	-	Cal.	Cal.	Cal.

Table 6.1: Set (input) and Calculated (output) values for MSF desalination model

6.4 MSF energy and exergy analysis

Energy and exergy analyses of MSF unit are rarely covered in the literature [72–74]. In particular, no previous study appears to have included details of all MSF stages in

an exergy analysis to investigate why this type of desalination exhibits low exergy efficiency.

Variation of any MSF model input parameter causes responses for all dependent unit variables to achieve a new equilibrium state. Therefore, energy and exergy analyses of the MSF unit are performed at full load condition (most operated case) and SWT of 27°C (the annual average SWT). Model outputs are used to calculate unit standard performance indicators, including steam consumption, distillate production, performance ratio, CR, electrical power consumption (EPC), power/water ratio (P/W ratio) and specific heat consumption (SHC). Table 6.2 shows these values, which fall in the range of design values for the unit studied.

Performance indicator	Unit	Result
Steam consumption	t/h	150.5
Water production	m ³ /h	1274
Performance ratio	–	8.47
Concentration ratio	–	1.67
P/W ratio	kWh/m ³	4.68
Specific heat consumption	kWh/m ³	73.2

Table 6.2: Model results for unit performance indicators

Table 6.3 shows the calculated thermodynamic properties for all numbered streams in Figure 6.1. Since all exit streams go from their exit state to the dead state for the purposes of exergy analysis, selection of the dead state (exergy datum) varies according to the researcher's objectives [46]. In this current exergy analysis, the dead state has been selected at $P_0 = 101.3$ kPa, $w_{s,0} = 40$ g/kg, and $T_0 = 27^\circ\text{C}$, which matches the average seawater intake parameters. The corresponding calculated dead state enthalpy (h_0) and entropy (s_0) of water and seawater are 114 (kJ/kg), 0.398 (kJ/(kg.K)), and 108 (kJ/kg) and 0.376 (kJ/(kg.K)), respectively. The last four streams (6-A, 9-A, 18-A, 21-A) in Table (6.3) represent the residual exergy when they move to the dead state at (P_0, T_0) to calculate the minimum separation work (W_{\min}) as explained in Section 4.1.2.

Stream	p (kPa)	T (°C)	w _s (g/kg)	\dot{m} (kg/s)	h (kJ/kg)	s (kJ/(kg.K))	e _{ph} (kJ/kg)	e _{ch} (kJ/kg)	e _T (kJ/kg)	E _T (MW)
1	101	27.2	40.0	2931	108	0.376	0.000	0.000	0.00	0.00
2	300	27.3	40.0	2931	108	0.376	0.193	0.000	0.19	0.57
3	210	36.2	40.0	2931	144	0.493	0.601	0.000	0.60	1.76
4	210	36.2	40.0	878.3	144	0.493	0.601	0.000	0.60	0.53
5	5.26	36.3	40.0	878.3	144	0.493	0.407	0.000	0.41	0.36
6	210	36.2	40.0	2054	144	0.493	0.601	0.000	0.60	1.24
7	5.26	34.5	67.0	3221	131	0.442	3.38	-2.52	0.87	2.79
8	5.26	34.5	67.0	524.4	131	0.442	3.38	-2.52	0.87	0.45
9	240	34.5	67.0	524.4	132	0.443	3.61	-2.52	1.09	0.57
10	5.26	34.5	67.0	2697	131	0.442	3.38	-2.52	0.87	2.34
11	5.26	35.0	60.4	3575	134	0.455	2.56	-1.90	0.66	2.35
12	685	35.1	60.4	3575	135	0.456	3.22	-1.90	1.32	4.72
13	109	90.5	60.4	3575	351	1.103	25.1	-1.90	23.25	83.10
14	88.5	97.2	60.4	3575	378	1.174	29.8	-1.90	27.95	99.92
15	7.89	42.0	66.2	3260	160	0.536	4.30	-2.44	1.86	6.05
16	148	111.0	0	41.79	2692	7.227	41.0	3.73	530	22.2
17	148	105.7	0	41.79	433	1.371	36.2	3.73	42.18	1.76
18	1058	105.9	0	41.79	433	1.371	47.2	3.73	43.01	1.80
19	7.89	41.3	0	315.0	173	0.589	0.744	3.73	4.47	1.41
20	5.26	33.8	0	353.9	142	0.488	-0.290	3.73	3.44	1.22
21	200	33.8	0	353.9	142	0.489	-0.090	3.73	3.64	1.29
6-A	101	27.2	40.0	2932	108	0.376	0.000	0.00	0.00	0.00
9-A	101	27.2	67.0	524.36	103	0.350	3.17	-2.52	0.66	0.34
18-A	101	27.2	0	41.79	114	0.398	-0.485	3.73	3.24	0.14
21-A	101	27.2	0	353.9	114	0.398	-0.485	3.73	3.24	1.15

Table 6.3: Thermodynamic properties of the indicated streams

The negative for either physical or chemical exergy in Table 6.3 is obtained when the stream is below the dead state condition. Interestingly, the above results validate the osmosis principle. The chemical exergy of the pure water (stream 21-A) is higher than the seawater (stream 9-A), which leads to the flow of the water towards seawater if both are in a container separated by a membrane at the same atmospheric pressure.

Table 6.4 summarizes the exergy analysis (all the numbered total exergies E_n in this calculation refer to the stream number in Figure 6.1). Equation 4.40 is applied to

calculate the overall exergy efficiency of the unit. The input exergy to the unit is the sum of the heating steam and pump work inputs (pump efficiency is assumed to be typically 75% [72, 74]). The output minimum separation work (for the exergy efficiency) is the sum of the discharge distillate and the discharge brine relative to the entering exergy of the cooling water to the unit. Exergy destruction in the unit components is evaluated by the differences between the input and output exergies of the individual components.

Equipment	Calculation Method	Result	Unit
Seawater pump exergy in	$E_2 - E_1$	0.567	MW
Brine recycle pump exergy in	$E_{12} - E_{11}$	2.37	MW
Blow down pump exergy in	$E_9 - E_8$	0.119	MW
Distillate pump exergy in	$E_{21} - E_{20}$	0.071	MW
Condensate Pump exergy in	$E_{18} - E_{17}$	0.035	MW
Pump input exergy in	$E_{PP} = (1/0.75) \times (\Sigma ((E_2 - E_1) + (E_{21} - E_{20}) + (E_{12} - E_{11}) + (E_9 - E_8) + (E_{18} - E_{17})))$	4.21	MW
Heating steam exergy	E_{16}	22.2	MW
Exergy in	$E_{16} + E_{PP}$	26.4	MW
Minimum separation work	$W_{min} = E_{(9-A)} + E_{(21-A)} - E_{(1-A)}$	1.49	MW
Exergy efficiency	$\eta_{II} = \frac{W_{min}}{E_{16} + E_{PP}}$	5.66	%
Total exergy destruction	$E_d = E_{Input} - E_{Output}$ $E_d = (E_{16} + E_P) - W_{min}$	24.9	MW
Exergy destroyed in pumps	$E_{d,PP} = (1 - 0.75) \times E_{PP}$	1.05	MW
Exergy destroyed in brine heater	$E_{d,BH} = (E_{16} + E_{13} - E_{14} - E_{17})$	3.57	MW
Exergy destroyed in HRC stages	$E_{d,HRC} = (E_{14} + E_{12} - E_{15} - E_{19} - E_{13})$	14.1	MW
Exergy destroyed in HRJ stages	$E_{d,HRJ} = (E_{15} + E_{19} + E_5 + E_2 - E_8 - E_{20} - E_{11} - E_3)$	2.60	MW
Exergy destroyed in cooling	$E_{d,C} = E_6$	1.24	MW
Exergy destroyed in product	$E_{d,P} = (E_{21} - E_{(21-A)})$	0.140	MW
Exergy destroyed in brine disposal	$E_{d,B} = (E_9 - E_{(9-A)})$	0.230	MW
Exergy destroyed in condensate disposal	$E_{d,C0} = (E_{18} - E_{(18-A)})$	1.66	MW
Exergy destroyed in throttling valve	$E_{d,Th} = (E_4 - E_5)$	0.170	MW

Table 6.4: MSF exergy analysis results

Consequently, Figure 6.6 shows the percentage exergy destruction as a ratio of the component exergy destruction to the total exergy destruction of the MSF unit [78]. The results show that the overall exergy efficiency of the MSF unit studied is only 5.8%. More than 64% of the exergy destruction occurs in the MSF evaporator, shared between 54% at the heat recovery stages 1–16 and only 10% at the heat rejection stages 17–19. Pumps, brine heater, and streams' disposal to the dead state each contribute 4%, 17%, and 13%, respectively to the overall exergy destruction, in general agreement with most published studies of exergy analysis for MSF desalination units [72–74].

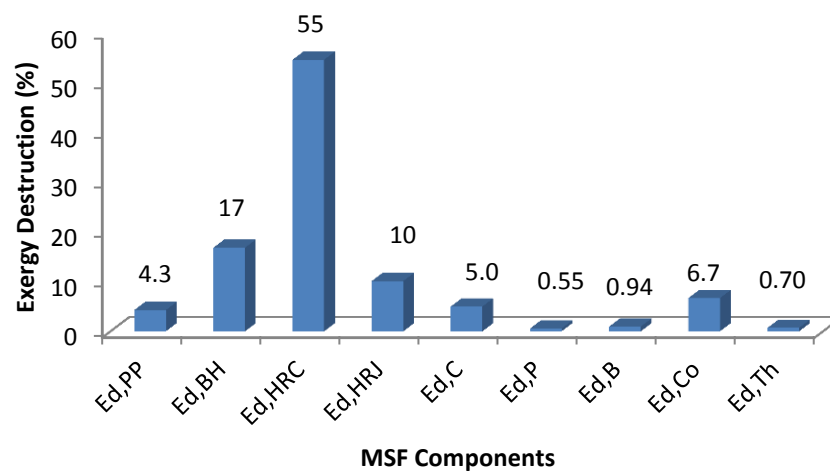


Figure 6.6: Exergy Destruction (%) in MSF desalination components.

(For key to abbreviations see Nomenclature)

However, going beyond these previous studies, this current study covers the detail of the location of the exergy destruction in the MSF unit as a first initiating step for future improvement and enhancement of the unit. During this detailed stage exergy analysis, it is essential that the sum of the individual stage exergy destructions matches the overall exergy destruction given in Table 6.4. To carry out a detailed exergy analysis of all the stages using Equation 4.41 to calculate the stage exergy destruction and stage efficiency, the stage inlet and outlet parameters for the cooling water, distillate, and brine are listed in Tables 6.5, 6.6, and 6.7.

Stage	Seawater Cooling Inlet						Seawater cooling Outlet					
	Mass Flow \dot{m} (kg/s)	Temperature T ($^{\circ}$ C)	Pressure P (bar)	Salinity w_s (g/kg)	Specific Exergy, e_T (kJ/kg)	Total Exergy E_T (MW)	Mass Flow \dot{m} (kg/s)	Temperature T ($^{\circ}$ C)	Pressure P (bar)	Salinity w_s (g/kg)	Specific Exergy, e_T (kJ/kg)	Total Exergy E_T (MW)
1	3575	87.0	1.45	60	21.0	75.0	3575	90.5	1.09	60	23.2	83.1
2	3575	83.6	1.81	60	18.8	67.4	3575	87.0	1.45	60	21.0	75.0
3	3575	80.1	2.17	60	16.8	60.1	3575	83.6	1.81	60	18.8	67.4
4	3575	76.6	2.53	60	14.9	53.1	3575	80.1	2.17	60	16.8	60.1
5	3575	73.2	2.89	60	13.0	46.6	3575	76.6	2.53	60	14.9	53.1
6	3575	69.7	3.25	60	11.3	40.6	3575	73.2	2.89	60	13.0	46.6
7	3575	66.2	3.61	60	9.80	34.9	3575	69.7	3.25	60	11.3	40.6
8	3575	62.8	3.97	60	8.30	29.6	3575	66.2	3.61	60	9.80	34.9
9	3575	59.3	4.33	60	7.00	24.9	3575	62.8	3.97	60	8.30	29.6
10	3575	55.9	4.69	60	5.70	20.5	3575	59.3	4.33	60	7.00	24.9
11	3575	52.4	5.05	60	4.70	16.6	3575	55.9	4.69	60	5.70	20.5
12	3575	48.9	5.41	60	3.70	13.2	3575	52.4	5.05	60	4.70	16.6
13	3575	45.5	5.77	60	2.90	10.3	3575	48.9	5.41	60	3.70	13.2
14	3575	42.0	6.13	60	2.20	7.90	3575	45.5	5.77	60	2.90	10.3
15	3575	38.5	6.49	60	1.70	6.10	3575	42.0	6.13	60	2.20	7.90
16	3575	35.1	6.85	60	1.30	4.70	3575	38.5	6.49	60	1.70	6.10
17	2932	33.2	2.40	40	0.30	1.00	2932	36.2	2.10	40	0.60	1.80
18	2932	30.2	2.70	40	0.20	0.60	2932	33.2	2.40	40	0.30	1.00
19	2932	27.3	3.00	40	0.20	0.60	2932	30.2	2.70	40	0.20	0.60

Table 6.5: Cooling water inlet/outlet stage parameters

Stage	Distillate water Inlet						Distillate water Outlet					
	Mass Flow \dot{m} (kg/s)	Temperature T ($^{\circ}$ C)	Pressure P (bar)	Salinity w_s (g/kg)	Specific Exergy, e_T (kJ/kg)	Total Exergy E_T (MW)	Mass Flow \dot{m} (kg/s)	Temperature T ($^{\circ}$ C)	Pressure P (bar)	Salinity w_s (g/kg)	Specific Exergy, e_T (kJ/kg)	Total Exergy E_T (MW)
1	0	0.0	0.000	0	0.0	0	21.3	92.8	0.780	0	29.4	0.63
2	21.3	92.8	0.780	0	29.4	0.63	42.4	89.4	0.685	0	26.8	1.14
3	42.4	89.4	0.685	0	26.8	1.14	63.2	85.9	0.600	0	24.4	1.54
4	63.2	85.9	0.600	0	24.4	1.54	83.8	82.5	0.524	0	22.1	1.85
5	83.8	82.5	0.524	0	22.1	1.85	104	79.1	0.456	0	19.9	2.08
6	104	79.1	0.456	0	19.9	2.08	124	75.6	0.396	0	17.9	2.22
7	124	75.6	0.396	0	17.9	2.22	144	72.2	0.343	0	15.9	2.30
8	144	72.2	0.343	0	15.9	2.30	164	68.7	0.296	0	14.1	2.32
9	164	68.7	0.296	0	14.1	2.32	184	65.3	0.254	0	12.5	2.29
10	184	65.3	0.254	0	12.5	2.29	203	61.9	0.217	0	10.9	2.21
11	203	61.9	0.217	0	10.9	2.21	222	58.4	0.186	0	9.48	2.11
12	222	58.4	0.186	0	9.48	2.11	241	55.0	0.158	0	8.20	1.98
13	241	55.0	0.158	0	8.20	1.98	260	51.6	0.133	0	7.05	1.83
14	260	51.6	0.133	0	7.05	1.83	278	48.1	0.113	0	6.05	1.68
15	278	48.1	0.113	0	6.05	1.68	297	44.7	0.094	0	5.19	1.54
16	297	44.7	0.094	0	5.19	1.54	315	41.3	0.079	0	4.47	1.41
17	315	41.3	0.079	0	4.47	1.41	328	38.8	0.069	0	4.05	1.33
18	328	38.8	0.069	0	4.05	1.33	341	36.3	0.060	0	3.70	1.26
19	341	36.3	0.060	0	3.70	1.26	354	33.8	0.053	0	3.44	1.22

Table 6.6: Distillate water inlet/outlet stage parameters

Stage	Brine Inlet						Brine Outlet					
	Mass Flow \dot{m} (kg/s)	Temperature T ($^{\circ}\text{C}$)	Pressure P (bar)	Salinity w_s (g/kg)	Specific Exergy, e_T (kJ/kg)	Total Exergy E_T (MW)	Mass Flow \dot{m} (kg/s)	Temperature T ($^{\circ}\text{C}$)	Pressure P (bar)	Salinity w_s (g/kg)	Specific Exergy, e_T (kJ/kg)	Total Exergy E_T (MW)
1	3575	97.2	0.885	60.4	28.0	99.9	3554	93.8	0.780	60.7	25.5	90.5
2	3554	93.8	0.780	60.7	25.5	90.5	3533	90.3	0.685	61.1	23.1	81.6
3	3533	90.3	0.685	61.1	23.1	81.6	3512	86.9	0.600	61.5	20.8	73.1
4	3512	86.9	0.600	61.5	20.8	73.1	3491	83.4	0.524	61.8	18.6	65.1
5	3491	83.4	0.524	61.8	18.6	65.1	3471	80.0	0.456	62.2	16.6	57.6
6	3471	80.0	0.456	62.2	16.6	57.6	3451	76.5	0.396	62.5	14.6	50.5
7	3451	76.5	0.396	62.5	14.6	50.5	3431	73.1	0.343	62.9	12.8	43.9
8	3431	73.1	0.343	62.9	12.8	43.9	3411	69.6	0.296	63.3	11.1	37.8
9	3411	69.6	0.296	63.3	11.1	37.8	3391	66.2	0.254	63.6	9.49	32.2
10	3391	66.2	0.254	63.6	9.49	32.2	3372	62.7	0.217	64.0	8.01	27.0
11	3372	62.7	0.217	64	8.01	27.0	3353	59.3	0.186	64.4	6.66	22.3
12	3353	59.3	0.186	64.4	6.66	22.3	3334	55.8	0.158	64.7	5.43	18.1
13	3334	55.8	0.158	64.7	5.43	18.1	3315	52.4	0.133	65.1	4.33	14.4
14	3315	52.4	0.133	65.1	4.33	14.4	3297	48.9	0.113	65.5	3.37	11.1
15	3297	48.9	0.113	65.5	3.37	11.1	3278	45.5	0.094	65.8	2.54	8.33
16	3278	45.5	0.094	65.8	2.54	8.33	3260	42.0	0.079	66.2	1.86	6.05
17	3260	42.0	0.079	66.2	1.86	6.05	3247	39.5	0.069	66.5	1.45	4.71
18	3247	39.5	0.069	66.5	1.45	4.71	3234	37.0	0.060	66.7	1.12	3.61
19	3234	37.0	0.060	66.7	1.12	3.61	3221	34.5	0.053	67.0	0.870	2.79

Table 6.7: Brine inlet/outlet stage parameters

Consequently, Figures 6.7 and 6.8 show the exergy efficiency and exergy destruction of the heat recovery and heat rejection stages, respectively. These figures show that the exergy efficiency reduces gradually over the heat recovery stages from the high temperature to the low temperature stages, mainly because of the high evaporation rate in the early stages, reflecting a high production rate in these stages. In particular, stage 1 has maximum exergy efficiency not only because the maximum evaporation rate occurs but also because there is distillate production without an input exergy from an upstream distillate stream. The rates of increase of exergy efficiency and of

decrease of exergy destruction in the heat rejection stages are greater than for the heat recovery stages, but with similar trends. In particular, special consideration has to be taken in calculating the exergy efficiency and exergy destruction for the last stage because here, the mixing of the makeup and the brine takes place, resulting in poor exergy efficiency and high exergy destruction.

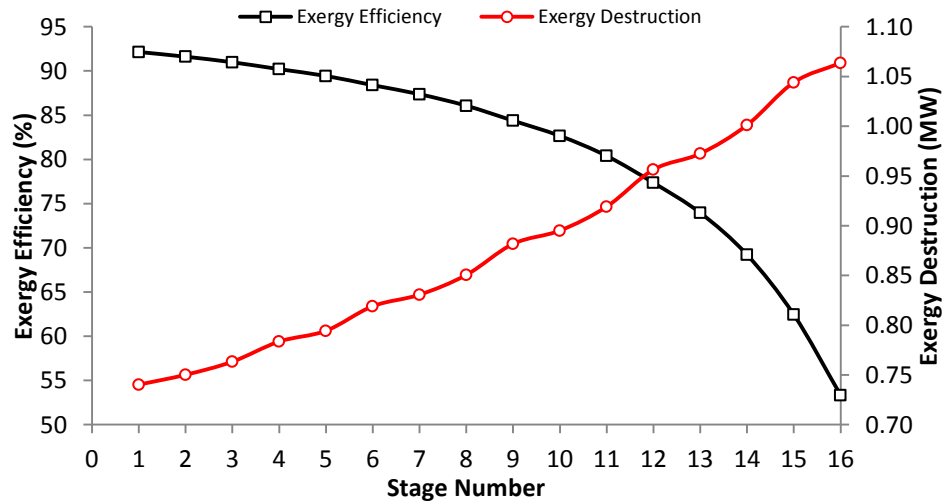


Figure 6.7: Exergy efficiency and exergy destruction of heat recovery stages

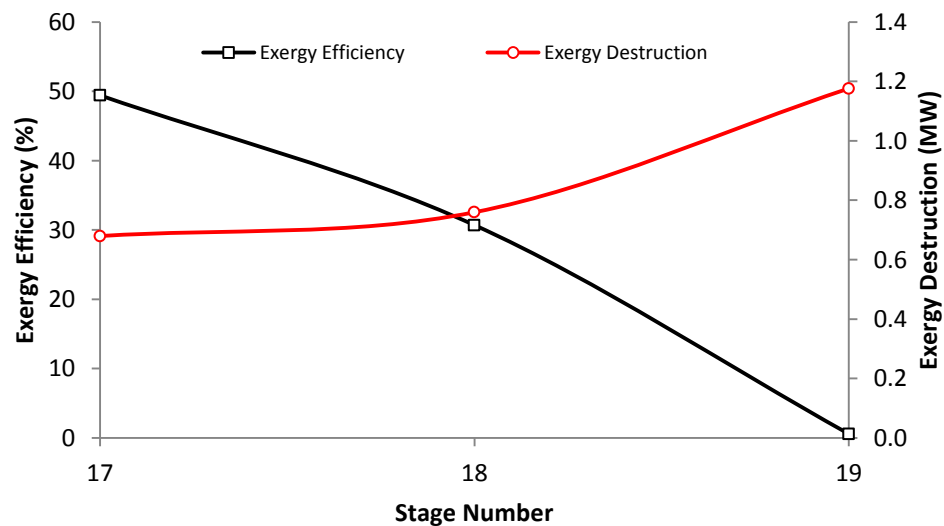


Figure 6.8: Exergy efficiency and exergy destruction of heat rejection stages

6.5 MSF exergy efficiency enhancement possibilities

Exergy efficiency of a cogeneration system depends on the sum of the net power generated (W_{\min} in MSF desalination) plus the net exergy of any heat stream out of

the system boundary [46, 163]. In the case of the typical MSF desalination unit analysed above, no outlet stream has a thermal energy that can be calculated as useful exergy out. However, the accumulated distillate production with high temperature after the condensation process moves from the first stage through to the last stage [85]. During this process, the distillate mass flow rate increases at each stage and the temperature reduces due to the reduction of pressure in the later stages. Most of the exergy leaving the early stages is destroyed in the vacuum system by subsequent mixing with stages at lower temperatures and pressure. Therefore, recovering the distillate water from the early stages and utilizing its exergy into another thermal process could enhance the exergy efficiency of MSF desalination.

Figure 6.9 illustrates the potential improvement of MSF unit exergy efficiency by recovering the accumulated distillate from the early stages. The exergy efficiency of this particular unit increases from the 5.7% calculated previously to 15%, with distillate recovery up to stage 8, reducing to 10% with distillate recovery up to stage 19. The continuous reduction of the accumulated distillate water exergy content is due to the reduction of the distillate temperature in spite of the increase of the accumulated mass flow rate as can be seen from Table 6.6. This combination of mass flow rate and the working temperature of the thermal process are the two main parameters that will identify the optimum stage up to which distillate extraction could be beneficial in any particular plant. The recovered hot water can be utilized for heat input to thermal processes, such as MED, AC, district heating, and ORC [92, 164]. The primary desalination process requirements will influence the selection of this thermal process.

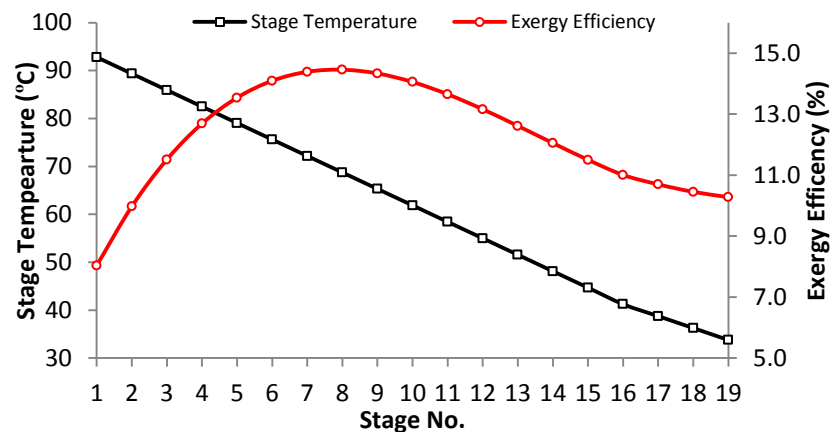


Figure 6.9: MSF exergy enhancement by recovering hot distillate water

6.6 MSF parametric analysis

Operation of the MSF unit is subject to continuous variation due to external factors such as seawater feed temperature and seawater feed salinity and operational factors like UL, seawater feed flow, brine recirculation flow, and brine recirculation temperature. This dynamic nature of the system requires a parametric study of the effect of these variations to identify the optimal operational condition and to provide a clear understanding of the response of these variables on the unit from the technical and economical sides. Consequently, a parametric analysis was performed to discover the influence of these variations on unit: distillate production, Performance Ratio (PR), Specific Heat Consumption (SHC), P/W ratio, Exergy Efficiency (η_{II}), and Total Power Consumption (TPC).

6.6.1 MSF Unit load variations

A simple example of the interdependence of the MSF unit operating variables can be obtained by the varying UL from the maximum vendor operating condition of 100% UL and to a minimum at 60% UL. This change in UL is followed by linear changes in brine recirculation flow, steam flow, makeup flow, and rejected brine flow, to maintain the mass and salt balance of the new equilibrium condition. Figure 6.10 describes the respond of these variable as a result of the UL variation.

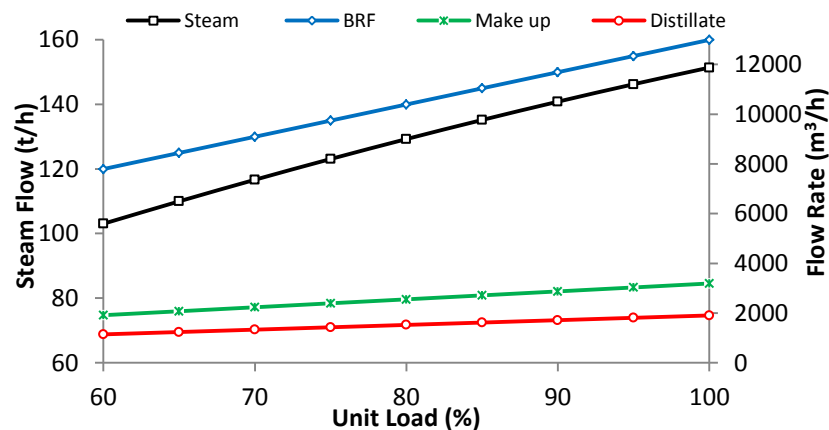


Figure 6.10: Variation of unit variables as the UL changes

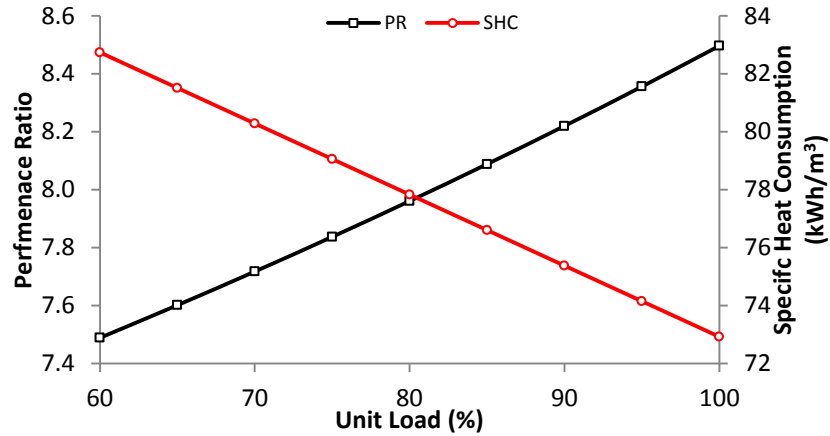


Figure 6.11: PR and SHC versus load variation

Moreover, the PR varies from low value of 7.49 at 60 % UL and exhibits a maximum of 8.49 at 100% UL. This can be explained by the 3% reduction in SHC for every 10% load change (Figure 6.11). Reduction of the PR as the load increases can be justified from the exergy analysis. The exergy efficiency of the unit rises by 3.2% for every 10% UL increase due to high exergy destruction in the brine heater and heat rejection stages at low UL, although there is slight exergy destruction improvement in the disposed streams. In addition, the pump's exergy destruction is not linear, which can be clarified from the pump characteristics curves and is shown in the P/W ratio (Figure 6.12). Appendix 6-B shows the detailed exergy analysis for the load variation.

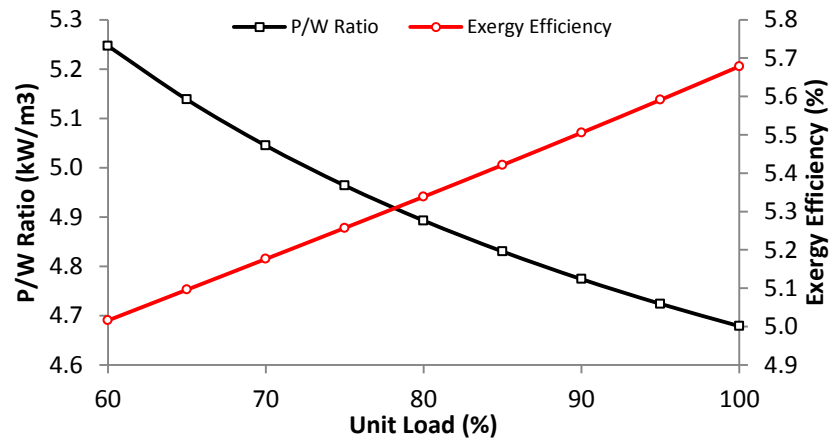


Figure 6.12: P/W ratio and exergy efficiency versus load change

6.6.2 Seawater feed temperature (T_1)

Variation of seawater inlet temperature was investigated at constant steam consumption ($\dot{m}_{16} = 151 \text{ t/h}$), brine recirculation flow ($\dot{m}_{12} = 12873 \text{ m}^3/\text{h}$), and CR of 1.67. An increase of 1°C in T_1 enhances distillate production by 0.12% due to the raise in the heat absorption in heat rejection, which causes an increase in the brine recirculation temperature (Figure 6.13). More flow for makeup and rejected brine is observed due to this variation in T_1 , to maintain the unit salt balance within the cycle. Moreover, this increase in T_1 rises the PR by 0.13% for each 1°C increase because of reduction in the SHC, that is, more distillate is produced with the same steam consumption (Figure 6.13).

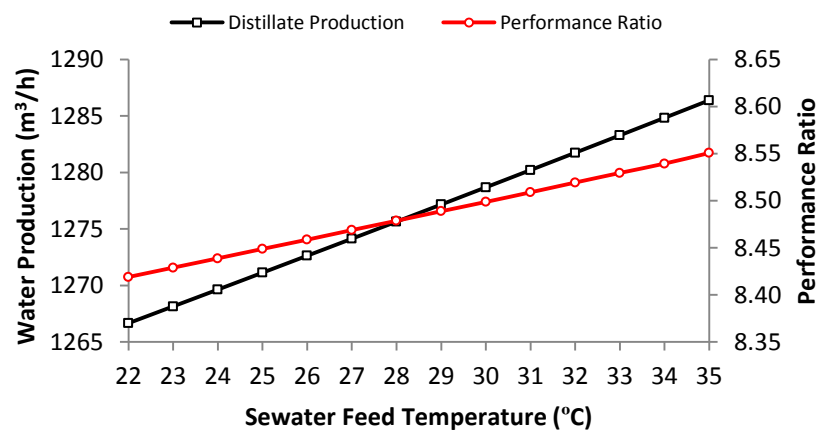


Figure 6.13: Effect of seawater feed temperature variation on distillate production and PR

Figure 6.14 presents the respond of exergy efficiency and P/W ratio change in T_1 . A 1°C variation a causes 0.5% and 0.2% rise in exergy efficiency and P/W ratio, respectively. This increase in exergy efficiency reflects the rise in W_{\min} because of more distillate production, in spite of the rise in pumping power, which is reflected by an increasing P/W ratio. Appendix 6-B describes the detailed effect of a seawater feed temperature (T_1) change on unit performance indicators and component exergy destruction.

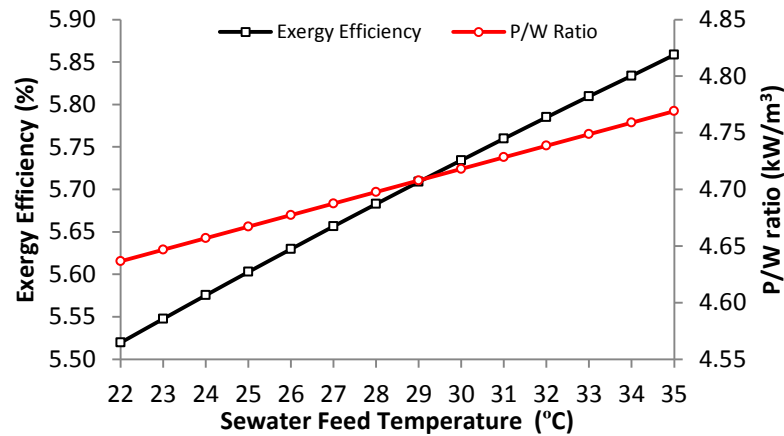


Figure 6.14: Effect of seawater feed temperature variation on exergy efficiency and P/W ratio

The trend shown in Figure 6.14 suggests the possibility of recovering heat from other thermal sources to increase SWT T_1 . The main reason for not investigating this option in MSF is that more than 30% of the seawater feed will be rejected back to the sea, which makes this a nonviable economical option. Another technical reason for increasing T_1 causes an increase in temperature of the heat rejection stages, which affects the performance of the vacuum ejector system considerably.

6.6.3 Seawater feed salinity ($w_{s,1}$)

The influence of the seawater salinity is investigated for the 35–45 g/kg range at a constant unit load, TBT, and brine recirculation flow (\dot{m}_{12}). Both makeup flow (\dot{m}_5) and rejected brine flow (\dot{m}_9) respond to the salinity change, by increasing flow to maintain the inlet salinity for the HRC stages at 60 g/kg. It was observed from the seawater enthalpy calculation that it increases with salinity; therefore, increasing unit salinity reduces the steam consumption and enhances performance ratio, but by less than 0.3% (Figure 6.15).

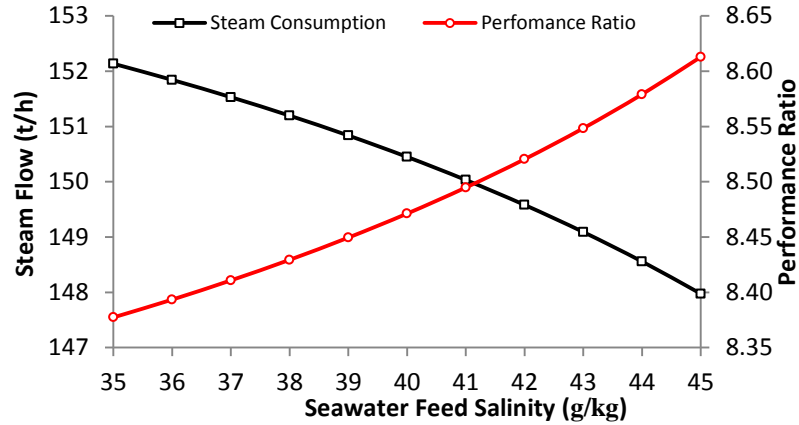


Figure 6.15: Influence of seawater feed salinity change on steam consumption and PR

Thus, the exergy efficiency rises with increasing seawater feed salinity, due to an increase in the inlet enthalpy, despite the increases in makeup, rejected brine, and condensate pump power consumption (as results of flow increases). Figure 6.16 presents the influence of seawater feed salinity variation on both exergy efficiency and the pump’s power consumption (PC), and Appendix 6-B shows a detailed unit response to feed salinity change.

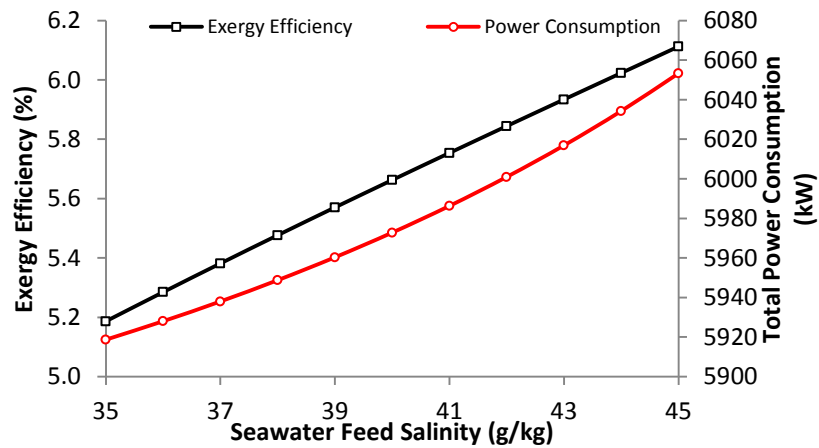


Figure 6.16: Influence of seawater feed salinity change on exergy efficiency and PC

However, an important design and operation limitation should be mentioned for the variation in the seawater feed salinity. The increase in seawater feed salinity causes a rise in concentration ratio, which can enhance the scaling phenomenon in the unit and increase the requirement for anti-scalant, resulting in significant increase of maintenance and operation costs.

6.6.4 Seawater feed flow (\dot{m}_1)

It is informative to examine the influence of the seawater feed flow on unit performance by running the model for a range of values of seawater feed flow. This influence was checked at constant UL, TBT, make up seawater flow (\dot{m}_5), rejected brine flow (\dot{m}_9), and brine recirculation flow (\dot{m}_{12}). As the seawater feed flow reduced, the steam flow reduces and thus the PR was enhanced as shown in Figure 6.17. This can be explained by the increase in the last stage temperature, which has a significant influence on the HRC stages and brine heater temperature profile; therefore, steam consumption reduces for same TBT value.

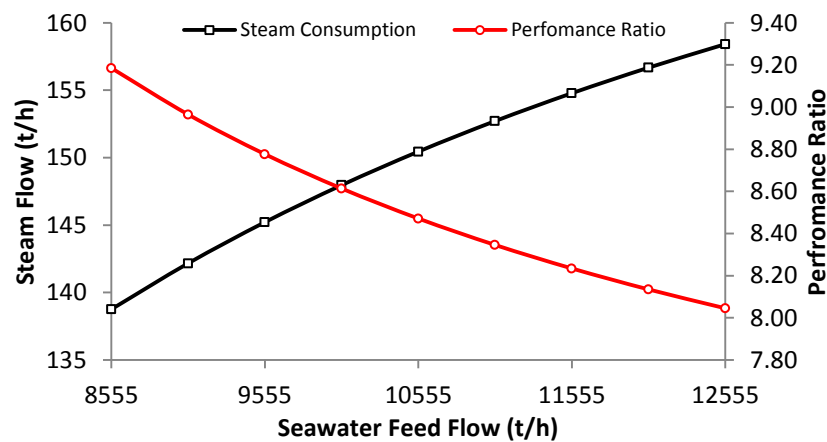


Figure 6.17: Influence of seawater feed flow on steam consumption and PR

A 500 t/h rise in seawater feed flow reduces exergy efficiency by 2% (Figure 6.18). This trend is due to the increase in exergy destruction of the HRC stages at higher flow and lower HRC stage inlet temperatures, with relatively insignificant changes of exergy destruction in other components. Moreover, using more inlet seawater consumed more electrical pumping power, which results in a reduction in the exergy efficiency of the MSF unit. Appendix 6-B shows the details of the exergy calculations. However, the operation engineers raised an operational concern. Reducing this flow causes an increase in heat rejection stage temperatures, which can affect the evaporation rate, especially at high SWTs and therefore, distillate production is reduced. Therefore, with this reduction in flow, a modification in the vacuum system to adjust the evaporation rate is suggested to remove the excess non-condensable gases produced.

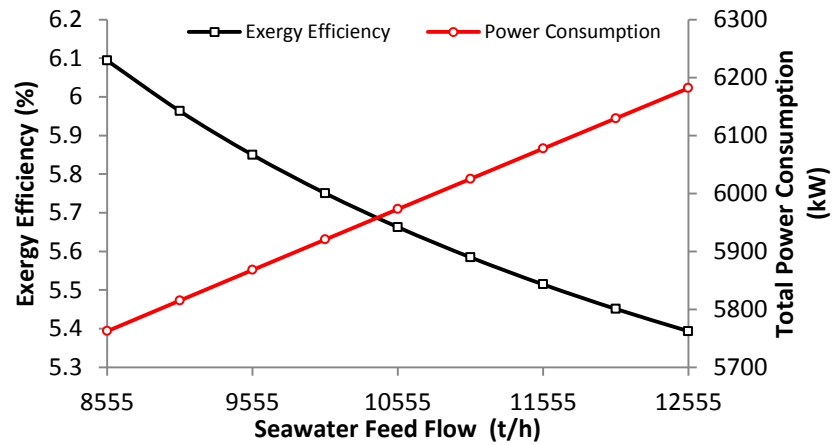


Figure 6.18: Influence of seawater feed flow on exergy efficiency and PC

6.6.5 Brine recirculation flow (\dot{m}_{12})

The influence of brine recirculation flow was examined by variation of the flow from 100% to 60% at constant TBT and CR. Other variables: steam flow (\dot{m}_{16}), distillate production (\dot{m}_{21}), makeup flow (\dot{m}_5), and rejected brine flow (\dot{m}_9) respond to this change proportionally to maintain the new equilibrium condition (Figure 6.19).

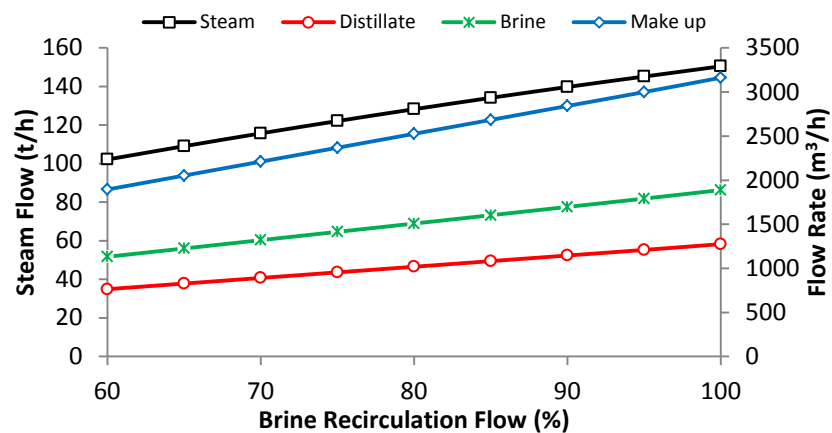


Figure 6.19: Influence of brine recirculation flow on steam, distillate, rejected brine, and make up flow rates

Interestingly, the PR exhibits a reduction of 3.4% for every 10% decrease of brine recirculation flow (Figure 6.20). This is as a result of decline of the SHC to back up the energy and salt balance of the unit at the same TBT and stage temperature profile.

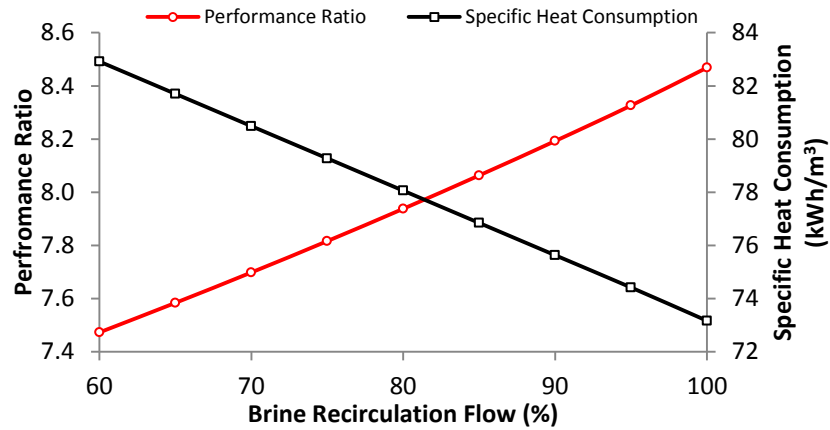


Figure: 6.20: Influence of brine recirculation flow on performance ration and specific heat consumption

Exergy efficiency declines by 3.2% for every 10% decrease in brine recirculation flow due to the reduction in distillate production, causing less W_{\min} to be achieved (Figure 6.21). Exergy destruction within the unit relatively stays without major changes, except the condensate disposal stream is reduced significantly as a result of the drop in condensate return to the power plant. Appendix 6-B presents the exergy analysis for the variation in brine recirculation flow.

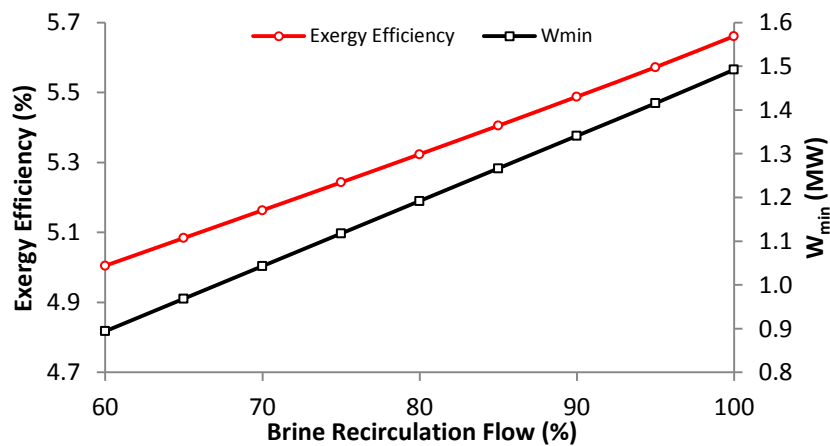


Figure: 6.21: Influence of brine recirculation flow on exergy efficiency and W_{\min}

6.6.6 Brine recirculation temperature (T_{12})

The variation in the brine recirculation temperature was investigated at constant make up flow (\dot{m}_5), rejected brine flow (\dot{m}_9), distillate production (\dot{m}_{21}), and TBT. The rise in brine recirculation temperature is followed by increase in the inlet temperature of all series connected stages until the brine heater inlet. Consequently,

holding TBT constant, the brine heater seawater inlet/outlet temperature difference ($T_{14} - T_{13}$) reduces, causing a significant steam flow reduction (16% for every 1°C increase in brine recirculation temperature). Thus, the PR changes by the same percentage at a constant unit load or distillate production (Figure 6.22).

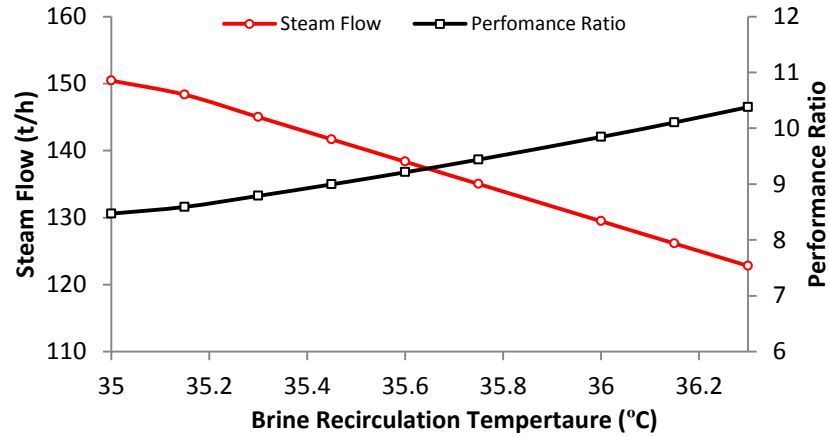


Figure 6.22: Effect of brine recirculation temperature on steam flow and PR

Furthermore, the unit overall exergy analysis is affected highly by the changes in brine recirculation temperature, and the exergy efficiency is enhanced by 11% for every 1°C rise in brine recirculation temperature for two reasons: firstly, a reduction in exergy destruction at the brine heater and HRC stages due to less specific heat consumption; secondly, decrease in the power consumption of the unit pumps, especially the condensate pump, due to the reduction of condensate return flow to power plant (\dot{m}_{18}). Figure 6.23 is plotted to explain this justification, and Appendix 6-B shows the detailed exergy analysis.

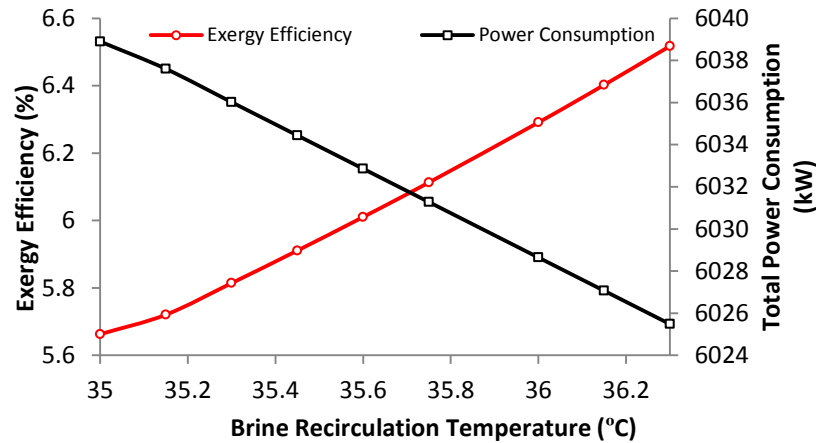


Figure 6.23: Effect of brine recirculation temperature change on exergy efficiency and unit PC

It is important to emphasise that if there is a possibility to utilize a heat source to increase brine recirculation temperature, the unit product cost could reduce significantly due to a sharp reduction in steam flow. Reduction in steam consumption for the three MSF units can either decrease the amount of natural gas used to produce this steam or it can generate more power if directed to the steam turbine.

6.7 Closing Remarks

The MSF desalination plant has been modelled and validated against vendor testing data at four different vendor testing conditions with the highest difference between the modelled and vendor data 3.9%.

The study found the MSF unit exergy efficiency was very low at only 5.7 %. The sources of exergy destruction were shared by the brine heater, heat recovery stages, heat rejection stages, pumps and streams disposal at 17 %, 55 %, 10 %, 4 % and 13 %, respectively. A unique exergy analysis of individual heat recovery and rejection stages pinpointed the exact sources of this exergy destruction. It was found the lowest exergy destruction occurs in the first heat recovery stage, increasing gradually in later stages (but more sharply in the heat rejection stages as would be expected). The study showed that the MSF desalination exergy efficiency could be improved

from 5.7 % to 15 % by recovering the hot distillate water from heat recovery stages 1 to 8, consequently providing a hot water source which can be utilized in other thermal processes (for example parametric study showed the unit is highly influenced by brine recirculation temperature).

Chapter 7

Performance enhancement of MSF desalination using recovered heat from stages

Chapter 6 revealed two features which can improve MSF unit performance: Firstly, a raising the brine recirculation temperature as revealed from the parametric study. Secondly, extracting the hot distillate from the MSF stages not only reduces the exergy destruction in the stages, but also provides a source that could power thermal technologies. This Chapter therefore, focuses on utilizing the extracted MSF stages hot distillate to power the simple form of heat exchanger (i.e. single pass shell and tube) to increase make-up temperature which results in brine recirculation temperature rise. Furthermore, the study will investigate the possibility of utilizing part of this recovered heat on other technologies to appraise the optimal level of heat utilization that ensures no impact on the performance of the original MSF desalination unit.

7.1 MSF desalination unit with Internal Heating (IH)

The parametric study of the MSF unit (Chapter 6) identified that raising the brine recirculation temperature slightly had a positive effect on the unit performance indicators. Therefore, this chapter discusses the possibility of recovering the heat from the hot distillate water extracted from the MSF stages to raise this temperature using the simplest configuration of heat exchanger, that is, a single pass shell and tube.

While investigating this possibility, it is important to discuss the effect of distillate extraction on the MSF unit performance. As was explained in the MSF desalination process description (Section 2.4.1), the condensed distillate moves from MSF stage to stage and re-flashes due to the pressure drop at each stage, as well as due to being re-condensed by the recycled brine in the tubes. Therefore, extraction of the hot distillate from each MSF stage (with reconnection to the suction of the distillate pump) will increase the heat transfer area, which could be utilized by the flashing brine at that stage and thus, increase unit production. On other hand, the hot distillate raising the brine recirculation temperature slightly was noticed; therefore, extracting the distillate could result in increasing the unit steam consumption. However, only part of the heat is transferred to the recycled brine due to the irreversibility produced from distillate re-flashing and re-condensing between stages. Consequently, heating the brine recirculation using an external heat exchanger will increase MSF unit production and reduce steam flow.

Sommoriva et al [12] discussed two ways of raising the brine recirculation temperature: direct heating of the recirculation or indirect by heating the make-up flow to the deaerator, which mixes later with the recycled brine. In this study, heating of the makeup flow was identified to be more beneficial than heating the brine recirculation directly. This is because the make-up flow is lower than the brine recirculation flow by almost 65% and a heat exchanger pressure drop would increase the brine recirculation pump power consumption. The study considers the extraction of the distillate from the first eight MSF stages, which guarantees better exergy efficiency (Figure 6.9) of the unit suitable temperature for powering low-grade heat recovery technologies. Figure 7.1 shows the extracted distillate mass flow rate and its temperature at the unit full load of the MSF and an average SWT of 27°C. Appendix 7-A provides the simulation results of the MSF model with IH recovering the heat from the first eight stages. The numbers in the table refer to the original MSF model in Figure 6.1.

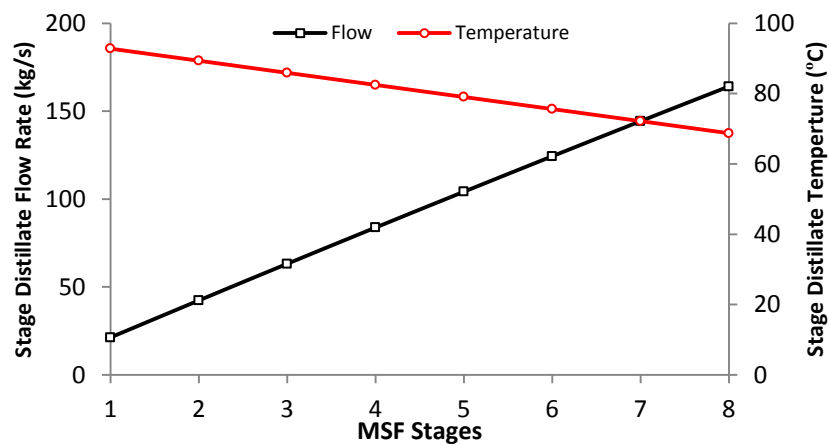


Figure 7.1: Extracted distillate mass flow rate and temperature at unit full load MSF and an average SWT of 27°C

The original IPSEpro model of the MSF was modified for further energy and exergy analysis (Figure 7.2) by adding the heat exchanger component for the make-up flow. The heat exchanger used IH within the MSF model is validated using the effectiveness and NTU method [149, 151]. Since the study considers recovery of the hot distillate water from different MSF stages having different mass flow rates and temperatures (Figure 7.1), heat exchanger effectiveness and NTU were maintained constant at an average of 0.85 and 1.95, respectively. These values were selected based on the most available industrial heat exchanger characteristics [105].

In this study, fouling of the heat exchanger was neglected due to the low brine recirculation temperature (average at 35°C), and it was assumed normal anti-scalant chemical injection was maintained [15]. It was found that as the number of MSF stages recovered increased, the heat exchange overall heat transfer conductance (UA) also increased (Figure 7.3), with a rise of 1 t/h in hot distillate water flow corresponding with a 1.9 kW/K increase in the overall heat transfer conductance of the heat exchanger.

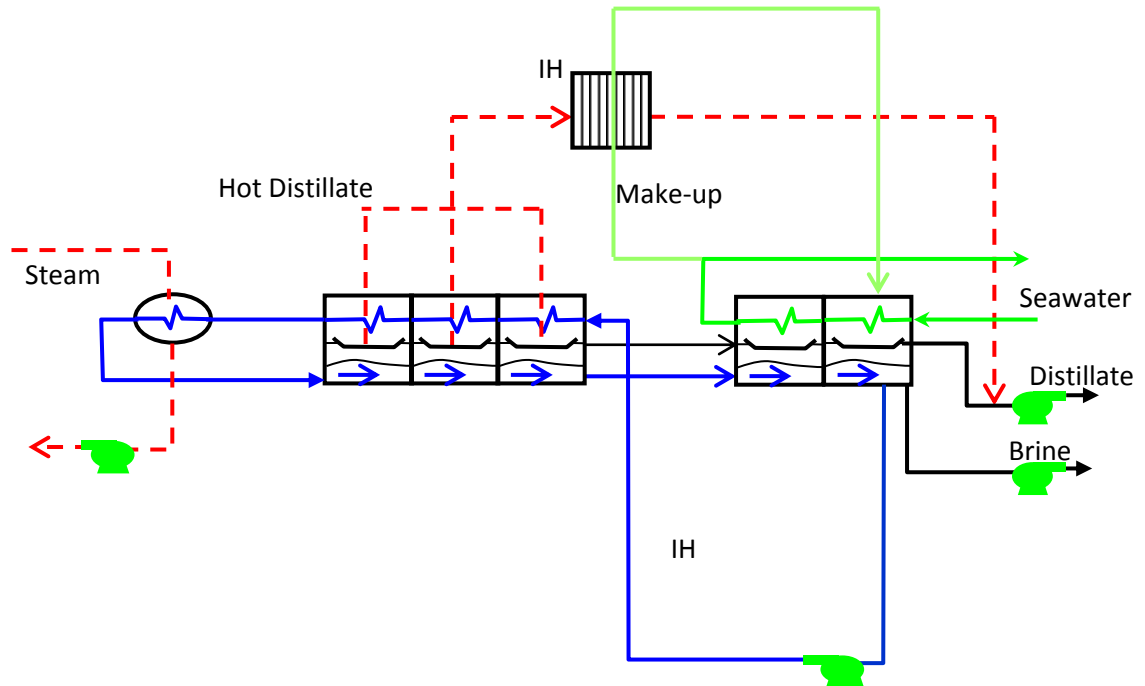


Figure 7.2: Schematic drawing of MSF desalination with IH

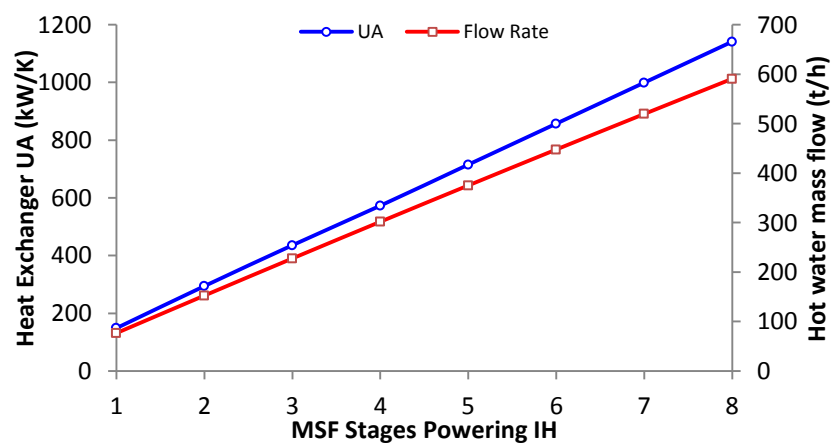


Figure 7.3: Effect of increasing number of MSF power stages on heat exchanger UA and distillate mass flow rate

7.2 MSF desalination unit with IH energy and exergy analyses

As the number of recovered distillate stages increases, the MSF unit production rises due to rise of the flashing temperature range ($T_{14}-T_{15}$). In contrast, steam consumption reduces as a result of the increase in brine heater inlet temperature (T_{13}) by heating the make-up. However, both curves in Figure 7.4 start to flatten at stage 8, proving that stage is the optimal maximum number of stages for distillate extraction (this agrees with the results found previously in Chapter 6). A 2.0% increase in unit production and a 4.9% decrease in steam consumption, respectively are found up to stage 8. Therefore, the MSF PR increases linearly from 8.4, at the original case, to 9.1 when extracting distillate from stage 8's power IH.

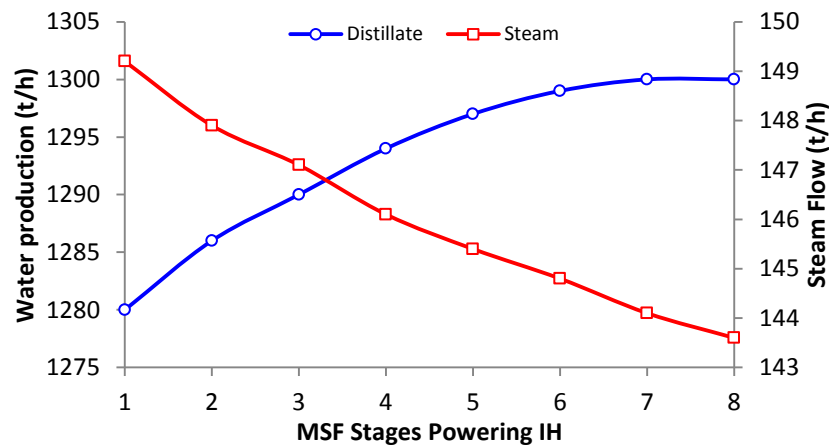


Figure 7.4: Effect of increasing number of MSF stages powering IH on unit production and steam flow

Extracting this distillate leads to a decrease of seawater cooling water flow and thus seawater feed pump power consumption, in agreement with other studies [10, 83], with a 7 kW power consumption decrease for every stage of distillate recovered (Figure 7.5). This decrease was because the heat of the accumulated distillate would otherwise have been rejected at the MSF heat rejection stages to the feed seawater, so distillate extraction reduces the amount of heat released to the seawater and consequently, the seawater flow can be reduced.

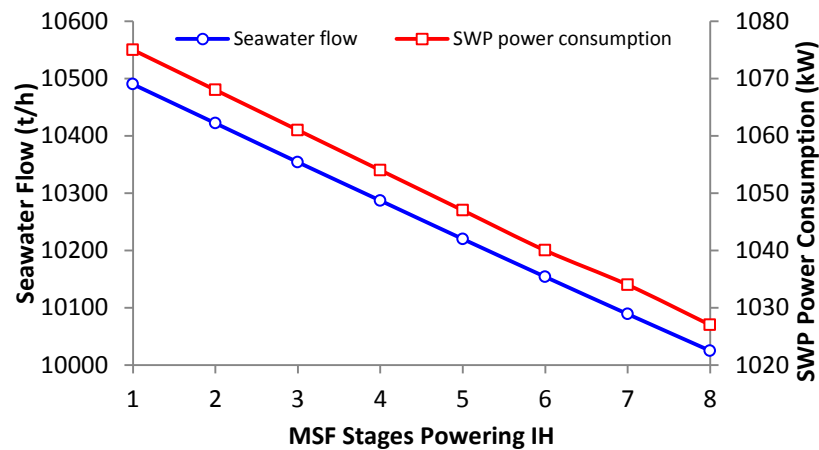


Figure 7.5: Reduction of seawater flow and seawater pump power consumption as MSF stages power increases

Exergy analysis of MSF with IH was performed at the same dead state selected in Chapter 6: $p_0 = 101.3$ kPa, $T_0 = 27^\circ\text{C}$, and $w_{s0} = 40$ g/kg. Recovering hot distillate water heat from MSF stages to power the IH, in principle, could improve the unit exergy efficiency compared with the original MSF, but taking into account the exergy destruction within the IH, this reduced to 7.3%. It should be mentioned that this enhancement was in addition to production enhancement up to 30 t/h of the distillate (at optimal stage). Otherwise, if the unit maintained the full load figure (1274 t/h), the exergy efficiency enhancement could reach up to 16%.

The impact on this enhancement is more from the higher temperature stages, reducing with further stages. This can be explained by the reduction in the steam feed flow to the unit, thus decreasing the input exergy to the unit while maintaining the original minimum separation work at almost the same level. Figure 7.6 shows MSF exergy enhancement, as the number of recovered stages increases through IH compared with the original MSF configuration. Furthermore, using MSF hot distillate water to power IH to increase the make-up temperature reduces the total exergy destruction of the MSF unit components compared with the original configuration. Figure 7.7 shows the reduction of the MSF unit total exergy destruction as a result of heat recovery from up to the eight stages compared with the original configuration.

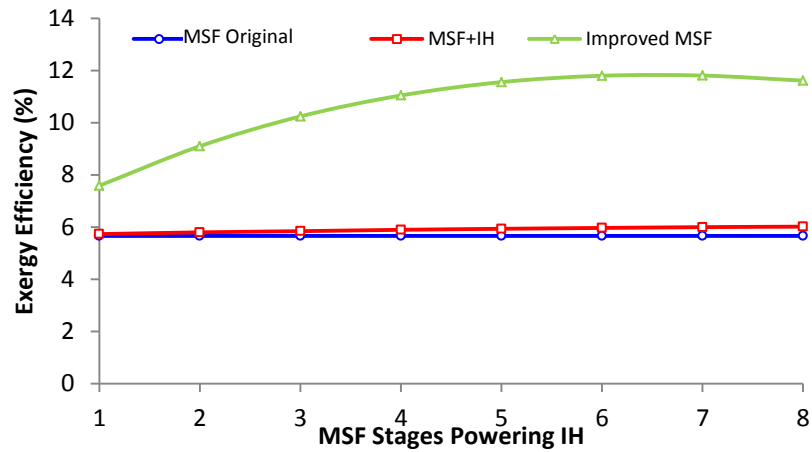


Figure 7.6: Exergy efficiency enhancement of the MSF desalination unit using IH powered by stage extracted hot distillate

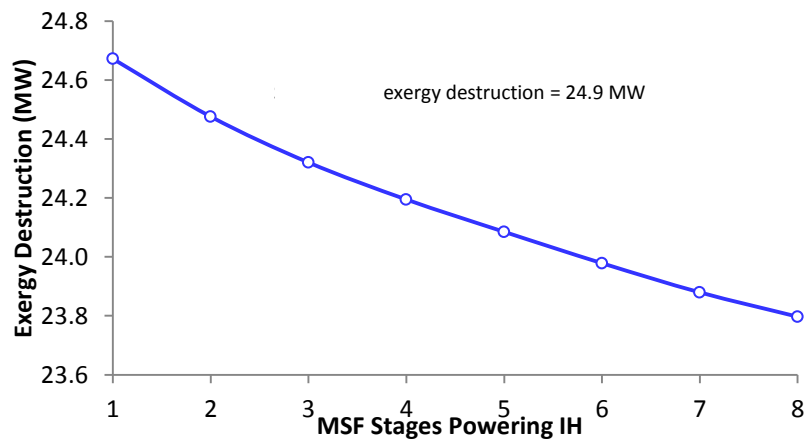


Figure 7.7: Total exergy destruction reduction of the MSF desalination unit using IH powered by stage extracted hot distillate

7.3 Impact of using IH in MSF on the cogeneration plant

The saved exergy destruction is 3.3 MW from the three identical MSF units considered in this study. In addition to this saving, the decrease of steam consumption causes a reduction of cogeneration plant gas consumption. To estimate this saving in terms of natural gas amount or electrical power that could be produced, actual operating scenarios should be considered because this modification impacts on other plant components, including the HRSG, duct burner, reduction station, and steam turbine, since the MSF powering steam was originally from the HRSG. This steam was either extracted from the steam turbine (operating scenarios I and III) or taken from the reduction station when the steam turbine is in shutdown condition. Therefore, a reduction in the powering steam has the most impact in operating

scenario II since it represents non- avoidable and non-efficient MSF steam supply method due to seasonal changes. In addition, as extraction of the hot distillate from the stages increases unit production, an additional amount of natural gas should be consumed to produce this quantity, but this section will count the natural gas saving resulting from the reduction in the steam consumption only.

Figure 7.8 shows that a decrease in MSF steam consumption reduces natural gas flow as the number of MSF stages IH power increases. This is up to the optimal recovery stage (stage 8), with a 0.34%, 2.5%, and 0.8% gas reduction for scenarios I, II, and III respectively, equivalent to annual natural gas saving of up to 1675 tonne/year, 3035 tonne/year, and 258 tonne/year (scenario III has a lower figure because operating the plant in this scenario is only 8% annually). This amount of natural gas saved will be the key to improving other cogeneration plant performance indicators and economic viabilities. Figure 7.9 shows the enhancement of cogeneration plant energy efficiency resulting from the reduction in the steam consumption by IH. As usual, scenario II achieved the highest energy efficiency improvement of 3.2% while scenarios I and III recorded only 0.5% and 0.7%, respectively.

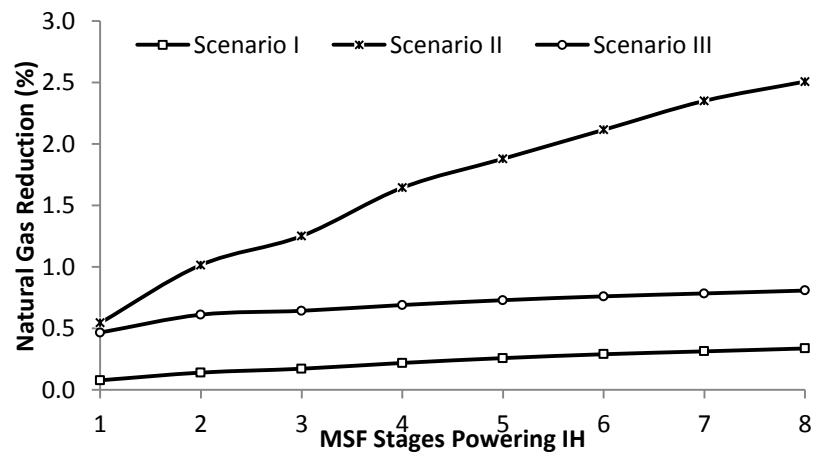


Figure 7.8: Effect of increasing the amount of heat recovered from the MSF stages by IH on reducing the cogeneration plant natural gas consumption

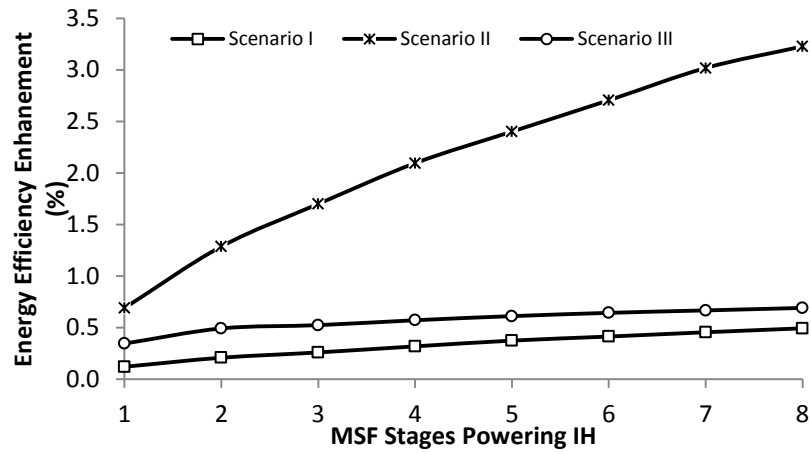


Figure 7.9: Effect of increasing the heat recovered from the MSF stages by IH on enhancing the cogeneration plant energy efficiency

The overall exergy efficiency of the cogeneration plant responded positively to this MSF modification by enhancements of 0.4%, 2.7%, and 1.0% for operating scenarios I, II, and III, respectively (Figure 7.10). This enhancement is due to two reasons: the primary one is the reduction of the natural gas input exergy and the secondary is operating plant components (e.g., HRSG, duct burner, reduction station, steam turbine) at lower loads, which causes a reduction in the exergy destruction. The high exergy enhancement of operating scenario II is because this modification reduced the steam produced from the HRSG directly and therefore, the exergy destruction at the reduction station dropped significantly, unlike in the other two scenarios, where the steam should pass through the steam turbine.

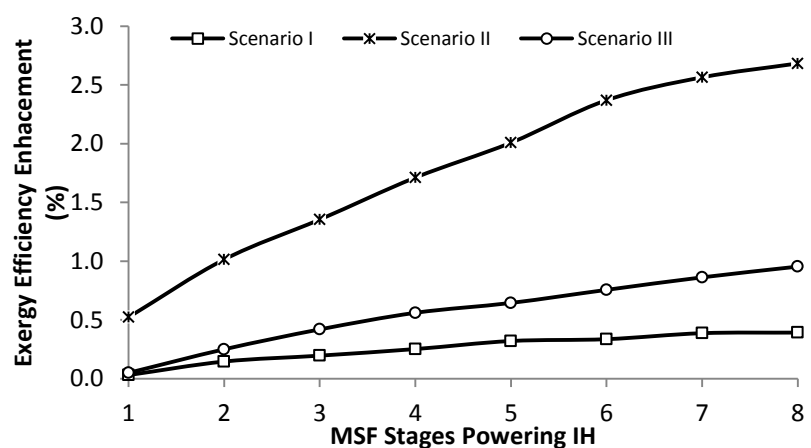


Figure 7.10: Effect of increasing the amount of heat recovered from MSF stages by IH on enhancing the cogeneration plant exergy efficiency

The reduction of the cogeneration plant exergy destruction could be counted as saving on equivalent electrical energy since the natural gas has perfect exergy (from 0.95% to 100%) [64]. Figure 7.11 shows this equivalent electrical energy saved. The annual saved exergy destruction at the optimal MSF heat recovery (stage 8) was 34109 MWh, 48576 MWh, and 4594 MWh for operating scenarios I, II, and III, respectively.

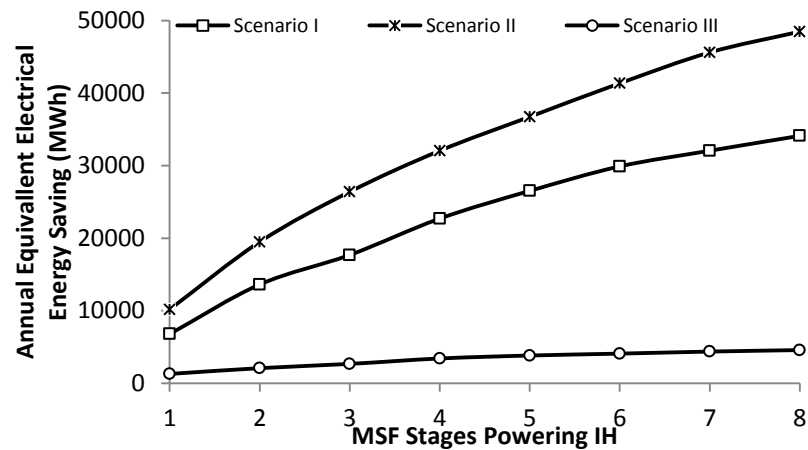


Figure 7.11: Effect of increasing the amount of heat recovered from MSF stages by IH on enhancing the cogeneration plant equivalent electrical energy saving

Environmentally, reduction of natural gas consumption and plant components' exergy destruction decreases the CO₂ emissions considerably (Figures 7.12 and 7.13). The above electrical power saving results in a reduction of CO₂ emissions by 1.2%, 10%, and 2.5% for scenarios I, II and III, respectively, representing 3364 kg/h, 13734 kg/h and 3568 kg/h. Taking into account the percentage of operating each scenario annually, savings in CO₂ emissions increase sharply from 11961 tonne/year to 56991 tonne/year, as heat is recovered from MSF stages 1 to 8 (Figure 7.13).

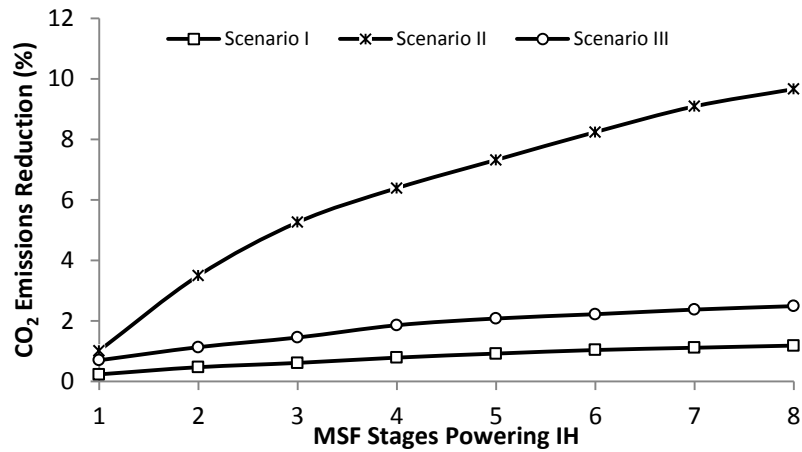


Figure 7.12: Effect of increasing the amount of heat recovered from MSF stages by IH on reducing cogeneration plant CO₂ emissions

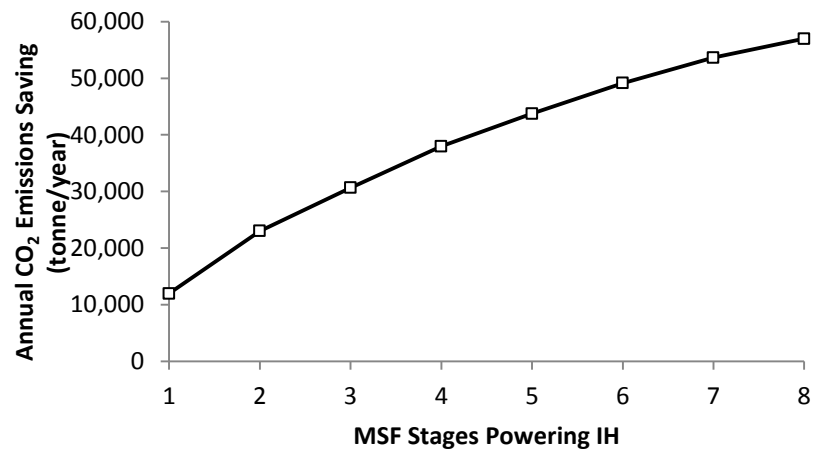


Figure 7.13: Effect of increasing amount of heat recovered from MSF stages by IH on annual CO₂ emissions savings

7.4 Utilization of the extracted distillate heat in addition to IH

The previous sections discussed utilizing the whole of the recovered heat for IH but in principle, part of this heat could be exploited for other heat recovery applications (AC, SED, and ORC are available in the market for low heat applications) before connecting it to the IH exchanger. The level of utilization should be studied to ensure that such heat usage would not increase steam consumption. It was found that utilizing part of the heat before the IH exchanger will not affect the reported production enhancement whatever the heat utilization level, but that the main effect is on unit steam consumption and thus unit PR.

Figure 7.14 shows the heat absorbed by the MSF IH exchanger at five different conditions IH (full utilization), 5°C heat utilization before IH; 10°C heat utilization before IH; 15°C heat utilization before IH; and 20°C heat utilization before IH. In all five cases, MSF IH effectiveness and NTU were kept constant.

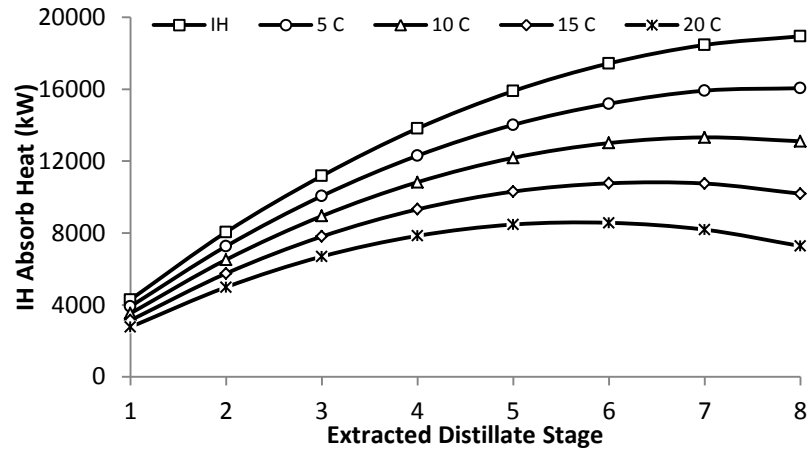


Figure 7.14: IH heat absorption at different heat utilization levels before IH

As can be seen from Figure 7.15, the level of heat utilization still has a positive effect (reduction in steam consumption and consequently reduction in cogeneration plant natural gas consumed) up to level of utilization below 10°C. Increasing the level of heat utilization above 10°C leads to rising unit steam consumption. Therefore, for utilizing part of the recovered heat with heat recovery technologies, the utilization (in heat recovery technologies) temperature difference of the heat source should be less than 10°C. Figure 7.16 describes the trend of the MSF unit PR at different heat utilization levels, which has a realistic trend opposite to the steam consumption (the dashed line represents the MSF desalination unit configuration without distillate heat recovery).

The coming chapters will discuss the exploitation of the recovered heat partially (at levels of 10°C or less) in the AC, ORC, and SED. With the AC, water will be produced to enhance power generation through cooling the gas turbine inlet air, while with the ORC; the heat will be used to produce more electrical power. SED will utilize the heat to supply more water.

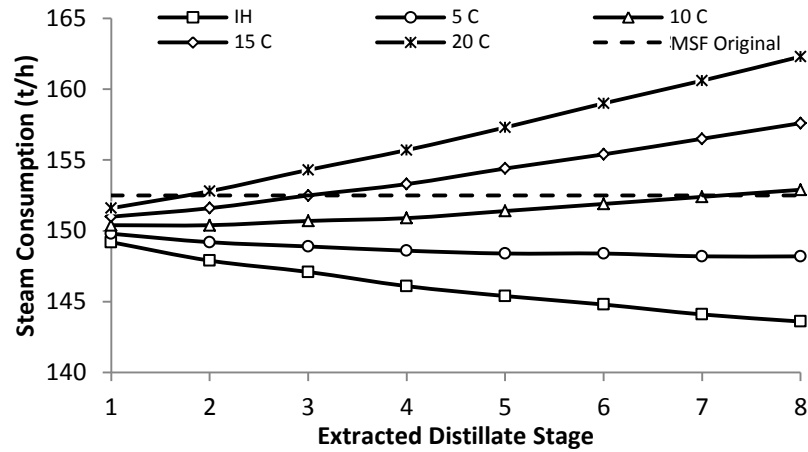


Figure 7.15: MSF steam consumption at different levels of heat utilization from extracted distillates

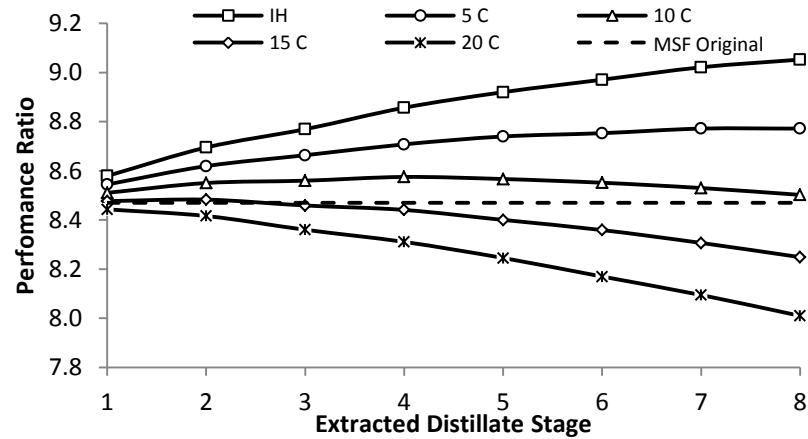


Figure 7.16: MSF PR at different levels of heat utilization from extracted distillates

7.5 Closing Remarks

It has been found that extracting the distillate from the MSF stages up to stage 8 (for this particular plant) increases the MSF unit production by up to 2% and reduces seawater feed pump power consumption. In addition, this extracted heat can be used to increase brine recirculation temperature through increasing make-up temperature using an internal heat exchanger. Increasing this temperature reduced MSF unit steam consumption by up to 5% and therefore increased the unit performance ratio by a similar percentage. Consequently, unit exergy efficiency could be improved by up to 16% due to reduction of total exergy destruction (reaching up to 3.3 MW for the three MSF units).

In practice, this improvement of the MSF unit is reflected by enhancement of the cogeneration plant performance indicators at the three normal operating scenarios; with scenario II was mostly affected. The cogeneration plant gas consumption could reduce by 1675 tonne/year, 3035 tonne/year and 258 tonne/year for scenario I, II and III, increasing cogeneration plant energy efficiency by 0.5%, 3.2%, and 0.7 %, respectively. Exergy efficiency improved up to 0.4%, 2.7% and 1.0% for operating scenarios I, II and III due to reduction of exergy destruction (equivalent to 34100 MW, 48600 MW and 4590 MW saved electrical power).

This MSF modification resulted on high reduction of the CO₂ emissions: 3364 kg/h, 13734 kg/h and 3568 kg/h for scenarios I, II and III respectively. This percentage led to saved 57000 tonne/year CO₂ at last possible MSF powering stage.

Furthermore, the study investigated using part of the heat before the internal heat exchanger. It was found any level of utilization of the heat below 10 °C has a positive impact on the MSF unit. This utilization will be addressed in details for absorption chiller, organic Rankine cycle and single effect desalination in coming chapters.

Chapter 8

Single-effect Absorption Chiller (AC) powered by hot distillate water from the MSF stages

8.1 Single-effect Absorption Chiller (AC) modelling and validation

8.1.1 Validation of single effect AC model

A LiBr–H₂O single-effect AC energized by the hot distillate water recovered from the MSF stages provides a cooling effect that can be used to reduce GT inlet temperature and thus augment the cogeneration plant power produced. The single-effect AC was modelled using the IPSEpro refrigeration library and validated against the existing unit and its physical possibility confirmed on a Dühring chart. The model was then modified to fit with Oman climate parameters, and the Dühring chart used again to confirm its continuing thermal applicability in these new conditions.

The model-simulated data were used to perform detailed energy and exergy analyses of this system with distillate extracted up to various MSF power stages to investigate the effect of change of powering source parameters on unit performance indicators. In addition, the single-effect AC exergy analysis takes into account the chemical exergy that most authors in this field have neglected [100, 107]. A parametric study was carried out to find the impact of variations of the chilled water temperature and cooling water temperature on a single-effect AC performance.

While cooling, the GT inlet temperature is an established technology, and the single-effect AC powered from MSF stage hot distillate water is considered to be original. The effect of this hybridization on cogeneration plant performance was investigated for the three actual operation scenarios studied in Chapter 3.

To ensure the model reflects a realistic AC performance, working data for an existing unit were obtained from the literature [165] and accordingly, a model for this case was built. Table 8.1 presents the specifications uploaded into the IPSEpro model described in Figure 8.1. The labelled components are linked by the numbered streams used to indicate the thermodynamic properties of the fluid transferring from one component to another. Some of these properties were fixed in the model (called set values) as they were obtained from the unit specifications and the model (represented as calculated values) calculated the others. Appendix 8-A identifies the stream properties and whether set or calculated.

Description	Unit	Specifications
Manufacturer	–	Carrier Sanyo
Model	–	LJ
Heat source	–	Hot water
Cooling type	–	Series (absorber/condenser)
Working fluid	–	LiBr–H ₂ O
Capacity	kW	2213
Hot water temperature	°C	90
Hot water flow	l/s	151
Cooling water temperature (inlet/outlet)	°C	28.5/34.5
Chilled water temperature (inlet/outlet)	°C	16/6.0
Pressure (high/low)	bar (abs)	0.067/0.0084
solution concentration (strong/weak)	%	59.5/55.0

Table 8.1: Single-effect AC specifications [165]

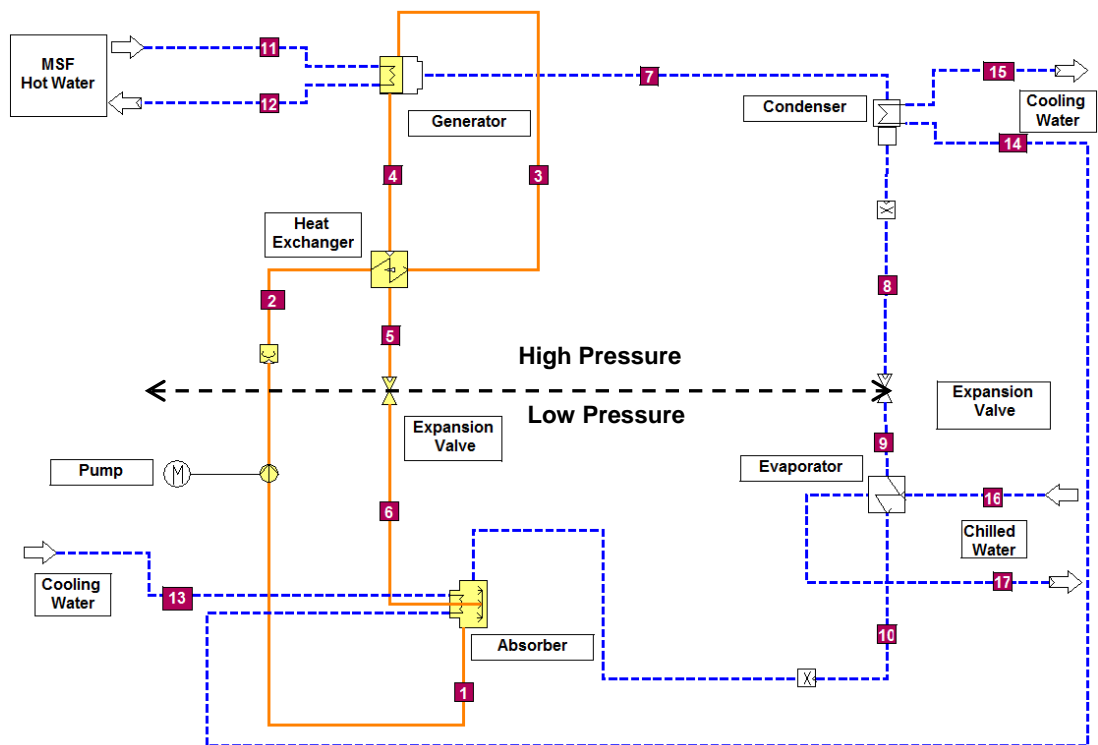


Figure 8.1: Schematic drawing of LiBr–H₂O AC IPSEpro model

For model validation comparisons between model results and existing unit, the performance data [165] are shown in Table 8.2. The compared values have a maximum difference of 4.1% for COP, while other parameters have acceptable matching. Moreover, Sanyo AC suggests an energy balance requires that the heat amount coming into the chiller cycle (heat transfer to the generator and evaporator) should be almost equal to the heat rejected from the cycle (heat rejected to cooling water of absorber and condenser) [166]. The model energy balance results reflected exact matching between both these heat amounts but a 7 kW difference can be observed for the existing unit. This small difference could be due to the assumption of specific heat values for the heat calculations or minor heat losses to atmosphere (which are neglected in the model).

Parameter	Unit	Existing unit data	Model Result	Differences (%)
Coefficient of performance (COP)	–	0.74	0.77	4.1
Refrigeration capacity	kW	2213	2283	3.2
Generator heat transfer	kW	2987	2957	1.0
Generator outlet temperature	°C	85.0	85.2	0.24
Generator and evaporator heat transfer	kW	5200	5240	0.77
Absorber and condenser heat transfer	kW	5193	5240	0.91
Cooling water flow	kg/s	211	209	0.95
Chilled water flow	kg/s	52.6	54.3	3.2

Table 8.2: Single-effect AC validation

Any proposed AC cycle should be checked for thermal practicality by superimposing thermodynamic state points on a Dühring chart [92, 167], as this helps avoid a number of pitfalls, such as avoiding the crystallization [167]. On Figure 8.1, points (1, 4, and 8) are saturated liquid; (10) is saturated vapour; (2, 3, and 5) are sub-cooled liquid; (7) is superheated vapour; and the other two (6, 9) are the two-phase vapour-liquid phase. These thermodynamic state points plotted on the Dühring chart (Figure 8.2) show a practical thermodynamic working AC cycle with working parameters away from the crystallization line.

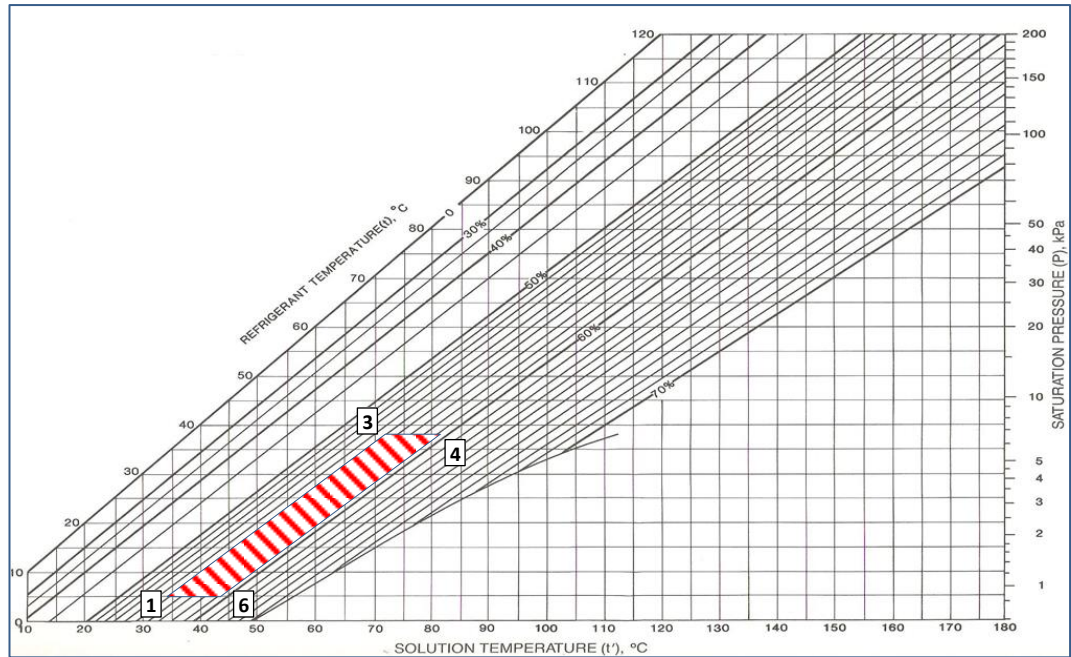


Figure 8.2: Single-effect AC (Table 8.1 and 8.2) on a Dühring chart

8.1.2 AC powered by MSF hot distillate

As mentioned in Chapter 7, the hot distillate water from the different MSF desalination stages (i.e., the powering source for the single-effect AC) varies in temperature and mass flow rate. The hot distillate water temperature drops as stage number increases, while the accumulative distillate mass flow rate increases (Figure 7.1), so it was concluded that using only the first eight stages both guarantees a higher exergy efficiency of the MSF desalination and a suitable temperature for powering heat recovery technologies.

The previous model was updated with the MSF minimum hot distillate water temperature, and with the average site recorded cooling temperature (27°C) while maintaining the 2°C pinch point between the cooling water temperature and absorber outlet temperature (T_1). From this updated model, it was found that the minimum working temperature that could be used to power the single-effect AC (at 1.4 kPa low pressure cycle and 4.5% solution concentration difference between strong and weak LiBr solutions) is 72°C. This matches with the stage 7 MSF hot distillate parameters. The impact on the low pressure side caused an increase in saturated vapour evaporator temperature (T_{10}) to 12.0°C, leading to an increase in chilled water outlet temperature. The chilled water inlet temperature was chosen to be 18°C, the minimum ambient temperature recorded for this site, whereas the outlet was kept at 14°C to maintain the 2°C pinch point temperature between the temperatures of the evaporator (T_{10}) and the chilled water (T_{17}) [104]. In addition, the

temperature difference ($T_{11}-T_{12}$) was kept constant at 4.85°C to ensure no impact on the original MSF desalination unit (Figure 7.15).

To ensure realistic thermodynamic representation, the modified single-effect AC model state points were plotted for all power stages on a Dühring chart. Figure 8.3 shows the working envelope for the AC powered by the first and last (7th) hot distillate water stage, with the other stages located between these (Appendix 8-B lists the details for each heat recovery stage).

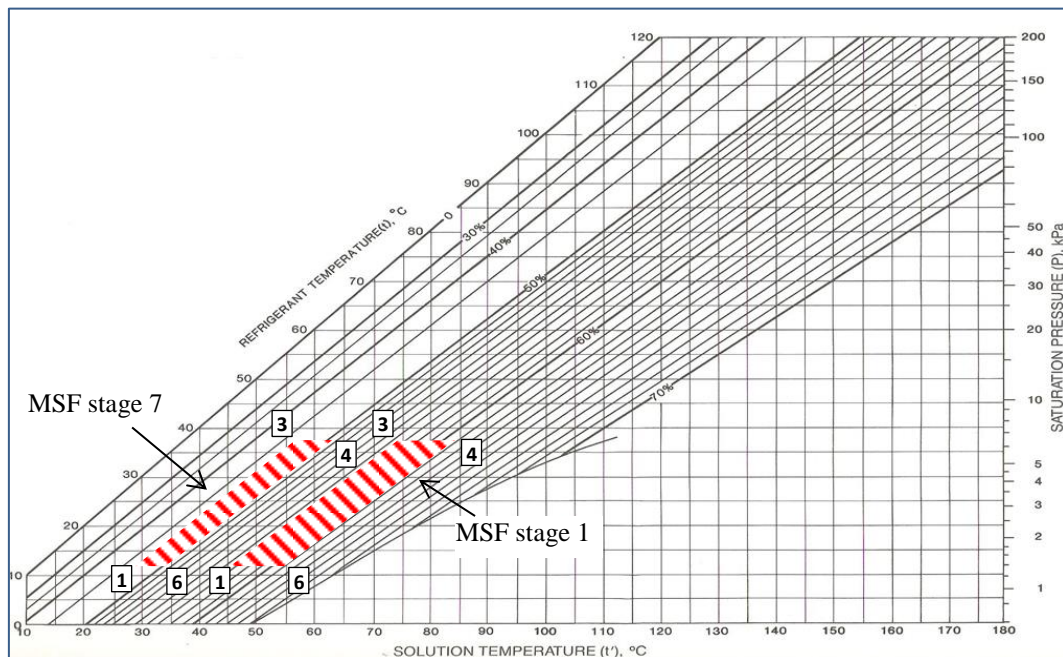


Figure 8.3: Single-effect AC powered by MSF hot distillate water (Stages 1 and 7) on Dühring chart

8.2 Analysis of single effect AC powered by MSF stages

8.2.1 Energy analysis

The simulation results for the single-effect AC IPSEpro model (listed in Appendix 8-C) were used to carry out the energy analysis for the system. This analysis was performed at the average cooling water temperature of 27°C with fixed inlet/outlet chilled water temperatures ($18^{\circ}\text{C}/14^{\circ}\text{C}$).

The results show that as the heat recovered from the MSF stages increases, the refrigeration capacity produced from the AC rises linearly (Figure 8.4), at 100 tonne (352 kW) of refrigeration for every powering stage. This is because the powering distillate recovered from MSF follows a similar trend despite the distillate temperature drops.

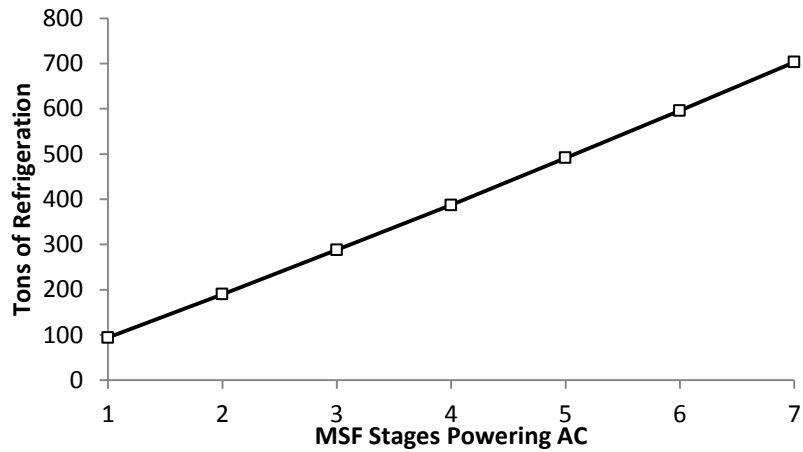


Figure 8.4: Effect of increase of MSF heat recovery stages on AC refrigeration capacity

The results (Figure 8.5) show the MSF stages with the lower distillate temperature giving a higher single-effect AC COP (e.g., stage 1 with temperature 92°C and COP 0.76 compared with stage 7 with 72°C and 0.84), in agreement with published theoretical and experimental studies [92, 168, 169]. These studies claim the reason behind this behaviour is a rise in heat transfer irreversibility at higher temperatures resulting in a reduction in COP. The manufacturer SONNENKLIMA's AC COP curve at 28°C cooling water temperature and 15°C chilled water temperature shows a similar trend when the generator inlet temperature (hot distillate water temperature in this study) is varied [169].

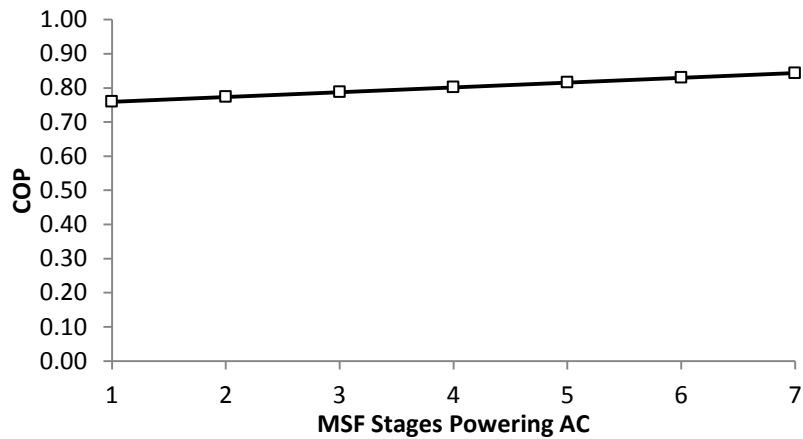


Figure 8.5: Effect of the increase of MSF heat recovery stages on AC COP

As the MSF recovery stages increases, the mass flow rate increases, despite the decreasing distillate temperature with this recovery. Thus, a single-effect AC responds to this increase by increasing the heat transfer to all cycle components (Figure 8.6).

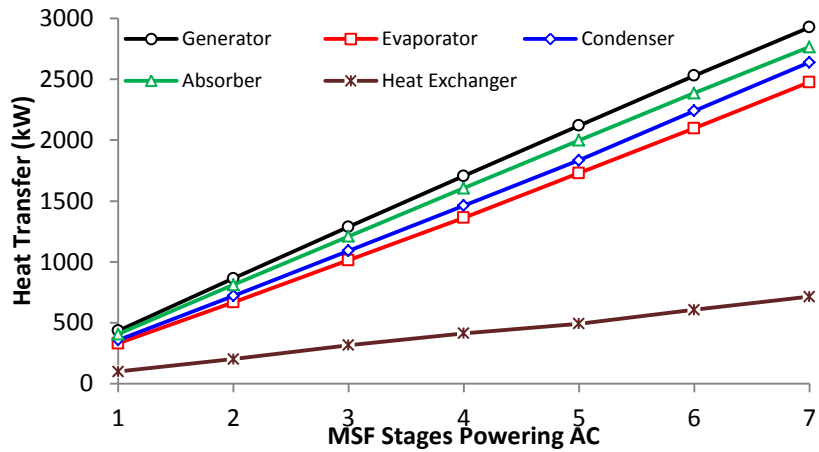


Figure 8.6: Variation of cycle component heat transfer as the MSF recovery stages increase

This increase in powering distillate flow is accompanied by a rise in chilled water flow (\dot{m}_{17}), though this enhancement per recovery stage is not directly proportional, as can be seen from Figure 8.7. The ratio (m_{11}/m_{17}), which defines the amount of chilled water produced per distillate water recovered, is at 1.09 stage 1 and drops to 0.983 at stage 7. The reason could be the rising COP at lower temperature stages. This relation and others, such as cooling water flow, cycle (weak and strong) LiBr–H₂O solution flow, and refrigerant flow are presented in Appendix 8-C.

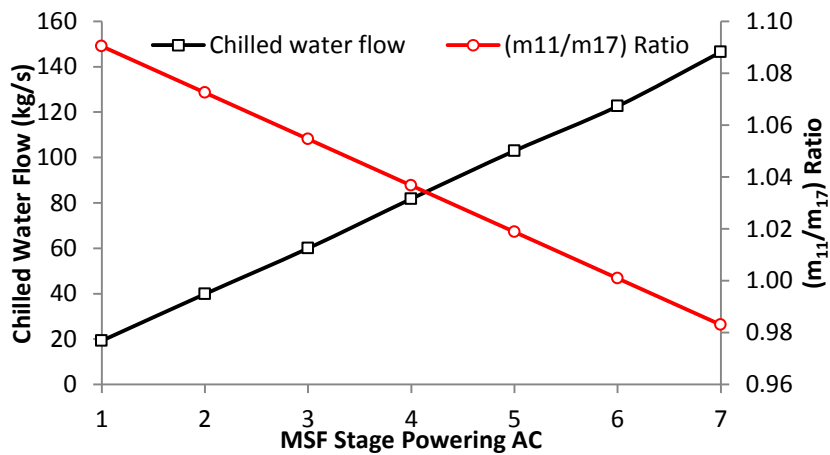


Figure 8.7: Variation of chilled water flow and (m_{11}/m_{17}) ratio as the MSF recovery stage increases

Due to an increase the heat transfer duty of all cycle components as more MSF stages are recovered, the cooling water flow should rise to absorb the increase of heat rejected from both condenser and absorber (Figure 8.8).

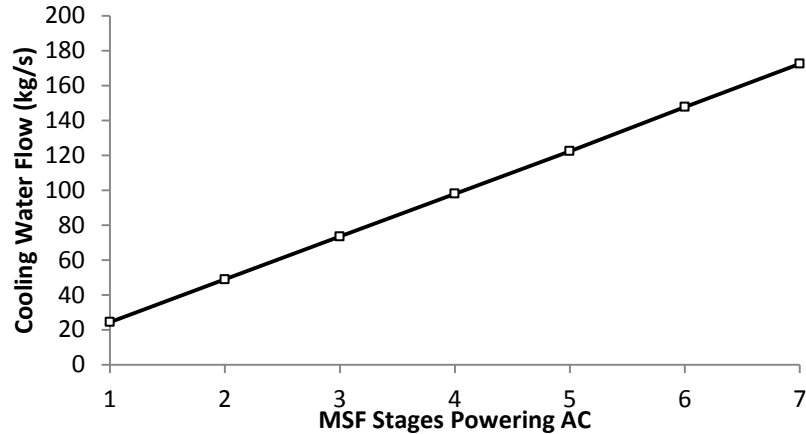


Figure 8.8: Variation of cooling water flow as the MSF recovery stages increase

8.2.2 Exergy analysis

The exergy analysis of the single-effect AC was performed at the chosen dead state of average cooling water temperature T_0 of 25°C and pressure of p_0 of 101.3 kPa. The exergy efficiency and exergy destruction calculation methods of the AC components are listed in Table 8.3. The simulated data presented in Appendix 8-C were used to conduct the exergy analysis at the various MSF stages used to power the single-effect AC.

During the AC exergy analysis, it is necessary to account for the chemical exergy of all streams of the single-effect AC cycle in addition to the physical exergy. The chemical exergy destruction due to dissolving LiBr should be added to the standard chemical exergy of pure LiBr, which Szargut et al [49] estimated experimentally. The difficulty of chemical exergy estimation for a LiBr solution caused this to be neglected in most previous published studies [94, 100, 103, 105], which could have led to incorrect conclusions concerning the AC and its components' exergy destruction and the cycle exergy efficiency of the AC cycle. The inlets and outlets of the absorber and generator do not have the same chemical composition [107]. Figure 8.9 presents the variation of the standard chemical exergy along with additional chemical exergy destruction due to dissolution for the weak and strong solutions at the possible MSF power stages (stream 1 and 4). The standard LiBr solution chemical exergy for both strong and weak solutions reduces linearly with the number of recovered MSF stages as a result of the reduction in the heating source temperature (T_{11}) and a decrease in LiBr concentration while maintaining the ($X_{\text{Strong}}/X_{\text{Weak}}$) ratio constant at 4.5%. However, the chemical exergy destruction due to the dissolving LiBr tends to reduce more at higher temperatures and higher element concentrations and then flattens at lower temperature MSF stages (e.g., stages 6 and 7).

These reductions have a significant effect on improving exergy efficiency and this will be presented next.

Equipment	Exergy Efficiency (%)	Exergy Destruction (MW)
Generator	$\frac{\dot{E}_4 + \dot{E}_7 + \dot{E}_{12}}{(\dot{E}_{11} + \dot{E}_3)}$	$\dot{E}_{11} + \dot{E}_3 - \dot{E}_4 - \dot{E}_7 - \dot{E}_{12}$
Condenser	$\frac{\dot{E}_8 + \dot{E}_{15}}{(\dot{E}_7 + \dot{E}_{14})}$	$\dot{E}_7 + \dot{E}_{14} - \dot{E}_8 - \dot{E}_{15}$
Evaporator	$\frac{\dot{E}_{10} + \dot{E}_{17}}{(\dot{E}_9 + \dot{E}_{16})}$	$\dot{E}_9 + \dot{E}_{16} - \dot{E}_{10} - \dot{E}_{17}$
Absorber	$\frac{\dot{E}_{13} + \dot{E}_1 + \dot{E}_{14}}{(\dot{E}_6 + \dot{E}_{10})}$	$\dot{E}_6 + \dot{E}_{10} + \dot{E}_{13} - \dot{E}_1 - \dot{E}_{14}$
Expansion Valves	$\frac{\dot{E}_9}{\dot{E}_8}$	$\dot{E}_8 - \dot{E}_9$
Heat Exchanger	$\frac{\dot{E}_3 + \dot{E}_5}{(\dot{E}_2 + \dot{E}_4)}$	$\dot{E}_2 + \dot{E}_4 - \dot{E}_3 - \dot{E}_5$

Table 8.3: Exergy efficiency and destruction calculation of single-effect AC components

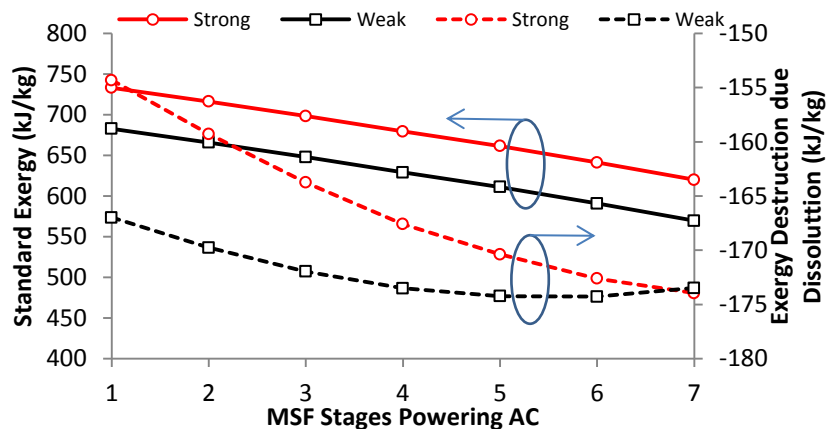


Figure 8.9: Standard chemical exergy and chemical exergy destruction due to dissolving of strong and weak solutions

Like the COP, the single-effect AC cooling exergy efficiency is higher at the later low distillate water temperature stages (Figure 8.10) because of the higher exergy destruction at the higher temperature stages [92, 103]. The exergy efficiency varies from 10% at stage 1 to 16% at stage 7, which is in agreement with previous published work [99, 103]. It was found that a 10°C reduction in the heating source temperature enhances the exergy efficiency by 27%. The increase of cycle exergy destruction in Figure 8.10 is a result of the increase in distillate mass flow rate, although the rate of increase starts to flatten off at

the low temperature stages, which justifies the behaviour of the COP and exergy efficiency trends.

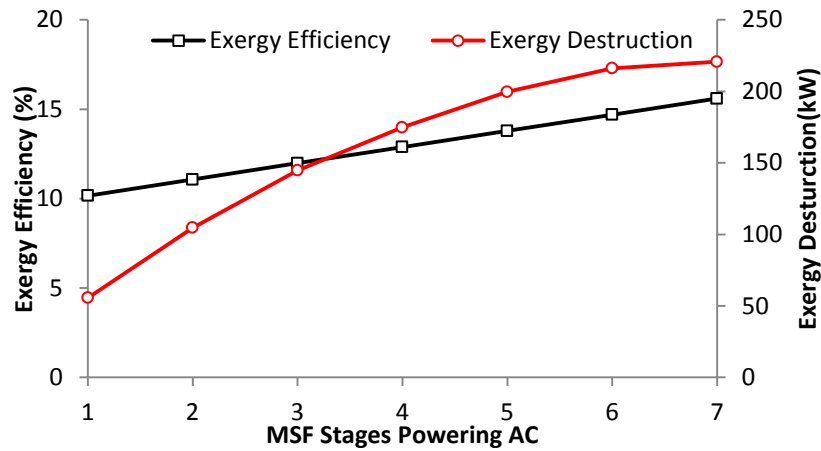


Figure 8.10: Effect of the number of MSF recovery stages on the AC exergy efficiency and destruction

Figure 8.11 presents the variation of the exergy destruction ratio of the AC cycle components as the number of MSF recovery stages is increased. Up to the first five recovery MSF stages, the AC absorber is the main contributor to cycle exergy destruction in agreement with published studies [170, 171] but generator destruction increases to become significant at the remaining stages. This absorber percentage represents around 52% of total exergy destruction at stage 1, reducing at the lower temperature stages to only 17% at stage 7 due to a decrease in the refrigerant mass flow rate ratio per recovered stage and a reduction of the chemical exergy at low temperature powering stages. By contrast, like the generator, the evaporator and condenser exergy destruction ratios recorded a noticeable increase as the number of recovered stages rises, due to the rise in the cooling water flow as recovery stage increases and reflected in both components since they are cooled in a series configuration. The exergy destruction of the heat exchanger and expansion valve were insignificant compared with the other components. Appendix 8-D lists all cycle component exergy efficiencies and exergy destructions at all possible power MSF stages.

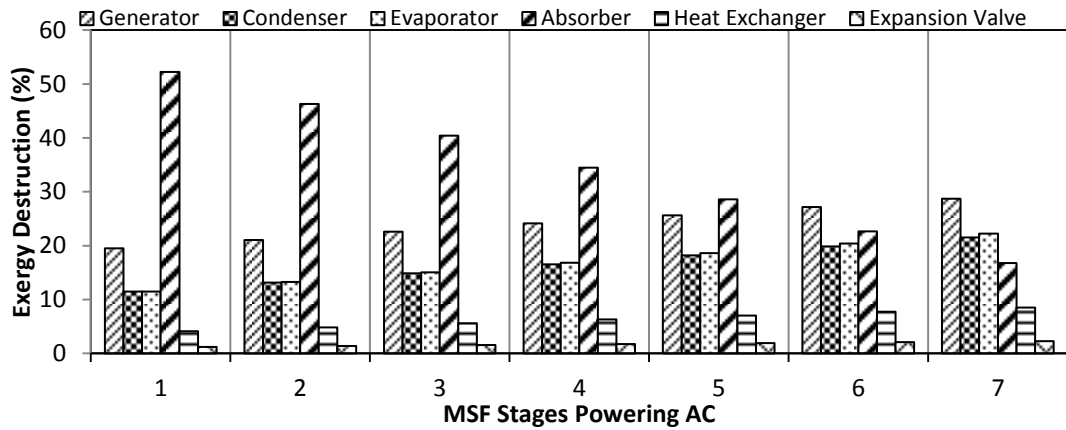


Figure 8.11: Exergy destruction ratio (%) of AC cycle components as the MSF recovery stage increases

Powering the single-effect AC by MSF stages hot distillate water achieves an increase of the MSF exergy efficiency compared with its original configuration (without heat recovery), because the exergy output is the sum of the MSF W_{\min} and AC generator feed exergy difference ($E_{11}-E_{12}$) divided by the same MSF exergy input (Figure 8.12). However, considering both systems (MSF and AC) together, this improvement is reduced due to the exergy destruction within the AC. The net saving through powering the AC from MSF hot distillate is 8780 kW of thermal energy for the three identical MSF units. This saving is equivalent to 1169 kW of exergy, which can be imagined as electrical power.

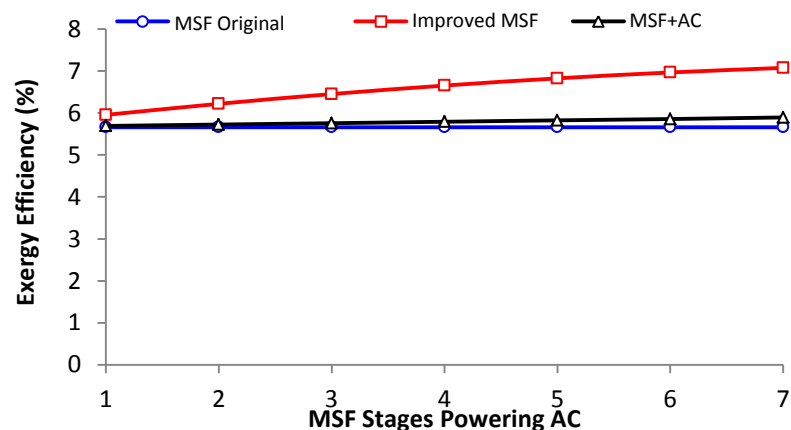


Figure 8.12: MSF exergy enhancement resulting from powering a single-effect AC

8.2.3 Single-effect AC parametric study

Besides the impact of the heating source parameters on the performance of the AC

machine that was addressed in Section 8.2.2, two main external factors affect the single-effect AC: the cooling water temperature and the chilled water temperature [92, 167]. The simulation was used to test for both variations of parameters, selecting their variation range from the possible actual variation that was obtained from meteorological data analysis (Section 3.3.2).

The influence of the inlet chilled water (T_{16}) temperature was examined over a wide range of chilled water temperature (14–22°C), while fixing the other input parameters (defined previously), except the chilled water outlet temperature (T_{17}), which remained unset (calculated). Figure 8.13 shows the effect of this variation in inlet chilled water temperature. Both the COP and cooling capacity varied a little (only 0.86% for every 1°C), with a slight increasing trend because the rise in the inlet chilled water temperature is accompanied by slight changes for the low pressure side at evaporator and absorber, which enhanced the heat transfer potential in the evaporator [92, 167]. These results corroborate the findings of previous work in this field, as well as manufacturer testing curves [169].

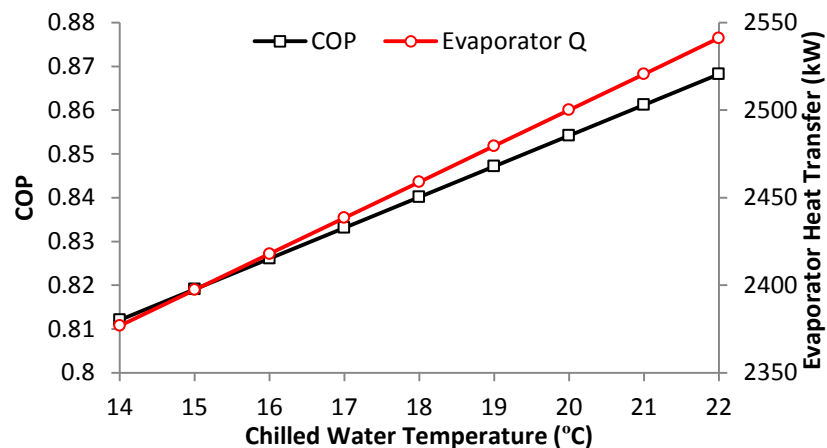


Figure 8.13: Effect of the chilled water inlet temperature on the COP and capacity of a single-effect AC

However, contrary to expectations, an increase in chilled water inlet temperature reduces the exergy efficiency significantly (a 2.2% decline for every 1°C increase) as can be seen from Figure 8.14. This is mainly due to the increase in the specific physical exergy of stream 10 as a result of the rise in the evaporator and absorber pressure, leading to greater generator exergy destruction. Appendix 8-E shows a detailed exergy analysis of the cycle components due to the variation of the chilled water inlet temperature.

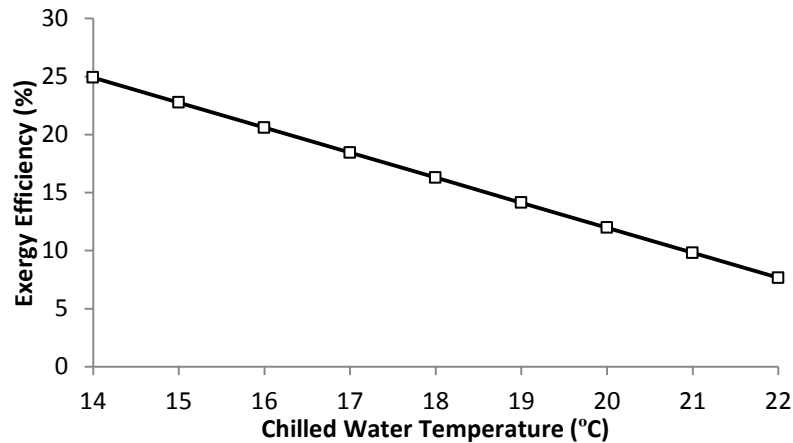


Figure 8.14: Effect of the chilled water inlet temperature on the exergy efficiency of a single-effect AC

Like the seasonal variation of the ambient temperature in arid countries, the cooling water temperature also varies seasonally. The single-effect AC model was based on the annual average cooling water temperature (27°C). Consequently, the impact of cooling water temperature changes over the range of the highest/lowest (33°C/22°C) recorded temperature was investigated. This study was performed at a constant cooling water flow of 172 kg/s. Changing the cooling temperature moves the single-effect AC operating envelope LP/HP pressure to maintain a fixed solution concentration and absorber/condenser pinch point.

Again the COP varies only slightly (a 0.02% difference for a 1°C increase of cooling water temperature), as the combined effects of the temperature and capacity changes effectively cancel one another [92, 99] (Figure 8.15). The cycle capacity decreases as the cooling water temperature increases as a result of a rise in the heat transfer potential at the evaporator. In general, the COP is found to be less sensitive to the cooling water temperature (Figure 8.15) compared with chilled water temperature (Figure 8.14). This result is in agreement with previously published studies [92]; however, other studies [94] found it more sensitive to the cooling water than the chilled water temperature in the case of parallel cooling.

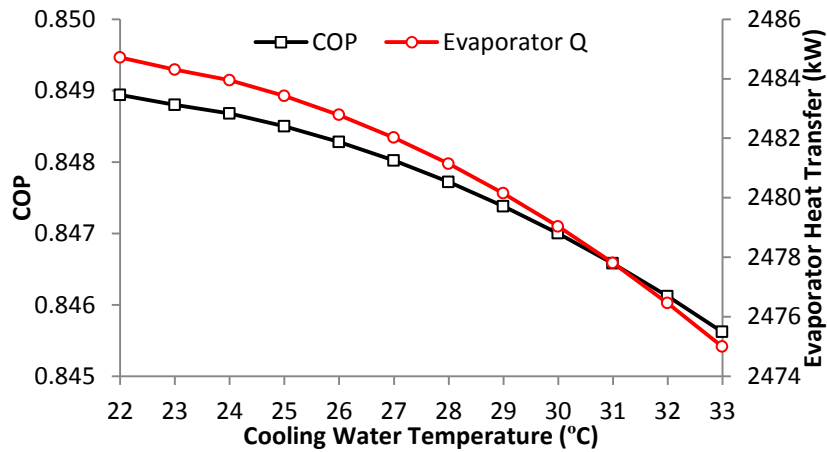


Figure 8.15: The effect of the cooling water temperature on the COP and capacity of a single-effect AC

The exergy efficiency shows a significant drop as a result of a rise in the cooling water temperature, agreeing with previous studies [92, 99] (Figure 8.16). It drops sharply from 31% at 22°C to only 3% at 33°C. This reduction could be a result of the higher rate of exergy destruction for the generator and evaporator compared with other cycle components (Figure 8.11). The detailed component exergy analysis is presented in Appendix 8-E.

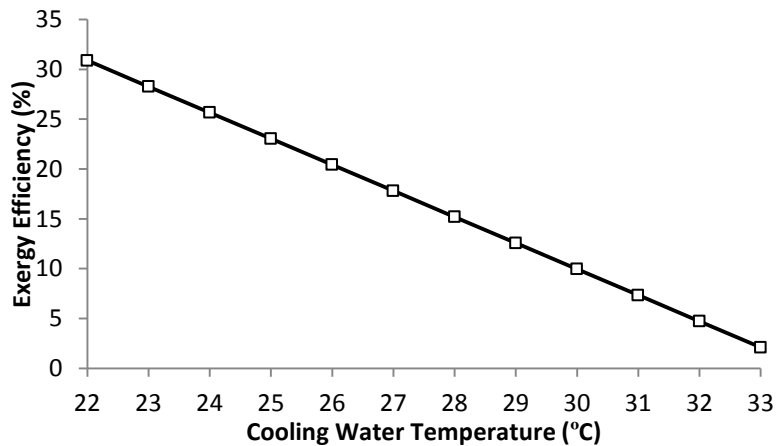


Figure 8.16: The effect of the cooling water temperature on the exergy efficiency of a single-effect AC

8.3 Gas turbine inlet temperature cooling using AC powered from MSF

The parametric study of the power plant (Section 5.5.1) showed the ambient temperature variation affects it highly. Therefore, controlling or reducing the GT air inlet temperature will result in the enhancement of the cogeneration plant performance indicators [95, 109,

115]. This section focuses on utilizing the produced chilled water from the single-effect AC to cool down the GT air inlet temperature using a simple cross flow air cooler. Since, the number of AC units is three (one powered from each of three MSF desalination units), the assumption is made that each GT inlet temperature is cooled down by 50% of the total chilled water produced. The cooling water stream temperatures (inlet and outlet) were kept constant as set for the single-effect AC (14°C/18°C).

During the simulation process, the air cooler effectiveness and NTU were calculated to ensure they fell in the acceptable range for the cooler design. Figure 8.17 describes a schematic for the usage of the single-effect AC powered by heat recovered from the MSF stages' distillate to cool down the GT inlet temperature. The analysis of this configuration was carried out at all possible MSF stages that could be used to power the single-effect AC and the average air ambient temperature (29°C). As the number of recovery stages increases, the single-effect AC cooling capacity rises and thus, its ability to cool down the GT inlet air temperature is enhanced.

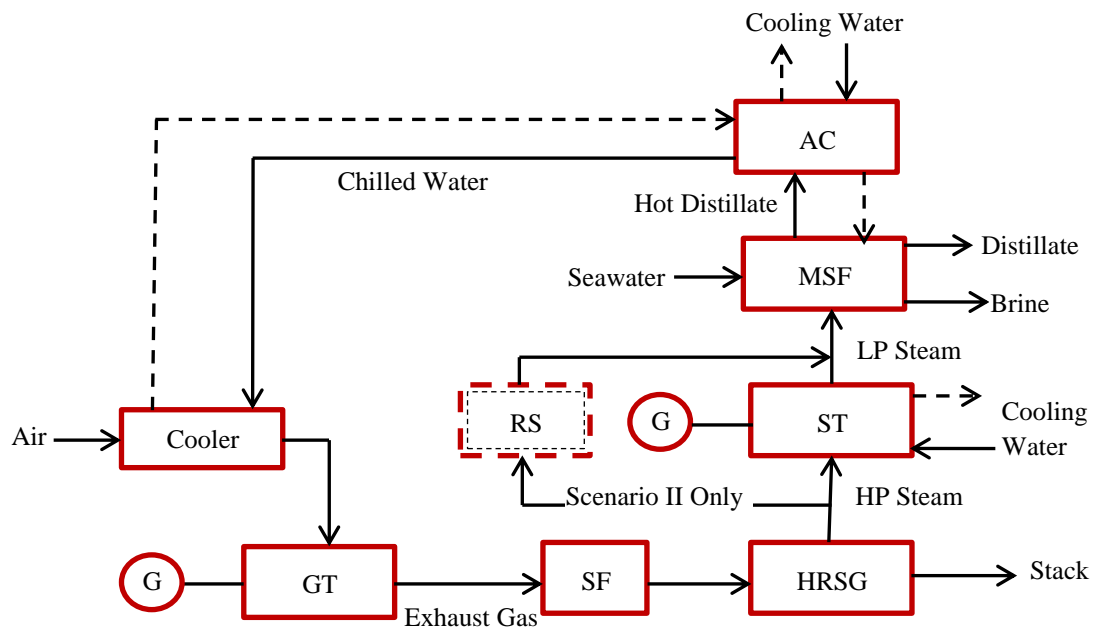


Figure 8.17: Schematic drawing of GT air inlet cooling using a single-effect AC

Figure 8.18 illustrates the effect of the GT air inlet cooling using a single-effect AC powered by the MSF stages on the power and efficiency. The results show that as AC power stage increases, the GT power is augmented significantly as a result of a reduction of the turbine inlet temperature, which is caused by the rise in chiller water mass flow rate. The enhancement of GT power and plant net power are 3.8% and 2.4%, respectively, for

every 5°C decrease in the GT inlet temperature (this percentage is equivalent to a 18 MW increase from both GTs). Consequently, the GT efficiency improves because of reduction in the GT gas/power ratio. These findings seem consistent with other research in the same field [95, 109]. Furthermore, this enhancement will not be limited to the GT but will extend to the overall plant, as was discussed in the parametric study of the power plant (Section 5.5.1).

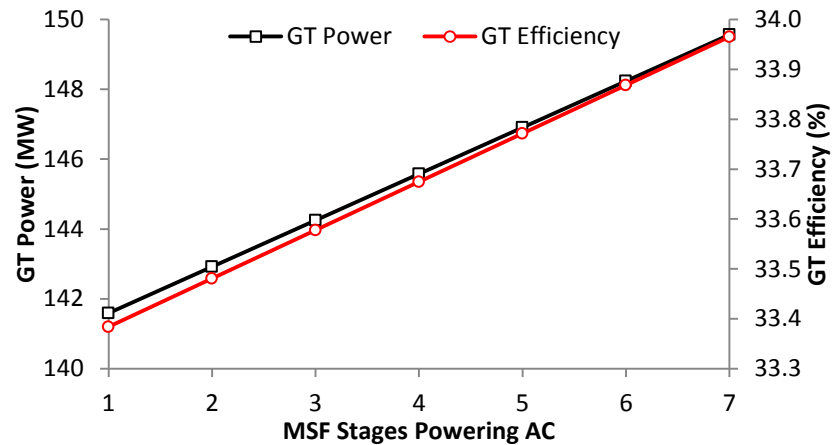


Figure 8.18: Effect of the GT air inlet temperature cooling using AC powered by the MSF stages

To obtain a realistic understanding of any technical benefits from this configuration, its impact should be studied for the actual plant operating scenarios. For all three operating scenarios, cooling the GT by the single-effect AC improved the power plant efficiency, and this improvement rose as number of power stages increased (Figure 8.19). Scenario II benefits more from this cooling methods compared with the other two scenarios. This is because the GT is the only source for power in this scenario with the ST shutdown; hence, the impact of the GT inlet cooling is highest.

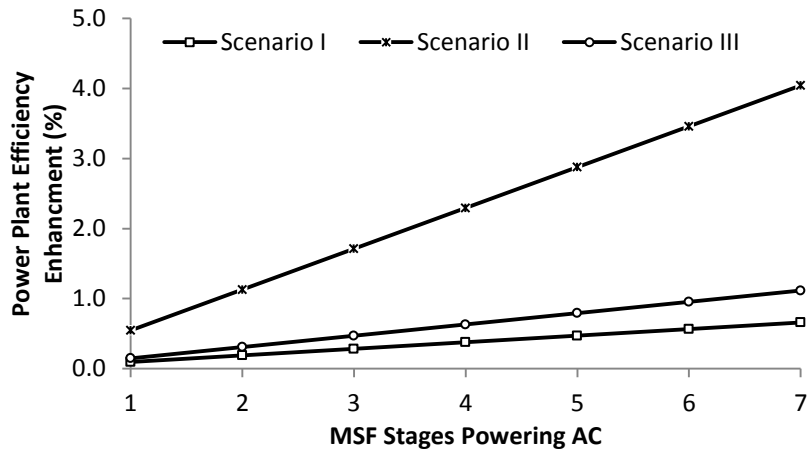


Figure 8.19: Effect of AC GT cooling on power plant efficiency for the three operating scenarios

Although the increase in cogeneration plant gross power due to using a single-effect AC for cooling the GT inlet temperature is clear (Figure 8.19), there is a corresponding increase in total natural gas consumption. However, as the GT inlet temperature reduces, the gas/power ratio decreases for the three operating scenarios (Figure 8.20), which results in the enhancement of the scenario operating efficiencies. Scenario II achieves the highest reduction in gas/power ratio, with scenario I the lowest (Figure 8.20). Savings of natural gas from a reduction of the gas/power ratio are 3984 tonne/year, 5808 tonne/year, and 404 tonne/year for scenarios I, II, and III, respectively using MSF power up to stage 7.

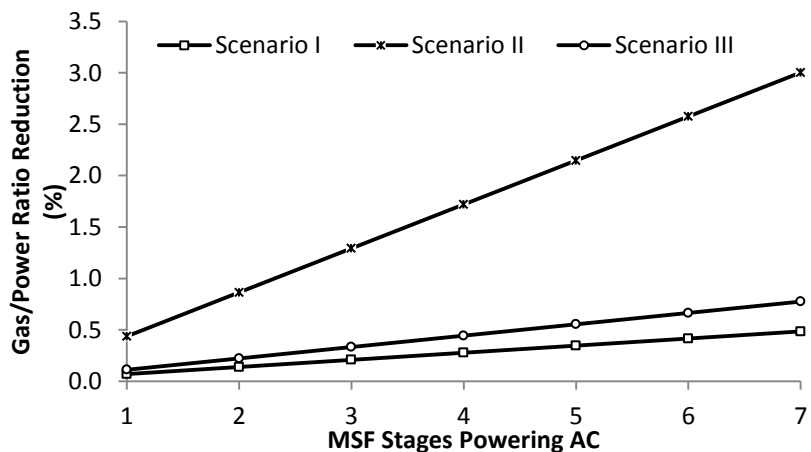


Figure 8.20: Effect of AC GT cooling on gas/power ratio at the three operating scenarios

The exergy efficiency of the cogeneration plant follows the same trends as previous performance indicators: as the number of MSF stages used to power a single AC increases for all three operating scenarios, exergy efficiency is enhanced (Figure 8.21). The highest overall exergy efficiency enhancement (compared with the scenarios without the modified

configuration) is for powering up to MSF stage 7. These findings support the results of Ehyaei et al [115].

The enhancement of exergy efficiency could be represented by the equivalent electrical energy saved from this modification, since the exergy analysis standardizes all streams by their ability to produce electrical power [45]. This representation can help in quantifying the applicability of this modification saving and to estimate equivalent CO₂ emissions for this modification.

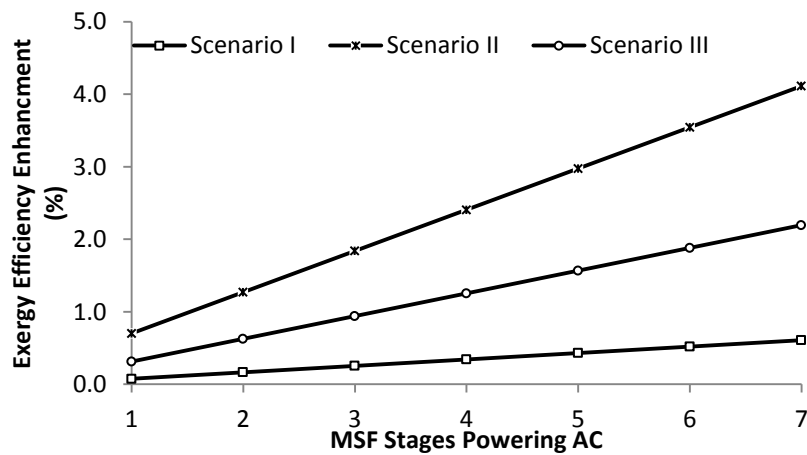


Figure 8.21: Effect of AC GT cooling on plant exergy efficiency for the three operating scenarios

Figure 8.22 presents the equivalent electrical energy saved annually as a result of implementing the cooling of the GT inlet temperature using a single-effect AC powered by the hot distillate water from the MSF stages. As can be seen, this saving is proportional to an increased number of the MSF stages powering the single-effect AC. The savings from scenario I and II are similar due to the high percentage of operating time for scenario I (62%) compared with scenario II (32%), despite this modification affecting scenario II more highly (Figure 8.21).

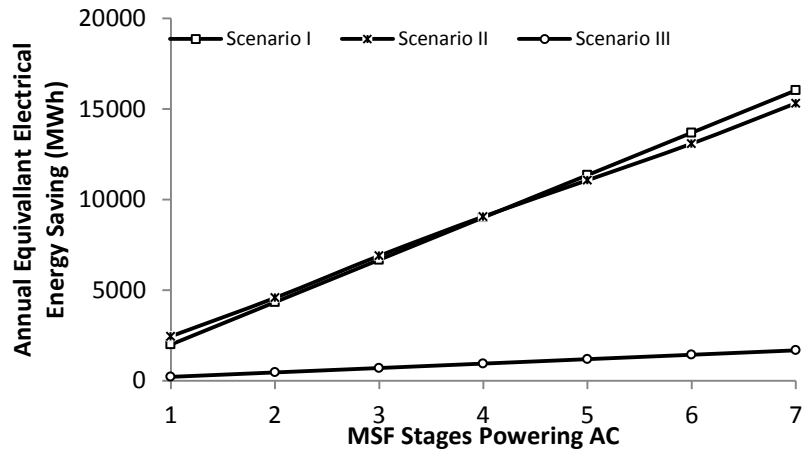


Figure 8.22: Equivalent electrical energy saved from the cooling of the GT inlet by a single-effect AC powered by the hot distillate from the MSF stages

Furthermore, using only part of the heat (4.85°C) to power the AC and then utilizing the rest in heating the MSF make-up flow results in a reduction in the unit steam consumption. Consequently, the natural gas consumption reduces at all three operating scenarios. Figure 8.23 illustrates the natural gas saving arising from both steam consumption and additional water produced from the distillate extraction compared with the original MSF.

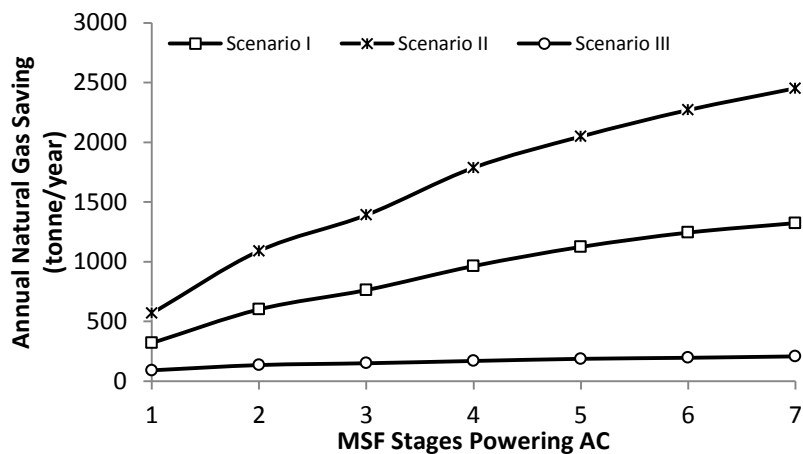


Figure 8.23: Annual natural gas saving for the three scenarios resulting from coupling the MSF with the AC for GT inlet cooling

Usage of single-effect AC cooling for the GT reduces CO₂ emissions significantly since it saves the natural gas, which emits CO₂ if burned to produce electrical power. Figure 8.24 presents CO₂ emission reductions for different MSF stages powering the AC. The savings amounts are 2436 kg, 5535 kg, and 2001 kg hourly for scenarios I, II, and III, respectively.

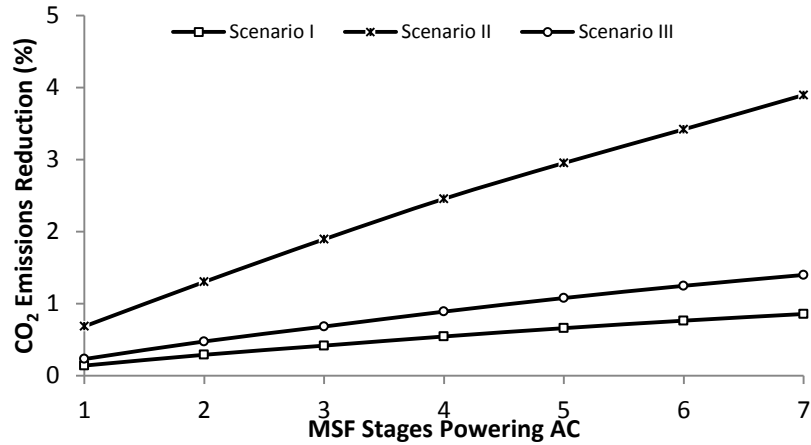


Figure 8.24: CO₂ emissions reduction from cooling the GT inlet temperature by a single-effect AC powered by hot distillate from the MSF stages

Annually (based on operating percentage for each scenario), CO₂ emissions are reduced as more heat is recovered from the MSF stages powering the AC (Figure 8.25). When the AC is powered by only stage 1, 4932 tonne/year are saved, increasing linearly up to 29219 tonne/year at stage 7.

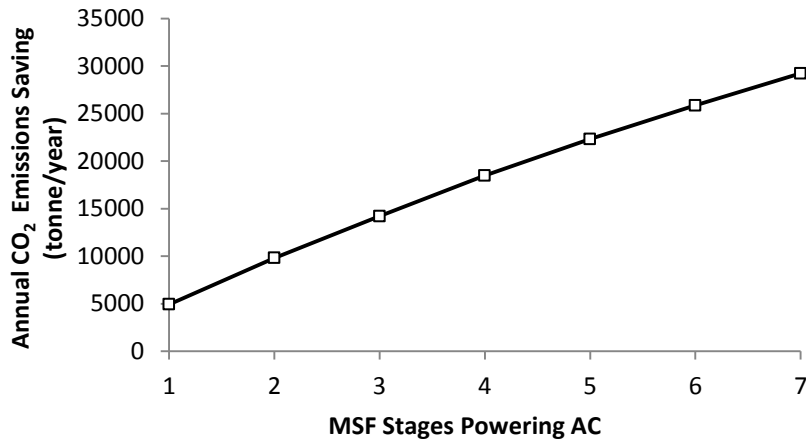


Figure 8.25: Annual CO₂ emissions saving from powering the AC by the hot distillate water from the MSF

8.4 Closing Remarks

The IPSEpro refrigeration library has been used to model a single-effect H₂O/LiBr AC chiller powered by the hot the hot distillate water from the MSF stages. The model was validated against an existing unit with highest difference in output parameters of 4%.

The results showed the cooling capacity of the single-effect AC rising as the number of

powering stages from the MSF increased. Both single-effect AC COP and cooling exergy efficiency increased as the number of recovered MSF stages increased as a result of rise of accumulative distillate flow rate and despite reduction of the stage temperature. However, a relatively high temperature favours the H₂O/LiBr AC, while Chapter 7 previously suggested distillate extraction up to stage 8, the enhancements observed for AC suggest MSF stage 7 is the highest possible recovering stage for AC. The absorber was the main contributor to exergy destruction among the AC components.

A parametric study was performed for variation of the AC chilled water inlet temperature and cooling water temperature. The study found that AC COP is more sensitive to the change of chilled water temperature compared with the cooling water temperature. Moreover, both parameters reduce the AC exergy efficiency as the temperature increases.

Using the single-effect AC cooling capacity to reduce the GT inlet temperature was found to increase GT power by 3.8% for every 5 °C reduction. Consequently, all performance indicators for all three operating scenarios of the cogeneration plant recorded an enhancement due to this cooling with scenario II most affected. The highest power plant efficiency improvement compared with the original configuration was around 4.0% at scenario II, with overall exergy efficiency enhancements 0.61%, 4.1% and 2.2% for scenario I, scenario II and scenario III respectively, giving saving of natural gas from the reduction of the gas/ power ratio of 3984 tonne/year, 5808 tonne/year and 404 tonne/year. Extracting the distillate to power AC saved natural gas by 1323 tonne/year, 2542 tonne/year and 207 tonne/year for scenario I, II and III, with CO₂ emissions reduction by 0.9%, 3.9% and 1.4% (equivalent to 2436 kg, 5535 kg and 2001 kg hourly). Annually CO₂ saving was 29000 tonne/year.

Chapter 9

Organic Rankine Cycle (ORC)
powered by hot distillate water from
MSF stages

9.1 ORC modelling and validation

9.1.1 Validation of ORC model

This Chapter investigates utilizing recovered heat from MSF hot distillate water to energize an ORC cycle. The IPSEpro refrigeration library was used to create the ORC model for an existing unit utilizing the heat from an underground hot spring in Chena, Alaska to power a 250 kW ORC unit [172]. Specifications of the modelled unit are presented in Table 9.1.

Parameter	Unit	Value
Working fluid	–	R134a
Heat source type	–	Hot spring water
Heat source temperature inlet	°C	73.3
Hot water mass flow rate	kg/s	33.3
Gross power	kW	250
Pump power	kW	40.0
Turbine inlet pressure	bar	16.0
Turbine outlet pressure	bar	4.39
Turbine mechanical efficiency	%	80
Cooling water inlet/outlet temperature	°C	4.44/10.0

Table 9.1: Specifications of the Chena Alaska ORC unit

Figure 9.1 describes the schematic of the IPSEpro model developed for the Chena ORC unit. The ORC components are joined by streams that carry the moving working fluid from one component to another. The numbers on the streams were used to indicate the stream's thermodynamic properties. Some of these properties are fixed values (set) obtained from unit specifications and others are calculated from the model. Appendix 9-A describes the set and calculated stream properties.

The ORC model was validated through the comparison between the model results and the existing unit data as presented in Table 9.2. As can be seen from the comparisons, the model predicted a close estimation to the actual ORC unit performance, with the highest deviation of 3.27% for the condenser cooling water flow. This model showed less deviation from the unit data compared with the study conducted for the same unit by Aneke et al. [156].

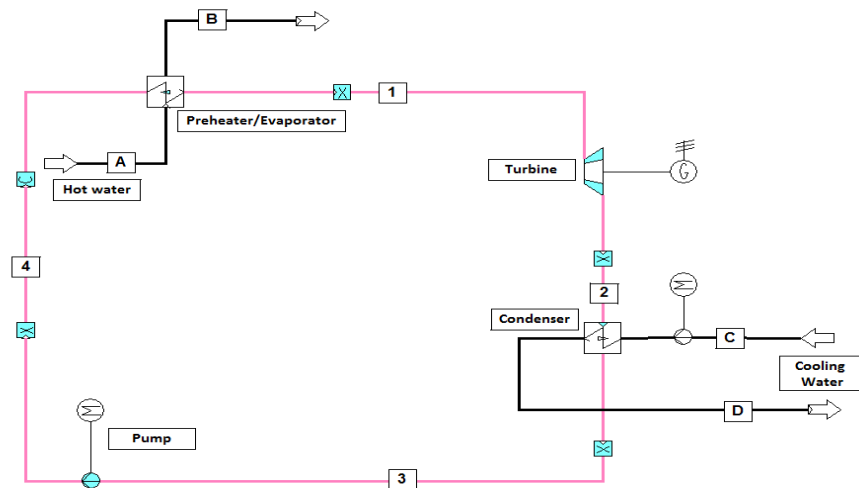


Figure 9.1: Schematic drawing of the IPSEpro ORC

Parameter	Unit	Existing unit data	Model result	Difference (%)
Gross power	kW	250	250	0.00
Net power	kW	210	209	0.467
Pump power consumption	kW	40.0	40.7	1.75
ORC efficiency	%	8.20	8.04	1.95
Cooling water flow	kg/s	101	97.7	3.27
Working fluid flow	kg/s	12.2	12.5	2.46
Evaporator outlet temperature	°C	54.4	54.7	0.551
Evaporator heat transfer	kW	2580	2602	0.853
Condenser heat transfer	kW	2360	2297	2.67
Evaporator heat conductance	kW/K	–	98.0	–
Condenser heat conductance	kW/K	–	594	–
Evaporator effectiveness	%	–	82	–
Condenser effectiveness	%	–	30	–
Evaporator NTU	–	–	1.71	–
Condenser NTU	–	–	1.45	–

Table 9.2: Validation of the ORC IPSEpro model

Figure 9.2 shows the plot of the state points of the ORC on the p-h diagram for the R134a working fluid. Process 1–2 is the expansion process in the turbine of the slightly superheated vapour to the vapour-liquid state at the turbine exit. Process 2–3 describes the constant-pressure heat rejection process in the condenser. In process 3–4, the refrigerant pump compresses the refrigerant to the operating pressure of the preheater and evaporator. Process 4–1 shows the constant pressure heat addition in the evaporator after the refrigerant absorbs the required heat to move to saturated liquid in the preheater.

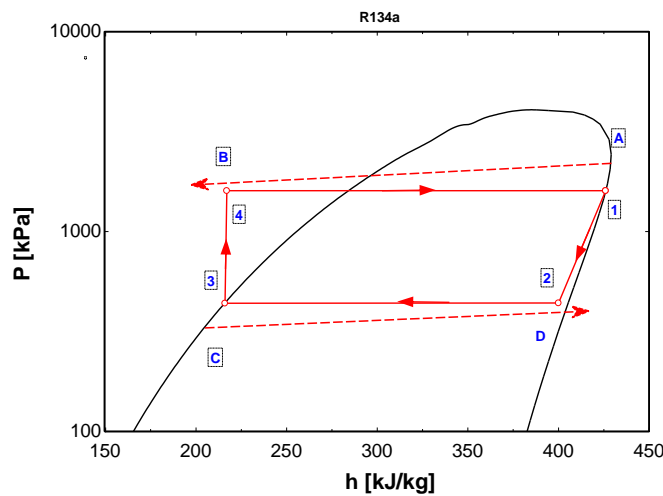


Figure 9.2: p-h diagram of the Chena ORC unit using the R134a working fluid

9.1.2 ORC working fluid investigation

As was mentioned earlier in the literature review (Section 2.4.2.2.1), the most suitable ORC refrigerants that can utilize low-grade temperature, such as that recovered from the hot distillate water of the MSF stages, are R134a and R245fa. These two working fluids are characterized compared with other working fluids by high molecular weight, low vaporization heat, non-flammability, with less impact environmental and negligible ozone depletion potential [122, 123, 127].

The validated model of the Chena ORC was tested by using an alternative working fluid R245fa at the same original existing equipment design data (e.g., evaporator and condenser effectiveness and turbine mechanical efficiency). It should be noted in this case, evaporator pressure (p_1) and condenser pressure (p_3) were the corresponding pressures for the condenser and evaporator fixed design temperatures,

respectively. Therefore, the turbine differential pressure (p_1-p_2) and the condenser differential temperature (T_2-T_3) will differ from those for R134a. Furthermore, due to R245fa being a dry working fluid, the turbine outlet quality falls in the superheated region (compared with vapour-liquid region with R134a), as seen in Figure 9.3 [118, 173].

The hot distillate water recovered from MSF stages should power both ORC models (R134a and R245fa). Fortunately, the MSF stage 7 hot water temperature almost matches with the Chena powering stream; therefore, it can be used easily after considering the cooling water temperature. The remaining parameters were simulated in the model with respect to the actual unit design parameters: 82% evaporator effectiveness, 30% condenser effectiveness, and 80% turbine mechanical efficiency. Maintaining the original model effectiveness of the condenser and evaporator the same as the original unit guaranteed both equipment pinch points (T_A-T_B) and (T_2-T_D). In addition, (T_A-T_B) was maintained constant at 10°C to ensure no effect on the original MSF desalination unit (Figure 7.16).

Although the objectives of this study do not include a detailed investigation of alternative ORC working fluids, to demonstrate a practical application of heat recovery in this new context, it is important to investigate whether refrigerant choice is a key issue. Therefore, to assess the role of working fluid selection on the ORC, a comparison between R134a and R245fa refrigerants was performed for the same heat input to the evaporator. It can be seen from the output results in Table 9.3 that R-245fa performs well and gives a better overall performance than R-134a. Selecting R-245fa over R-134a yields less gross power but more net power due to less power consumption of the working fluid pump. Moreover, R245fa has less cycle refrigerant mass flow and condenser and evaporator UA values, and a lower cycle PR, all of which lead to less equipment cost and lower operating costs. The R245fa ORC exergy efficiency is higher than for R134a by 9.7%, reflecting the higher utilization of the available energy in the cycle. This comparison agrees with published studies in this field [129, 174].

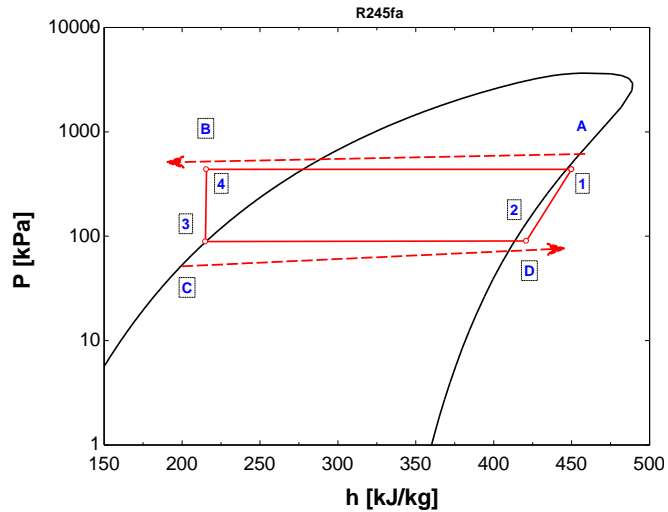


Figure 9.3: p-h diagram of the Chena ORC unit using R245fa working fluid

Description	Unit	Working fluid	
		R134a	R245fa
Gross power	kW	250	241
Net power	kW	209	232
Pump power consumption	kW	40.7	9.07
Thermal efficiency	%	8.04	8.90
Exergy efficiency	%	20.5	22.7
Turbine differential pressure	bar	11.6	3.49
Condenser cooling water flow	kg/s	97.7	97.4
Working fluid flow rate	kg/s	12.5	11.1
Evaporator UA	kW/K	98.0	97.2
Condenser UA	kW/K	594	269
Evaporator NTU	–	1.70	1.72
Condenser NTU	–	1.45	0.66

Table 9.3: Results of both the refrigerants modelled

9.2 Analysis of ORC powered by MSF stages

The study performs a comparison between two of the promising ORC working fluids: R134a and R245fa. Both models are investigated with the same unit components designed to be powered by the hot distillate water extracted from the first eight MSF desalination stages. The model simulation results for both R134a and R245fa are used to conduct a thermal assessment of powering the ORC cycles from

the hot distillate, as well as a detailed parametric study of the impact of ORC cooling water temperature and evaporator temperature. Energy and exergy analyses of both R134a and R245fa were carried at an average cooling water temperature of 27°C.

9.2.1 ORC system energy analysis

Appendix 9-B presents the simulation results for both working fluids powered by the hot distillate water from the first eight stages of the MSF. As the heating source (MSF hot distillate water) is varied in its temperature and mass flow rate depending on how many MSF stages were extracted, the ORC cycle changes in the cycle operational parameters to reach a new equilibrium condition. Figure 9.4 describes the ORC working fluid mass flow rate trend (for both R134a and R245fa) as heat input to the evaporator increases due to the rise in the hot distillate flow rate from MSF stage 1 to 8, despite the decrease in its temperature. In both cases, the working fluid mass flow rate is proportional to the increase in the input heat to the evaporator, but R245fa shows a lower rising refrigerant flow trend compared with R134a.

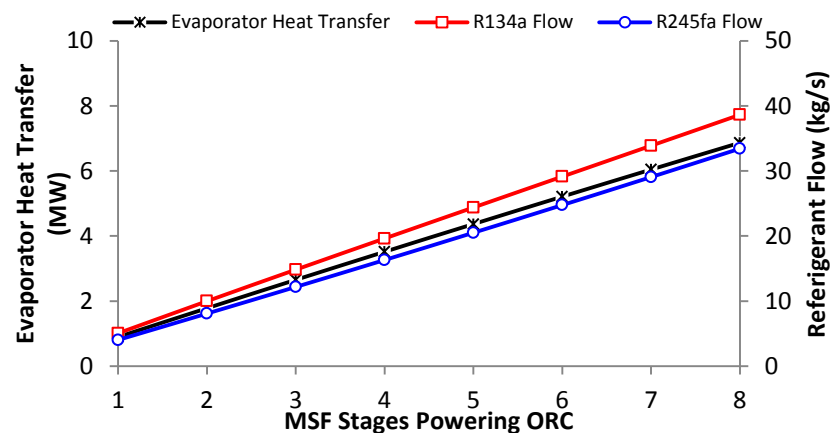


Figure 9.4: ORC mass flow and evaporator heat transfer for R134a and R245fa for the MSF power stages

Figure 9.5 presents the variation of evaporator and condenser overall heat transfer conductance (UA) for R134a and R245fa for various MSF power stages. The evaporator and condenser (UA) increase continuously in concert with the rise of the hot water power stream flow and the refrigerant mass flow rate. Both working fluids have similar UA evaporator profiles as the power in the MSF stage varies due to the same heat input, although R245fa shows slightly lower UA as a result of a smaller

working fluid mass flow rate. However, R245fa has a lower condenser UA compared with R134a as a result of less refrigerant and cooling water mass flow rate.

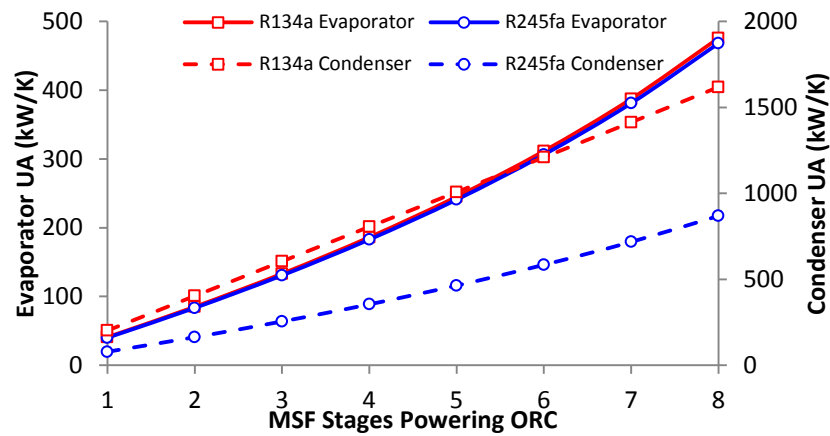


Figure 9.5: ORC evaporator and condenser UA for both refrigerants for the MSF power stages

In addition, the ORC gross power produced from both ORC cycles rises as the MSF powering stage hot distillate mass flow rate increases, recording the highest power generation at stage 8, (390 kW and 379 kW for R134a and R245fa, respectively), before the trend starts reducing (Figure 9.6). This can be explained by the higher working fluid enthalpy reduction at the turbine inlet at the lower MSF stage power temperature while maintaining the exit enthalpy almost constant. Again, more net power is produced by R245fa due to lower working fluid pump power consumption, which was, on average 22.5% from gross power for R134a and only 5.4% for R245fa (Figure 9.6).

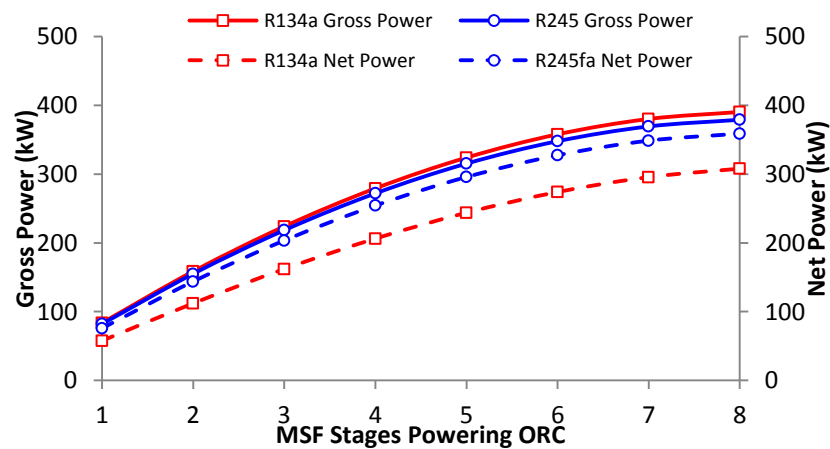


Figure 9.6: ORC gross and net power produced for R134a and R245fa for the MSF power stages

Consistent with other researchers who found a higher heating source temperature results in achieving better ORC efficiency [174, 175], the ORC thermal efficiency drops for both working fluids as the MSF power stage increases (Figure 9.7). In this application, this is mainly due to the reduction of the heating source temperature, which causes a decrease in the upper operating envelope shown in Figures 9.2 and 9.3.

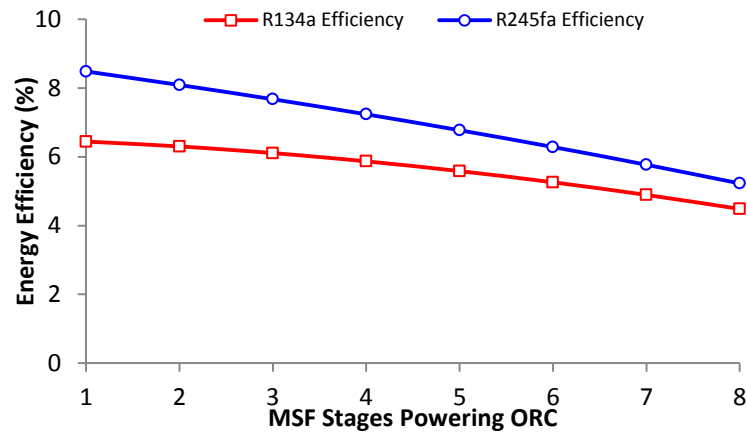


Figure 9.7: Variation of thermal efficiency of both ORC working fluids for the MSF power stages

9.2.2 ORC system exergy analysis

The ORC model simulation results for R134a and R245fa were used to perform an exergy analysis at the dead state of temperature T_0 of 25°C and pressure (P_0) of 101.3kPa. Chemical exergy was neglected since the component inlet and outlet streams have same chemical composition. Table 9.4 describes the calculation method for the ORC component exergy efficiencies and exergy destructions (Appendix 9-C lists these for both working fluids).

Equipment	Exergy Efficiency (%)	Exergy Destruction (MW)
Evaporator	$\frac{\dot{E}_1 - \dot{E}_4}{\dot{E}_A - \dot{E}_B}$	$\dot{E}_A + \dot{E}_4 - \dot{E}_B - \dot{E}_1$
Turbine	$\frac{\dot{W}_{ORC}}{\dot{E}_1 - \dot{E}_2}$	$\dot{E}_1 - \dot{W}_{ORC} - \dot{E}_2$
Condenser	$\frac{\dot{E}_D - \dot{E}_C}{\dot{E}_2 - \dot{E}_3}$	$\dot{E}_C + \dot{E}_2 - \dot{E}_D - \dot{E}_3$
Pump	$\frac{\dot{E}_4 - \dot{E}_3}{\dot{W}_{pp}}$	$\dot{E}_3 + \dot{W}_{pp} - \dot{E}_4$

Table 9.4: Exergy efficiency and exergy destruction calculation methods for the ORC

Figure 9.8 illustrates the variation of the exergy efficiency as the MSF power stage changes. The exergy analysis showed the ORC with the 245fa working fluids achieved higher exergy efficiency than the R134a working fluid (on average at 48% compared with only 39% for R134a). The exergy efficiency of R245fa decreases continuously as the number of MSF power stages increases, however R134a increases slightly up to MSF powering stage 6 and then starts dropping. These values of exergy efficiency fall within the range of published studies [131, 176,177].

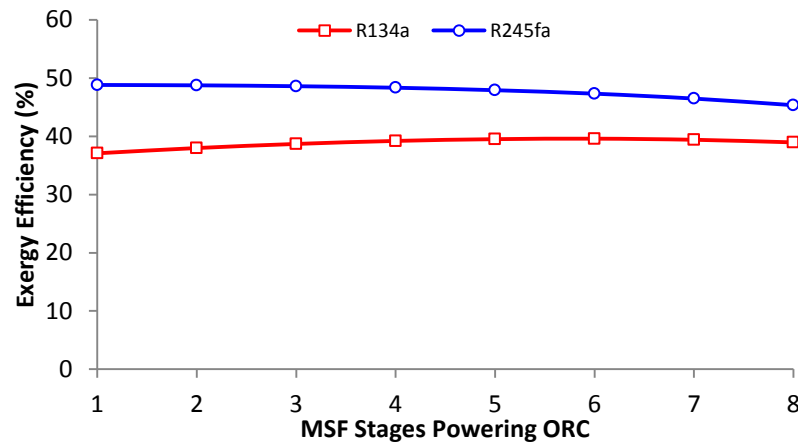


Figure 9.8: ORC exergy efficiency for both refrigerants at different MSF power stages

For ORC cycles, changing the power stream from the MSF stages does not affect the condenser and turbine exergy efficiencies significantly. Exergy efficiency is on average 76% and 53% for the R134a turbine and condenser, respectively, with the same exergy efficiency for the R245fa turbine but 52.5% for the condenser. In

contrast, however, the exergy efficiency of the evaporator and working fluid pumps varies as the power source changes (Figure 9.9). While the working fluid pump exergy efficiency continues improving as the MSF power stages increase, the evaporator follows a similar trend to the exergy efficiency.

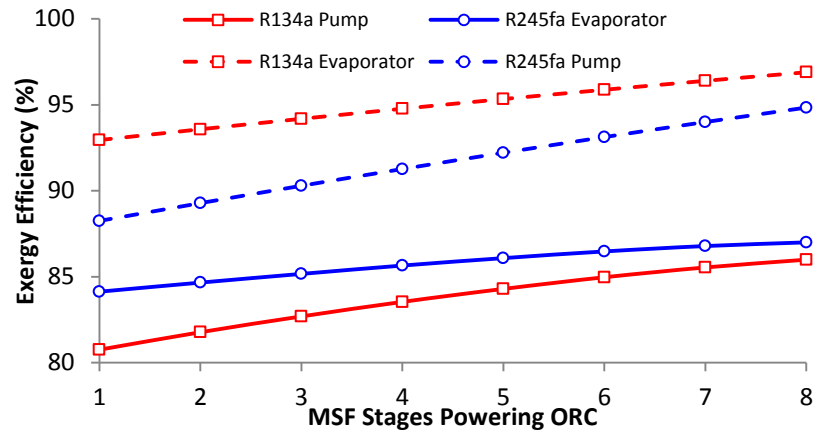


Figure 9.9: Exergy efficiency for both working fluids evaporator and pump for the MSF power stages

Comparison of the exergy destruction between the ORC components for R134a and R245fa are presented in Figures 9.10 and 9.11, respectively. As can be seen from both figures, the exergy destruction for all ORC components rises as the number of the power stages rises as a result of the increase in the mass flow rate of the power stream.

The ORC turbine is the main contributor to the ORC cycle exergy destruction for both refrigerants, representing on average 32% for R134a and 38% for R245fa. The exergy destruction for the evaporator and condenser are 32% and 19% on average for R134a from total input exergy, with 33% for the evaporator and 23% for the condenser in the case of R245fa. The working fluid pump exergy destruction amounts (as can be seen from both figures) are the lowest among the cycle components for both working fluids. However, the exergy destruction ratio of the pump significantly drops as the MSF power stage increases. For example, for R134a, it shared 20% from the total exergy destruction at stage 1, falling to 14% at stage 8 (for R245fa, 6.1% at stage 1 and 4.0% at stage 8). These results are consistent with those from other studies [176,177].

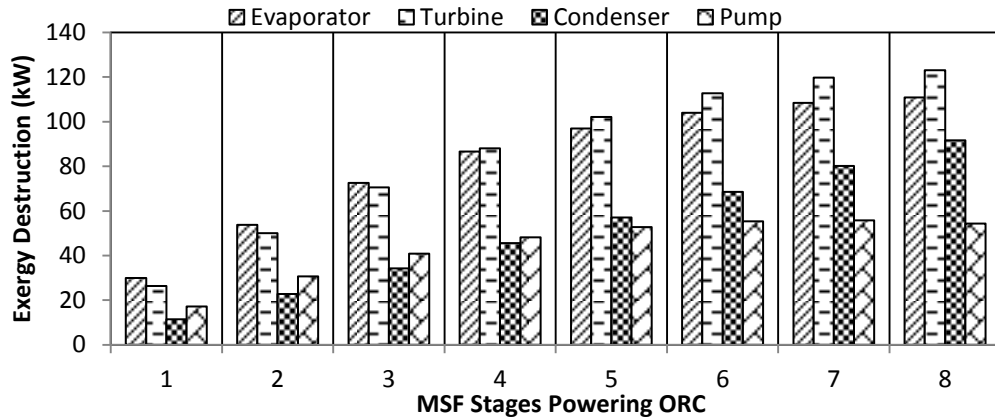


Figure 9.10: The R134a ORC cycle component exergy destruction for different MSF power stages

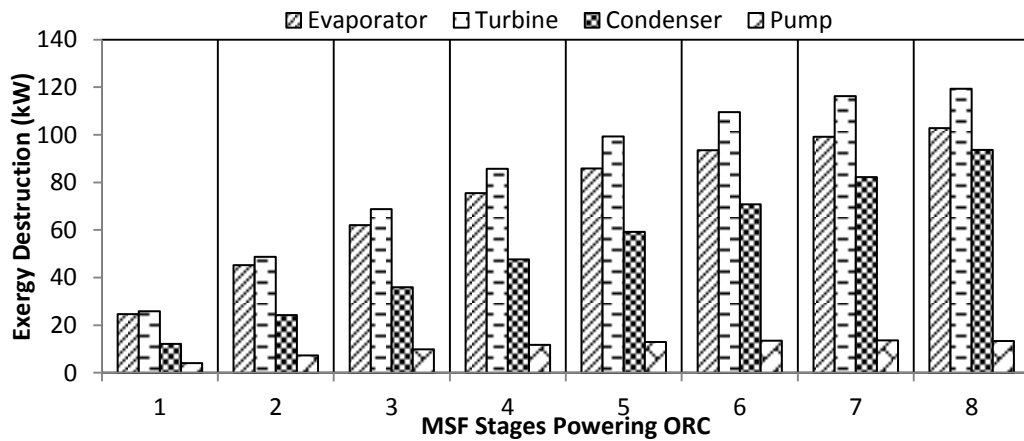


Figure 9.11: R245fa ORC cycle component exergy destruction for different MSF power stages

Figure 9.12 shows the impact of coupling with ORC on MSF exergy efficiency enhancement. As noted previously, recovering the heat from the MSF stage hot distillate water causes an exergy efficiency enhancement of the MSF itself. If part of the recovered heat is utilized in producing extra power from ORC units, the enhancement is reduced for both working fluids due to the ORC exergy destruction.

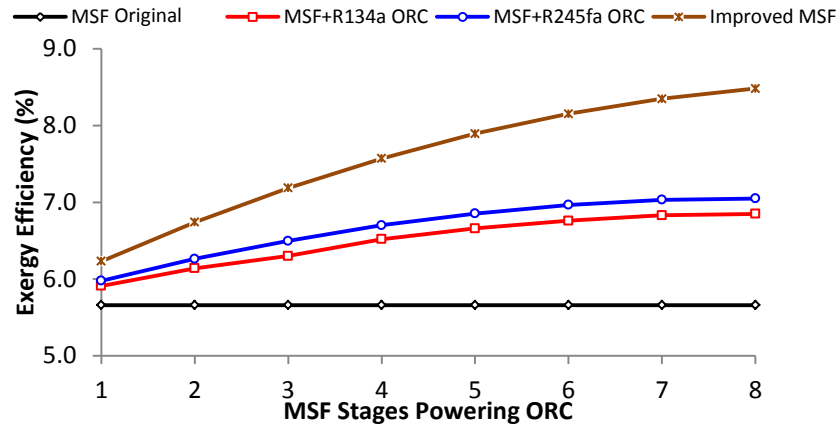


Figure 9.12: Exergy efficiency enhancement of MSF with R134a and R245fa refrigerants as the MSF power stage increases

9.2.3 ORC parametric study

The two main factors affecting the ORC cycle are the heating source temperature and the cooling water temperature. The effect of the variation of cooling water temperature (T_C) on the cycle performance will be analysed. However, the heating source temperature influence has been discussed in detail since this study deals with variable heating source temperatures (from 68°C to 100°C). Consequently, this part of the study focuses on the influence of changing the evaporator temperature (T_1), since it is the key temperature for determination of the evaporator pinch point ($T_1 - T_B$). Both of these analyses will be performed for MSF power stage 8 and for both R134a and R245fa working fluids.

The effect of the evaporator temperature was studied over $\pm 3^\circ\text{C}$ of the evaporator design temperature 60.7°C at MSF power stage 8 with a fixed annual average cooling water temperature of 27°C . Increasing the evaporator outlet temperature (T_1) raises the corresponding pressure; therefore, the enthalpy for the turbine inlet, and consequently, both the gross and net power are increased for both working fluids (Figure 9.13).

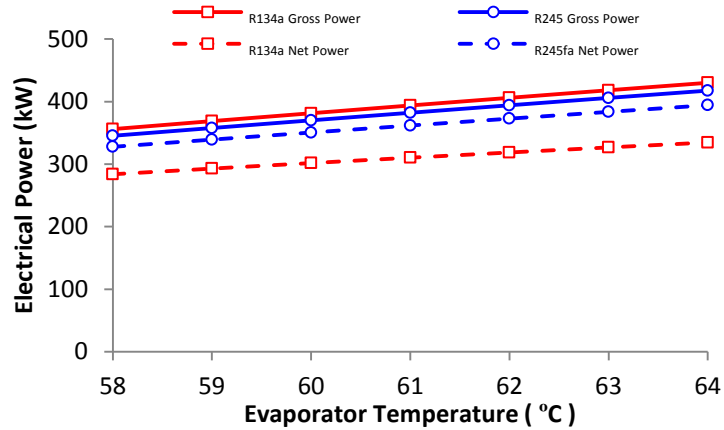


Figure 9.13: Influence of the evaporator temperature on gross and net power for both the R134a and R245fa ORC unit

Variation of evaporator temperature affects refrigerant pump power consumption considerably (Figure 9.14). A 1°C increase in the evaporator temperature causes, on average, a 5.2% rise in pump power consumption for both refrigerants. Interestingly, the rise in the evaporator temperature reduces the refrigerant mass flow rate required within the ORC cycle (Figure 9.14). This behaviour can be justified as a result of the equal heat amounts absorbed in the evaporator over the considered evaporator temperature range. Thermodynamically, the mass flow rate should decrease to adjust to changes in the inlet and outlet evaporator temperature differences.

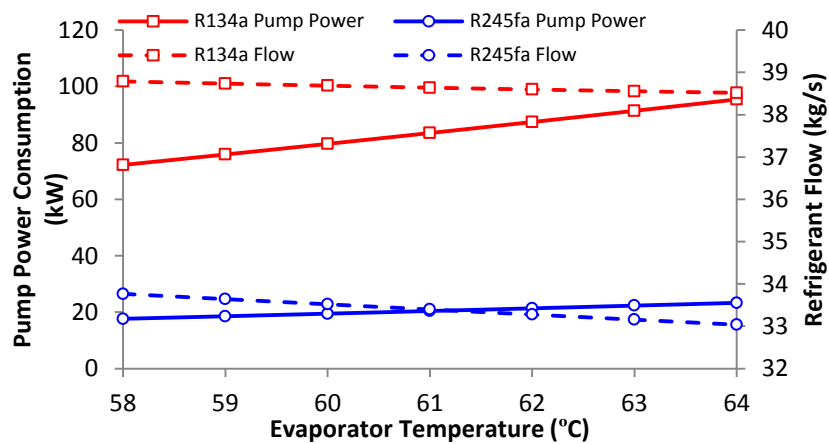


Figure 9.14: Influence of the evaporator temperature on refrigerant pump power consumption and working fluid mass flow rate for both the R134a and R245fa ORC units

The rise in evaporator temperature is accompanied by increases in evaporator heat transfer conductance (UA) and evaporator NTU (Figure 9.15), due to a reduction in

evaporator effectiveness, which is almost 99% at 58°C (pinch point = 0.15°C) dropping to 47% at 64°C (pinch point = 5.3°C) for both R134a and R245fa. Consequently, a 1°C increase in evaporator temperature increases evaporator UA and NTU by the almost same percentage for both refrigerants, 4.3% and 8.6%, respectively for R134a and R245fa.

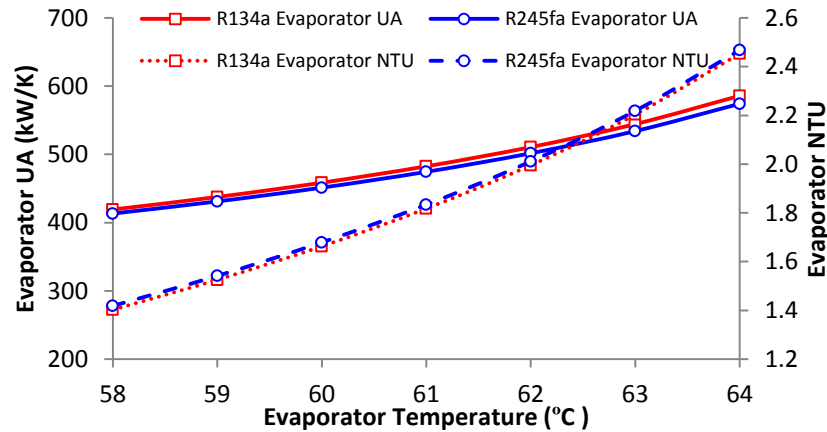


Figure 9.15: Influence of the change in evaporator temperature on evaporator UA and NTU for both the R134a and R245fa ORC units

Increasing the evaporator temperature increases the ORC energy efficiency and decreases the condenser cooling water flow for both working fluids (Figure 9.16). The rise in thermal efficiency is due to the increase in net produced power for the same evaporator heat input due to an increase of turbine inlet enthalpy. However, reduction of the cooling water flow results from a decrease in the working fluid mass flow rate.

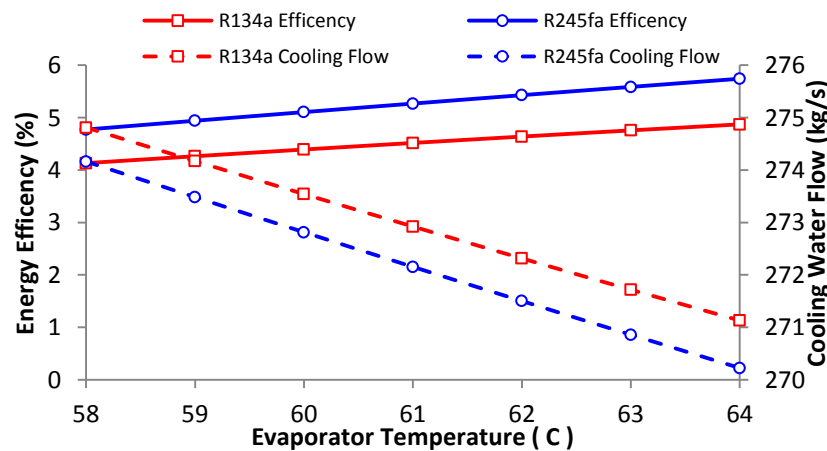


Figure 9.16: Influence of the evaporator temperature on ORC efficiency and cooling water flow for R134a and R245fa

The exergy analysis shows the evaporator temperature has a significant effect on the ORC exergy efficiency (Figure 9.17), with the exergy efficiency varying by 6.4% and 8.4% for R134a and R245fa, respectively, over the considered temperature range. This enhancement of exergy efficiency correlated to a clear reduction in ORC cycle component exergy destruction (Figure 9.17). Appendix 9-C presents the exergy efficiency and exergy destruction ratio for all ORC components for both refrigerants.

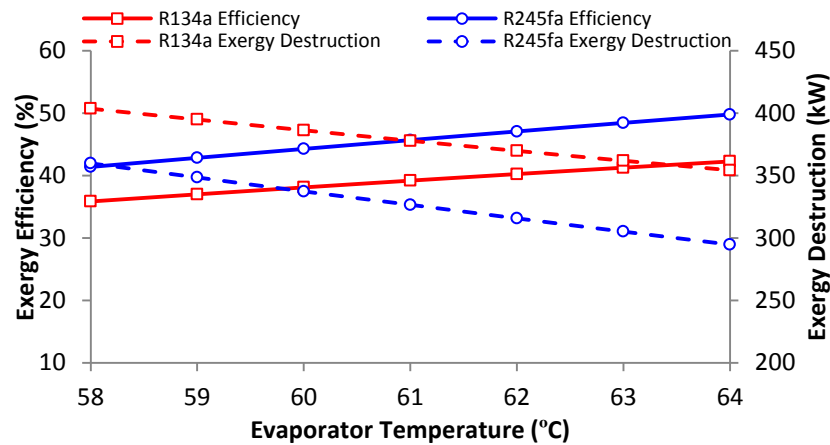


Figure 9.17: Influence of the evaporator temperature on ORC exergy efficiency and exergy destruction for both ORC refrigerants

The influence of the condenser cooling water temperature was studied over the range of 22°C to 33°C, the historically recorded minimum and maximum cooling water temperatures in Oman. The effectiveness of both evaporator (81%) and condenser (31%) as maintained and, therefore, for both these pinch points, were sustained.

Figure 9.18 shows the reduction of gross and net power for both ORC refrigerants as cooling water temperature increases. Averagely, a 1°C rise in cooling water temperature reduces the net power and gross power by 12 kW for R134a and 13 kW for R245fa, because the increase of cooling water temperature causes a rise in condenser temperature (T_3), and consequently, the corresponding ORC turbine exit pressure increases.

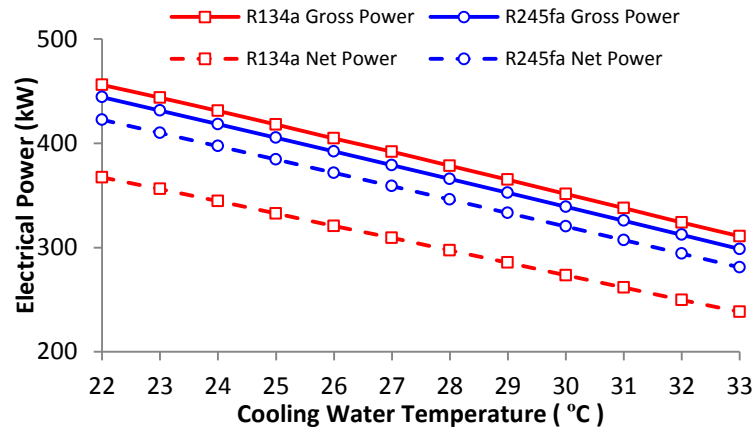


Figure 9.18: Influence of cooling water temperature on ORC gross and net power for both ORC working fluids

For both working fluids, the working fluid pump power consumption reduces by almost 18% for every 10°C rise in the cooling water temperature (Figure 9.19), due to the increase of condenser temperature for higher cooling water temperature and therefore, a corresponding pressure rise. In contrast, the cycle working fluid mass flow rate increases by 9.4% for R134a and 8.0% for R245fa for the same 10°C increase in cooling water temperature, to compensate for the reduction in the evaporator inlet temperature (T_4) to meet the same heat absorption in the evaporator (Figure 9.19).

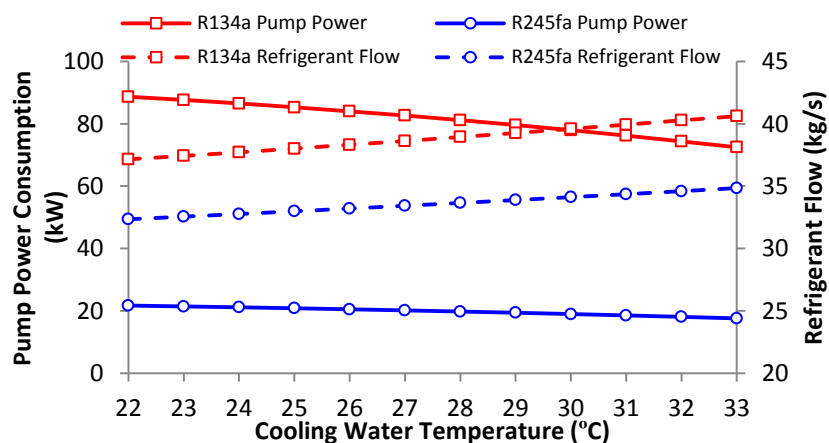


Figure 9.19: Effect of cooling water temperature change on ORC pump power consumption and refrigerant mass flow rate for both refrigerants

The higher working fluid mass flow rate for both refrigerants leads to increases in condenser UA and NTU (Figure 9.20), with the R245fa condenser more affected than the R134a condenser.

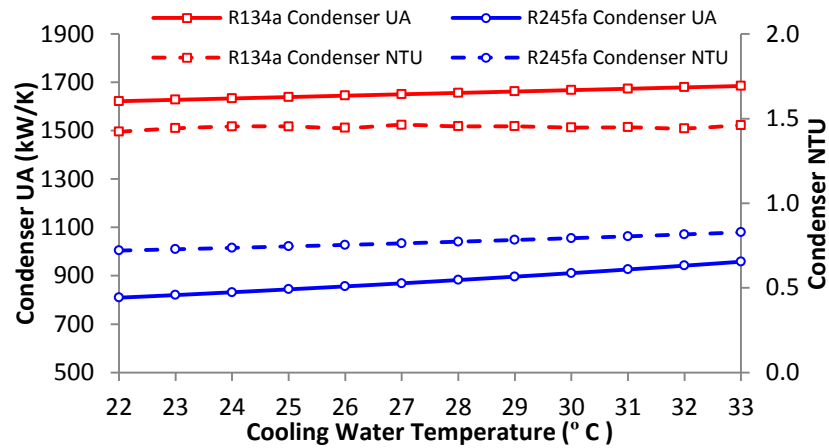


Figure 9.20: Effect of cooling water temperature change on ORC condenser UA and NTU for both working fluids

The rise in the cooling water temperature is accompanied by increase in condenser temperature (T_3), thus with the corresponding pressure for this temperature, turbine output is reduced, reducing ORC efficiency almost equally for both working fluids. On other hand, the cooling water flow shows a 3.0% increase for both working fluids as the cooling water temperature rises by 10°C to cope with the rise in the working fluid mass flow rate (Figure 9.21).

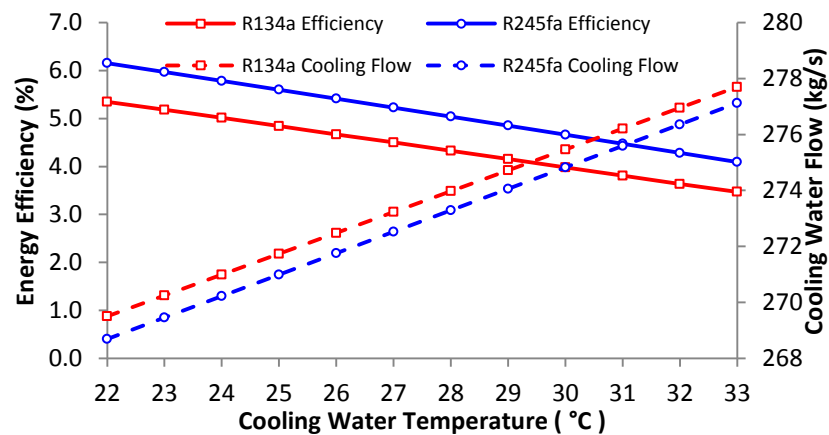


Figure 9.21: Influence of cooling water temperature on ORC thermal efficiency and refrigerant mass flow rate for both working fluids

The cooling water temperature influence on exergy efficiency behaves similarly to the energy efficiency trend (Figure 9.22). The reduction of the exergy efficiency is due to a decrease in net power produced with the same input exergy. The ORC component exergy efficiency varies slightly for all of them except the condenser, which shows a considerable change as shown in Appendix 9-C.

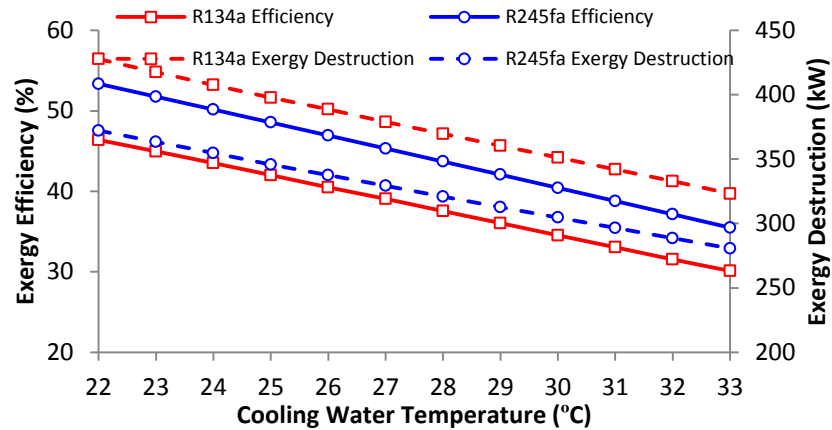


Figure 9.22: Effect of cooling water temperature change on ORC exergy efficiency and total exergy destruction for both working fluids

9.3 Impact on the cogeneration plant of powering ORC from MSF

This section presents the impact of powering the ORC unit from MSF hot distillate water on the cogeneration plant actual operation scenarios. Figure 9.23 shows the cogeneration plant scheme after recovering part of the heat from the MSF to power the ORC. In this scheme, the cogeneration plant produces net power in addition to the both GTs and ST from the ORC unit. The water production enhancement will be similar to the other heat recovery technologies, that is, 90 tonne/h from the three distillers, with negligible effect on steam consumption since the heat utilized in the ORC uses only 10°C.

Only the R245fa ORC cycle (from the first eight MSF power stages) gives a better performance compared with R134a. The impact of this hybridization of the MSF and ORC is investigated in comparison to the original MSF configuration.

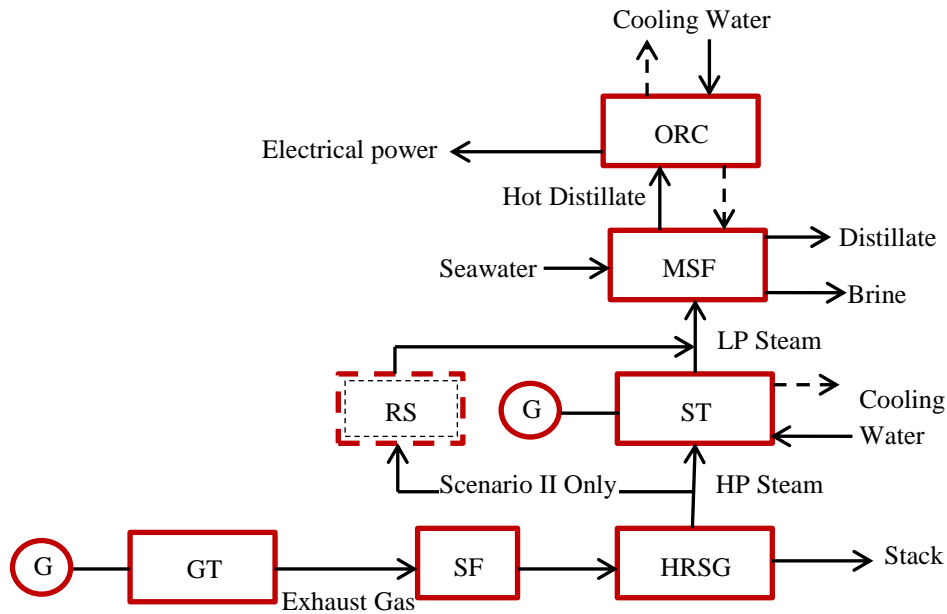


Figure 9.23: schematic drawing of cogeneration plant with ORC technology recovering the heat from MSF desalination

Powering the ORC from the MSF augments the cogeneration plant net power, as the number of power stages increases (Figure 9.24). This augmentation reaches a maximum of 0.9% for scenario II (at stage 8) compared with 0.2% and 0.4% for scenarios I and III, respectively. The high impact on scenario II is justified by the low net power produced in this scenario compared with the other two, while the additional net power from the ORC is the same for all three operating scenarios (three ORC units powered from three MSF units). This enhancement results in annual electrical energy augmentations of 5840 MWh, 2842 MWh, and 600 MWh from scenarios I, II, and III, respectively.

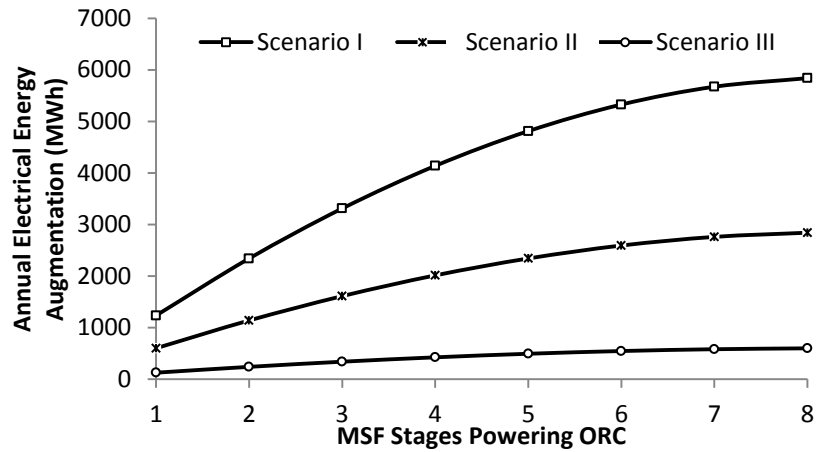


Figure 9.24: Operating scenarios' annual energy augmentation resulting from powering the ORC from the MSF

Adding more electrical power from the ORC to the net power generated from the cogeneration plant enhances the overall plant energy efficiency, since the ORC is powered from waste heat and not by additional burning natural gas (Figure 9.25). Consequently, cogeneration plant performance indicators, such as G/P ratio and heat utilization factor, also improve, as for thermal energy.

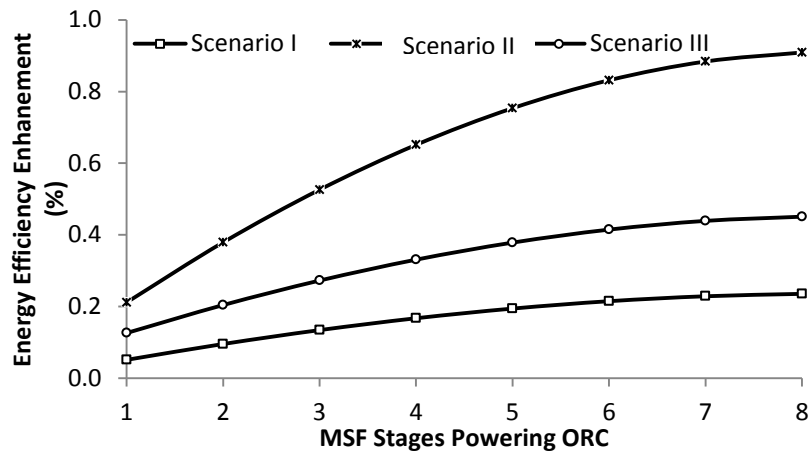


Figure 9.25: Operating scenarios' energy efficiency enhancement resulting from powering the ORC from the MSF

Figure 9.26 shows the exergy efficiency is enhanced more as the MSF power stage for the ORC increases, with scenario II achieving the highest enhancement due to low produced net electrical power compared with the other two scenarios. The enhanced percentage is linked to the total MSF exergy destruction contribution.

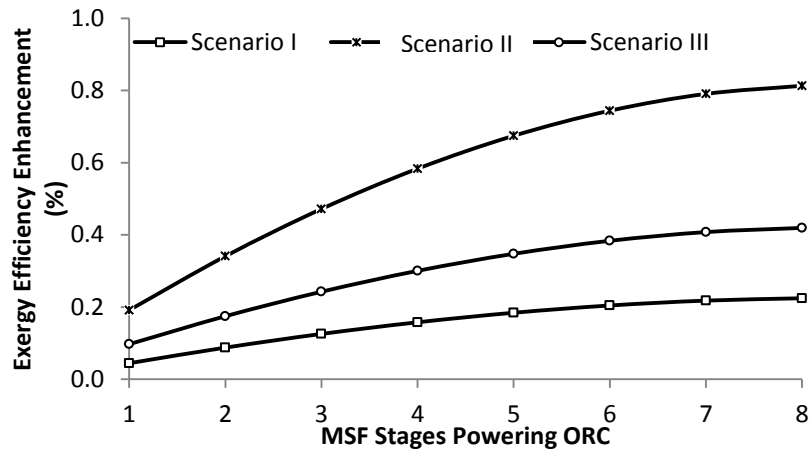


Figure 9.26: Operating scenarios' exergy efficiency enhancement resulting from powering the ORC from the MSF

Environmentally, powering the ORC from hot distillate water from the MSF stages reduces CO₂ emissions as result of producing extra electrical power and water from the extracted heat. The CO₂ emissions reduction percentage was found to be similar to the trend of the enhancement of the net power and thermal efficiency since it counts the electrical power produced from the three ORC powered from the three identical MSF distillers. Although scenario II was most affected by this modification, the total CO₂ emissions reduction shows higher savings at scenario I (1431 kg/h while the other two scenarios are 2001 kg/h and 1160 kg/h, respectively). Figure 9.27 shows the annual CO₂ saving the highest at power stage 8 (13373 tonne/year).

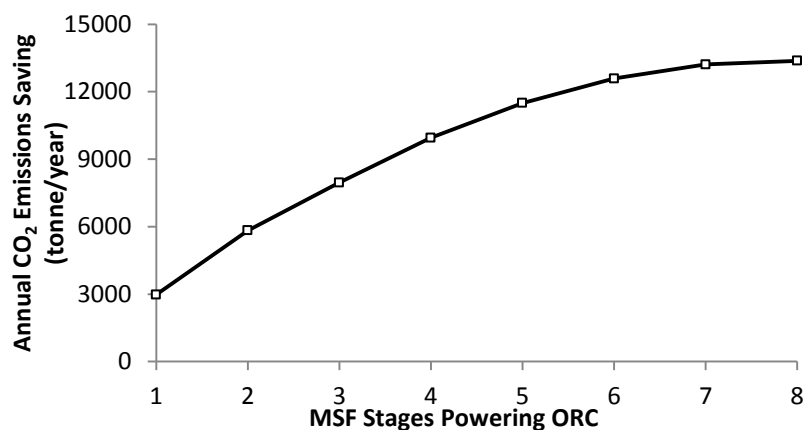


Figure 9.27: Annual CO₂ emissions saving from powering the ORC from the MSF desalination

9.4 Closing Remarks

The study presented an attempt to recover part of the heat from MSF desalination plant hot distillate water to power an ORC. The model used design characteristics of an existing R134a ORC unit, and it was validated against the output of this unit [172]. Then the hot distillate water from various MSF stages is utilized to provide heat to the ORC. Through a detailed study of ORC working fluids is beyond the scope of this investigation, to confirm the importance of correct working fluid choice, the ORC is modelled using R134a and R245fa working fluids at 27 °C cooling temperature and performances are investigated when both of these working fluids are used.

Both refrigerants exhibit an increase of power output and decrease of energy efficiency as heat recovered from more MSF stages. The results showed that the net power produced is highest when distillate hot water up to MSF stage 8 is recovered, generating 359 kW when R245fa is used and 308 kW when R134a is used. The ORC turbine was main contributor of cycle exergy destruction for both refrigerants working fluids. An exploratory parametric study was performed to find the influence of the evaporator temperature and cooling water temperature for both R134a and R245fa with MSF powering stage 8. Both parameters significantly affected the net produced power, and ORC energy and exergy efficiencies.

Powering an ORC from the MSF hot distillate added 5840 MWh, 2842 MWh and 600 MWh annually for scenario I, II and III over and above the original cogeneration plant produced power. This power augmentation increased thermal efficiency, heat utilization factor, exergy efficiency and reduced the G/P ratio and CO₂ emissions. The total CO₂ emissions reduction by this technology was 1431 kg/h, 2001 kg/h and 1160 kg/h for scenario I, II and III respectively, and equivalent to 13000 tonne/year.

Chapter 10

Single Effect Desalination (SED)
powered by hot distillate water from
MSF stages

10.1 Hot water SED modelling and validation

10.1.1 Validation of SED model

This Chapter discusses for the first time the concept of recovering the heat from the hot distillate water from the MSF stages to power an additional Single Effect Desalination (SED), producing additional fresh water to that produced by the MSF. In the literature, there are few studies on MED powered by hot water; normally, it is powered by LP steam [21, 137, 178]. MED is characterized by its ability to recover waste heat from 100°C down to 65°C [179], and the first eight MSF stages provide these temperatures at various mass flow rates.

The IPSEpro desalination library was used to develop a model using actual data from an SED (available in Alfa Laval Marine & Diesel product catalogue [139]) adapted from Wang et al. [139] (Figure 10.1). The model inputs (set values) were obtained from the catalogue, whereas the model output (the SED water production, represented by stream 13 in Figure 10.1) was considered as a calculated value. Appendix 10-A shows the model set and calculated values.

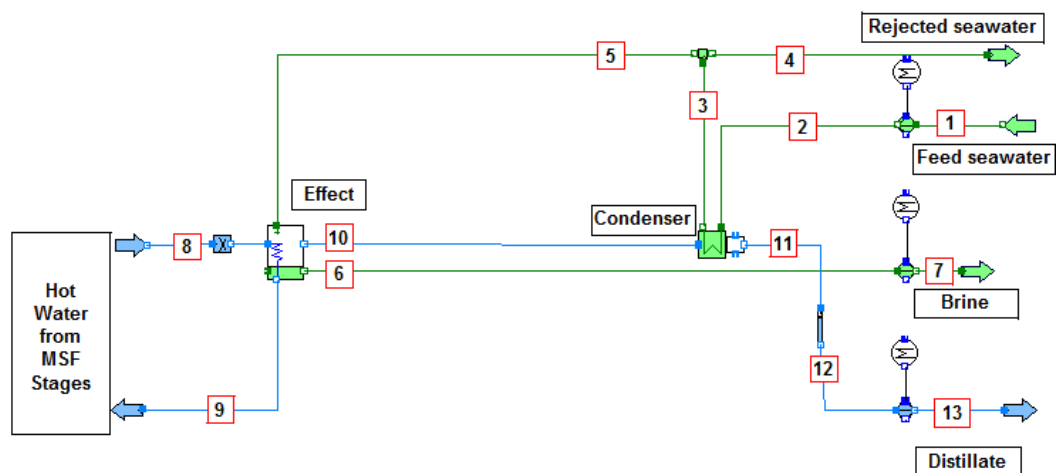


Figure 10.1: The IPSEpro model of SED

Model validation was by comparison between actual performance data and the model results for water production. To ensure the model validation covers an acceptable range of data, 48 cases were selected for validation at different hot powering water flows (\dot{m}_8), hot water powering temperatures (T_8), hot water return temperatures (T_9), and seawater cooling mass flow rates (\dot{m}_1). Seawater salinity (w_1) and seawater cooling temperature were maintained at 35000 ppm and 32°C,

respectively. Figure 10.2 shows the comparison between actual data and the model results, with an average difference of 3.2%, a lower difference compared with the study conducted by Wang et al. for the same SED unit [139].

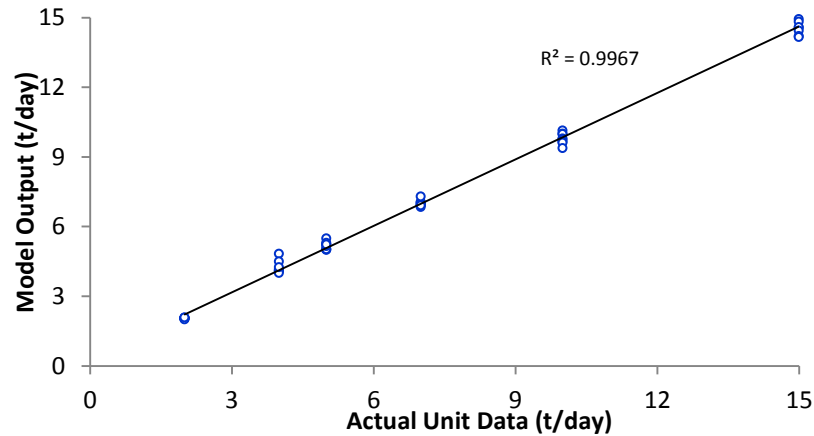


Figure 10.2: Comparison between the actual SED data and the model prediction

10.2 Analysis of SED powered by MSF hot distillate

10.2.1 Hot water SED system energy analysis

Alfa Laval indicates this SED design can be adopted to be powered by hot water at varying temperatures [180]. Thus, hot water recovered from the MSF stages at different temperatures and mass flow rates was used to power the same SED model. Cooling water temperature and salinity was set at 27°C (average Oman seawater condition) and 40000 ppm, respectively. The effect temperature difference ($T_8 - T_9$) was fixed at 10°C based on the average value of the actual unit data from Alfa Laval Marine & Diesel. Appendix 10-B presents the model simulation results for an SED unit powered by heat recovered from the MSF hot distillate water up to the initial eight stages.

Figure 10.3 shows the variation of fresh water production and SED Gain Output Ratio (GOR) as more MSF stage heat is recovered. SED water production rose sharply from 29 tonne/day to 221 tonne/day, as the heat recovered from MSF increased from stage 1 to 8, as a result of the powering stream mass flow rate rising, despite the drop in its temperature. The SED GOR is also enhanced by 10% as the power stages increase from stage 1 to 8. This could be due to high irreversibility at the higher temperature power stages, which will be investigated in detail by exergy analysis (Section 10.2.2). Interestingly, for this SED, the GOR is much lower than

the typical GOR of SED powered by low pressure steam, which is typically from 5 to 9 [32, 181]. The reason is the low enthalpy difference ($h_8 - h_9$) in the case of this hot water SED since no phase change occurs, whereas with a steam SED, a saturated vapour to saturated liquid phase change occurs.

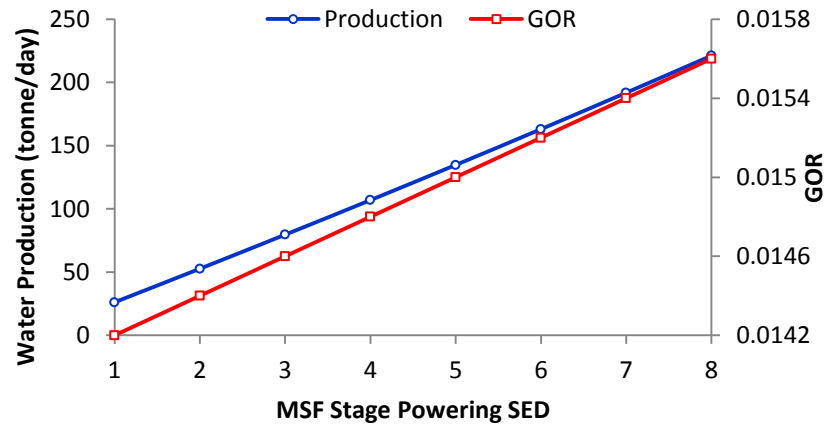


Figure 10.3: Influence of MSF powering stage on SED production and GOR

Due to the increase of power stream mass flow rate as more MSF stages are recovered, the effect vapour production (represented by stream 10) rises. Therefore, the cooling water flow increases (Figure 10.4) to remove the heat required to change the state of stream 10 to saturated liquid. However, 95% of this water is rejected back to the sea due to the low effect seawater requirement.

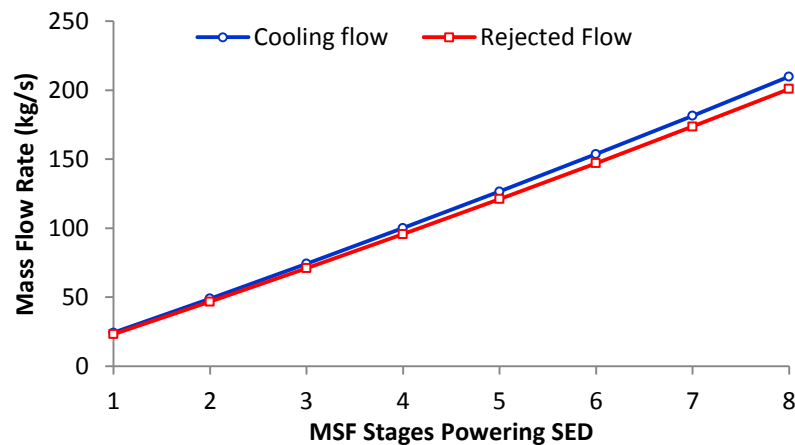


Figure 10.4: Influence of MSF powering stage on cooling and rejected seawater mass flow rate

Heat absorbed from the distillate vapour produced in the SED effect increases as this vapour mass flow rate increases. Thus, the condenser heat duty rises from 698 kW to

6060 kW as the number of MSF recovery stages increases from 1 to stage 8 (Figure 10.5). Consequently, overall condenser heat transfer conductance (UA) exhibits a similar behaviour, varying from 14 kW/K to 238 kW/K, as MSF power stages increase from 1 to 8 (Figure 10.5). In comparison, SED effect heat duty and UA are higher (Figure 10.6) than the condenser (Figure 10.5).

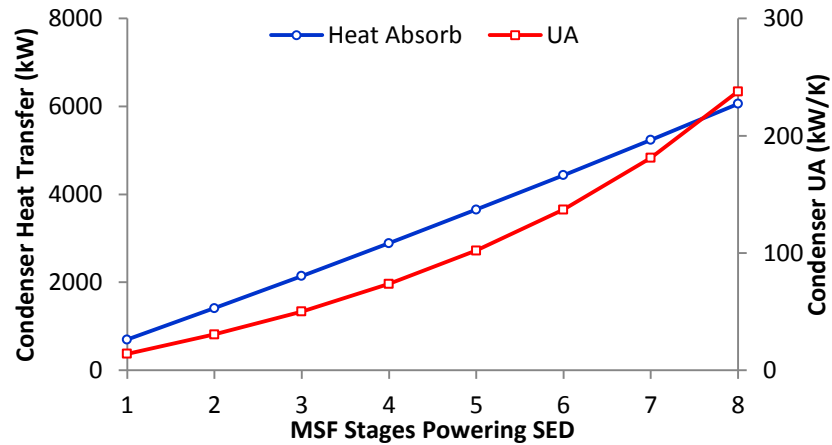


Figure 10.5: Influence of MSF powering stage on SED condenser heat duty and UA

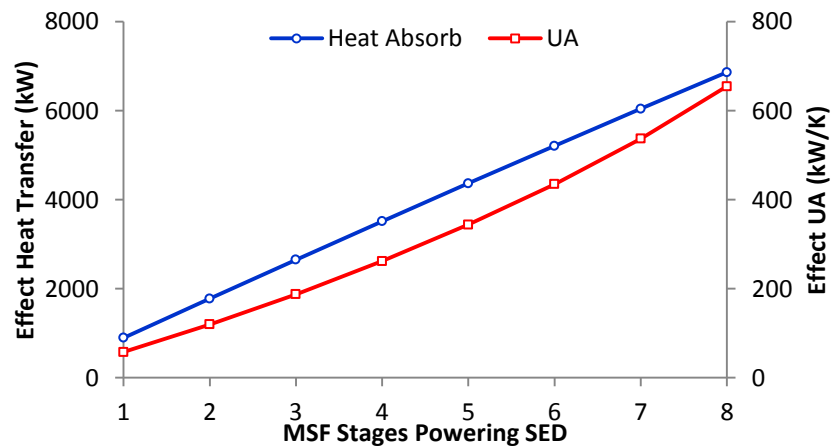


Figure 10.6: Influence of MSF powering stage on SED effect heat duty and UA

SED total power consumption of seawater pump (SWP), brine pump (BP), and distillate pump (DP) increases as heat is recovered from more MSF stages (Figure 10.7) and is in line with increasing flows through all of these.

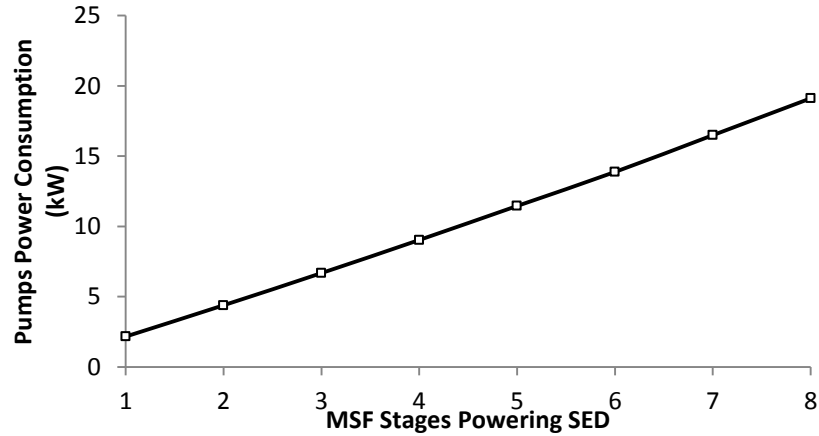


Figure 10.7: Influence of MSF powering stage on the pumps' total power consumption

10.2.2 Hot water SED system exergy analysis

Scant literature exists on the exergy analysis of hot water MED, possibly due to the unavailability of the operational data necessary to perform such a task. Therefore, this is one of the first detailed exergy analyses of an SED powered by hot water, including physical and chemical aspects. The dead state was selected to be the average seawater cooling temperature T_0 of 27°C, pressure p_0 of 101.3 kPa, and seawater salinity $w_{s,0}$ of 40 g/kg. Table 10.1 describes the calculation method for the exergy efficiency and exergy destruction of the SED, and Appendix 10-B gives the results for the stream exergy analysis at different MSF power stages.

This study revealed that the exergy efficiency of SED powered by hot distillate water from MSF stages is too low, similar to other thermal desalination technologies [71, 77]. The hot water SED exergy efficiency is only 0.8% at power stage 1 rising to 1.3% with stage 8 (Figure 10.7), and this is in good agreement with Sayyaadi and Saffari [182]. The low exergy efficiency at the high temperature power stages is due to the higher irreversibility at these stages relative to the input exergy, as indicated by the exergy destruction trend as more MSF stages recover (Figure 10.7), despite the higher SED power mass flow rates.

Equipment	Calculation Method
Seawater pump exergy in	$E_2 - E_1$
Blow down pump exergy in	$E_7 - E_6$
Distillate pump exergy in	$E_{13} - E_{12}$
Pump input exergy in	$E_{PP} = (1/0.75) \times (\Sigma ((E_2 - E_1) + (E_7 - E_6) + (E_{13} - E_{12})))$
Hot water exergy	$E_8 - E_9$
Exergy in	$(E_8 - E_9) + E_{PP}$
Minimum separation work	$W_{min} = E_{(13-A)} + E_{(7-A)} - E_{(1-A)}$
Exergy Efficiency	$\eta_{II} = \frac{W_{min}}{(E_8 - E_9) + E_{PP}}$
Total exergy destruction	$E_d = E_{Input} - E_{Output}$ $E_d = ((E_8 - E_9) + E_{PP}) - W_{min}$
Exergy destroyed in pumps	$E_{d,PP} = (1 - 0.75) \times E_{PP}$
Exergy destroyed in effect	$E_{d,E} = (E_8 + E_5 - E_{10} - E_6 - E_9)$
Exergy destroyed in condenser	$E_{d,C} = (E_2 + E_{10} - E_3 - E_{11})$
Exergy destroyed in cooling process	$E_{d,C} = E_4$
Exergy destroyed in product	$E_{d,P} = (E_{13} - E_{(13-A)})$
Exergy destroyed in brine disposal	$E_{d,B} = (E_7 - E_{(7-A)})$

Table 10.1: Exergy analysis method for hot water SED

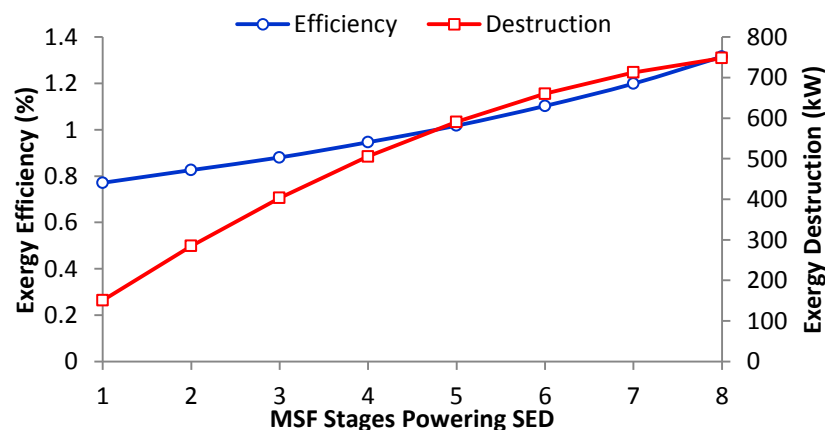


Figure 10.8: Influence of MSF powering stage on SED exergy efficiency and destruction

Figures 10.9 and 10.10 present the exergy destruction and exergy destruction ratio among the SED components at the possible MSF power stages. The condenser is the

dominant contributor of exergy destruction in SED. It represents 66% (101 kW) at power stage 1, reduced to 63% (470 kW) at power stage 8. Figure 10.8 shows the condenser exergy destruction increasing as the number of stages increases, but Figure 10.9 shows that the exergy destruction ratio for the condenser falls as the number of stages increases. The second largest contribution is from the SED effect. Its share varied from 15% (23 kW) at power stage 1 to 20% (150 kW) at power stage 8. By comparison, destruction from cooling (C) disposal, brine (B) disposal, product (P) disposal, and pump (PP) are all small.

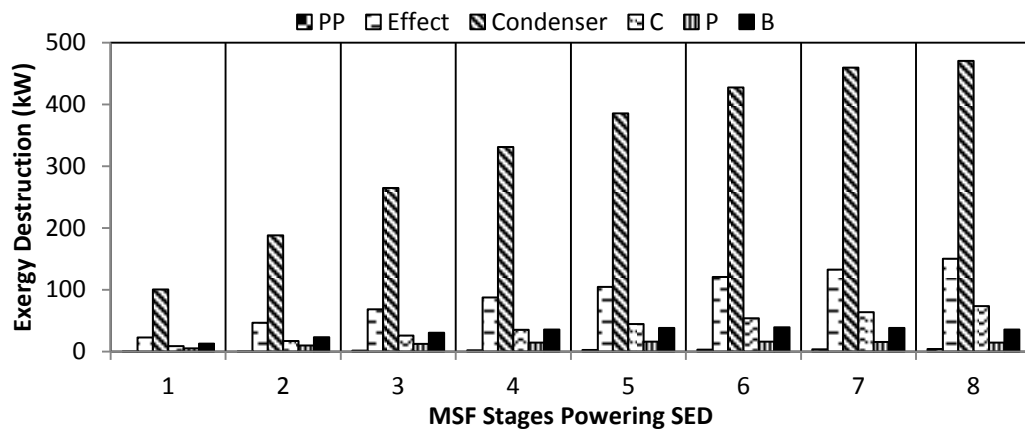


Figure 10.9: Influence of MSF powering stage on the exergy destruction of SED components

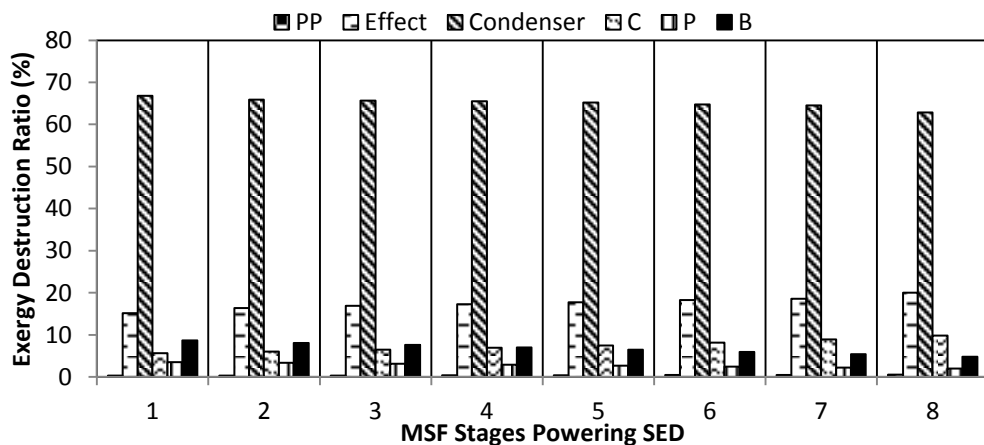


Figure 10.10: Influence of MSF powering stage on the exergy destruction ratio of the SED components

Figure 10.11 describes the exergy efficiency enhancement of the MSF unit at two cases when the MSF counted exergy gained from powering the SED (improved MSF) and when the MSF and SED were considered as one system, where the SED

system exergy destruction is counted (MSF + SED). MSF exergy efficiency improved by 10% at power stage 1, and this enhancement was reached at a maximum of 50% at power stage 8. However, when MSF and SED are considered as one system, the new exergy efficiency of combined system dropped significantly due to the high exergy destruction of the SED system, as was discussed earlier.

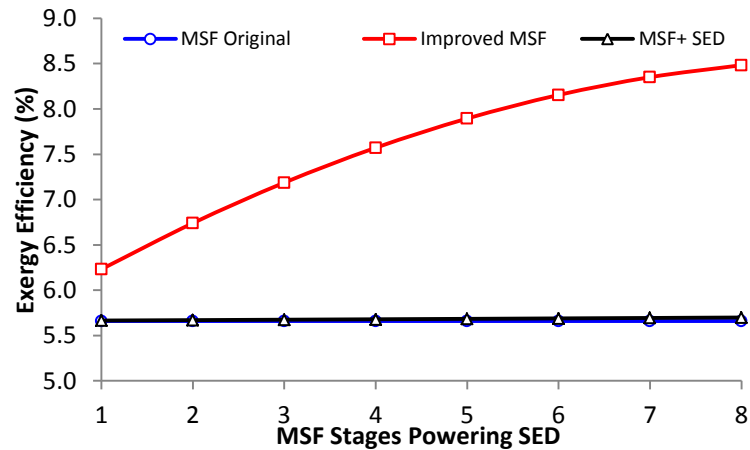


Figure 10.11: Influence of MSF powering stage on the exergy efficiency enhancement of the MSF desalination.

10.2.3 Hot water SED parametric studies

The two main parameters that have a significant influence on the performance of SED are the cooling water temperature and the number of effects [183, 184]. Therefore, these two parameters were investigated over their application ranges.

Seawater cooling temperature was varied over the minimum/maximum Oman seawater temperature range of 22–33°C. The study was carried out at a fixed inlet seawater feed mass flow rate of 209 kg/s with seawater salinity of 40000 ppm. Raising the effect inlet seawater temperature led to an increase of fresh water production and hence GOR at the same heat input (Figure 10.12).

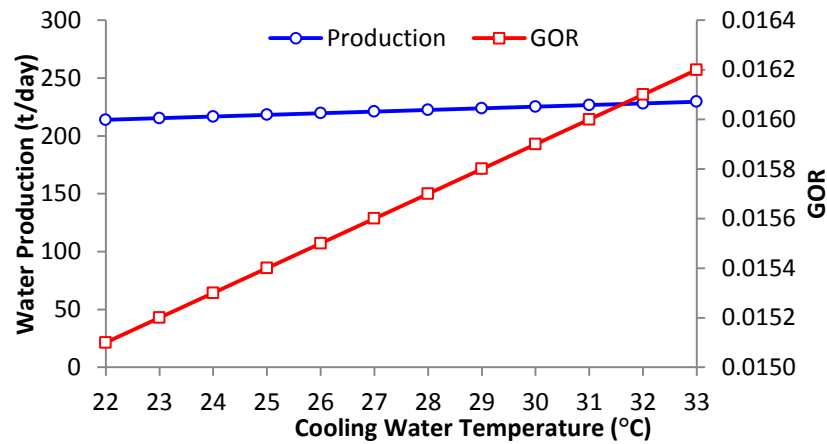


Figure 10.12: Influence of cooling water temperature on SED water production and GOR

The exergy efficiency is increased by raising the cooling water temperature (Figure 10.13). The reason is clear from the drop of exergy destruction at the higher seawater cooling temperatures.

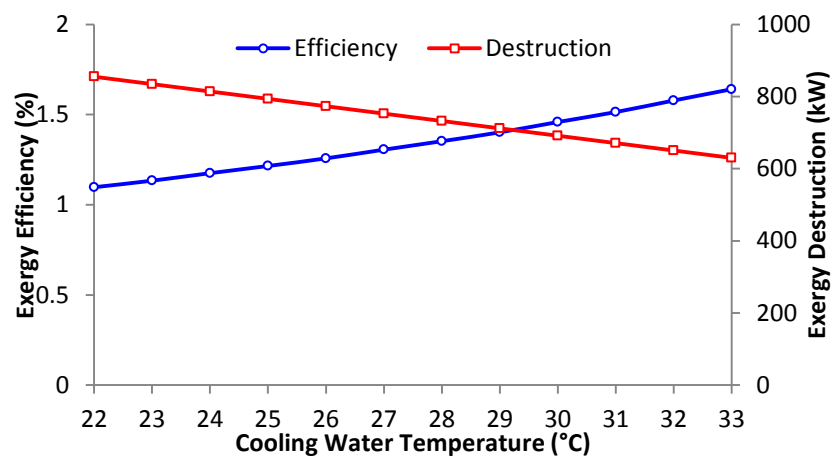


Figure 10.13: Influence of cooling water temperature on SED exergy destruction and exergy destruction ratio

Researchers have investigated the optimal number of SED effects related to unit performance [183–186]. For this parametric study, the SED input parameters were kept constant and only the number of effects in the unit was varied, from one to seven effects maintaining a 1°C difference between neighbouring effects. Figure 10.14 shows the IPSEpro model of these seven effects.

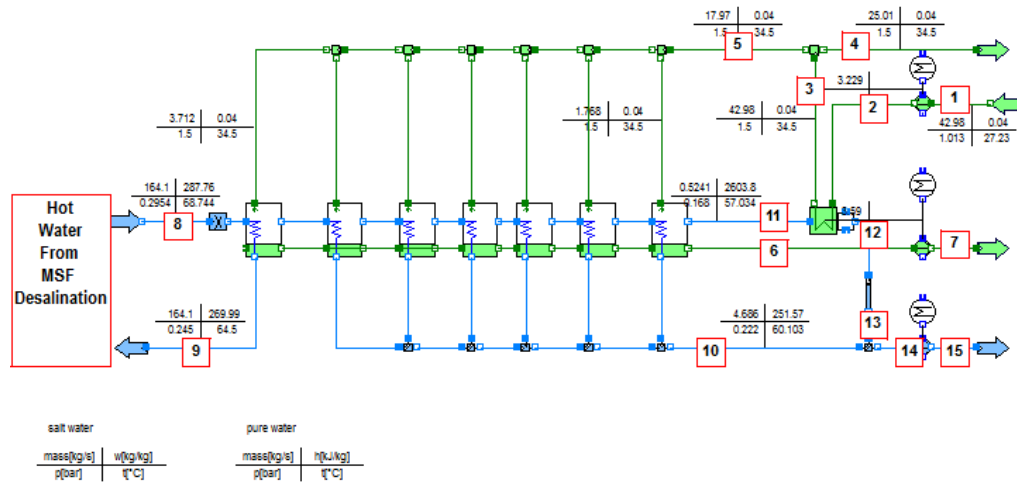


Figure 10.14: IPSEpro model of the seven effects

The fifth effect is the optimal effect, with the water production reaching a maximum (537 t/day). Figure 10.15 describes the trend of water production and GOR as the effect number increases. This result agrees with Ameri et al [183]. Thermodynamically, increasing the number of effects causes a drop on the first effect outlet temperature (T_9), thus the effect fresh water vapour production (\dot{m}_{10}) reduces continuously. However, this vapour is utilized again to produce more fresh water vapour in the adjacent effect. This process is repeated as more effects are added, until the drop in vapour production from the first effect becomes more than the additional water produced from the newly added effect, causing a drop in total water production.

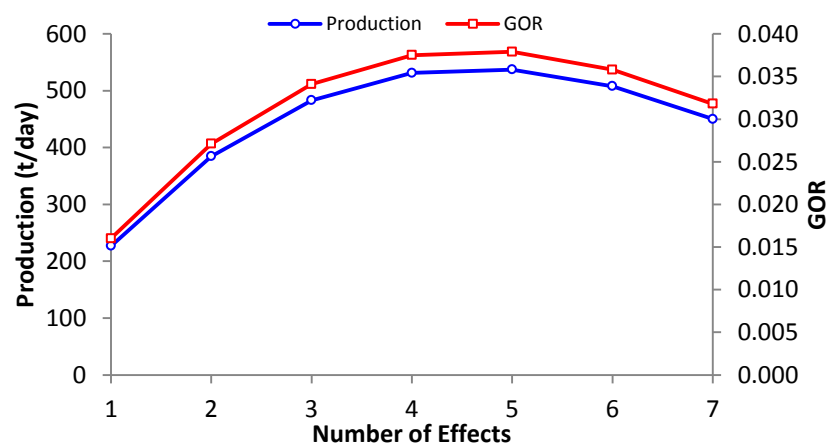


Figure 10.15: Influence of number of effects on water production and GOR

Another benefit from increasing the number of effects is reduction of the seawater cooling water flow (Figure 10.16), with, on average, a drop of 20% in cooling water

flow for one more effect added. The decrease of seawater cooling flow is due to the drop of water production from the effect adjacent to the condenser, since for the proceeding effects, the water produced is condensed in the neighbour effect, unlikely a single effect where all the vapour is condensed in the condenser. Consequently, this reduction of cooling water flow leads to reduced heat duty for the condenser (Figure 10.17).

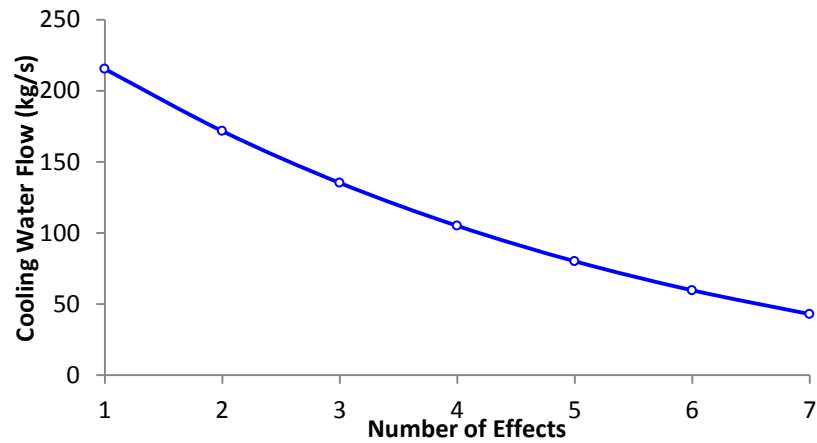


Figure 10.16: Influence of number of effects on seawater cooling flow

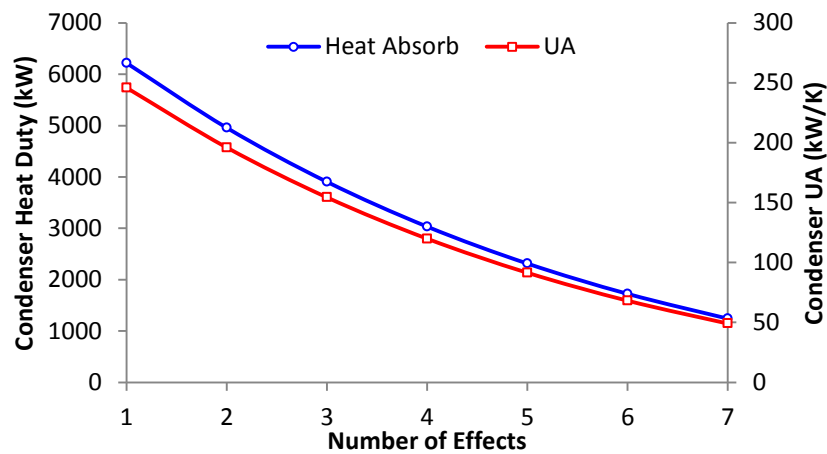


Figure 10.17: Influence of number of effects on condenser duty and UA

Exergy efficiency exhibits an increasing trend as the number of effects rises (Figure 10.18). However, this increasing trend flattens out the optimal production effect (1.3% at one effect to 5.0% at seven effects). This can be explained by a reduction in exergy destruction at a higher number of effects as a result of the utilization of more exergy.

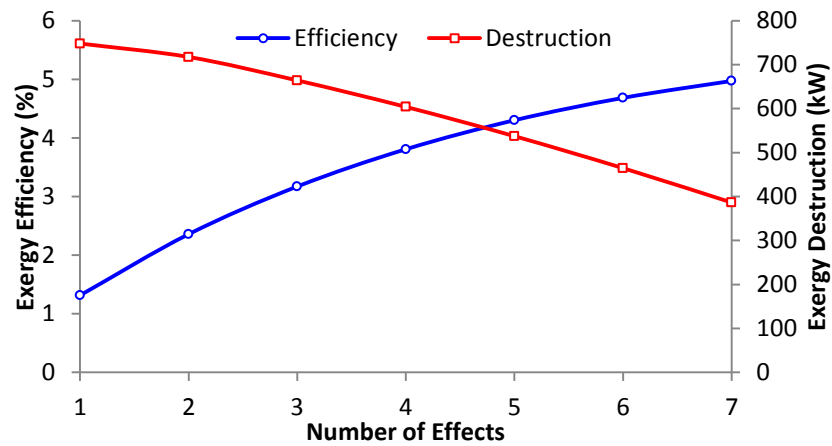


Figure 10.18: Influence of the number of effects on exergy efficiency and destruction

This reduction of total exergy destruction in Figure 10.17 can be explained more from Figures 10.19 and 10.20. The condenser is confirmed as the component most affected by the increase in number of effects. Its exergy destruction reduces from 470 kW (representing 63% of total exergy destruction) at the first effect to 97 kW at the seventh (represent only 25% from total exergy destruction). This reduction results from the decrease of heat absorbed mentioned previously. The effect exergy destruction is almost uniform around 200 kW, but the effect exergy destruction ratio rises from 20% at effect 1 to 40.7% at effect 7 due to a reduction in the condenser share.

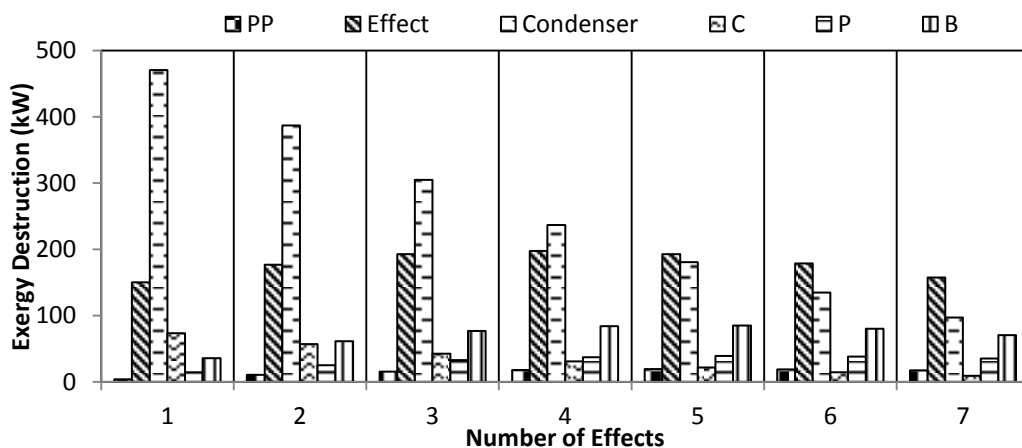


Figure 10.19: Influence of number of effects on component exergy destruction

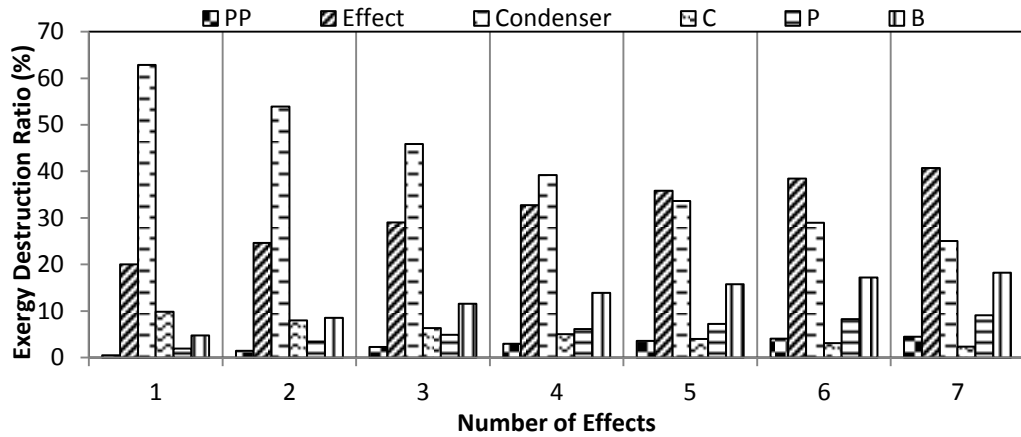


Figure 10.20: Influence of number of effects on component exergy destruction ratio

10.3 Impact of powering SED from MSF hot water on the cogeneration plant

Figure 10.21 illustrates the new configuration of the cogeneration power and water plant powering additional SED from the MSF stages. The main impact of powering SED from the hot distillate water of the MSF is to increase the water production from the free energy source recovered from the MSF stages.

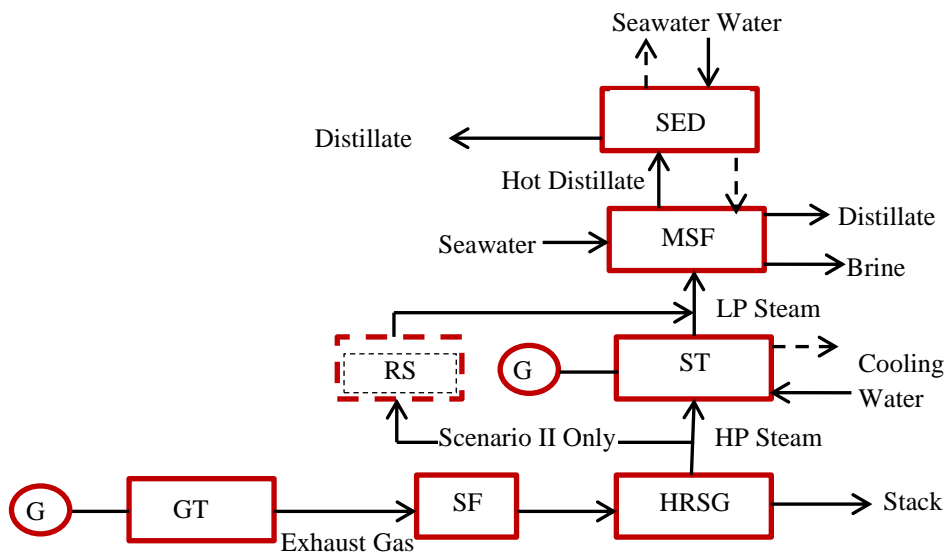


Figure 10.21: Cogeneration plant configuration showing the MSF powering the SED

At the three operating scenarios, water production enhancement is the same, 663 tonne/day from the three identical MSF units at the optimal powering stage. This represents around 0.7% of total plant water production, and it increases as the number of MSF power stages increases. Furthermore, from the parametric study of the number optimal of effects, the water production enhancement can reach 1.8% at

the optimal effect suggested (Section 10.2.2). The annual additional fresh water from the SED at the three operating scenarios and power stage 8 is 149945 tonne, 72982 tonne and 15392 tonne for scenarios I, II, and III, respectively (Figure 10.22).

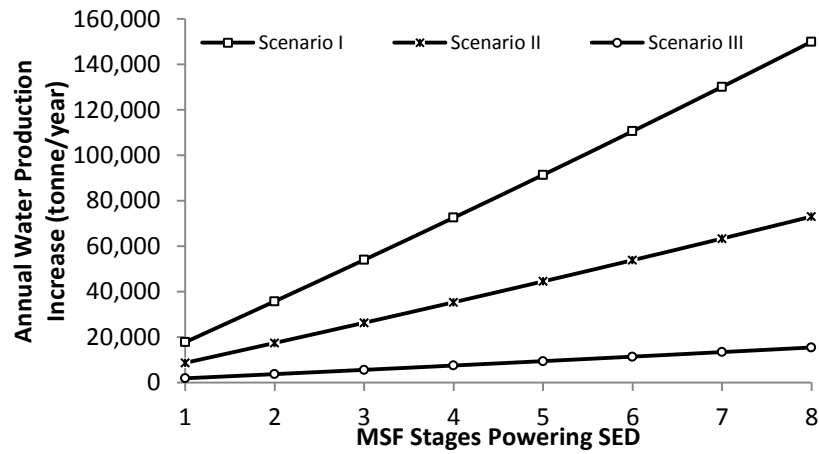


Figure 10.22: Annual impact of powering the SED from the MSF stages on water production from the cogeneration plant operating scenarios.

Additional water production saves MSF input exergy consumption. In the original configuration, each MSF unit consumed around 20.4 kW (equivalent electrical power) to produce 1 m³ of water. Therefore, the water produced from the three SEDs coupled to the MSF was able to save 564 kWh, 564 kWh, and 451 kWh from scenarios I, II and III, respectively, achieving an annual saving of 4862 MWh (Figure 10.23). The equivalent electrical energy saving is equal for scenarios I and II since the MSF is almost in full load operation, but scenario III saves less due to the lower MSF load.

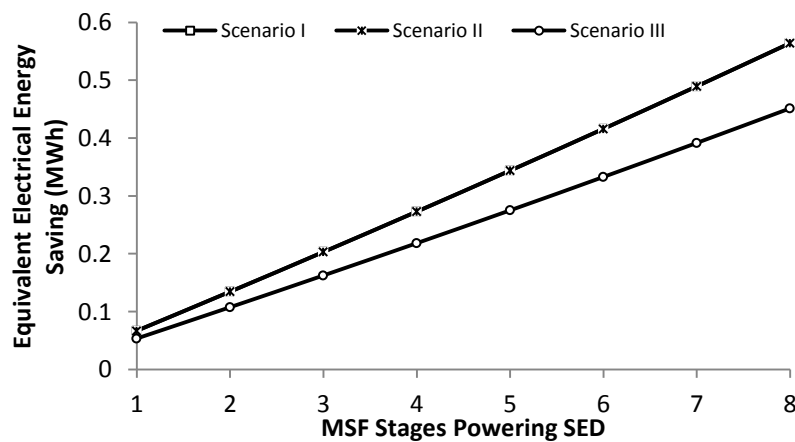


Figure 10.23: Equivalent electrical energy saving result from powering the SED from the MSF

Figure 10.24 presents this saving as exergy efficiency enhancement at the three operating scenarios. Scenario II has the highest enhancement in exergy efficiency, due to supplying MSF steam through the reduction station not the steam turbine, unlike the other scenarios.

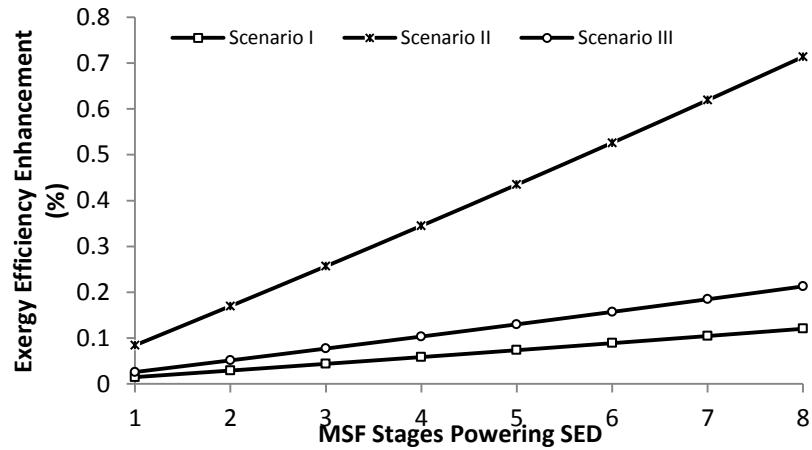


Figure 10.24: Impact of powering the SED from the MSF on the exergy efficiency enhancement of the cogeneration plant at the three operating scenarios

Carbon dioxide emissions reduce as a result of the electrical energy saving (Figure 10.25). Figure 10.26 describes the annual CO₂ saving based on the operating percentage of each scenario.

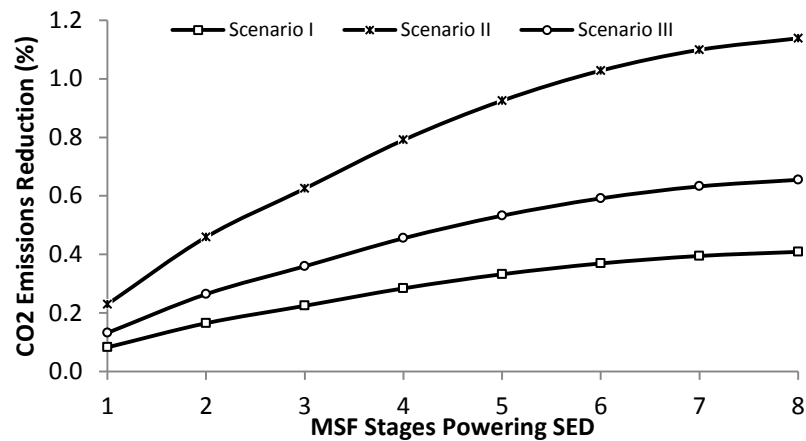


Figure 10.25: Impact of powering SED from MSF on the CO₂ reduction of the cogeneration plant at the three operating scenarios

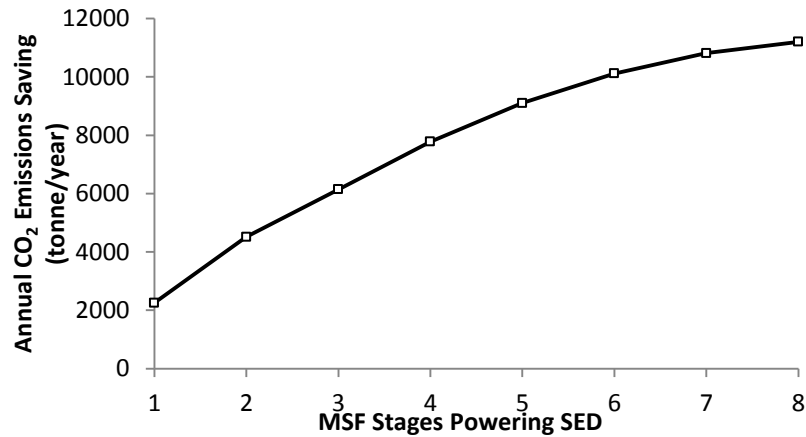


Figure 10.26: Impact of powering SED from the MSF on annual CO₂ emissions saving

10.4 Closing Remarks

This Chapter presented a novel method of producing additional fresh water from SED powered by recovering heat from the MSF hot distillate water. To investigate this, an IPSEpro model was developed for a commercial SED and validated against manufacturer actual data with an average error of only 3.2%.

An investigation of powering the SED from increasing MSF stages has been carried out, showing the highest water production of 221 tonne/day at the last possible recovering MSF stage 8. The SED GOR trend followed that of water production with the highest value of 0.0156 at stage 8, which was much lower than for a typical SED conventionally powered by low pressure steam. Similarly, the SED exergy efficiency increased from 0.8% to 1.3% as MSF powering stages increased from 1 to 8. The condenser was the highest contributor of exergy destruction, representing averagely 63%, whereas the SED effect share was around 20%. In addition, powering SED from MSF to increase MSF exergy efficiency up to 50% compared with the original configuration.

A parametric study on unit performance included the influence of seawater cooling water temperature and modelling SED to MED with a number of effects. Cooling water temperature raises water production and GOR by 7.3% for each 10 °C increase. Exergy efficiency of the SED rose from 1.1% to 1.6% for 10°C increase in cooling water temperature as a result of a drop in condenser exergy destruction. The study revealed MED was highly affected by the number of effects with five effects

found optimal to be for water production. At the optimal effect number, water production increased sharply to 140% higher GOR compared to SED. However, exergy efficiency continues to improve almost linearly as more effects are added, rising from 1.1 % to 5.0% as the number of MED effect varied from 1 to 7.

The additional water produced from SED improved overall cogeneration plant water production by 0.7%, equal to 240000 m³ annually, and saved an equivalent electrical power of 4862 MW, increasing cogeneration plant exergy efficiency and reducing CO₂ emissions by 11000 tonne/year.

Chapter 11

Economic assessment

11.1 Introduction

This Chapter assesses economically the four modifications options: MSF + IH only, AC + IH, ORC + IH, and SED + IH, which have been investigated for MSF desalination. Certain assumptions were made to conduct this economic assessment: 20 years project lifetime, zero taxation on all newly installed equipment and the revenue obtained, and zero discount rate. Where necessary costs were updated using the British pound Retail Prices Index (RPI), for example, for 1992 heat exchanger costs [151], this was assumed as 180% [187]. Additionally, contingencies and salvage value are assumed as 10% and 1% of technical equipment cost [46, 94].

Revenue estimation is based on Oman selling prices of electricity, water, and natural gas, while other requirements of the study, such as costs of equipment, operation cost, maintenance cost, and other elements of project implementation were obtained from the literature. To perform the profitability analysis, IPSEpro economics was used to calculate the economic study indicators. The indicators chosen are payback period, net present value, and average rate of return.

11.2 Estimation of initial and operation and maintenance costs

The initial cost of the project or any modification within the plant is the sum of direct and indirect costs. The direct costs include cost of purchased equipment, installation, piping, instrumentation, control system, wiring, civil work, and land. Indirect costs consist of costs of supervision, engineering, and construction. In this study, the initial costs were either calculated or obtained from official sources.

The recurrent operation and maintenance costs are linked with revenue but are estimated normally based on the nature of the equipment and area obtained from the literature or through contacting official personnel at the working site.

11.2.1 Heat Exchanger Option

For all four modification options, the IH exchanger is included, but its size is different in each option because of the absorbed heat. The heat exchanger cost was estimated using a well-known method obtained from ESDU 92013 [151] since obtaining direct quotations for the heat exchanger was difficult. ESDU has gained a good reputation among British heat exchanger manufacturers, such as IMI Marston [150]. This method depends on the estimation of heat exchanger NTU with available

data for both cold/hot stream inlet/outlet temperatures and an assumption that heat exchanger material is 316L stainless steel:

$$NTU = \frac{UA}{(\dot{m}c_p)_{smaller}} \quad (11 - 1)$$

UA is the overall heat transfer conductance (kW/K) calculated by IPSEpro, whereas $(\dot{m}c_p)_{smaller}$ is the product of the stream flow rate and specific heat capacity of the streams. By knowing the NTU the ratio of heat exchanger load and logarithmic mean temperature difference, $\frac{\dot{Q}}{\Delta T_m}$ can be calculated by:

$$\frac{\dot{Q}}{\Delta T_m} = (\dot{m}c_p)_{smaller} NTU \quad (11 - 2)$$

This value of $\left(\frac{\dot{Q}}{\Delta T_m}\right)$ is used to read off the values of coefficients C_1 and C_2 from ESDU 92013 Table 9.2 based on the type of fluid and the inlet and outlet pressures of the heat exchanger. For the four modification options in the MSF desalination, the heat exchanger is selected as a simple shell and tube heat exchanger, which is the most common available type and has a wide range of applications in the process industry. However, for GT inlet cooling, the heat exchanger was selected as a multi-pass unmixed shell and tube heat exchanger, with the coolant as LP treated process water (chilled water) and the hot stream as LP gas (air). Finally, a C-value was determined by:

$$C = \exp \left[\log_e C_1 + \frac{\log_e \left(\frac{C_1}{C_2}\right) \log_e \left[\frac{\dot{Q}}{\Delta T_m} / \left(\frac{\dot{Q}}{\Delta T_m}\right)_1 \right]}{\log_e \left[\left(\frac{\dot{Q}}{\Delta T_m}\right)_1 / \left(\frac{\dot{Q}}{\Delta T_m}\right)_2 \right]} \right] \quad (11 - 3)$$

The final heat exchanger cost is obtained by multiplying the C value at $\left(\frac{\dot{Q}}{\Delta T_m}\right)$. All these formulae were incorporated into a MS Excel spreadsheet to calculate the heat exchanger cost as illustrated by the example in Figure 11.1.

Heat Exchanger Cost Calculation		
Hot Side		
Temperature In	69	°C
Temperature Out	41	°C
Cold Side		
Temperature In	36	°C
Temperature Out	42	°C
Heat Load	18,551,050	W
ΔT	28	°C
$(mc_p)_{\text{smaller}}$	671070	
NTU	2.00	
$Q/\Delta T_m$	1,342,139	W/°C
C1	0.116	
C2	0.058	
$(Q/\Delta T_m)_1$	100,000	
$(Q/\Delta T_m)_2$	1,000,000	
C-value	0.053	£/(W/K)
Heat Exchanger Cost Calculation	128241	£

Figure 11.1: MS Excel worksheet for the heat exchanger cost calculations

Costs of the heat exchangers for the four modifications are illustrated in Table 11.1. The AC heat exchanger has the lowest cost since it is powered only up to MSF stage 7 (the optimal powering stage for the AC) whereas the others are powered up to stage 8. The cogeneration plant consists of three identical distillers; therefore, the final cost is the sum of three heat exchangers. Furthermore, as informed by the plant site manager [188], the operation and maintenance (O&M) cost for the heat exchangers varies but be assumed as 5% of the purchased cost. During heat exchanger installation, piping costs from the MSF stages to the heat exchanger should be included, covering installation, supervision and engineering, and construction. The piping and installation were assumed to be 30% of purchased equipment cost, whereas supervision and construction were 30% [46].

Modification	Unit	IH	AC	ORC	SED
Absorbed heat	kW	18551	15916	13101	13101
C-value	£/(W/K)	0.053	0.055	0.053	0.053
Single heat exchanger cost	£	128241	119081	130218	130218
For the three distiller	£	384723	357243	390654	390654
GT inlet heat exchanger	£	–	448793	–	–
O&M cost	£	19236	40302	19533	19533
Piping cost	£	115417	241811	117196	117196
Construction cost	£	76945	161207	78131	78131
Engineering and supervision	£	76945	161207	78131	78131
Installation cost	£	115417	241811	117196	117196
Contingencies	£	38472	80604	39065	39065
Salvage value	£	385	806	391	391

Table 11.1: Heat exchanger costs for the four enhancement options

11.2.2 Absorption Chiller

AC skid costs are normally estimated by specific cost £/kW and varies based on the thermal cooling capacity of the unit. As cooling capacity increases, the unit specific cost reduces [189, 190], based on prices from eight manufacturers at different cooling cost capacities. With the studied AC capacity around 2476 kW, average specific cost is found at 76.8 £/kW, including the unit instrumentation and control system. The unit operation and maintenance cost is estimated as 2% of the unit purchased cost [190]. Table 11.2 shows the breakdown of AC modification cost.

Description			
Initial and installation cost			(£)
1	AC skid unit skid	[189, 190]	570470 (3 units)
2	Piping cost	[46]	171141
3	Construction cost	[46]	114094
4	Engineering and supervision	[46]	114094
5	Installation cost	[46]	171141
6	Contingencies	[94]	57047
7	Salvage value	[94]	5705
O & M annual cost			£/year
1	Operation Cost	[94]	11409
2	Maintenance Cost	[190]	11409

Table 11.2: AC option initial and operation maintenance cost estimation

11.2.3 Organic Rankine Cycle

The ORC unit is assembled commercially as one unit mounted on a skid or in a package. The ORC unit capacity varies from 0.1 MW to 1 MW, and recently reached 5 MW as manufactured by Geocal [94]. The ORC unit specific prices (£/kW) have

been analyzed in many studies and decrease as unit capacity increases [94, 191]. In this study, the ORC produces 390 kW from each distiller, with the unit specific cost found to be 1422 £/kW. Annual operation and maintenance costs of the unit vary, typically from 13438 to 30958 £/year when the ORC unit production capacity changes from 100 kW to 1000 kW [191], so linear interpolation is used to obtain the corresponding values based on power produced from the ORC unit. Table 11.3 shows initial and operation and maintenance cost estimations.

Descriptions			(£)
Initial and installation cost			
1	Skid-mounted R245fa ORC unit	[94, 191]	1663740 £ (3 units)
2	Piping cost	[46]	499122
3	Construction cost	[46]	332748
4	Engineering and supervision	[46]	332748
5	Installation cost	[46]	499122
6	Contingencies	[94]	166374
7	Salvage value	[94]	16637
O & M annual cost			£/year
1	Operation and Maintenance Cost	[191] Using linear interpolation	57249 (3 units)

Table 11.3: ORC option initial and operation maintenance

11.2.4 Single Effect Desalination

The hot water SED initial cost is estimated from the literature [192] based on the annual amount of water produced. Each SED unit in the study was able to supply 221 m³/day. The initial cost of the SED was found to be 525 £/(m³/day) [192]. The operation and maintenance cost was estimated annually at 68 £/(m³/day) [192]. Table 11.4 shows the initial and operation and maintenance costs for all three units.

Descriptions			(£)
Initial and installation cost			
1	SED unit	[192]	348075
2	Piping cost	[46]	104423
3	Construction cost	[46]	69615
4	Contingencies	[94]	69615
5	Engineering and supervision	[46]	104423
6	Installation cost	[46]	34808
7	Salvage value	[94]	3481
O & M annual cost			£/year
1	Operation and Maintenance Cost	[192]	45084

Table 11.4: SED option initial and operation maintenance cost estimation

11.3 Revenue Estimation

For the four heat recovery technologies, the annual financial revenues can be estimated based on saving of natural gas, generating more electrical power, or producing additional water. The distillate extraction improves the original MSF desalination unit production equally (90 tonne/h from the three MSF distillers) for all the heat recovery options. However, in the case of IH and AC, additional water production capacity was accompanied by natural gas reduction; therefore, for both these options, natural gas savings were estimated from the simulation model. By contrast, additional electrical power from the ORC and more water production from the SED were calculated. Table 11.5 describes the economic improvements achieved from the different heat recovery technologies.

Enhancement technology	Unit	MSF + IH only	MSF + AC + IH	MSF + ORC + IH	MSF + SED + IH
Water	m ³ /year	788400	788400	788400	238319+788400 =1026719
Natural gas saving	t/year	4968	2484 (from MSF steam reduction)+ 10196 (From GT efficiency improvement)	Nil	Nil
Electrical Energy	MWh/year	Nil	Nil	9282	Nil

Table 11.5: Summary of heat recovery technology improvements

To understand the revenue estimation of these heat recovery options, it is necessary to clarify the contracts nature of power and water industry in Oman. Most companies producing electrical power and water are private companies (local or global) and have long-term contracts with the Oman government. The revenue of these companies comes from selling the power and water at a fixed rate and purchasing from the government-fixed subsidized natural gas price. The power and water selling prices are 20 £/MWh and 0.9 £/m³ [7, 8], whereas the gas subsidized fixed price is 0.96 £/MMBTU [7, 8, 9]. Table 11.6 shows the revenue estimation for all four heat recovery options.

Enhancement technology	Unit	MSF+IH only	MSF+AC+IH	MSF+ORC+IH	MSF+SED+IH
Water	£/year	709560	709560	709560	924047
Natural gas saving	£/year	211724	540392	–	–
Electrical energy	£/year	–	–	185640	–
Total annual saving	£/year	921284	1249952	895200	924047

Table 11.6: Summary of heat recovery technology revenue estimation

11.4 Profitability Analysis

This section presents the profitability analysis of the four heat recovery technology options. IPSEpro PS economics (explained in Chapter 4) was used to calculate the profitability indicators, including payback period, net present value, average rate of return, and net-benefit cost ratio.

The payback period refers to the time of the year (j) requiring returning initial investment cost from the revenues or cash inflow. Mathematically, this is obtained by [46]:

$$TCI = \sum_{j=1}^{PBP} CFN_j \quad (11 - 4)$$

where TCI and CFN are total capital investment and cash flow net, respectively.

Figure 11.1 shows the payback period for the four heat recovery options. All four options had less than a 5.2-year payback period, mainly due to high revenues from the distillate produce resulting from stage distillate extraction. It was observed that by not incorporating this original MSF distillate, enhancement revenue could move up the payback period by four times the current figure. Using IH alone in MSF desalination achieved the lowest payback period of around 1 year, whereas SED, AC, and ORC achieved 1.8 years, 2.4 years, and 5.2 years, respectively. It worthy to mention that the high unit selling price of water played a main role on reducing the payback period for the four options and for SED specifically.

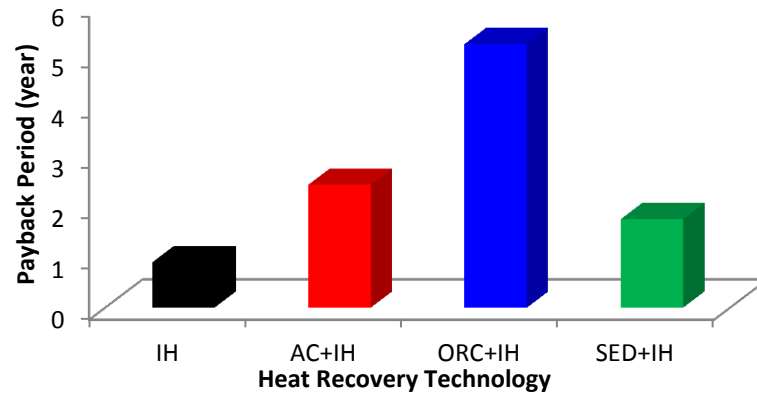


Figure 11.2: Payback period for four heat recovery technology implementations

The net present value of a project is defined as the difference between the sum of all the net cash inflows and the initial investment cost. This value could be positive or negative: a positive one means the project is preferable and earns more income than investment cost; however, negative refers to the inability to cover the initial investment cost and should be avoided. Mathematically, the NPV is calculated from [46]:

$$NPV = \sum_{j=1}^t \frac{CFN_j}{(1+r)^j} - TCI \quad (11 - 5)$$

where CFN_j and r are the net cash flow at time (j) and r is the discount rate.

Figure 11.2 illustrates the net present value for the implementation of the four heat recovery technologies. AC gained the highest net present value despite the lower payback period compared with IH and SED. This could be justified as the annual income from the AC option was more than the other two options after returning the initial investment cost.

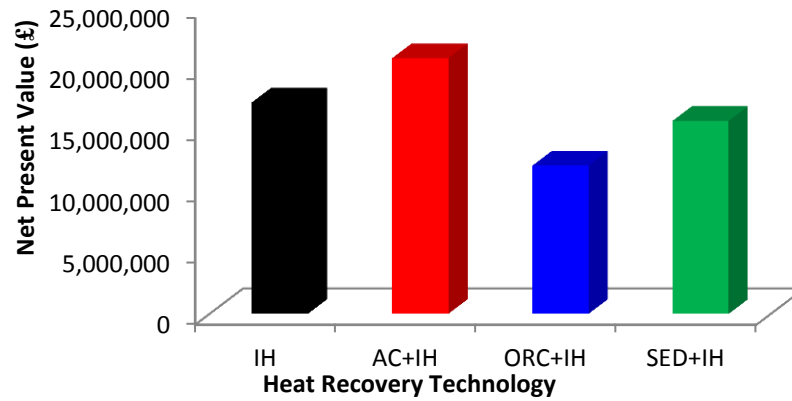


Figure 11.3: Net present value for four heat recovery technology implementations

The average rate of return is defined as the ratio of the average annual net profits to the total capital investment. It is obtained from [46]:

$$ARR = \frac{\overline{NP}}{TCI} \quad (11 - 6)$$

where \overline{NP} is the average net profit of the investment.

The ARR of the four heat recovery technologies is shown in Figure 11.4, which shows a similar trend to the payback period graph.

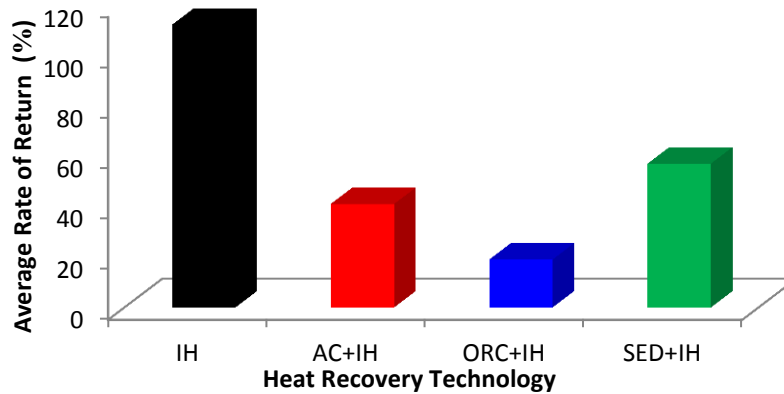


Figure 11.4: Average rate of return for four heat recovery technology implementations

Chapter 12

Conclusions and future recommendations

12.1 Use of simulation models for cogeneration plant development

12.1.1 Identification of real plant operational requirements and conditions

To satisfy objective (a) (Section 1.2), actual operational data for a cogeneration plant were gathered to identify and appreciate its typical operation scenarios, not only to give realistic inputs for simulation but also to facilitate predications of annual production, carbon footprint, and economics. The outcomes showed that the normal operation of this plant is dominated by the following three seasonal scenarios (Section 3.5):

- Scenario I (represents 62% annually): the summer season requires all the plant equipment for both power and desalination, to supply almost full water production and power but with some power load variation due to ambient temperature fluctuation. The variation in load was accommodated by reduction of supplementary firing or of gas turbine load.
- Scenario II (represents 30% annually): for the winter season, power demand is less but with almost a full supply of water required. In this scenario, one GT, one HRSG, and one steam turbine are kept under shutdown condition, with low pressure steam supplied to the MSF distillers through a pressure reduction station from the one HRSG.
- Scenario III (represents 8% annually): in the transition period from summer to winter, the load demand starts to reduce, with the steam turbine maintained at low load and one GT with HRSG kept under shutdown condition.

12.1.2 Applicability of modelling software (e.g. IPSEpro)

To enable objectives (b) and (c) (Section 1.2) to be fulfilled, the cogeneration plant (power plant and MSF desalination) and four proposed heat recovery technologies (IH, AC, ORC, and SED) were modelled using IPSEpro software and these models were validated in line with objectives (f) and (g). The modelling confidence level was assessed by estimating the relative difference between the actual data (either measured directly from the site or collected from the manufacturer) and model outputs. The results showed that IPSEpro has the capability to model the cogeneration plant studied (power plant and MSF desalination) and the four heat recovery technologies with within a difference considered to be acceptable while

taking issues, such as minor modelling assumptions and measurement uncertainties in actual plant data, into consideration.

The power plant was modelled at the three operating scenarios and validated by comparison with site measured data. The differences between the measured data and model results varied from 1.0% to 3.7%. As site operational data were not available, the MSF desalination model was validated against vendor testing data at different loads and seawater temperatures. The highest difference found was 3.9%. In the MSF modelling, non-equilibrium effects were not taken into consideration, with the prospect of including those in future studies to improve the model. The single effect LiBr–H₂O AC model was validated against an actual unit, with a maximum 4% difference, the model thermodynamic applicability confirmed on a Dühring chart and the manufacturer's operating curve (Section 8.1.2). The ORC model validation was achieved by comparison of model results with an existing unit (Section 9.1.1). The highest difference was 3.3%, and its applicability was checked on refrigerant T-s diagrams. The SED was validated against manufacturer data at different operating parameters (Section 10.1.1) with a maximum difference of 3.2%.

These results suggest that these IPSEpro plant simulation models are a legitimate tool to carry out the core objectives (b) and (c) (Section 1.2). While performance enhancements may be only of a similar order to the larger model differences, the conclusion has to be that in terms of overall behaviour, the simulations are broadly correct, with the inference that improvements to the model performance are likely to manifest themselves as improvement to actual plant performance of similar (if not actually identical) scale.

12.2 Plant performance enhancement

Objectives (b) and (c) (Section 1.2) are the central engineering focus of this study, that is, to enhance the thermodynamic, environmental, and economic performance of a cogeneration power and water plant of the general type of the actual installation investigated. By further investigation and development of a previously suggested MSF plant enhancement, the study found that extraction of distillate from the MSF desalination stages increased unit water production by 2% (equivalent to 788400 m³/year) due to the rise in flashing range of the brine (Section 7.2). Furthermore, utilization of the hot extracted distillate through a heat exchanger to raise the brine

recirculation temperature resulted in a reduction of steam consumption by 5%. This suggested utilizing part of this heat for other heat recovery technologies.

Section 7.4 revealed that any partial utilization of the heat for less than 10°C of the available temperature has no impact on the original MSF desalination performance, suggesting partial heat utilization in different heat recovery technologies could result in performance enhancement (either more electricity or more water) beyond the original MSF production. Consequently, this study investigated, for first time, hybridization of the MSF with four options heat recovery technologies: IH, AC, ORC, and SED, which improved MSF exergy efficiency by 16%, 25%, 23%, and 50%, respectively.

Option 1: Internal Heating (IH) to raise the brine recycle temperature (Section 7.2) reduces steam consumption. Location of the IH exchanger at the brine recycle stream could be studied to assess its thermal and economic benefits compared with the current study. This option gives the greatest CO₂ saving (57000 tonne/year) and the best economic return (1-year payback period from an average rate of return of 112%), though over 20 years, the NPV lifetime return at £17.2 M is less than for option 2.

Option 2: The hot distillate water from the MSF was found able to produce up to 700 tonne chilling load through a LiBr–H₂O single effect AC with 0.84 COP and an exergy efficiency of 16% (Section 8.2). A parametric study (Section 8.2.3) found that both AC cooling temperature and chilled water temperature have a slight effect on AC COP and a significant effect on exergy efficiency. The chilled water was used to reduce GT inlet temperature in the same cogeneration plant and was able to increase cogeneration plant gross power by up to 18 MW and thermal efficiency by 4%. This improvement led to 12680 tonne/year saving in natural gas consumption due to MSF steam reduction and GT inlet cooling by the AC, leading to 29000 tonne/year CO₂ saving. This option gives the best 20 years NPV lifetime return £20.8M but less rapid payback than option 1 (only 2.4 years with average rate of return at 41%). The study ignored the effect of humidity on AC cooling performance, future investigation of this issue is recommended.

Option 3: Powering an ORC cycle (to generate additional power) by the MSF hot distillate water was investigated for two refrigerants R134a and R245fa (Section

9.2). R245fa was found to give better thermal and exergy efficiencies than R134a, and a parametric study found that both evaporator and cooling water temperature have a significant effect on thermal and exergy efficiencies. This hybridization resulted in additional energy of 9000 MWh/year to the cogeneration plant, but with significantly lower CO₂ savings compared with options 1 and 2 (only 13000 tonne/year). Economically, it is the weakest of the options; with longest payback period (5.2 years at 18.5% average rate of return) and lowest NPV lifetime return (£ 12.1 M).

Option 4: Using the hot MSF distillate to energize an additional SED is able to produce 242000 tonne/year additional water, though the SED exergy efficiency obtained by this powering is low at 1.3% (not far from the MSF) with a low GOR at 0.0156 (Section 10.2). The study also found the SED is affected highly by increasing the number of effects, but did not cover the possibility of flashing the extracted hot water to power MED. Studying this in future would enable a comparison between hot water SED and steam MED. This option gives the lowest CO₂ savings (11000 tonne/year). Economically, it is better than option 3 on all three criteria used (1.8 year payback, 41% average rate of rate, and £15.7M).

12.3 Benefits from exergy analysis approach

In arriving at all the above conclusions, objectives (d) and (e) (Section 1.2) have been crucial to the methodology used. Both the conventional cogeneration plant and suggested heat recovery technologies have been analysed using both the conventional energy and exergy approaches. In this application, where the thermal system outputs are different in quality (i.e., electrical power and water), the exergy approach was found more effective than the conventional energy approach. In particular, the exergy efficiency was found to be a more powerful approach to assessing such a plant than the heat utilization factor (common practice up to this time). The heat utilization factor counts the thermal energy (that is, heat added to the MSF) as equivalent to electrical power, but the case against this can be argued for two reasons: firstly, the thermal energy supplied to the MSF is different in quality to electrical power and, secondly, this energy (LP steam to MSF) in reality, is an input (internally), while the electrical power is an output from the system. The exergy approach analyses both power and MSF desalination plants based on their ability to

produce useful work; therefore, both products (system outputs) are assessed as being similar in quality.

This study covered the estimation of the exergy efficiency of a cogeneration (combined and MSF desalination) power plant for the first time. Using the simulation model, the results revealed heat utilization factors of 69.4%, 78.1%, and 81.3 % for scenarios I, II, and III, respectively, in contrast to 36%, 21%, and 32% for the exergy efficiencies. The exergy efficiencies are not simply lower than heat utilization factors, but more significantly, they lead to different performance rankings between the three scenarios. These conventional operating scenarios due to seasonal changes can cause a huge loss in exergy content (e.g., reduction station at scenario II destroyed 100 MW).

In a similar fashion, the conventional MSF desalination system assessment by the PR (amount of distillate per amount of steam consumed) does not compare the separation work to produce the distillate with the energy required to produce the steam, in contrast to the exergy analysis. This study confirmed previous low exergy efficiency (only 5.8%) for MSF desalination, and its unique detailed exergy analysis of MSF desalination was also able to specify the location of the plant equipment exergy destruction and consequently, help to focus more on this equipment for improvements. The sources of MSF exergy destruction were found to be 17%, 55%, 10%, 4%, and 13% in the brine heater, heat recovery stages, heat rejection stages, pumps, and stream disposal, respectively. This MSF detailed exergy analysis revealed that recovering heat from the hot distillate water of the MSF stages (as implemented in the Layyah plant in 2005) could increase the exergy efficiency of the MSF unit by up to 15%. In addition, it indicated that the distillate water in temperature range of 65°C to 100°C is suitable to power low-grade heat recovery technologies as indicated in the options above.

In addition, using an energy based approach in evaluating CO₂ emissions shows a lower emissions rate and hence, a higher thermal energy CO₂ saving potentially due to its evaluation of thermal energy and electrical power without regard to their differing thermodynamic qualities. By contrast, the exergy approach gives a higher emissions rate resulting from the lower available energy in thermal energy compared with the electrical power. This study found that for the cogeneration power plant

studied, CO₂ emissions (energy base) are only 371 g/kWh, 329 g/kWh, and 314 g/kWh for scenarios I, II, and III, respectively but the exergy base shows significant increases at 535 g/kWh, 748 g/kWh and 542 g/kWh, respectively. Therefore, where waste heat is recovered for any output other than additional electrical power, the realized CO₂ emissions estimation needs to be based on exergy and not energy.

References

- [1] Bachellerie, I. J. (2012) *Renewable energy in GCC countries resources, potential, and prospects*. Gulf Research Centre. Kingdom of Saudi Arabia.
- [2] Qader, M. (2009) “Electricity Consumption and GHG Emissions in GCC Countries”, *Energies*, 2, pp: 1201-1213.
- [3] Dziuban, M. (2011) *Scarcity and strategy in the GCC*. Center for Strategic International Studies.
- [4] Economist Intelligence Unit. (2010) *The GCC in2020: resources for the future*. The Economist intelligent Unit Limited.
- [5] UNEP-Regional Officer of West Asia (ROWA). (2005) “Environmental impacts of the arab oil and gas sector”, *Arab regional conference on energy for sustainability development*, Cairo, Egypt.
- [6] <http://www.omanet.om>. (2013) *Useful information about Oman*. Ministry of Information, Oman.
- [7] Oman Power and Water Procurement Co. (2012) *OPWP’s 7-years statement (2012-2018)*.
- [8] Oman Power and Water Procurement Co. (2011) OPWP’s 2011 annual report.
- [9] Authority for Electricity Regulation. (2008) *Study on renewable energy resources, Oman*.
- [10] Awerbuch, L, Sommariva, C. (2008). *MSF distillate driven desalination process and apparatus* . European patent specification office, UK.
- [11] *E-mail from president of Leading Edge Technology: Leon Awerbuch*. 18-04-2013.
- [12] Sommariva, C, et al. (1999) “Innovative configuration of multistage flash desalination plant”, *IDA Proceeding Conference*, San Diego, US.
- [13] Dincer, I, Rosen, M. A. (2007). *Exergy, energy, environment and sustainable development*. 1st edn. Oxford : Elsevier.
- [14] Abdul-Wahab, S, et al. (2012) “Development of a steady-state mathematical model for multistage flash (MSF) desalination plant”, *International Journal of Energy Research*, 36, pp: 710-723.
- [15] Barka Plant. (2003). *Plant operation and maintenance manual*. Oman.

- [16] Darwish, M. A, Darwish, A, Darwish, A. (2011) “Fifty years of MSF desalination in Kuwait and sustainability”, *Desalination and Water Treatment*, 29, pp: 343-354.
- [17] Téllez, D. et al (2009) “Evaluation of technologies for a desalination operation and disposal in the Tularosa Basin, New Mexico”, *Desalination*, 249, pp: 983-990.
- [18] Shatat, M, Riffat, S. B. (2012) “Water desalination technologies utilizing conventional and renewable resources”, *International Journal of Low-Carbon Technologies*, 0, pp: 1-19.
- [19] MENA Regional Water Outlook. (2011) *Desalination using renewable energy part II*. FICHTNER.
- [20] Borsani, R, Rebagliati, S. (2005) “Fundamental and costing of MSF desalination plants and comparative with other technologies”, *Desalination*, 182, pp: 29-37.
- [21] Budhiraja, P, Fares, A. A. (2008) “Studies of scale formation and optimization of antiscalant dosing in multi-effect thermal desalination units”, *Desalination*, 220, pp: 313-325.
- [22] <http://www.sidem-desalination.com>
- [23] Wangnick, K. (2000) *IDA worldwide desalting plants inventory*. Report no:16. Wangnick Consulting.
- [24] Ghaffour, N, Missimer, T. M, Amy, G. L. (2013) “Technical review and evaluation of the economics of water desalination for water supply and sustainability”, *Desalination*, 309, pp: 197-207.
- [25] Khawaji, A. D, Kutubkhanah, I. K, Wie, J. M. (2008) “Advances in seawater desalination technologies”, *Desalination*, 221, pp: 47-69.
- [26] Australian Sustainable Industry Research Center. (2005) *Overview of treatment process for the production of fit for purpose water: desalination and membrane technologies*. ASIRC report no. R05-2207.
- [27] United Nation. (2001) *Water desalination technologies in the ESCWA member countries* . UN report no. 172.
- [28] Gacem, Y, et al. (2012) “Physical and chemical assessment of MSF distillate and SWRO product”, *Desalination*, 290, pp: 107-114.
- [29] Gude, V. G, Nirmalakhandan, N, Deng, S. (2010) “Renewable and sustainable approaches for desalination”, *Renewable and Sustainable Energy Reviews* , 14, pp: 2641-2654.

- [30] Berktaç, A. (2011) “Environmental approach and influence of red tide to desalination process in the Middle East region”, *International Journal of Chemical and Environmental Engineering*, 2, pp: 1-6.
- [31] Ammar, Y, et al. (2013) “Reprint of desalination using low grade heat in the process industry: challenges and prospective”, *Applied Thermal Engineering*, 223, pp: 448-456.
- [32] Eltawil, M. A, Zhengming, Z, Yuan, L. (2009) “A review of renewable energy technologies integrated with desalination systems”, *Renewable and Sustainable Energy Reviews* , 13, pp: -2254-2262.
- [33] Karagiannis, I, Soldatos, P, G. (2008) “Water desalination cost literature: review and assessment”, *Desalination*, 223, pp: 448-456.
- [34] Al-Mutaz, I. S, Al-Namleh, A, M. (2004) “Characteristics of dual purpose MSF desalination plants”, *Desalination*, 166, pp: 287-294.
- [35] Darwish, M. A, Abdulrahim, H, K. Amer, A. B. (2008) “On better utilization of gas turbine in Kuwait”, *Desalination*, 33, pp: 571-588.
- [36] Sommariva, C. (2008) “Utilization of power plant waste heat steams to enhance efficiency in thermal desalination”, *Desalination*, 222, pp: 592-595.
- [37] Darwish, M. (2007) “Desalting fuel energy cost in Kuwait in view of \$75 barrel oil price”, *Desalination*, 208, pp: 306-320.
- [38] Çengel, Y, Boles, M. (2002). *Thermodynamics: an engineering approach*. 4th edn. New York: McGraw-Hill.
- [39] Al-Katheeri, E, Agashichev, S, P. (2008) “Feasibility of the concept of hybridization of existing co-generative plant with reverse osmosis and aquifer storage”, *Desalination*, 222, pp: 87-95.
- [40] Petchtl, P, et al.(2003) “Integrated thermal power and desalination plant optimization”, *PowerGen Middle East*, 1, pp: 1-20.
- [41] Shafaghat, R, et al. (2012) “Design of MSF desalination plant to be supplied by new specific 42 MW power plant located in Iran”, *World Academy of Science, Engineering and Technology*, 62, pp: 515-521.
- [42] Al-Weshahi, M. A, Anderson, A, Tian, G. (2013) “Validation of simulation model of cogeneration power and water desalination plant”, *International Journal of Modeling and Optimization*, 3, pp: 46-51.
- [43] Fellah, G, Mgherbi, F, Aboghres, S. (2010) “Exergoeconomics analysis for unit GT14 of South Tripoli Gas turbine power plant”, *Jordan Journal of Mechanical and Industrial Engineering*, 4, pp: 507-95.

- [44] Arora, S. C, Domkundwar, S. (2001). *A course in power plant engineering*. 1st edn. Dhanpat Rai & Co.: Delhi.
- [45] Dincer, I, Rosen, M. A. (2010). *Thermal energy storage systems and applications*. 2nd edn. New York: Wiley.
- [46] Bejan, A, Tsatsaronis, G, Moran, M. (1996). *Thermal design & optimization*. 1st edn. New York: Wiley.
- [47] Bejan, A. (2006). *Advanced engineering thermodynamics*. 3rd edn. New York: Wiley.
- [48] Kotas, T. J. (1995). *The exergy method in thermal plant analysis*. 2nd edn. Malabar: Krieger.
- [49] Szargut, J, Morris, D. R, Steward, F. R. (1988). *Exergy Analysis of thermal chemical and metallurgical processes*. 1st edn. New York: Hemisphere.
- [50] Kanoglu, M, Dincer, I, Rosen, M. A. (2007) “Understanding energy and exergy efficiencies for improved energy management in power plants”, *Energy Policy*, 35, pp:3967-3978.
- [51] Hepbasli, A. (2008) “A key review on exergetic analysis and assessment of renewable energy resources for sustainable future”, *Renewable & Sustainable Energy Reviews*, 12, pp:593-661.
- [52] Kilkis, I. B. (1999) “Utilization of wind energy in space heating and cooling with hybrid”, *Energy Buildings*, 30, pp:147-153.
- [53] Frangopoulos, C. (2000). Exergy, Energy system analysis and optimization. *Encyclopaedia of Life Support Systems*, 1, pp:1-33.
- [54] Szargut, J. (2005). “Exergy Analysis”, *Academia Research in Progress*, 7, pp: 31-33.
- [55] Cornelissan, R. L. (1997). The use of exergy analysis and the reduction of the irreversibility. *PhD Thesis*, Enschede, Netherlands.
- [56] Kaushik, S. C, Reddy, V. S, Tyagi, S. K. (2011) “Energy and exergy analyses of thermal power plants: a review”, *Renewable and Sustainable Energy Reviews*, 15, pp: 1857-1872.
- [57] Dincer, I, Rosen, M. A. (2005) “Thermodynamics aspects of renewable and sustainable development”, *Renewable and Sustainable Energy Reviews*, 4, pp: 507-95.
- [58] Darwish, M. A, Al-Najem, N. M, Lior, N. (2009) “Towards sustainable seawater desalting in Gulf area”, *Desalination*, 235, pp: 58-87.

- [59] Fischer, M, et al. (2008) “Exergy-efficiency as enhancement of energy-efficiency- an LCA prospective”, Study prepared by: Fraunhofer Institute for Building Physics, University of Stuttgart, PE International GmbH.
- [60] Al-Ghandoor, A, Jaber, J. O, Al-Hinti, I. (2009) “Assessment of energy and exergy efficiencies of power generation sub-sector in Jordan”, *Jordan Journal of Mechanical and Industrial Engineering*, 3, pp: 1-8.
- [61] Saidur, R, Ahamed, J. U, Masjuki, H. H. (2010) “Energy, exergy and economics analysis of industrial boilers”, *Energy Policy*, 38, pp: 2188-2197.
- [62] Rosen, M. A. (2013) “Using exergy to assess regional and national energy utilization: a comparative review”, *Arab Journal of Science and Engineering*, 38, pp: 251-261.
- [63] Koroneos, C. J, Nanaki, E. A, Xydis, G. A. (2012) “Sustainability indicators for the use of resources-the exergy approach”, *Sustainability*, 4, pp: 1867-1878.
- [64] Kennedy, S, et al. (2012) “CO₂ allocation for power and water production in Abu Dhabi”, *Masdar Working Paper*, pp: 774-778.
- [65] Ozkan, D. B, Kiziler, O, Bilge, D. (2012) “Exergy analysis of a cogeneration plant”, *World Academy of Science, Engineering and Technology*, 61, pp: 774-778.
- [66] Modesto, M, Nebra, S. A. (2009) “Exergoeconomic analysis of power generation system using blast furnace and coke oven gas in a Brazilian steel mill”, *Applied Thermal Engineering*, 29, pp: 2127-2136.
- [67] Shi, X, Che, D. (2007) “Thermodynamic analysis of an LNG fuelled combined cycle power plant with waste heat recovery and utilization system”, *International Journal of Energy Research*, 31, pp: 975-998.
- [68] Cihan, A, Hacıhafizoğlu, O, Kahveci, K. (2006) “Energy-exergy analysis and modernization suggestions for a combined-cycle power plant”, *International Journal of Energy Research*, 30, pp: 115-126.
- [69] Ameri, M, Ahmadi, P, Khanmohammadi, S. (2008) “Exergy analysis of a 420 MW combined cycle power plant”, *International Journal of Energy Research*, 32, pp: 175-183.
- [70] Khaliq, A, Dincer, I. (2011) “Energetic and exergetic performance analyses of a combined heat and power plant with absorption inlet cooling and evaporative aftercooling”, *Energy*, 36, pp: 2662-2670.

- [71] Kempton, R, et al. (2010) “ Thermodynamics efficiencies and GHG emissions of alternative desalination process”, *Water Science Technology: Water Supply-WWTWS*, 10.3, pp: 416-427.
- [72] Kahraman, N, Cengel, Y. A. (2005) “ Exergy analysis of a MSF distillation plant”, *Energy*, 46, pp: 2625-2636.
- [73] Cerci, Y. (2002) “ Exergy analysis of a reverse osmosis desalination plant in California”, *Desalination*, 142, pp: 257-266.
- [74] Sharqawy, M. H, Lienhard, V, Zubair, M. (2011) “On exergy calculations of seawater with applications in desalination systems”, *International Journal of Thermal Sciences*, 50, pp: 187-196.
- [75] Sharqawy, M. H, Lienhard, V, Zubair, M. (2010) “Thermophysical properties of seawater: a review of existing correlations and data”, *Desalination and Water Treatment*, 16, pp: 354-380.
- [76] Mabrouk, A. A, Nafey, A. S, Fath, H. E. S. (2007) “Thermoeconomic analysis of some exiting desalination processes”, *Desalination*, 205, pp: 354-373.
- [77] Mistry, K. H, et al. (2011) “Entropy generation analysis of desalination technologies”, *Entropy*, 13, pp:1829-1864.
- [78] Nafey, A. S, Fath, H. E. S, Mabrouk, A. A. (2006) “Exergy and thermoeconomic evaluation of MSF process using a new visual package”, *Desalination*, 201, pp: 224-240.
- [79] Tanios, B. (1984) “Marginal operation field of existing MSF desalination plants”, *Desalination*, 51, pp: 201-212.
- [80] Mussati, S. F, Aguirre, P. A, Scenna, N. J. (2004) “Improving the efficiency of the MSF once through (MSF-OT) and MSF-mixer (MSF-M) evaporator”, *Desalination*, 166, pp: 141-151.
- [81] Mussati, S. F, Aguirre, P. A, Scenna, N. J. (2003) “Novel configuration for a multistage flash-mixer desalination system”, *Industrial Engineering Chemical Research*, 42, pp: 4828-4839.
- [82] Helal, A. M, Al-Jafri, A, Al-Yafeai, A. (2012) “Enhancement of existing MSF plant productivity through design modification and change of operating conditions”, *Desalination*, 307, pp: 76-86.
- [83] Awerbuch, L. (2008). *Thermal desalination plant integrated upgrading process and apparatus*. Intellectual property office.
- [84] Atkinson, G. A. (2003) “Improvements in multistage flash desalination technology”, *PB Power Limited*, UK.

- [85] Junie, Y, et al. (2007) “Improvement of multi-stage flash seawater desalination system for cogeneration power plants”, *Desalination*, 217, pp: 191-202.
- [86] Wang, X, Chua, H. T. (2009) “Absorption cooling: A review of lithium bromide-water chiller technologies”, *Recent Patents on Mechanical Engineering*, 2, pp: 193-213.
- [87] Goodheart, K. A, Klein, S. A, Schultz, K. (2002) “Economic assessment of low firing temperature absorption chiller systems”, *ASHRAE Transactions*, 108, pp: 1-9.
- [88] Srihirin, P, Aphornratana, S, Chungpaibulpatana, S. (2001) “A review of absorption refrigeration technologies”, *Renewable and Sustainable Energy Reviews*, 5, pp: 344-372.
- [89] American Society of Heating, Refrigerating and Air-conditioning Engineers. (1989). *ASHRAE handbook fundamentals*. Atlanta.
- [90] Marcriss, R. A, Gutraj, J. M, Zawacki, T. S. (1988) “Absorption fluid data survey: final report on worldwide data”, *Institute of Gas Technology*, Chicago.
- [91] Kurosawa, S, et al. (1990) “Working fluids survey. In: working fluids and transport phenomena in advanced absorption heat pumps”, HHP-AN14-1.
- [92] Herold, K. E, Radermacher, R, Klein, S. A. (1996). *Absorption chillers and heat pumps*. 1st edn. USA :CRC Press.
- [93] Labus, J. (2011). *Modeling of small capacity absorption chillers driven by solar thermal energy or waste heat* . PhD thesis: University of Rovira I Virgili.
- [94] Masheiti, S. A. (2011). *A thermodynamic and economic simulation modelling study of utilizing low-temperature sources to power absorption and organic Rankine cycles*. PhD thesis: Newcastle University: UK.
- [95] Popli, S, Rodgers, P, Eveloy, V. (2013) “Gas turbine efficiency enhancement using waste heat powered absorption chillers in the oil and gas industry”, *Applied Thermal Engineering*, 50, pp: 918-931.
- [96] Wang, J, Zheng, D. (2009) “Performance of one and a half-effect absorption cooling cycle of H₂O/LiBr system ”, *Energy Conversion and Management*, 50, pp: 3087-3095.
- [97] Kalogirou, S. (2003) “The potential of solar industrial process heat applications”, *Applied Energy*, 76, pp: 337-361.

- [98] Mokhtar, M, et al. (2010) “Systematic comprehensive techno-economic assessment of solar cooling technologies using location specific-climate data”, *Applied Energy*, 87, pp: 3766-3778.
- [99] Kaushik, S. C, Arora, A. (2009) “Energy and exergy analysis of single effect and series flow double effect water-lithium bromide absorption refrigeration systems”, *International Journal of Refrigeration*, 32, pp: 1247-1258.
- [100] Talbi, M. M, Agnew, B. (2000) “Exergy analysis: an absorption refrigerator using lithium bromide and water as the working fluid”, *Applied Thermal Engineering*, 20, pp: 619-630.
- [101] Gomri, R. (2009) “Second law comparison of single effect and double effect vapour absorption refrigeration systems”, *Energy Conversion and Management*, 50, pp: 1279-1287.
- [102] Shahata, A. I, et al. (2012) “Energy and exergy analysis of single and parallel flow double effect water-lithium bromide vapor absorption systems”, *International Journal of Science and Technology*, 2, pp: 85-94.
- [103] Zadeh, F. P, Bozorgan, N. (2011) “The energy and exergy analysis of single effect absorption chiller”, *Majlesi Journal of Mechanical Engineering*, 4, pp: 19-26.
- [104] Mehrabian, M. A, Shahbeik, A. E. (2005) “Thermodynamic modeling of a single-effect LiBr-H₂O absorption refrigeration cycle”, *Proceedings of the Institute of Mechanical Engineers, Part E: Journal of Process Mechanical Engineering*, 219, pp: 261-273.
- [105] Al-Zahrani, K. S. (2010). *Operational simulation and an economical modelling study on utilizing waste heat energy in a desalination plant and an absorption chiller*. PhD thesis: Newcastle University: UK.
- [106] Misra, R. D, et al. (2003) “Thermoeconomic optimization of a single effect water/LiBr vapour absorption refrigeration system”, *International Journal of Refrigeration*, 26, pp: 158-169.
- [107] Palacios-Bereche, R, Gonzales, R, Nebra, S. A. (2012) “Exergy calculation of lithium bromide-water solution and its application in the exergetic evaluation of absorption refrigeration systems LiBr-H₂O”, *International Journal of Energy Research*, 36, pp: 166-181.
- [108] Alsairafi, A. A. (2013) “Effects of ambient conditions on the thermodynamics performance of hybrid nuclear-combined cycle power plant”, *International Journal of Energy Research*, 37, pp: 211-227.
- [109] Santos, P. P, Andrade, C. R, Zaparoli, E. L. (2012) “Comparisons of different gas turbine inlet air cooling methods”, *World Academy of Science, Engineering and Technology*, 61, pp: 40-45.

- [110] Alhazmy, M. M, Najjar, Y. S. H. (2004) “Augmentation of gas turbine performance using air coolers”, *Applied Thermal Engineering*, 61, pp: 40-45.
- [111] Erdem, H, et al. (2009) “Comparative energetic and exergetic performance analyses for coal-fired thermal power plant in Turkey”, *International Journal of Thermal Science*, 48, pp: 2179-2186.
- [112] Farzaneh-Gord, M, Deymi-Dashtebayaz, M. (2011) “Effect of various inlet air cooling methods on gas turbine performance”, *Energy*, 36, pp: 1196-1205.
- [113] Brooks, F. J. (2001) “GE gas turbine performance characteristics”, *GE Power Systems*, GER-3567H, pp: 1-16.
- [114] Kakaras, E, et al. (2006) “Inlet air cooling methods for gas turbine based power plants”, *Transactions of the ASME*, 128, pp: 312-317.
- [115] Ehyaei, M. A, et al. (2012) “Exergy, economic and environment (3E) analysis of absorption chiller inlet air cooler used in gas turbine power plants”, *International Journal of Energy Research*, 36, pp: 486-498.
- [116] Ameri, M, Hejazi, S. H. (2004) “The study of capacity enhancement of the Chabahar gas turbine installation using an absorption chiller”, *Applied Thermal Engineering*, 24, pp: 59-68.
- [117] Boonnasa, S, Namprakai, P, Muangnapoh, T. (2006) “Performance improvement of the combined cycle power plant by intake air cooling using an absorption chiller”, *Energy*, 31, pp: 2036-2046.
- [118] Chen, H, Goswami, D. Y, Stefanakos, E. K. (2010) “A review of thermodynamic cycles and working fluids for the conversion of low-grade heat”, *Renewable and Sustainable Energy Reviews*, 14, pp: 3059-3067.
- [119] <http://www.turboden.eu/en/rankine/rankine-advantages.php>
- [120] Quoilin, S, et al. (2013) “Techno-economic survey of Organic Rankine Cycle (ORC) systems”, *Renewable and Sustainable Energy Reviews*, 22, pp: 168-186.
- [121] <http://www.cycle-organique-rankine.com/market-markers.php>
- [122] Tchanche, B. F, et al. (2009) “Fluid selection for a low-temperature solar organic Rankine cycle”, *Applied Thermal Engineering*, 29, pp: 2468-2476.
- [123] Schuster, A, et al. (2009) “Energetic and economic investigation of Organic Rankine Cycle applications”, *Applied Thermal Engineering*, 29, pp: 1809-1817.

- [124] Kosmadakis, G, et al. (2009) “Comparative thermodynamic study of refrigerants to select the best for use in the high-temperature stage of a two-stage organic Rankine cycle for RO desalination”, *Desalination*, 243, pp: 74-94.
- [125] Saleh, B, et al. (2007) “Working fluids for low-temperature organic Rankine cycles”, *Energy*, 32, pp: 1210-1221.
- [126] Guo, T, Wang, H, Zhang, S. (2010) “Fluid selection for a low-temperature geothermal organic Rankine cycle by energy and exergy”, *Power and Energy Engineering Conference (APPEEC)*, pp: 1-5.
- [127] Papadopoulos, A. I, et al. (2010) “Power generation from low enthalpy geothermal fields by design and selection of efficient working fluids for organic Rankine cycles”, *Chemical Engineering Transactions*, 21, pp: 61-66.
- [128] Bao, J, Zhao, L. (2013) “A review of working fluid and expander selections for organic Rankine cycle”, *Renewable and Sustainable Energy Reviews*, 24, pp:325-342.
- [129] Kosmadakis, G, et al. (2010) “Design of a two organic Rankine cycle for reverse osmosis desalination supplied from a steady thermal source”, *Desalination*, 250, pp: 323-328.
- [130] Lakew, A. A, Bolland, O. (2010) “Working fluids for low-temperature heat source”, *Applied Thermal Engineering*, 30, pp: 1262-1268.
- [131] Tempesti, D, Manfrida, G, Fiaschi, D. (2012) “Thermodynamic analysis of two micro CHP systems operating with geothermal and solar energy”, *Applied Energy*, 97, pp: 609-617.
- [132] Aghahosseini, S, Dincer, I. (2013) “Comparative performance analysis of low temperature Organic Rankine Cycle (ORC) using pure and zeotropic working fluids”, *Applied Thermal Engineering*, 54, pp: 35-42.
- [133] Schuster, A, Karl, J. (2007) “Simulation of an innovative stand-alone solar desalination system using and Organic Rankine Cycle”, *International Journal of Thermodynamics*, 10, pp: 155-163.
- [134] Mago, P. J, Charma, L. M, Somayaji, C. (2007) “Performance analysis of different working fluids for use in organic Rankine cycles”, *Journal of Power and Energy*, 221, pp: 255-264.
- [135] Masheiti, S, Agnew, B, Walker, S. (2011) “An evaluation of R134a and R245fa as the working fluid in an organic Rankine cycle energized from a low temperature geothermal”, *Journal of Energy and Power Engineering*, 5, pp: 392-402.

- [136] Karytsas. (1996) “renewable energy source for water production”, *Mediterranean conference EURORED Network, Greece*, pp: 128-131.
- [137] Hughes, B. R, Rezazadeh, F, Chaudhry, H, N. (2013) “Economic viability of incorporating multi-effect distillation with district cooling systems in the United Arab Emirates”, *Sustainable Cities and Society*, 7, pp: 37-43.
- [138] Michelle, L. S. Z, et al. (2013) “Geothermal desalination in Singapore”, *The IES Journal Part A: Civil & Structural Engineering*, 6, pp: 42-50.
- [139] Wang, X, et al. (2011) “Low grade heat driven multi-effect distillation technology”, *International Journal of Mass and Heat Transfer*, 54, pp: 5497-5503.
- [140] Holladay, W. L. (1973) “Suggested revision of weather data design temperature”, *ASHRAE*, 221, pp: 44-46.
- [141] Makhdoum, B. M. A. (2011). An energy, exergy and economic modelling study based on utilizing waste heat of a C200 microturbine to power ORC, absorption chiller and desalination units. PhD thesis: Newcastle University: UK.
- [142] ASME. (1981). *PTC4.4 gas turbine heat recovery generators*. 1st edn. New York: ASME.
- [143] ASME. (1996). *PTC6 steam turbines*. 1st edn. New York: ASME.
- [144] Lior, N, Zhang, N. (2007) “Energy, exergy and second law performance criteria”, *Energy*, 32, pp: 281-296.
- [145] Feuercker, G, Scharfe, J, Greiter, I. (1993) “Measurement of thermophysical properties of aqueous LiBr solution at high temperatures and concentrations”, *ASME International Absorption Heat Pump Conference*, 31, pp: 493-499.
- [146] Kaita, Y. (2001) “Thermodynamics properties of lithium-water solution at high temperatures”, *International Journal of Refrigeration*, 24, pp: 374-390.
- [147] Rivero, R, Garfias, M. (2006) “Standard chemical exergy of elements updated”, *Energy*, 31, pp: 3310-3326.
- [148] Kim, D. S, Ferreira, C. A. (2006) “A gibbs energy equation of LiBr aqueous solutions”, *International Journal of Refrigeration*, 29, pp: 36-46.
- [149] Kakac, S, Liu, H. (2002). *Heat exchangers selection, rating and thermal design*. 2nd edn. USA: CRC.

- [150] Kays, W. M, London, A. L. (1984). *Compact heat exchangers*. 3rd edn. USA: McGraw-Hill.
- [151] ESDU92013. (1992). *Selection and costing of heat exchanger*. 1st edn. UK: ESDU.
- [152] SimTec Simulation Technology. (2003). *IPSEpro process simulation manual: process simulation environment*. 1st edn. Austria: SimTec.
- [153] SimTec Simulation Technology. (2003). *IPSEpro process simulation manual: advanced power plant library*. 1st edn. Austria: SimTec.
- [154] SimTec Simulation Technology. (2003). *IPSEpro process simulation manual: advanced desalination library*. 1st edn. Austria: SimTec.
- [155] Perz, E, Bergmann, S. (2007) “A simulation environment for the techno-economic performance predication of water and power cogeneration systems using renewable energy and fossil energy source”, *Desalination*, 203, pp: 337-345.
- [156] Aneke, M, Agnew, B, Underwood, C. (2011) “Performance analysis of Chena binary geothermal power plant”, *Applied Thermal Engineering*, 31, pp: 1825-1832.
- [157] Dubey, S, Tiwari, F. (2008) “Thermal modelling of a combined system of photovoltaic thermal (PV/T) solar water heater”, *Solar Energy*, 82, pp: 602-612.
- [158] Kanoglu, M, Dincer, I. (2009) “Performance assessment of cogeneration plants”, *Energy Conversion and Management*, 50, pp: 76-81.
- [159] Sanjay. (2011) “Investigation of effect of variation of cycle parameters on thermodynamic performance of gas-steam combined cycle”, *Energy*, 36, pp: 157-167.
- [160] Ganapathy, T, et al. (2009) “Exergy analysis of operating lignite fired thermal power plant”, *Journal of Engineering Science and Technology Review*, 2, pp: 123-130.
- [161] Ganapathy, V. (2003). *Industrial boilers and heat recovery steam generators: design applications and calculations*. 1st edn. New York: Marcel Dekker.
- [162] Siemens. (2006). *Introduction to the complementary fired combined power cycle power plant*. 1st edn. Orlando: Siemens.
- [163] Atmaca, M. (2011) “Efficiency analysis of a combined cogeneration systems with steam and gas turbines”, *Energy Source*, 33, pp: 360-369.

- [164] Sarinvas, S, et al. (2009) “Studies on water-based absorption heat transformer for desalination using MED”, *Desalination and Water Treatment*, 1, pp: 75-81.
- [165] Carrier-Sanyo. (2005). *Specifications of Falun absorption chiller*. China: Carrier-Sanyo.
- [166] Carrier-Sanyo. *Absorption chiller service training manual*. China: Carrier-Sanyo.
- [167] Masheiti, S, Agnew, B. (2010) “The influence of coolant temperature on a single-effect lithium bromide-water absorption chiller when energized from a low-temperature source”, *Journal of Power and Energy*, 224, pp: 947-955.
- [168] Asdrubali, F, Grignaffini, S. (2005) “Experimental evaluation of the performance of a H₂O-LiBr absorption refrigerator under different service condition”, *International Journal of Refrigeration*, 28, pp: 489-497.
- [169] SONNENKLIMA. (2010). *Features of SONNENKLIMA absorption chiller*. Berlin.
- [170] Hu, T. (2012). *Advanced exergy analysis for a solar double stage absorption chiller*. Carnegie Mellon University: Pittsburgh.
- [171] Ahmadi, P, Rosen, M. A, Dincer, I. (2011) “Greenhouse gas emission and exergo-environmental analysis of trigeneration energy system”, *International Journal of Greenhouse Gas Control*, 5, pp: 1540-1549.
- [172] Alaska Energy Authority Chena Power. (2007). *400 kW geothermal power plant at Chena hot springs*. Alaska: Final report.
- [173] Wang, X. D, et al. (2010) “Performance evaluation of a low-temperature solar Rankine cycle system utilizing R245fa”, *Solar Energy*, 84, pp: 353-364.
- [174] Salah, B, et al. (2007) “Working fluids for organic Rankine cycle”, *Energy*, 32, pp: 1210-1221.
- [175] Bruno, J. C, et al. (2008) “Modelling and optimization of solar organic rankine cycle engines for reverse osmosis desalination”, *Applied Thermal Engineering*, 28, pp: 2212-2226.
- [176] Sami, S. M. (2008) “Energy and exergy analysis of an efficient organic Rankine cycle for low temperature power generation”, *International Journal of Ambient Energy*, 29, pp: 1-10.
- [177] Li, J, et al. (2012) “Energetic and exergitic investigation of an organic Rankine cycle at different heat source temperature”, *Energy*, 38, pp: 85-95.

- [178] Chacartegui, R, et al. (2009) “Feasibility analysis of a MED desalination plant in a combined cycle based cogeneration facility”, *Applied Thermal Engineering*, 29, pp: 412-417.
- [179] Wang, Y, Lior, N. (2011) “Thermoeconomic analysis of a low-temperature multi-effect thermal desalination system coupled with an absorption pump”, *Energy*, 36, pp: 3878-3887.
- [180] Alfa Laval product catalogues. Available at: www.alfalaval.com, accessed on 12-02-2013.
- [181] Saidur, R, et al. (2011) “An overview of different distillation methods for small scale applications”, *Renewable and Sustainable Energy Review*, 15, pp: 4756-4764.
- [182] Sayyaadi, H, Saffari, A. (2010) “Thermoeconomic optimization of multi effect distillation desalination systems”, *Applied Energy*, 87, pp: 1122-1133.
- [183] Ameri, M, et al. (2009) “Effect of design parameters on multi-effect desalination system specifications”, *Desalination*, 245, pp: 266-283.
- [184] Kamali, R. K, Abbassi, A, Vanini, S. A. S. (2010) “A simulation model and parametric study of MED-TVC process”, *Desalination*, 235, pp: 340-351.
- [185] Kamali, R. K, et al. (2008) “Thermodynamic design and parametric study of MED-TVC”, *Desalination*, 222, pp: 596-604.
- [186] Kamali, R. K, Mohebinia. (2008) “Experience of design and optimization of multi-effects desalination systems in Iran”, *Desalination*, 222, pp: 639-645.
- [187] <http://safalra.com/other/historical-uk-inflation-price-conversion>. Accessed on 12-02-2013.
- [188] E-mail from Barka plant operation manager. On 10-02-2014.
- [189] International Energy Agency. (1999). *District cooling balancing the production and demand in CHP*. USA: Novem.
- [190] Bailey, O, et al. (2002). *An engineering-economics analysis of combined heat and power technologies in a µgrid application*. USA: United State Environmental Protection Agency.
- [191] Chandrasekharam, D, Bundschuh, J. (2008). *Low-enthalpy geothermal resources for power generation*. 1st edn. UK: CRC.
- [192] Water Treatment Engineering Research Group. (2003). *Desalting for planner*. 3rd edn. USA.

Appendices

Appendix 3-A

- Seawater daily average temperature (°C) of hourly measurement

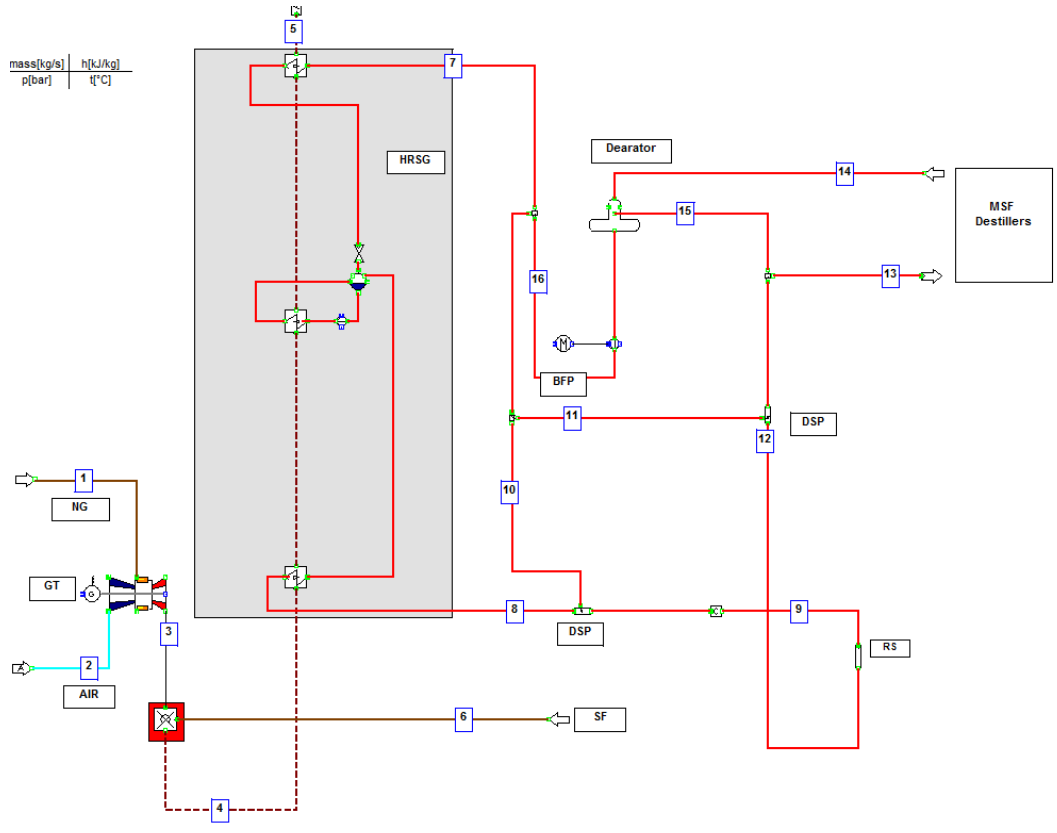
Day	Jan.	Feb.	Mar.	Apr.	May	Jun.	Jul.	Aug.	Sep.	Oct.	Nov.	Dec.
1	22.7	21.9	24.6	31.7	32.6	36.7	37.4	31.4	30.7	29.4	27.9	22.7
2	21.0	23.2	24.0	29.4	30.9	31.6	33.1	31.8	30.6	29.9	28.4	22.7
3	21.5	23.7	24.4	28.8	32.0	29.5	31.8	34.4	31.9	29.7	27.6	22.1
4	20.8	25.2	23.1	27.9	33.3	25.8	31.9	37.0	31.0	33.4	27.5	22.8
5	21.0	25.8	24.1	27.3	32.5	28.1	33.0	36.1	29.8	32.2	27.3	23.6
6	21.1	24.3	22.8	28.9	32.1	29.7	33.8	32.0	29.5	30.9	26.8	22.6
7	21.3	21.6	23.0	28.2	31.1	31.4	33.3	30.3	31.3	29.9	26.8	22.0
8	21.2	20.1	23.6	29.2	31.6	29.5	32.8	31.3	32.0	30.8	27.1	22.1
9	21.0	19.4	23.9	33.3	32.2	30.0	31.8	31.6	30.3	32.4	27.6	21.8
10	21.0	19.8	25.7	34.0	33.4	30.3	31.1	31.1	29.8	31.4	27.0	22.1
11	19.6	20.5	27.0	33.3	31.8	30.4	33.2	31.2	30.9	31.4	26.7	22.4
12	20.2	20.9	25.7	30.8	35.2	32.5	38.8	31.6	31.5	31.8	27.1	22.6
13	19.9	21.3	26.0	30.9	36.1	34.8	40.0	31.5	30.4	30.3	26.6	23.7
14	20.3	21.2	26.3	33.9	35.2	34.8	34.3	31.1	31.7	30.1	26.9	25.0
15	20.3	21.4	26.9	33.2	37.5	33.2	32.0	31.3	30.5	30.0	25.9	23.5
16	20.1	21.8	27.3	33.1	36.8	33.2	32.5	31.1	30.0	29.9	25.6	22.7
17	20.5	22.4	26.9	32.5	35.2	35.6	32.2	31.3	30.1	31.1	24.7	22.1
18	21.0	22.7	25.8	33.6	33.5	35.0	32.2	31.5	30.9	31.3	24.0	22.2
19	21.5	23.2	25.6	31.7	33.7	33.5	32.0	30.8	30.1	30.9	23.7	21.7
20	21.9	22.8	27.0	30.2	37.7	35.8	31.9	31.2	29.6	30.9	23.6	21.9
21	21.9	25.1	28.6	29.4	38.0	35.9	30.9	30.9	28.2	30.6	23.6	21.8
22	21.6	22.7	29.0	29.8	37.7	35.3	31.5	30.2	29.0	30.5	24.1	21.9
23	22.9	22.2	27.2	29.5	36.6	36.3	31.4	30.4	30.9	29.8	24.6	21.7
24	21.8	24.0	27.0	30.1	34.7	34.8	30.6	31.4	30.2	28.2	24.0	21.9
25	22.2	24.0	28.5	34.4	37.3	33.9	31.7	32.0	29.5	27.4	23.7	22.2
26	22.6	24.9	31.1	32.7	38.2	32.7	33.3	30.6	29.4	27.4	23.1	22.2
27	22.8	27.5	31.4	31.4	35.2	32.0	34.8	29.9	30.3	28.4	23.5	21.8
28	21.9	25.9	29.3	33.1	33.1	34.5	34.8	30.3	29.5	29.3	23.4	18.2
29	21.5		27.9	34.3	33.9	39.7	32.8	30.5	30.4	28.7	23.4	19.2
30	21.2		29.8	35.2	36.3	38.9	32.5	31.4	29.1	28.6	23.2	19.0
31	21.9		32.4		38.2		31.6	31.3		28.9		19.5

- Daily Average Relative Humidity (%) of hourly measurement

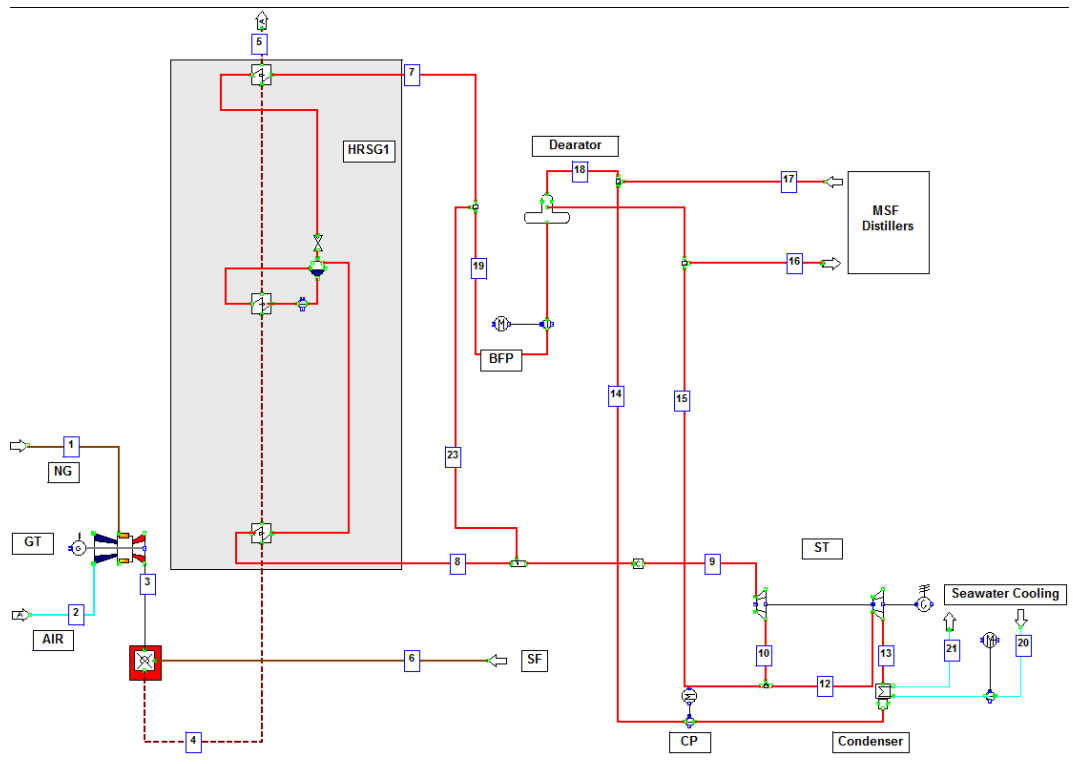
Day	Jan.	Feb.	Mar.	Apr.	May	Jun.	Jul.	Aug.	Sep.	Oct.	Nov.	Dec.
1	68	58	76	24	60	49	41	75	81	73	69	61
2	70	53	78	39	81	78	77	76	84	75	50	62
3	64	61	76	35	71	81	75	54	68	67	58	63
4	72	72	59	46	41	94	74	34	72	42	64	62
5	73	58	45	66	41	78	69	42	86	43	57	63
6	73	76	63	60	47	70	74	74	83	61	65	63
7	67	89	72	69	47	72	79	82	72	78	67	62
8	72	71	70	49	31	85	75	77	68	73	63	69
9	67	65	67	35	25	85	68	76	79	47	68	67
10	54	69	40	27	31	87	79	80	84	50	74	62
11	65	73	33	23	42	86	70	78	73	51	66	59
12	58	72	46	40	26	72	38	75	70	56	62	59
13	61	71	61	38	26	57	32	71	73	80	67	53
14	67	71	52	29	41	59	72	78	60	74	67	42
15	71	71	40	36	25	65	84	73	72	62	69	61
16	74	70	44	36	28	64	80	79	79	69	53	67
17	72	72	56	36	40	59	81	79	81	47	42	69
18	76	72	75	30	53	63	72	76	71	44	44	66
19	72	61	85	38	54	75	71	79	67	52	52	69
20	76	69	57	45	29	51	76	74	41	57	51	74
21	66	61	31	52	28	54	79	74	50	59	43	72
22	69	62	29	52	28	63	77	80	62	48	54	71
23	65	64	60	65	37	53	75	79	53	52	56	70
24	66	51	66	73	61	41	79	76	74	68	64	69
25	67	75	46	35	41	49	77	76	77	65	64	72
26	73	77	27	33	40	74	72	83	63	48	56	68
27	73	63	31	46	62	78	66	83	55	40	56	49
28	66	76	63	32	81	51	59	80	65	50	65	70
29	65		76	24	76	23	70	81	67	69	70	49
30	72		36	27	54	28	69	77	66	73	67	39
31	63		25		35		71	75		68		43
Avg.	68	58	76	24	60	49	41	75	81	73	69	61

Appendix 5- A

- Scenario II: IPSEpro model:



- Scenario III: IPSEpro model



- Scenario II: Streams compositions and model Cal. /Set properties

Stream No.	Composition	Flow	Temperature	Pressure	Entropy	Enthalpy	Specific volume
1	Natural Gas	Cal.	Set	Set	Cal.	Cal.	Cal.
2	Air	Cal.	Set	Set	Cal.	Cal.	Cal.
3	GT exhaust	Cal.	Cal.	Cal.	Cal.	Cal.	Cal.
4	GT exhaust after SF	Cal.	Cal.	Cal.	Cal.	Cal.	Cal.
5	HRSO exhaust	Cal.	Cal.	Cal.	Cal.	Cal.	Cal.
6	Natural Gas	Set	Set	Set	Cal.	Cal.	Cal.
7	Water	Cal.	Cal.	Cal.	Cal.	Cal.	Cal.
8	HP steam	Cal.	Set	Set	Cal.	Cal.	Cal.
9	HP steam	Cal.	Set	Cal.	Cal.	Cal.	Cal.
10	Water	Cal.	Cal.	Cal.	Cal.	Cal.	Cal.
11	Water	Cal.	Cal.	Cal.	Cal.	Cal.	Cal.
12	HP steam	Cal.	Cal.	Cal.	Cal.	Cal.	Cal.
13	LP steam	Set	Set	Set	Cal.	Cal.	Cal.
14	Condensate	Set	Set	Cal.	Cal.	Cal.	Cal.
15	LP steam	Cal.	Cal.	Cal.	Cal.	Cal.	Cal.
16	LP steam	Set	Cal.	Cal.	Cal.	Cal.	Cal.

- Scenario III: Streams compositions and model Cal. /Set properties

Stream No.	Composition	Flow	Temperature	Pressure	Entropy	Enthalpy	Specific volume
1	Natural Gas	Cal.	Set	Set	Cal.	Cal.	Cal.
2	Air	Cal.	Set	Set	Cal.	Cal.	Cal.
3	GT exhaust	Cal.	Cal.	Cal.	Cal.	Cal.	Cal.
4	GT exhaust after SF	Cal.	Cal.	Cal.	Cal.	Cal.	Cal.
5	HRSG exhaust	Cal.	Cal.	Cal.	Cal.	Cal.	Cal.
6	Natural Gas	Set	Set	Set	Cal.	Cal.	Cal.
7	Water	Cal.	Cal.	Cal.	Cal.	Cal.	Cal.
8	HP steam	Cal.	Set	Set	Cal.	Cal.	Cal.
9	HP steam	Cal.	Set	Set	Cal.	Cal.	Cal.
10	LP steam	Cal.	Cal.	Set	Cal.	Cal.	Cal.
12	LP steam	Cal.	Cal.	Cal.	Cal.	Cal.	Cal.
13	LP steam	Cal.	Cal.	Set	Cal.	Cal.	Cal.
14	LP steam	Cal.	Cal.	Cal.	Cal.	Cal.	Cal.
15	LP steam	Cal.	Cal.	Cal.	Cal.	Cal.	Cal.
16	LP steam	Set	Cal.	Cal.	Cal.	Cal.	Cal.
17	Condensate	Set	Set	Set	Cal.	Cal.	Cal.
18	Condensate	Cal.	Cal.	Cal.	Cal.	Cal.	Cal.
19	Water	Cal.	Cal.	Cal.	Cal.	Cal.	Cal.
20	Water	Cal.	Set	Set	Cal.	Cal.	Cal.
21	Water	Cal.	Set	Cal.	Cal.	Cal.	Cal.
23	Water	Cal.	Cal.	Cal.	Cal.	Cal.	Cal.

Appendix 5- B

- Scenario I validation

T _a (°C) / RH (%)	Unit	28.5/81.3		29.0/83.6		29.1/75.5		29.6/82.1	
		Measured Data	Model Result						
GT 1 Load	MW	120	120	140	140	120	120	125	125
GT2 Load	MW	120	120	131	131	120	120	125	125
SF1 flow	kg/s	1.47	1.47	1.58	1.58	1.47	1.47	1.48	1.48
SF2 flow	kg/s	1.68	1.68	0.91	0.91	1.69	1.69	1.43	1.43
MSF steam flow	kg/s	143	139	143	139	141	138	144	140
Steam P	bar	72.3	72.3	69.0	69.0	72.5	72.5	72.5	72.5
Steam T	°C	515	515	507	507	515	515	513	513
GT1 gas flow	kg/s	8.66	8.66	9.77	9.58	8.65	8.65	8.92	8.91
GT 2 gas flow	kg/s	8.66	8.66	9.13	9.16	8.65	8.65	8.91	8.91
HRSG1 steam flow	kg/s	310	299	351	348	312	298	321	312
HRSG2 steam flow	kg/s	332	313	308	282	331	314	327	308
ST Load	MW	125	123	128	126	126	124	126	128
Condensate flow	kg/s	98.7	97.6	116	113	106	103	98.9	97.3

T _a (°C) / RH (%)	Unit	29.9/88.85		30.0/95.9		30.5/84.4		30.9/95.9	
		Measured Data	Model Result						
GT 1 Load	MW	125	125	141	141	125	125	139	139
GT2 Load	MW	125	125	138	138	125	125	134	134
SF1 flow	kg/s	1.46	1.46	1.62	1.62	1.47	1.47	1.69	1.69
SF2 flow	kg/s	1.13	1.13	0.900	0.90	1.06	1.06	1.22	1.22
MSF steam flow	kg/s	141	137	143	141	138	135	142	141
Steam P	bar	72.8	72.8	68.9	68.9	72.7	72.7	71.2	71.2
Steam T	°C	512	512	507	507	512	512	515	515
GT1 gas flow	kg/s	8.91	8.90	9.77	9.52	8.90	8.94	9.50	9.50
GT 2 gas flow	kg/s	8.89	8.90	9.56	9.47	8.88	8.94	9.22	9.34
HRSG1 steam flow	kg/s	319	311	354	351	320	314	349	354
HRSG2 steam flow	kg/s	312	288	319	299	308	285	328	314
ST Load	MW	120	120	132	131	120	121	137	138
Condensate flow	kg/s	95.5	90.9	128	127	101	97.7	137	140

T _a (°C) / RH (%)	Unit	31.0/57.4		31.6/24.6		31.9/89.9		32.0/11.9	
		Measured Data	Model Result						
GT 1 Load	MW	126	126	139	139	137	137	130	130
GT2 Load	MW	126	126	135	135	133	133	130	130
SF1 flow	kg/s	1.32	1.32	1.44	1.44	1.71	1.71	1.41	1.41
SF2 flow	kg/s	1.10	1.10	1.12	1.12	1.33	1.33	1.03	1.03
MSF steam flow	kg/s	138	135	142	141	146	147	140	140
Steam P	bar	69.8	69.8	69.9	69.9	72.9	72.9	70.1	70.1
Steam T	°C	507	507	509	509	515	515	507	507
GT1 gas flow	kg/s	8.97	8.98	9.58	9.49	9.65	9.43	9.11	9.24
GT 2 gas flow	kg/s	8.97	8.98	9.35	9.39	9.37	9.34	9.11	9.24
HRSG1 steam flow	kg/s	313	306	337	335	350	356	323	322
HRSG2 steam flow	kg/s	314	290	325	307	332	325	314	296
ST Load	MW	119	119	130	130	137	140	122	123
Condensate flow	kg/s	103	98	115	117	129	132	102	99

T _a (°C) / RH (%)	Unit	32.5/64.8		32.9/61.77		33.1/37.5		33.5/51.0	
		Measured Data	Model Result						
GT 1 Load	MW	130	130	126	125	137	136	137	137
GT2 Load	MW	132	132	124	124	133	133	134	134
SF1 flow	kg/s	1.46	1.46	1.77	1.77	1.48	1.48	1.28	1.28
SF2 flow	kg/s	1.10	1.10	1.37	1.37	1.44	1.44	1.44	1.44
MSF steam flow	kg/s	142	140	143	143	141	143	141	143
Steam P	bar	72.7	72.7	72.3	72.3	70.1	70.1	70.2	70.2
Steam T	°C	511	511	518	518	511	511	510	510
GT1 gas flow	kg/s	9.21	9.19	9.01	9.00	9.55	9.46	9.61	9.44
GT 2 gas flow	kg/s	9.27	9.22	8.92	8.89	9.31	9.36	9.40	9.37
HRSG1 steam flow	kg/s	326	325	335	336	336	337	326	324
HRSG2 steam flow	kg/s	321	301	321	308	337	337	340	332
ST Load	MW	125	127	130	132	136	136	133	133
Condensate flow	kg/s	108	105	113	112	133	132	124	122

T _a (°C) / RH (%)	Unit	33.9/63.0		34.0/16.8		34.4/41.0		34.9/18.4	
		Measured Data	Model Result						
GT 1 Load	MW	130	130	130	130	136	136	134	134
GT2 Load	MW	129	129	133	133	132	132	130	130
SF1 flow	kg/s	1.57	1.57	1.29	1.29	1.15	1.15	1.63	1.63
SF2 flow	kg/s	1.15	1.15	1.45	1.45	0.960	0.96	1.40	1.40
MSF steam flow	kg/s	146	146	145	145	139	138	144	142
Steam P	bar	73.0	73.0	70.1	70.1	69.7	69.7	67.8	67.8
Steam T	°C	513	513	510	510	505	505	505	505
GT1 gas flow	kg/s	9.2	9.2	9.1	9.2	9.54	9.42	9.39	9.41
GT 2 gas flow	kg/s	9.2	9.2	9.3	9.3	9.34	9.34	9.13	9.27
HRSG1 steam flow	kg/s	336	335	314	314	319	316	344	347
HRSG2 steam flow	kg/s	320	305	338	329	317	298	335	325
ST Load	MW	126	129	127	129	121	123	136	136
Condensate flow	kg/s	101	100	106	105	104	104	132	131

T _a (°C) / RH (%)	Unit	35.0/41.9		35.6/53.6		35.9/67.8		36.0/58.1	
		Measured Data	Model Result						
GT 1 Load	MW	133	132	133	133	134	134	125	125
GT2 Load	MW	130	129	129	129	130	129	125	125
SF1 flow	kg/s	1.53	1.53	1.99	1.99	1.73	1.73	1.59	1.59
SF2 flow	kg/s	1.44	1.44	1.62	1.62	1.23	1.23	1.26	1.26
MSF steam flow	kg/s	140	142	143	146	142	143	141	141
Steam P	bar	71.5	71.5	71.2	71.2	72.6	72.6	73.1	73.1
Steam T	°C	513	513	513	513	513	513	515	515
GT1 gas flow	kg/s	9.42	9.36	9.46	9.4	9.44	9.39	8.97	9.07
GT 2 gas flow	kg/s	9.23	9.21	9.21	9.21	9.12	9.24	8.97	9.07
HRSG1 steam flow	kg/s	331	340	361	372	348	355	329	330
HRSG2 steam flow	kg/s	333	327	341	338	325	314	321	308
ST Load	MW	134	135	147	147	137	138	129	131
Condensate flow	kg/s	131	136	159	161	134	135	113	113

T _a (°C) / RH (%)	Unit	36.4/48.5		36.9/20.1		37.0/44.2		37.5/38.3	
		Measured Data	Model Result						
GT 1 Load	MW	134	134	132	132	132	132	132	132
GT2 Load	MW	129	129	129	129	123	123	128	128
SF1 flow	kg/s	0.36	0.36	1.77	1.77	1.59	1.59	1.59	1.59
SF2 flow	kg/s	1.98	1.98	2.02	2.02	1.13	1.13	1.93	1.93
MSF steam flow	kg/s	140	142	140	143	142	142	141	142
Steam P	bar	72.3	72.3	71.9	71.9	73.1	73.1	72.1	72.1
Steam T	°C	516	516	518	518	514	514	516	516
GT1 gas flow	kg/s	9.20	9.38	9.30	9.37	9.36	9.37	9.13	9.35
GT 2 gas flow	kg/s	8.95	9.24	9.09	9.22	8.83	9.00	8.84	9.21
HRSG1 steam flow	kg/s	268	258	346	352	340	344	344	343
HRSG2 steam flow	kg/s	363	363	361	363	312	295	356	359
ST Load	MW	120	125	151	151	128	130	146	147
Condensate flow	kg/s	96	95	174	176	111	111	164	167

T _a (°C) / RH (%)	Unit	37.9/30.3		38.2/16.1		38.4/15.4		38.8/24.8	
		Measured Data	Model Result						
GT 1 Load	MW	132	132	130	130	131	131	131	131
GT2 Load	MW	128	128	126	126	127	127	127	127
SF1 flow	kg/s	3.03	3.03	1.16	1.16	1.78	1.78	1.34	1.34
SF2 flow	kg/s	1.09	1.09	1.57	1.57	2.02	2.02	1.74	1.71
MSF steam flow	kg/s	141	144	141	142	139	142	141	142
Steam P	bar	72.2	72.2	69.9	69.9	71.9	71.9	70.0	70.0
Steam T	°C	519	519	512	512	518	518	516	516
GT1 gas flow	kg/s	9.28	9.34	9.21	9.34	9.25	9.33	9.25	9.32
GT 2 gas flow	kg/s	9.05	9.20	8.97	9.17	9.06	9.19	9.02	9.18
HRSG1 steam flow	kg/s	418	436	312	312	348	353	323	322
HRSG2 steam flow	kg/s	309	300	338	332	356	362	347	343
ST Load	MW	158	156	128	130	151	151	136	136
Condensate flow	kg/s	186	191	111	112	173	179	134	134

T _a (°C) / RH (%)	Unit	39.0/22.7		39.3/10.9		39.9/20.4		40.1/17.9	
		Measured Data	Model Result						
GT 1 Load	MW	130	130	129	129	129	129	129	129
GT2 Load	MW	127	127	126	126	126	126	126	126
SF1 flow	kg/s	1.68	1.68	1.16	1.16	2.21	2.21	2.31	2.31
SF2 flow	kg/s	1.37	1.34	1.57	1.57	1.48	1.48	1.48	1.48
MSF steam flow	kg/s	143	145	141	144	141	144	142	146
Steam P	bar	70.3	70.3	69.8	69.8	70.6	70.6	70.8	70.8
Steam T	°C	514	515	512	512	517	517	520	520
GT1 gas flow	kg/s	9.26	9.32	9.16	9.31	9.20	9.29	9.18	9.29
GT 2 gas flow	kg/s	9.07	9.22	8.94	9.17	9.03	9.20	8.97	9.20
HRSG1 steam flow	kg/s	342	347	312	311	368	382	369	387
HRSG2 steam flow	kg/s	329	321	337	333	333	328	333	328
ST Load	MW	136	137	128	130	149	148	147	149
Condensate flow	kg/s	126	128	110	109	164	168	164	166

T _a (°C) / RH (%)	Unit	40.4/12.0		40.9/14.4		41.2/16.2		41.6/13.4	
		Measured Data	Model Result						
GT 1 Load	MW	129	129	128	128	128	128	128	128
GT2 Load	MW	126	126	125	125	123	123	125	123
SF1 flow	kg/s	1.55	1.55	1.99	1.99	1.35	1.35	1.18	1.18
SF2 flow	kg/s	1.34	1.34	1.44	1.44	1.56	1.56	1.56	1.56
MSF steam flow	kg/s	139	140	140	144	139	142	139	142
Steam P	bar	70.3	70.3	70.4	70.4	70.0	70.0	70.0	70.0
Steam T	°C	515	515	516	516	516	516	515	515
GT1 gas flow	kg/s	9.16	9.29	9.12	9.27	9.10	9.27	9.09	9.26
GT 2 gas flow	kg/s	8.98	9.20	8.92	9.23	8.86	9.14	8.92	9.12
HRSG1 steam flow	kg/s	333	336	356	366	321	322	310	311
HRSG2 steam flow	kg/s	327	318	331	327	335	331	337	331
ST Load	MW	133	134	143	144	131	133	128	130
Condensate flow	kg/s	129	132	151	154	125	124	116	113

▪ Scenario II validation

T _a (°C) / RH (%)	Unit	17.54/73.54		17.87/74.42		18.32/68.62		18.85/73.91	
		Measured Data	Model Result						
GT Load	MW	148	148	147	147	147	148	148	148
SF flow	kg/s	2.57	2.57	2.56	2.56	2.57	2.57	2.52	2.52
MSF steam flow	kg/s	138	140	138	139	139	139	138	139
Steam P	bar	71.5	71.5	71.0	71.0	72.5	72.5	72.8	72.8
Steam T	°C	420	420	420	420	420	420	420	420
GT gas flow	kg/s	9.97	9.96	9.95	9.92	9.96	9.93	9.94	9.91
HRSG steam flow	kg/s	409	397	407	399	410	400	406	397

T _a (°C) / RH (%)	Unit	19.1/74.1		19.5/53.2		19.9/73.8		20.0/73.6	
		Measured Data	Model Result						
GT Load	MW	148	148	147	147	142	142	147	147
SF flow	kg/s	2.63	2.63	2.62	2.62	2.37	2.37	2.32	2.32
MSF steam flow	kg/s	139	139	139	139	135	134	135	134
Steam P	bar	71.9	71.9	72.0	72.0	76.0	76.0	74.8	74.8
Steam T	°C	419	419	419	419	415	415	414	414
GT gas flow	kg/s	9.92	9.96	9.90	9.87	9.69	9.65	9.90	9.85
HSRG steam flow	kg/s	410	408	408	405	390	380	391	385

T _a (°C) / RH (%)	Unit	20.5/74.2		20.9/77.4		21.0/68.9		21.5/51.2	
		Measured Data	Model Result						
GT Load	MW	142	142	148	148	147	147	145	144
SF flow	kg/s	2.45	2.45	1.42	1.42	2.45	2.45	1.97	1.97
MSF steam flow	kg/s	135	134	112	110	135	135	127	126
Steam P	bar	74.0	74.0	74.4	74.4	74.0	74.0	73.5	73.5
Steam T	°C	415	415	402	402	415	415	410	410
GT gas flow	kg/s	9.68	9.69	10.0	9.93	10.0	9.93	9.84	9.77
HSRG steam flow	kg/s	389	389	340	328	389	398	373	358

T _a (°C) / RH (%)	Unit	21.9/70.4		22.0/76.3		22.4/58.7		22.9/19.7	
		Measured Data	Model Result						
GT Load	MW	141	141	147	147	144	144	145	145
SF flow	kg/s	1.45	1.45	1.89	1.89	2.62	2.62	1.98	1.98
MSF steam flow	kg/s	114	112	126	124	139	138	128	128
Steam P	bar	75.0	75.0	71.9	71.9	74.6	74.6	73.2	73.2
Steam T	°C	407	407	409	409	424	424	412	412
GT gas flow	kg/s	9.65	9.62	10.08	9.93	9.81	9.78	9.73	9.78
HSRG steam flow	kg/s	346	331	371	362	408	407	378	363

T _a (°C) / RH (%)	Unit	23.0/58.9		23.5/51.2		23.9/82.7		24.0/84.9	
		Measured Data	Model Result						
GT Load	MW	142	142	140	140	144	144	145	145
SF flow	kg/s	2.39	2.39	1.42	1.42	1.26	1.30	2.85	2.85
MSF steam flow	kg/s	135	134	115	112	113	110	141	141
Steam P	bar	76.4	76.4	74.1	74.1	72.1	72.1	74.5	74.5
Steam T	°C	415	415	411	411	405	405	419	419
GT gas flow	kg/s	9.69	9.69	9.54	9.60	9.86	9.70	10.10	9.82
HSRG steam flow	kg/s	390	390	343	330	341	328	414	428

T _a (°C) / RH (%)	Unit	24.5/52.5		24.9/98.3		25.0/55.9		25.5/72.7	
		Measured Data	Model Result						
GT Load	MW	146	146	144	144	144	144	140	140
SF flow	kg/s	2.30	2.30	1.31	1.31	1.90	1.90	1.87	1.87
MSF steam flow	kg/s	132	132	115	113	125	125	124	125
Steam P	bar	74.5	74.5	73.0	73.0	73.3	73.3	70.8	70.8
Steam T	°C	420	420	405	405	411	411	412	412
GT gas flow	kg/s	9.94	9.79	9.87	9.76	9.86	9.76	9.54	9.56
HSRG steam flow	kg/s	388	387	344	328	369	365	369	355

T _a (°C) / RH (%)	Unit	25.9/74.9		26.0/77.6		26.5/41.1		26.9/66.9	
		Measured Data	Model Result						
GT Load	MW	142	142	142	142	143	143	143	143
SF flow	kg/s	1.24	1.24	1.26	1.26	2.62	2.62	1.37	1.37
MSF steam flow	kg/s	113	110	113	112	138	137	116	114
Steam P	bar	72.9	72.9	75.6	75.6	73.1	73.1	72.9	72.9
Steam T	°C	408	408	408	408	387	387	406	406
GT gas flow	kg/s	9.80	9.70	9.83	9.67	9.83	9.67	9.81	9.70
HSRG steam flow	kg/s	338	323	338	324	405	412	342	329

T _a (°C) / RH (%)	Unit	27.0/47.9		27.5/34.3		27.9/50.2		28.0/65.5	
		Measured Data	Model Result						
GT Load	MW	139	139	141	141	140	140	140	140
SF flow	kg/s	1.42	1.42	1.85	1.85	2.76	2.76	1.29	1.29
MSF steam flow	kg/s	115	113	123	123	139	138	114	113
Steam P	bar	70.7	70.7	69.9	69.9	75.0	75.0	74.2	74.2
Steam T	°C	405	405	408	408	413	413	406	406
GT gas flow	kg/s	9.58	9.53	9.74	9.62	9.68	9.59	9.63	9.59
HSRG steam flow	kg/s	342	326	367	358	405	421	342	326

T _a (°C) / RH (%)	Unit	31.0/42.6		31.5/38.9		31.8/30.4		32.1/26.5	
		Measured Data	Model Result						
GT Load	MW	140	140	137	137	138	138	137	137
SF flow	kg/s	2.00	2.00	1.49	1.49	2.04	2.04	2.07	2.07
MSF steam flow	kg/s	126	125	115	115	126	125	126	125
Steam P	bar	75.4	75.4	72.7	72.7	74.2	74.2	72.9	72.9
Steam T	°C	412	412	405	405	412	412	412	412
GT gas flow	kg/s	9.71	9.50	9.51	9.49	9.65	9.48	9.59	9.47
HSRG steam flow	kg/s	371	371	343	341	370	372	370	374

T _a (°C) / RH (%)	Unit	32.8/25.8		33.2/27.8		34.7/31.7		35.4/19.9	
		Measured Data	Model Result						
GT Load	MW	137	137	137	137	138	138	134	134
SF flow	kg/s	1.94	1.94	1.94	1.94	1.92	1.92	2.03	2.03
MSF steam flow	kg/s	125	125	125	125	126	125	126	125
Steam P	bar	72.9	72.9	72.5	72.5	73.6	73.6	71.0	71.0
Steam T	°C	413	413	413	413	414	414	413	413
GT gas flow	kg/s	9.40	9.46	9.39	9.44	9.49	9.42	9.23	9.40
HSRG steam flow	kg/s	368	366	369	366	369	364	369	371

▪ Scenario III validation

T _a (°C) / RH (%)	Unit	21.2/37.9		21.5/32.2		21.9/48.4		22.1/24.0	
		Measured Data	Model Result						
GT Load	MW	145	145	144	144	142	142	140	140
SF flow	kg/s	2.94	2.94	2.94	2.94	3.01	3.01	2.93	2.93
MSF steam flow	kg/s	92.5	88.0	92.4	90.0	92.3	88.0	92.2	90.0
Steam P	bar	66.6	66.6	67.3	67.3	66.7	66.7	67.3	67.3
Steam T	°C	511	511	512	512	509	509	512	512
GT gas flow	kg/s	9.96	9.78	9.85	9.78	9.77	9.68	9.70	9.62
HSRG steam flow	kg/s	441	426	441	426	442	430	441	420
ST Load	MW	81.9	85.4	81.0	84.9	83.2	86.2	80.0	83.5
Condensate flow	kg/s	99.7	95.7	92.5	89.4	103.7	99.3	85.0	84.2

T _a (°C) / RH (%)	Unit	22.4/43.6		22.9/30.7		23.1/82.6		23.5/44.1	
		Measured Data	Model Result						
GT Load	MW	142	142	140	140	142	142	140	140
SF flow	kg/s	2.94	2.94	2.94	2.94	3.01	3.01	3.00	3.00
MSF steam flow	kg/s	92.8	88.5	92.7	89.5	92.7	91.0	92.8	89.5
Steam P	bar	67.3	67.3	67.3	67.3	66.7	66.7	67.4	67.3
Steam T	°C	513	513	513	513	508	508	510	510
GT gas flow	kg/s	9.74	9.68	9.62	9.68	9.81	9.66	9.73	9.54
HSRG steam flow	kg/s	442	423	441	419	442	433	442	423
ST Load	MW	81.9	84.5	80.9	83.1	81.9	85.9	81.9	84.9
Condensate flow	kg/s	95.0	91.0	87.9	83.8	95.0	91.5	91.5	90.5

T _a (°C) / RH (%)	Unit	23.9/69.4		24.1/45.1		24.5/41.8		24.9/81.4	
		Measured Data	Model Result						
GT Load	MW	143	143	144	144	139	139	142	142
SF flow	kg/s	3.11	3.11	3.14	3.14	3.00	3.00	3.02	3.02
MSF steam flow	kg/s	93.0	91.0	93.0	89.0	92.9	91.0	92.4	92.5
Steam P	bar	67.8	67.8	67.1	67.1	67.3	67.3	66.6	66.6
Steam T	°C	517	517	516	516	510	510	509	509
GT gas flow	kg/s	9.82	9.70	9.70	9.75	9.72	9.55	9.81	9.70
HSRG steam flow	kg/s	441	443	440	444	442	431	443	441
ST Load	MW	85.1	88.8	87.7	90.6	81.9	84.0	82.0	85.6
Condensate flow	kg/s	105	101	112	109	91.4	90.0	95.3	92.4

T _a (°C) / RH (%)	Unit	25.0/67.8		25.6/32.1		25.9/76.2		26.0/59.6	
		Measured Data	Model Result						
GT Load	MW	145	145	139	139	142	142	145	144
SF flow	kg/s	3.03	3.03	2.93	2.93	3.02	3.02	3.04	3.04
MSF steam flow	kg/s	93.6	90.0	93.0	90.5	92.4	92.0	93.1	92.0
Steam P	bar	66.7	67.0	67.1	68.0	66.7	66.7	66.6	67.5
Steam T	°C	514	514	514	514	509	509	515	515
GT gas flow	kg/s	9.86	9.73	9.61	9.56	9.82	9.65	9.90	9.76
HSRG steam flow	kg/s	441	439	440	425	443	439	441	442
ST Load	MW	84.9	88.6	80.4	83.9	82.3	85.6	83.8	87.2
Condensate flow	kg/s	104	101	89.9	86.7	94.9	94.4	98.4	97.1

T _a (°C) / RH (%)	Unit	26.4/73.5		26.9/57.8		27.0/35.4		27.5/34.1	
		Measured Data	Model Result						
GT Load	MW	142	142	143	143	138	138	139	139
SF flow	kg/s	3.02	3.02	3.10	3.10	2.97	2.97	2.92	2.92
MSF steam flow	kg/s	92.6	92.0	93.6	93.0	93.2	91.5	90.8	90.5
Steam P	bar	66.7	66.0	66.8	68.0	67.1	69.0	67.0	67.0
Steam T	°C	509	509	515	515	513	513	515	515
GT gas flow	kg/s	9.83	9.65	9.83	9.70	9.63	9.42	9.71	9.48
HSRG steam flow	kg/s	443	440	441	446	440	427	439	426
ST Load	MW	82.4	85.6	84.9	88.0	80.5	83.4	80.4	83.0
Condensate flow	kg/s	93.3	94.8	96.5	97.6	88.5	85.4	90.8	87.4

T _a (°C) / RH (%)	Unit	27.9/49.6		28.0/34.8		28.4/80.0		28.8/57.4	
		Measured Data	Model Result						
GT Load	MW	141	141	138	138	142	142	140	140
SF flow	kg/s	3.09	3.09	3.00	3.00	2.96	2.96	3.08	3.08
MSF steam flow	kg/s	93.7	92.0	92.5	92.0	93.3	93.0	90.8	90.0
Steam P	bar	67.2	68.0	67.2	68.0	70.7	70.7	66.9	66.9
Steam T	°C	514	514	511	511	523	523	517	517
GT gas flow	kg/s	9.74	9.59	9.65	9.48	9.82	9.62	9.67	9.59
HSRG steam flow	kg/s	441	441	442	432	445	438	440	444
ST Load	MW	84.6	86.7	81.4	84.3	83.8	86.7	86.5	88.4
Condensate flow	kg/s	95.0	96.4	90.1	88.3	91.3	89.4	107.1	105.5

T _a (°C) / RH (%)	Unit	29.0/55.4		29.6/48.4		29.9/46.3		30.0/51.1	
		Measured Data	Model Result						
GT Load	MW	139	139	140	140	139	139	140	140
SF flow	kg/s	3.07	3.07	2.97	2.97	2.96	2.96	2.95	2.95
MSF steam flow	kg/s	90.6	90.0	96.2	92.0	95.9	92.0	95.7	91.0
Steam P	bar	67.0	67.0	68.9	68.9	68.9	68.9	69.2	520.0
Steam T	°C	517	517	533	520	534	520	533	10
GT gas flow	kg/s	9.58	9.53	9.78	9.55	9.75	9.52	9.85	9.52
HSRG steam flow	kg/s	440	440	436	436	435	435	435	432
ST Load	MW	85.7	89.3	89.7	88.4	86.8	89.9	89.0	89.7
Condensate flow	kg/s	105	102	95.8	91.8	93.3	91.1	95.6	91.7

T _a (°C) / RH (%)	Unit	31.2/43.9		31.9/45.1		32.1/45.7		32.6/27.4	
		Measured Data	Model Result						
GT Load	MW	139	139	137	137	137	137	137	137
SF flow	kg/s	3.07	3.07	3.14	3.14	3.15	3.15	3.07	3.07
MSF steam flow	kg/s	99.3	95.0	97.8	94.0	98.2	95.0	99.0	95.0
Steam P	bar	69.1	69.1	68.7	68.7	68.7	68.7	69.0	69.0
Steam T	°C	527	520	532	530	532	527	527	520
GT gas flow	kg/s	9.47	9.49	9.50	9.48	9.47	9.49	9.38	9.47
HSRG steam flow	kg/s	439	441	433	442	433	443	439	440
ST Load	MW	87.4	90.7	87.9	92.0	87.8	92.1	85.8	86.5
Condensate flow	kg/s	90.0	86.1	92.8	90.8	92.8	88.6	87.3	84.8

Appendix 5-C

- Simulated results of the cycle streams thermodynamics properties in scenario II.

Stream No.	\dot{m} (kg/s)	T (°C)	P (bar)	h (kJ/kg)	s (kJ/(kg.K))	E_{ph} (MW)	E_{ch} (MW)	E_T (MW)
1	9.58	25.0	18.0	52.1	9.75	4.26	492	497
2	480	29.0	1.01	29.5	6.96	0	0	0
3	489	556	1.02	612	8.20	124	1.93	126
4	492	796	1.01	913	8.56	225	1.94	227
5	492	142	1.01	152	7.48	9.72	1.94	11.7
6	3.16	25.0	1.11	52.1	11.1	1.41	162	164
7	108	109	104	465	1.40	5.64	0.270	5.91
8	108	720	83.0	3929	7.31	190	0.270	190
9	124	540	83.0	3494	6.83	181	0.310	181
10	15.5	109	104	465	1.40	0.810	0.040	0.850
11	17.2	109	104	465	1.40	0.890	0.040	0.940
12	124	265	1.50	3004	7.90	80.6	0.310	81.0
13	140	112	1.50	2694	7.23	76.2	0.350	76.6
14	140	104	1.30	436	1.35	5.26	0.350	5.61
15	0.819	112	1.50	436	7.23	0.450	0	0.45
16	141	109	104	465	1.40	7.34	0.350	7.69

- Simulated results of the cycle streams thermodynamics properties in scenario III.

Stream No.	\dot{m} (kg/s)	T (°C)	P (bar)	h (kJ/kg)	s (kJ/(kg.K))	E_{ph} (MW)	E_{ch} (MW)	E_T (MW)
1	9.58	25.0	18.0	52.1	9.75	4.26	492	497
2	480	29.0	1.01	29.3	6.92	0	0	0
3	489	556	1.02	608	8.16	123	1.93	125
4	492	798	1.01	909	8.52	224	1.94	226
5	492	143	1.01	151	7.44	9.69	1.93	11.6
6	3.16	25.0	1.11	52.1	11.1	1.41	162	164
7	107	109	104	465	1.40	5.59	0.270	5.86
8	107	725	83.0	3941	7.33	189	0.270	189
9	123	540	83.0	3494	6.83	180	0.310	180
10	123	111	1.50	2637	7.08	65.5	0.310	65.8
12	9.32	111	1.50	2637	7.08	4.95	0.020	4.98
13	9.32	45.8	0.100	2282	7.20	1.30	0.020	1.32
14	9.32	42.8	1.30	179	0.609	0.020	0.020	0.040
15	114	111	1.50	2637	7.08	60.5	0.280	60.8
16	112	111	1.50	2637	7.08	59.6	0.280	59.8
17	112	104	10.0	437	1.35	4.30	0.280	4.58
18	121	99.5	1.30	417	1.30	4.08	0.300	4.38
19	123	109	104	465	1.40	6.41	0.310	6.72
20	4320	25.0	1.01	105	0.368	0.880	10.8	11.6
21	4320	26.2	2.00	110	0.383	0.490	10.8	11.3
22	15.8	109	104	465	1.40	0.820	0.040	0.860

Appendix 5- D

- Influence of ambient temperature on equipment performance

PP+SF+MSF										
Equipment	Unit	10 °C	15 °C	20 °C	25 °C	30 °C	35 °C	40 °C	45 °C	50 °C
GT Efficiency	%	34.9	34.6	34.1	33.7	33.2	32.8	32.3	31.9	31.5
GT Load	MW	164	158	152	145	139	134	128	122	117
GT gas	kg/s	10.7	10.4	10.1	9.82	9.52	9.26	9.00	8.73	8.45
HRSG	%	81.5	81.8	82.4	83.0	83.6	84.2	84.8	85.2	85.4
HRSG	t/h	444	444	443	442	441	440	439	436	432
G/P ratio	kg/kW	0.18	0.18	0.18	0.18	0.18	0.18	0.18	0.18	0.18
ST load	MW	206	205	205	205	204	203	203	201	199

- Influence of ambient temperature on equipment exergy efficiency (%)

PP									
Equipment	10 °C	15 °C	20 °C	25 °C	30 °C	35 °C	40 °C	45 °C	50 °C
GT1	37.7	37.6	37.4	37.2	37.0	36.9	36.8	36.7	36.7
GT2	37.7	37.6	37.4	37.2	37.0	36.9	36.8	36.7	36.7
SFB 1	99.8	99.8	99.8	99.8	99.8	99.8	99.8	99.8	99.8
SFB 2	99.8	99.8	99.8	99.8	99.8	99.8	99.8	99.8	99.8
HRSG1	85.6	85.6	85.5	85.5	85.4	85.4	85.3	85.3	85.2
HRSG2	85.6	85.6	85.5	85.5	85.4	85.4	85.3	85.3	85.2
HPT	80.1	80.1	80.1	80.1	80.1	80.1	80.1	80.1	80.1
LPT	81.5	81.5	81.5	81.5	81.5	81.5	81.5	81.5	81.5
Condenser	8.7	8.7	8.7	8.7	8.7	8.7	8.7	8.7	8.7
Deaerator	41.4	41.4	41.5	41.5	41.7	41.8	42.0	42.2	42.5
DSP	99.8	99.7	99.6	99.4	99.3	99.1	99.0	98.8	98.7
MSF	5.70	5.70	5.70	5.70	5.70	5.70	5.70	5.70	5.70

PP+MSF									
Equipment	10 °C	15 °C	20 °C	25 °C	30 °C	35 °C	40 °C	45 °C	50 °C
GT1	37.7	37.6	37.4	37.2	37.0	36.9	36.8	36.7	36.7
GT2	37.7	37.6	37.4	37.2	37.0	36.9	36.8	36.7	36.7
SFB 1	99.8	99.8	99.8	99.8	99.8	99.8	99.8	99.8	99.8
SFB 2	99.8	99.8	99.8	99.8	99.8	99.8	99.8	99.8	99.8
HRSG1	85.6	85.6	85.5	85.5	85.4	85.4	85.3	85.3	85.2
HRSG2	85.6	85.6	85.5	85.5	85.4	85.4	85.3	85.3	85.2
HPT	80.1	80.1	80.1	80.1	80.1	80.1	80.1	80.1	80.1
LPT	81.5	81.5	81.5	81.5	81.5	81.5	81.5	81.5	81.5
Condenser	8.7	8.7	8.7	8.7	8.7	8.7	8.7	8.7	8.7
Deaerator	60.0	60.0	60.1	60.2	60.4	60.6	61.0	61.3	61.8
DSP	99.8	99.7	99.6	99.4	99.3	99.1	99.0	98.8	98.7
MSF	5.70	5.70	5.70	5.70	5.70	5.70	5.70	5.70	5.70

PP+SF									
Equipment	10 °C	15 °C	20 °C	25 °C	30 °C	35 °C	40 °C	45 °C	50 °C
GT1	37.7	37.6	37.4	37.2	37.0	36.9	36.8	36.7	36.7
GT2	37.7	37.6	37.4	37.2	37.0	36.9	36.8	36.7	36.7
SFB 1	77.9	78.0	78.1	78.1	78.2	78.3	78.4	78.4	78.5
SFB 2	77.9	78.0	78.1	78.1	78.2	78.3	78.4	78.4	78.5
HRSG1	85.6	85.6	85.6	85.6	85.6	85.6	85.6	85.7	86.1
HRSG2	85.6	85.6	85.6	85.6	85.6	85.6	85.6	85.7	86.1
HPT	80.1	80.1	80.1	80.1	80.1	80.1	80.1	80.1	80.1
LPT	81.5	81.5	81.5	81.5	81.5	81.5	81.5	81.5	81.5
Condenser	8.70	8.70	8.70	8.70	8.70	8.70	8.70	8.70	8.70
Deaerator	19.8	19.8	19.9	19.9	19.9	20.0	20.1	20.2	20.3
DSP	95.7	95.6	95.4	95.1	94.8	94.5	94.2	93.7	92.9
MSF	5.70	5.70	5.70	5.70	5.70	5.70	5.70	5.70	5.70

PP+SF+MSF									
Equipment	10 °C	15 °C	20 °C	25 °C	30 °C	35 °C	40 °C	45 °C	50 °C
GT1	37.7	37.6	37.4	37.2	37.0	36.9	36.8	36.7	36.7
GT2	37.7	37.6	37.4	37.2	37.0	36.9	36.8	36.7	36.7
SFB 1	77.9	78.0	78.1	78.1	78.2	78.3	78.4	78.4	78.5
SFB 2	77.9	78.0	78.1	78.1	78.2	78.3	78.4	78.4	78.5
HRSG1	85.6	85.6	85.6	85.6	85.6	85.6	85.6	85.7	86.1
HRSG2	85.6	85.6	85.6	85.6	85.6	85.6	85.6	85.7	86.1
HPT	80.1	80.1	80.1	80.1	80.1	80.1	80.1	80.1	80.1
LPT	81.5	81.5	81.5	81.5	81.5	81.5	81.5	81.5	81.5
Condenser	8.70	8.70	8.70	8.70	8.70	8.70	8.70	8.70	8.70
Deaerator	26.4	26.5	26.5	26.6	26.6	26.7	26.8	27.0	27.3
DSP	95.7	95.6	95.4	95.1	94.8	94.5	94.2	93.7	92.9
MSF	5.70	5.70	5.70	5.70	5.70	5.70	5.70	5.70	5.70

- Influence of ambient temperature on equipment exergy destruction (MW)

PP									
Equipment	10 °C	15 °C	20 °C	25 °C	30 °C	35 °C	40 °C	45 °C	50 °C
GT1	271	263	254	246	237	229	220	211	202
GT2	271	263	254	246	237	229	220	211	202
SFB 1	0.250	0.250	0.240	0.230	0.230	0.220	0.220	0.210	0.210
SFB 2	0.250	0.250	0.240	0.230	0.230	0.220	0.220	0.210	0.210
HRSG1	14.7	14.7	14.8	14.9	14.9	14.9	14.9	15.0	14.9
HRSG2	14.7	14.7	14.8	14.9	14.9	14.9	14.9	15.0	14.9
HPT	22.2	22.2	22.2	22.2	22.1	22.0	21.9	21.8	21.6
LPT	8.36	8.35	8.34	8.33	8.30	8.28	8.23	8.19	8.13
Condenser	17.2	17.2	17.2	17.1	17.1	17.0	16.9	16.9	16.7
Deaerator	3.32	3.31	3.31	3.31	3.30	3.29	3.27	3.25	3.23
DSP	0.43	0.55	0.82	1.09	1.35	1.63	1.89	2.16	2.42
Stack	49.9	48.9	46.9	45.0	43.1	41.3	39.5	37.8	36.1
MSF	0	0	0	0	0	0	0	0	0

PP+MSF									
Equipment	10 °C	15 °C	20 °C	25 °C	30 °C	35 °C	40 °C	45 °C	50 °C
GT1	271	263	254	246	237	229	220	211	202
GT2	271	263	254	246	237	229	220	211	202
SFB 1	0.250	0.250	0.240	0.230	0.230	0.220	0.220	0.210	0.210
SFB 2	0.250	0.250	0.240	0.230	0.230	0.220	0.220	0.210	0.210
HRSG1	14.7	14.7	14.8	14.9	14.9	14.9	14.9	15.0	14.9
HRSG2	14.7	14.7	14.8	14.9	14.9	14.9	14.9	15.0	14.9
HPT	22.2	22.2	22.2	22.2	22.1	22.0	21.9	21.8	21.6
LPT	0.69	0.68	0.67	0.66	0.63	0.61	0.57	0.53	0.47
Condenser	1.4	1.4	1.4	1.4	1.3	1.3	1.2	1.1	1.0
Deaerator	0.76	0.76	0.76	0.76	0.75	0.75	0.74	0.73	0.72
DSP	0.43	0.55	0.82	1.09	1.35	1.63	1.89	2.16	2.42
Stack	49.9	48.9	46.9	45.0	43.1	41.3	39.5	37.8	36.1
MSF	55.0	55.0	55.0	55.0	55.0	55.0	55.0	55.0	55.0

PP+SF									
Equipment	10 °C	15 °C	20 °C	25 °C	30 °C	35 °C	40 °C	45 °C	50 °C
GT1	271	263	254	246	237	229	220	211	202
GT2	271	263	254	246	237	229	220	211	202
SFB 1	64.2	64.0	63.5	63.1	62.7	62.2	61.8	61.4	60.9
SFB 2	64.2	64.0	63.5	63.1	62.7	62.2	61.8	61.4	60.9
HRSG1	30.7	30.7	30.8	30.9	30.9	30.9	30.9	30.4	29.7
HRSG2	30.7	30.7	30.8	30.8	30.9	30.9	30.9	30.4	29.7
HPT	45.7	45.7	45.6	45.5	45.4	45.3	45.1	44.9	44.5
LPT	15.92	15.9	15.88	15.86	15.81	15.78	15.72	15.63	15.5
Condenser	32.7	32.7	32.6	32.6	32.5	32.4	32.3	32.1	31.9
Deaerator	6.42	6.41	6.4	6.39	6.38	6.36	6.34	6.3	6.25
DSP	16.08	16.53	17.59	18.62	19.68	20.74	21.82	24.05	27.04
Stack	27.9	27.1	25.6	24.1	22.6	21.2	19.9	19.1	18.5
MSF	0	0	0	0	0	0	0	0	0

PP+SF+MSF									
Equipment	10 °C	15 °C	20 °C	25 °C	30 °C	35 °C	40 °C	45 °C	50 °C
GT1	271	263	254	246	237	229	220	211	202
GT2	271	263	254	246	237	229	220	211	202
SFB 1	64.2	64.0	63.5	63.1	62.7	62.2	61.8	61.4	60.9
SFB 2	64.2	64.0	63.5	63.1	62.7	62.2	61.8	61.4	60.9
HRSG1	30.7	30.7	30.8	30.9	30.9	30.9	30.9	30.4	29.7
HRSG2	30.7	30.7	30.8	30.8	30.9	30.9	30.9	30.4	29.7
HPT	45.7	45.7	45.6	45.5	45.4	45.3	45.1	44.9	44.5
LPT	6.83	6.82	6.79	6.77	6.73	6.69	6.64	6.55	6.42
Condenser	14.0	14.0	14.0	13.9	13.8	13.8	13.6	13.5	13.2
Deaerator	2.53	2.53	2.52	2.52	2.50	2.49	2.48	2.45	2.41
DSP	16.08	16.53	17.59	18.62	19.68	20.74	21.82	24.05	27.04
Stack	27.9	27.1	25.6	24.1	22.6	21.2	19.9	19.1	18.5
MSF	65.2	65.2	65.2	65.2	65.2	65.2	65.2	65.2	65.2

- Influence of ambient temperature on equipment exergy destruction ratio (%)

PP									
Equipment	10 °C	15 °C	20 °C	25 °C	30 °C	35 °C	40 °C	45 °C	50 °C
GT1	24.5	24.4	24.3	24.1	24.0	23.8	23.6	23.4	23.1
GT2	24.5	24.4	24.3	24.1	24.0	23.8	23.6	23.4	23.1
SFB 1	0.00	0.00	0.00	0.00	0.00	0.00	0.00	0.00	0.00
SFB 2	0.00	0.00	0.00	0.00	0.00	0.00	0.00	0.00	0.00
HRSG1	1.33	1.37	1.41	1.46	1.51	1.56	1.60	1.65	1.71
HRSG2	1.33	1.37	1.41	1.46	1.51	1.56	1.60	1.65	1.71
HPT	2.01	2.06	2.12	2.18	2.24	2.29	2.35	2.41	2.47
LPT	0.760	0.780	0.800	0.820	0.840	0.860	0.880	0.910	0.930
Condenser	1.560	1.59	1.64	1.68	1.73	1.77	1.82	1.86	1.91
Deaerator	0.300	0.310	0.320	0.320	0.330	0.340	0.350	0.360	0.370
DSP	0.04	0.05	0.08	0.11	0.14	0.17	0.20	0.24	0.28
Stack	4.51	4.55	4.48	4.42	4.37	4.3	4.23	4.18	4.12
MSF	0.00	0.00	0.00	0.00	0.00	0.00	0.00	0.00	0.00

PP+MSF									
Equipment	10 °C	15 °C	20 °C	25 °C	30 °C	35 °C	40 °C	45 °C	50 °C
GT1	24.5	24.4	24.3	24.1	24.0	23.8	23.6	23.4	23.1
GT2	24.5	24.4	24.3	24.1	24.0	23.8	23.6	23.4	23.1
SFB 1	0.00	0.00	0.00	0.00	0.00	0.00	0.00	0.00	0.00
SFB 2	0.00	0.00	0.00	0.00	0.00	0.00	0.00	0.00	0.00
HRSG1	1.33	1.37	1.41	1.46	1.51	1.56	1.60	1.65	1.71
HRSG2	1.33	1.37	1.41	1.46	1.51	1.56	1.60	1.65	1.71
HPT	2.01	2.06	2.12	2.18	2.24	2.29	2.35	2.41	2.47
LPT	0.060	0.060	0.060	0.060	0.060	0.060	0.060	0.060	0.050
Condenser	0.130	0.13	0.13	0.13	0.13	0.13	0.12	0.12	0.11
Deaerator	0.070	0.070	0.070	0.070	0.080	0.080	0.080	0.080	0.080
DSP	0.04	0.05	0.08	0.11	0.14	0.17	0.20	0.24	0.28
Stack	4.51	4.55	4.48	4.42	4.37	4.3	4.23	4.18	4.12
MSF	4.55	4.55	4.55	4.55	4.55	4.55	4.55	4.55	4.55

PP+SF									
Equipment	10 °C	15 °C	20 °C	25 °C	30 °C	35 °C	40 °C	45 °C	50 °C
GT1	18.9	18.7	18.5	18.3	18.0	17.8	17.5	17.2	16.8
GT2	18.9	18.7	18.5	18.3	18.0	17.8	17.5	17.2	16.8
SFB 1	4.48	4.56	4.62	4.69	4.77	4.83	4.90	4.98	5.07
SFB 2	4.48	4.56	4.62	4.69	4.77	4.83	4.90	4.98	5.07
HRSG1	2.14	2.19	2.24	2.29	2.35	2.40	2.45	2.47	2.47
HRSG2	2.14	2.19	2.24	2.29	2.35	2.40	2.45	2.47	2.47
HPT	3.19	3.25	3.32	3.38	3.45	3.52	3.58	3.64	3.70
LPT	1.110	1.130	1.150	1.180	1.200	1.230	1.250	1.270	1.290
Condenser	2.280	2.33	2.37	2.42	2.47	2.52	2.56	2.61	2.65
Deaerator	0.450	0.460	0.470	0.480	0.490	0.490	0.500	0.510	0.520
DSP	1.12	1.18	1.28	1.38	1.50	1.61	1.73	1.95	2.25
Stack	1.95	1.93	1.86	1.79	1.72	1.65	1.58	1.55	1.54
MSF	0.00	0.00	0.00	0.00	0.00	0.00	0.00	0.00	0.00

PP+SF+MSF									
Equipment	10 °C	15 °C	20 °C	25 °C	30 °C	35 °C	40 °C	45 °C	50 °C
GT1	18.9	18.7	18.5	18.3	18.0	17.8	17.5	17.2	16.8
GT2	18.9	18.7	18.5	18.3	18.0	17.8	17.5	17.2	16.8
SFB 1	4.48	4.56	4.62	4.69	4.77	4.83	4.90	4.98	5.07
SFB 2	4.48	4.56	4.62	4.69	4.77	4.83	4.90	4.98	5.07
HRSG1	2.14	2.19	2.24	2.29	2.35	2.40	2.45	2.47	2.47
HRSG2	2.14	2.19	2.24	2.29	2.35	2.40	2.45	2.47	2.47
HPT	3.19	3.25	3.32	3.38	3.45	3.52	3.58	3.64	3.70
LPT	0.480	0.490	0.490	0.500	0.510	0.520	0.530	0.530	0.530
Condenser	0.980	1.00	1.02	1.03	1.05	1.07	1.08	1.09	1.10
Deaerator	0.180	0.180	0.180	0.190	0.190	0.190	0.200	0.200	0.200
DSP	1.12	1.18	1.28	1.38	1.50	1.61	1.73	1.95	2.25
Stack	1.95	1.93	1.86	1.79	1.72	1.65	1.58	1.55	1.54
MSF	5.00	5.00	5.00	5.00	5.00	5.00	5.00	5.00	5.00

Appendix 5- E

Effect of the supplementary firing flow:

- Equipment exergy efficiency (%)

Equipment	0%	10%	20%	30%	40%	50%	60%	70%	80%	90%	100%
GT1	38.0	38.0	38.0	38.0	38.0	38.0	38.0	38.0	38.0	38.0	38.0
GT2	38.0	38.0	38.0	38.0	38.0	38.0	38.0	38.0	38.0	38.0	38.0
SFB 1	99.8	95.0	91.3	88.3	85.9	84.0	82.3	81.0	79.8	78.8	78.0
SFB 2	99.8	95.0	91.3	88.3	85.9	84.0	82.3	81.0	79.8	78.8	78.0
HRSG1	85.9	86.3	86.1	86.0	85.9	85.8	85.7	85.7	85.6	85.6	85.6
HRSG2	85.9	86.3	86.1	86.0	85.9	85.8	85.7	85.7	85.6	85.6	85.6
HPT	80.1	80.1	80.1	80.1	80.1	80.1	80.1	80.1	80.1	80.1	80.1
LPT	81.5	81.5	81.5	81.5	81.5	81.5	81.5	81.5	81.5	81.5	81.5
Condenser	8.70	8.70	8.70	8.70	8.70	8.70	8.70	8.70	8.70	8.70	8.70
Deaerator	58.1	49.4	44.7	40.8	37.4	34.5	32.0	29.9	28.0	26.3	24.8
DSP	99.6	99.0	98.5	97.9	97.4	96.9	96.3	95.8	95.3	94.8	94.2
MSF	5.66	5.66	5.66	5.66	5.66	5.66	5.66	5.66	5.66	5.66	5.66

- Equipment exergy destruction (MW)

Equipment	0%	10%	20%	30%	40%	50%	60%	70%	80%	90%	100%
GT1	258	258	258	258	258	258	258	258	258	258	258
GT2	258	258	258	258	258	258	258	258	258	258	258
SFB 1	0.230	7.16	14.0	20.6	27.1	33.5	39.8	46.0	52.1	58.1	64.0
SFB 2	0.230	7.16	14.0	20.6	27.1	33.5	39.8	46.0	52.1	58.1	64.0
HRSG1	14.3	15.4	17.1	18.8	20.5	22.3	23.9	25.6	27.4	29.0	30.7
HRSG2	14.3	15.4	17.1	18.8	20.5	22.3	24.0	25.6	27.4	29.0	30.7
HPT	22.4	24.8	27.1	29.3	31.5	33.7	35.9	38.1	40.2	42.4	44.5
LPT	0.030	0.790	1.60	2.41	3.21	4.01	4.80	5.58	6.36	7.13	7.90
Condenser	0.050	1.62	3.30	4.96	6.61	8	9.9	11.5	13.1	14.7	16.3
Deaerator	0.750	0.940	1.11	1.30	1.50	1.72	1.94	2.18	2.42	2.67	2.92
DSP	0.650	1.92	3.33	4.95	6.79	8.69	11.0	13.4	15.9	18.7	21.8
Stack	50.3	48.7	45.7	42.8	40.2	37.6	35.3	33.2	31.1	29.2	27.5
MSF	59.0	59.0	59.0	59.0	59.0	59.0	59.0	59.0	59.0	59.0	59.0

- Equipment exergy destruction ratio (%)

Equipment	0%	10%	20%	30%	40%	50%	60%	70%	80%	90%	100%
GT1	24.0	23.3	22.6	22.0	21.4	20.8	20.3	19.8	19.3	18.8	18.4
GT2	24.0	23.3	22.6	22.0	21.4	20.8	20.3	19.8	19.3	18.8	18.4
SFB 1	0.020	0.65	1.22	1.75	2.25	2.70	3.13	3.52	3.89	4.24	4.56
SFB 2	0.020	0.65	1.22	1.75	2.25	2.70	3.13	3.52	3.89	4.24	4.56
HRSG1	1.33	1.39	1.50	1.60	1.69	1.78	1.84	1.89	1.95	1.99	2.02
HRSG2	1.33	1.39	1.50	1.60	1.69	1.78	1.84	1.89	1.95	1.99	2.02
HPT	2.08	2.23	2.37	2.49	2.61	2.72	2.82	2.91	3.01	3.09	3.17
LPT	0.000	0.07	0.14	0.21	0.27	0.32	0.38	0.43	0.48	0.52	0.56
Condens	0.010	0.15	0.29	0.42	0.55	0.67	0.78	0.88	0.98	1.07	1.16
Deaerato	0.070	0.08	0.10	0.11	0.12	0.14	0.15	0.17	0.18	0.19	0.21
DSP	0.060	0.17	0.29	0.42	0.56	0.70	0.86	1.03	1.18	1.37	1.56
Stack	4.67	4.39	4.00	3.65	3.33	3.03	2.78	2.54	2.32	2.13	1.96
MSF	5.50	5.29	5.14	4.99	4.86	4.73	4.61	4.49	4.38	4.28	4.18

Appendix: 6-A

Model Input	TBT=105 (°C)	SWT=35.0 (°C)	$T_{B,16}=49.8$ (°C)	$T_{B,19}=42.1$ (°C)	$\dot{m}_{12}=12900$ (m ³ /h)	
	Brine Temperature (°C)		Distillate Temperature (°C)		Cooling water Temperature (°C)	
Stage	Vendor	Model	Vendor	Model	Vendor	Model
1	101	102	99.5	100	98.2	98.5
2	97.8	98.0	96.4	97.0	94.7	94.9
3	94.3	94.5	92.9	93.5	91.2	91.4
4	90.7	91.0	89.4	90.0	87.7	87.9
5	87.2	87.5	85.9	86.5	84.1	84.4
6	83.6	84.0	82.2	83.1	80.6	80.9
7	79.9	80.5	78.6	79.6	76.9	77.3
8	76.3	77.0	74.9	76.1	73.3	73.8
9	72.7	73.5	71.4	72.6	69.7	70.3
10	69.1	70.0	67.8	69.1	66.1	66.8
11	65.5	66.5	64.2	65.6	62.5	63.3
12	62.0	63.0	60.7	62.1	58.9	59.7
13	58.6	59.5	57.2	58.7	55.4	56.7
14	55.2	56.0	53.8	55.2	51.9	52.7
15	51.9	52.5	50.4	51.7	48.6	49.2
16	48.9	49.0	47.1	48.2	45.3	45.7
17	46.9	46.5	44.7	45.7	42.5	44.0
18	44.8	44.0	42.5	43.2	40.1	41.0
19	42.1	42.1	40.1	40.7	37.6	38.0
Parameter	Vendor		Model			
Steam flow	154.0		152.9			
Distillate flow	1273		1286			
Makeup flow	3220		3192			

Model Input	TBT=91.0 (°C)	SWT=35.0 (°C)	T _{B,16} =45.1 (°C)	T _{B,19} =39.6 (°C)	$\dot{m}_{12}= 9535$ (m ³ /h)	
	Brine Temperature (°C)		Distillate Temperature (°C)		Cooling water Temperature (°C)	
Stage	Vendor	Model	Vendor	Model	Vendor	Model
1	88.0	88.1	86.7	87.2	85.6	85.9
2	85.0	85.3	83.7	84.3	82.7	83.0
3	82.1	82.4	80.8	81.5	79.8	80.1
4	79.2	79.5	77.9	78.6	76.9	77.2
5	76.2	76.7	75.0	75.8	74.0	74.3
6	73.2	73.8	72.0	72.9	71.0	71.5
7	70.2	70.9	69.0	70.1	68.0	68.6
8	67.2	68.1	66.0	67.2	65.0	65.7
9	64.3	65.2	63.0	64.3	62.0	62.8
10	61.3	62.3	60.1	61.5	59.0	59.9
11	58.4	59.4	57.1	58.6	56.1	57.1
12	55.6	56.6	54.2	55.8	53.2	54.2
13	52.8	53.7	51.4	52.9	50.1	51.3
14	50.1	50.8	48.6	50.1	47.5	48.4
15	47.4	48.0	45.9	47.2	44.8	45.5
16	44.9	45.1	43.2	44.3	42.5	42.6
17	43.0	43.3	41.0	42.5	39.4	39.9
18	41.2	41.4	39.1	40.7	37.7	38.3
19	39.6	39.6	37.3	38.9	36.2	36.7
Parameter	Vendor		Model			
Steam flow	84.6		85.9			
Distillate flow	771		780			
Makeup flow	2008		1934			

Model Input	TBT=99.0 (°C)	SWT=24.0 (°C)	T _{B,16} =39.1 (°C)	T _{B,19} =31.8 (°C)	$\dot{m}_{12}= 12250$ (m ³ /h)	
	Brine Temperature (°C)		Distillate Temperature (°C)		Cooling water Temperature (°C)	
Stage	Vendor	Model	Vendor	Model	Vendor	Model
1	95.0	95.3	93.6	94.3	91.8	92.1
2	91.1	91.5	89.8	90.6	87.9	88.3
3	87.3	87.8	85.9	86.8	84.0	84.6
4	83.4	84.0	82.1	83.1	80.2	80.8
5	79.6	80.3	78.3	79.4	76.4	77.1
6	75.6	76.6	74.3	75.7	72.5	73.3
7	71.7	72.8	70.4	71.9	68.6	69.6
8	67.8	69.1	66.5	68.2	64.6	65.8
9	63.9	65.3	62.6	64.5	60.7	62.0
10	60.1	61.6	58.7	60.7	56.8	58.3
11	56.3	57.8	54.9	57.0	53.0	54.5
12	52.6	54.1	51.2	53.3	49.2	50.8
13	49.1	50.4	47.5	49.6	45.5	47.0
14	45.6	46.6	43.9	45.8	41.9	43.2
15	42.3	42.9	40.7	42.1	38.5	39.5
16	39.1	39.1	37.0	38.4	35.1	35.7
17	36.9	36.6	34.3	35.9	31.8	32.6
18	34.7	34.1	32.0	33.4	29.3	29.8
19	31.9	31.6	29.5	30.9	26.7	26.9
Parameter	Vendor		Model			
Steam flow	153.3		149.3			
Distillate flow	1278		1298			
Makeup flow	3196		3222			

Model Input	TBT=85.0 (°C)	SWT=24.0 (°C)	T _{B,16} =35.0 (°C)	T _{B,19} =29.2 (°C)	m ₁₂ =8925 (m ³ /h)	
	Brine Temperature (°C)		Distillate Temperature (°C)		Cooling water Temperature (°C)	
Stage	Vendor	Model	Vendor	Model	Vendor	Model
1	81.6	81.9	80.3	81.0	79.2	79.5
2	78.3	78.8	77.1	77.9	76.0	76.3
3	75.1	75.6	73.8	74.7	72.7	73.2
4	71.8	72.5	70.6	71.6	69.5	70.0
5	68.6	69.4	67.4	68.5	66.0	66.9
6	65.3	66.3	64.0	65.4	63.0	63.8
7	62.0	63.1	60.8	62.3	59.7	60.6
8	58.7	60.0	57.5	59.2	56.4	57.5
9	55.5	56.9	54.2	56.1	53.1	54.3
10	52.3	53.8	51.0	53.0	49.0	51.2
11	49.2	50.6	47.8	49.8	46.6	48.1
12	46.2	47.5	44.7	46.7	43.5	44.9
13	43.3	44.4	41.7	43.6	40.5	41.8
14	40.4	41.3	38.7	40.5	37.6	38.6
15	37.6	38.1	35.9	37.4	34.7	35.5
16	35.0	35.0	33.1	34.3	31.9	32.4
17	32.8	33.1	30.6	32.3	28.8	28.8
18	31.0	31.1	28.5	30.4	27.0	27.2
19	29.2	29.2	26.7	28.5	25.5	25.6
Parameter	Vendor		Model			
Steam flow	84.2		87.3			
Distillate flow	774.1		782.2			
Makeup flow	1992		1941			

Appendix 6- B

- Effect of MSF unit load (UL)

UL (%)	Exergy In (MW)							
	SWP	BRP	RBP	DP	CP	Pumps total	Steam	W_{min}
100	0.567	2.39	0.120	0.0714	0.0347	4.20	22.3	1.51
95	0.567	2.27	0.114	0.0678	0.0335	4.10	21.5	1.43
90	0.567	2.15	0.108	0.0642	0.0323	24.6	20.7	1.36
85	0.567	2.03	0.102	0.0607	0.0310	23.6	19.9	1.28
80	0.567	1.91	0.0962	0.0571	0.0297	22.6	19.0	1.20
75	0.567	1.79	0.0902	0.0535	0.0282	21.5	18.1	1.13
70	0.567	1.67	0.0842	0.0500	0.0268	20.4	17.2	1.05
65	0.567	1.55	0.0782	0.0464	0.0252	19.2	16.2	0.98
60	0.567	1.43	0.0722	0.0428	0.0236	18.0	15.2	0.90

UL (%)	Exergy Destruction (MW)								
	$E_{d,PP}$	$E_{d,BH}$	$E_{d,HRC}$	$E_{d,HRJ}$	$E_{d,C}$	$E_{d,P}$	$E_{d,B}$	$E_{d,Co}$	$E_{d,Th}$
100	1.06	3.59	14.2	2.60	1.25	0.141	0.231	1.67	0.173
95	1.02	3.48	13.7	2.55	1.17	0.134	0.219	1.61	0.164
90	0.973	3.36	13.2	2.50	1.09	0.127	0.208	1.56	0.156
85	0.930	3.23	12.6	2.44	1.02	0.120	0.196	1.49	0.147
80	0.886	3.10	12.1	2.37	0.943	0.113	0.185	1.43	0.139
75	0.842	2.96	11.5	2.30	0.871	0.106	0.173	1.36	0.130
70	0.799	2.82	10.9	2.22	0.801	0.099	0.162	1.29	0.122
65	0.755	2.66	10.3	2.14	0.734	0.092	0.150	1.21	0.113
60	0.712	2.50	9.63	2.04	0.671	0.085	0.139	1.14	0.105

- Effect of feed seawater temperature (T_1)

T_1 (°C)	\dot{m}_{21} m ³ /h	SHC kWh/m ³	\dot{m}_5 m ³ /h	\dot{m}_9 m ³ /h	P/W ratio	P_{total} kWh	PR	η_{II} %
35	1286	72.47	3192	1906	4.77	6141	8.55	5.86
34	1285	72.56	3188	1903	4.76	6117	8.54	5.83
33	1283	72.65	3184	1901	4.74	6089	8.53	5.81
32	1282	72.73	3181	1899	4.74	6072	8.52	5.78
31	1280	72.82	3177	1897	4.73	6050	8.51	5.76
30	1279	72.91	3173	1894	4.72	6029	8.50	5.73
29	1277	73.00	3169	1892	4.70	6008	8.49	5.71
28	1276	73.08	3165	1890	4.69	5988	8.48	5.68
27	1274	73.17	3162	1888	4.68	5968	8.47	5.66
26	1273	73.26	3158	1885	4.67	5949	8.46	5.63
25	1271	73.34	3154	1883	4.67	5931	8.45	5.60
24	1270	73.43	3151	1881	4.66	5912	8.44	5.58
23	1268	73.52	3147	1879	4.65	5895	8.43	5.55
22	1267	73.60	3143	1877	4.64	5878	8.42	5.52

T ₁ (°C)	Exergy In (MW)							
	SWP	BRP	RBP	DP	CP	Pumps total	Steam	W _{min}
35	0.569	2.463	0.119	0.070	0.035	4.341	22.148	1.552
34	0.569	2.449	0.119	0.070	0.035	4.323	22.148	1.544
33	0.568	2.436	0.119	0.070	0.035	4.305	22.148	1.537
32	0.568	2.423	0.119	0.071	0.035	4.288	22.148	1.529
31	0.568	2.410	0.119	0.071	0.035	4.270	22.148	1.522
30	0.568	2.398	0.119	0.071	0.035	4.254	22.148	1.514
29	0.567	2.386	0.119	0.071	0.035	4.237	22.148	1.506
28	0.567	2.374	0.119	0.071	0.035	4.221	22.148	1.499
27	0.567	2.363	0.119	0.071	0.035	4.206	22.148	1.491
26	0.567	2.352	0.119	0.071	0.035	4.191	22.148	1.483
25	0.567	2.341	0.119	0.071	0.035	4.176	22.148	1.475
24	0.566	2.331	0.119	0.071	0.035	4.162	22.148	1.467
23	0.566	2.321	0.119	0.071	0.035	4.148	22.148	1.459
22	0.566	2.311	0.119	0.071	0.035	4.134	22.148	1.451

T ₁ (°C)	Exergy Destruction (MW)								
	E _{d,PP}	E _{d,BH}	E _{d,HRC}	E _{d,HRJ}	E _{d,C}	E _{d,P}	E _{d,B}	E _{d,Co}	E _{d,Th}
35	1.085	3.978	13.722	2.551	1.253	0.138	0.243	1.658	0.171
34	1.081	3.927	13.762	2.560	1.252	0.138	0.242	1.659	0.171
33	1.076	3.876	13.802	2.566	1.251	0.138	0.240	1.659	0.171
32	1.072	3.825	13.844	2.574	1.249	0.139	0.238	1.659	0.171
31	1.068	3.772	13.887	2.581	1.247	0.139	0.237	1.66	0.171
30	1.063	3.719	13.932	2.588	1.244	0.139	0.235	1.661	0.171
29	1.059	3.668	13.988	2.583	1.242	0.139	0.233	1.661	0.171
28	1.055	3.613	14.037	2.590	1.238	0.140	0.231	1.661	0.171
27	1.051	3.559	14.086	2.597	1.235	0.140	0.228	1.662	0.171
26	1.048	3.503	14.137	2.604	1.231	0.140	0.226	1.663	0.171
25	1.044	3.448	14.189	2.611	1.226	0.141	0.224	1.647	0.171
24	1.040	3.391	14.243	2.618	1.222	0.141	0.221	1.664	0.171
23	1.037	3.335	14.298	2.625	1.216	0.141	0.218	1.664	0.171
22	1.034	3.278	14.355	2.631	1.211	0.142	0.215	1.665	0.171

▪ Effect of seawater feed Salinity ($w_{s,1}$)

$w_{s,1}$ (g/kg)	\dot{m}_{21} m ³ /h	SHC kWh/m ³	\dot{m}_5 m ³ /h	\dot{m}_9 m ³ /h	P/W ratio	P_{total} kWh	PR	η_{II} %
45	1274	71.9	3881	2607	4.75	6053	8.61	6.11
44	1274	72.2	3713	2438	4.73	6034	8.58	6.02
43	1274	72.5	3558	2283	4.72	6017	8.55	5.93
42	1274	72.7	3416	2141	4.71	6001	8.52	5.84
41	1274	72.9	3284	2010	4.70	5986	8.49	5.75
40	1274	73.1	3163	1888	4.69	5973	8.47	5.66
39	1274	73.3	3050	1775	4.68	5960	8.45	5.57
38	1274	73.5	2944	1670	4.67	5949	8.43	5.48
37	1274	73.7	2846	1572	4.66	5938	8.41	5.38
36	1274	73.8	2755	1480	4.65	5928	8.39	5.28
35	1274	74.0	2668	1394	4.64	5919	8.38	5.19

$w_{s,1}$ (g/kg)	Exergy In (MW)							
	SWP	BRP	RBP	DP	CP	Pumps total	Steam	W_{min}
45	0.565	2.37	0.165	0.0707	0.0340	4.27	21.8	1.59
44	0.565	2.37	0.154	0.0707	0.0341	4.25	21.9	1.57
43	0.566	2.37	0.144	0.0707	0.0342	4.24	21.9	1.55
42	0.566	2.37	0.135	0.0707	0.0343	4.23	22.0	1.53
41	0.567	2.37	0.127	0.0707	0.0344	4.22	22.1	1.51
40	0.567	2.37	0.119	0.0707	0.0345	4.21	22.1	1.49
39	0.567	2.37	0.112	0.0707	0.0346	4.20	22.2	1.47
38	0.568	2.37	0.105	0.0707	0.0347	4.19	22.3	1.45
37	0.568	2.37	0.0992	0.0707	0.0348	4.18	22.3	1.43
36	0.569	2.37	0.0934	0.0707	0.0348	4.18	22.4	1.40
35	0.569	2.37	0.0880	0.0707	0.0349	4.17	22.4	1.38

$w_{s,1}$ (g/kg)	Exergy Destruction (MW)								
	$E_{d,PP}$	$E_{d,BH}$	$E_{d,HRC}$	$E_{d,HRJ}$	$E_{d,C}$	$E_{d,P}$	$E_{d,B}$	$E_{d,Co}$	$E_{d,Th}$
45	1.07	3.50	13.8	2.50	1.12	0.140	0.316	1.61	0.209
44	1.06	3.52	13.9	2.51	1.14	0.140	0.296	1.63	0.200
43	1.06	3.53	13.9	2.53	1.17	0.140	0.277	1.63	0.192
42	1.06	3.55	14.0	2.55	1.19	0.140	0.260	1.64	0.185
41	1.05	3.56	14.0	2.57	1.22	0.140	0.244	1.65	0.178
40	1.05	3.57	14.1	2.60	1.24	0.140	0.229	1.66	0.171
39	1.05	3.58	14.1	2.62	1.25	0.140	0.215	1.67	0.165
38	1.05	3.59	14.1	2.64	1.27	0.140	0.202	1.68	0.160
37	1.05	3.60	14.2	2.66	1.29	0.140	0.191	1.69	0.154
36	1.04	3.61	14.2	2.69	1.30	0.140	0.179	1.69	0.149
35	1.07	3.50	13.8	2.50	1.12	0.140	0.316	1.61	0.209

▪ Effect of seawater feed flow (\dot{m}_1)

\dot{m}_1 (m ³ /h)	Exergy In (MW)							
	SWP	BRP	RBP	DP	CP	Pumps total	Steam	W _{min}
12555	0.675	2.36	0.119	0.0707	0.0363	4.35	23.3	1.49
12055	0.648	2.36	0.119	0.0707	0.0359	4.32	23.1	1.49
11555	0.621	2.36	0.119	0.0707	0.0355	4.28	22.8	1.49
11055	0.594	2.37	0.119	0.0707	0.0350	4.25	22.5	1.49
10555	0.567	2.37	0.119	0.0707	0.0345	4.21	22.1	1.49
10055	0.540	2.37	0.119	0.0707	0.0339	4.17	21.8	1.49
9555	0.513	2.37	0.119	0.0707	0.0333	4.14	21.4	1.49
9055	0.486	2.37	0.119	0.0707	0.0326	4.10	20.9	1.49
8555	0.460	2.37	0.119	0.0707	0.0318	4.07	20.4	1.49

\dot{m}_1 (m ³ /h)	Exergy Destruction (MW)								
	E _{d,PP}	E _{d,BH}	E _{d,HRC}	E _{d,HRJ}	E _{d,C}	E _{d,P}	E _{d,B}	E _{d,Co}	E _{d,Th}
12555	1.09	3.79	14.8	2.88	1.18	0.14	0.229	1.75	0.172
12055	1.08	3.75	14.6	2.81	1.19	0.14	0.229	1.73	0.172
11555	1.07	3.69	14.5	2.74	1.21	0.14	0.229	1.71	0.171
11055	1.06	3.63	14.3	2.67	1.22	0.14	0.229	1.69	0.171
10555	1.05	3.57	14.1	2.60	1.24	0.14	0.229	1.66	0.171
10055	1.04	3.50	13.8	2.51	1.25	0.14	0.229	1.63	0.171
9555	1.03	3.43	13.6	2.43	1.27	0.14	0.229	1.60	0.171
9055	1.03	3.34	13.3	2.34	1.28	0.14	0.229	1.57	0.170
8555	1.02	3.25	13.0	2.24	1.30	0.14	0.229	1.53	0.170

▪ Effect of brine recirculation flow (\dot{m}_{12})

\dot{m}_{12} (%)	Exergy In (MW)							
	SWP	BRP	RBP	DP	CP	Pumps total	Steam	W _{min}
100	0.567	2.37	0.119	0.0707	0.0345	4.21	22.2	1.49
95	0.567	2.24	0.113	0.0671	0.0333	4.03	21.4	1.42
90	0.567	2.12	0.107	0.0636	0.0321	3.86	20.6	1.34
85	0.567	2.01	0.101	0.0600	0.0308	3.69	19.7	1.27
80	0.567	1.89	0.0952	0.0565	0.0294	3.51	18.9	1.19
75	0.567	1.77	0.0892	0.0530	0.0280	3.34	18.0	1.12
70	0.567	1.65	0.0833	0.0494	0.0265	3.17	17.0	1.04
65	0.567	1.53	0.0773	0.0459	0.0250	3.00	16.1	0.968
60	0.567	1.41	0.0714	0.0424	0.0234	2.82	15.0	0.894

\dot{m}_{12} (%)	Exergy Destruction (MW)								
	$E_{d,PP}$	$E_{d,BH}$	$E_{d,HRC}$	$E_{d,HRJ}$	$E_{d,C}$	$E_{d,P}$	$E_{d,B}$	$E_{d,Co}$	$E_{d,Th}$
100	1.05	3.57	14.1	2.60	1.24	0.140	0.229	1.66	0.171
95	1.01	3.45	13.6	2.55	1.16	0.133	0.217	1.60	0.162
90	0.965	3.34	13.1	2.49	1.08	0.126	0.206	1.54	0.154
85	0.922	3.21	12.5	2.43	1.00	0.119	0.194	1.48	0.146
80	0.879	3.08	12.0	2.36	0.93	0.112	0.183	1.42	0.137
75	0.835	2.94	11.4	2.29	0.86	0.105	0.172	1.35	0.129
70	0.792	2.79	10.8	2.21	0.79	0.098	0.160	1.28	0.120
65	0.749	2.64	10.2	2.13	0.73	0.091	0.149	1.20	0.112
60	0.706	2.48	9.54	2.03	0.66	0.084	0.137	1.13	0.103

- Effect of brine recirculation temperature (T_{12})

T_{12} (°C)	Exergy In (MW)							
	SWP	BRP	RBP	DP	CP	Pumps total	Steam	W_{min}
35.00	0.567	2.37	0.119	0.0707	0.0345	4.21	22.1	1.49
35.15	0.567	2.40	0.119	0.0707	0.0340	4.25	21.8	1.49
35.30	0.567	2.45	0.119	0.0707	0.0333	4.32	21.3	1.49
35.45	0.567	2.51	0.119	0.0707	0.0325	4.39	20.9	1.49
35.60	0.567	2.56	0.119	0.0707	0.0317	4.47	20.4	1.49
35.75	0.567	2.62	0.119	0.0707	0.0310	4.54	19.9	1.49
36.00	0.567	2.71	0.119	0.0707	0.0297	4.67	19.1	1.49
36.15	0.567	2.77	0.119	0.0707	0.0289	4.74	18.6	1.49
36.30	0.567	2.83	0.119	0.0707	0.0282	4.82	18.1	1.49

T_{12} (°C)	Exergy Destruction (MW)								
	$E_{d,PP}$	$E_{d,BH}$	$E_{d,HRC}$	$E_{d,HRJ}$	$E_{d,C}$	$E_{d,P}$	$E_{d,B}$	$E_{d,Co}$	$E_{d,Th}$
35.00	1.05	3.57	14.1	2.60	1.24	0.140	0.229	1.66	0.171
35.15	1.06	3.51	13.9	2.60	1.24	0.140	0.229	1.64	0.171
35.30	1.08	3.42	13.6	2.60	1.24	0.140	0.229	1.60	0.171
35.45	1.10	3.33	13.3	2.60	1.24	0.140	0.229	1.56	0.171
35.60	1.12	3.24	13.0	2.60	1.24	0.140	0.229	1.53	0.171
35.75	1.14	3.15	12.7	2.60	1.24	0.140	0.229	1.49	0.171
36.00	1.17	3.00	12.1	2.60	1.24	0.140	0.229	1.43	0.171
36.15	1.21	2.82	11.5	2.60	1.24	0.140	0.229	1.36	0.171
36.3	1.05	3.57	14.1	2.60	1.24	0.140	0.229	1.66	0.171

Appendix: 7-A

MSF with IH model simulation results

- IH powered by hot distillate water from stage 1

Stream	\dot{m} (kg/s)	T (°C)	P (kPa)	w_s (g/kg)	h (kJ/kg)	s (kJ/(kg.K))	e_{ph} (kJ/kg)	e_{ch} (kJ/kg)	E_T (MW)
1	2914	27.2	101	40.0	108	0.376	0.00	0.00	0.000
2	2914	27.3	300	40.0	108	0.376	0.193	0.00	0.564
3	2914	36.2	210	40.0	144	0.493	0.601	0.00	1.75
4	883	36.2	210	40.0	144	0.493	0.601	0.00	0.531
5	883	37.5	5.17	40.0	149	0.509	0.556	0.00	0.491
6	2031	36.2	210	40.0	144	0.493	0.601	0.00	1.22
7	3220	34.2	5.17	67.0	130	0.438	3.35	-2.52	2.70
8	527	34.2	5.17	67.0	130	0.438	3.35	-2.52	0.442
9	527	34.2	240	67.0	130	0.439	3.58	-2.52	0.562
10	2693	34.2	5.17	67.0	130	0.438	3.35	-2.52	2.26
11	3576	35.0	5.17	60.2	135	0.456	2.55	-1.89	2.36
12	3576	35.1	685	60.2	136	0.457	3.21	-1.89	4.73
13	3576	90.6	109	60.2	352	1.104	25.2	-1.89	83.24
14	3576	97.2	88.5	60.2	378	1.174	29.8	-1.89	99.93
15	3259	41.7	7.76	66.2	159	0.533	4.24	-2.44	5.86
16	41.4	111	148	0.00	465	1.430	41.0	3.73	21.96
17	41.4	106	148	0.00	443	1.371	36.2	3.73	1.75
18	41.4	106	1000	0.00	445	1.373	37.2	3.73	1.78
19	295	40.9	7.76	0.00	171	0.585	0.685	3.73	1.30
20	356	33.5	5.17	0.00	140	0.484	-0.317	3.73	1.21
21	356	33.5	200	0.00	141	0.485	-0.118	3.73	1.28
6-A	2914	27.2	101	40.0	108	0.376	0.000	0.00	0.000
9-A	527	27.2	101	67.0	103	0.350	3.17	-2.52	0.346
18-A	356	27.2	101	0.0	114	0.398	-0.485	3.73	1.15
21-A	41.4	27.2	101	0.0	114	0.398	-0.485	3.73	0.134

- IH powered by hot distillate water from stage 2

Stream	\dot{m} (kg/s)	T (°C)	P (kPa)	w_s (g/kg)	h (kJ/kg)	s (kJ/(kg.K))	e_{ph} (kJ/kg)	e_{ch} (kJ/kg)	E_T (MW)
1	2895	27.2	101	40.0	108	0.376	0.00	0.00	0.000
2	2895	27.3	300	40.0	108	0.376	0.193	0.00	0.560
3	2895	36.2	210	40.0	144	0.493	0.601	0.00	1.74
4	887	36.2	210	40.0	144	0.493	0.601	0.00	0.533
5	887	38.5	5.08	40.0	153	0.523	0.701	0.00	0.622
6	2009	36.2	210	40.0	144	0.493	0.601	0.00	1.21
7	3219	33.9	5.08	67.0	129	0.435	3.33	-2.52	2.62
8	529	33.9	5.08	67.0	129	0.435	3.33	-2.52	0.430
9	529	33.9	240	67.0	129	0.435	3.56	-2.52	0.551
10	2689	33.9	5.08	67.0	129	0.435	3.33	-2.52	2.19
11	3576	35.1	5.08	60.2	135	0.457	2.56	-1.89	2.38
12	3576	35.2	685	60.2	136	0.458	3.22	-1.89	4.75
13	3576	90.6	109	60.2	352	1.104	25.2	-1.89	83.38
14	3576	97.2	88.5	60.2	378	1.174	29.8	-1.89	99.93
15	3257	41.4	7.64	66.2	158	0.529	4.19	-2.44	5.68
16	41.1	111	148	0.00	465	1.430	41.0	3.73	21.78
17	41.1	106	148	0.00	443	1.371	36.2	3.73	1.73
18	41.1	106	1000	0.00	445	1.373	37.2	3.73	1.77
19	276	40.6	7.64	0.00	170	0.581	0.630	3.73	1.20
20	357	33.2	5.08	0.00	139	0.480	-0.342	3.73	1.21
21	357	33.2	200	0.00	139	0.481	-0.143	3.73	1.28
6-A	2895	27.2	101	40.0	108	0.376	0.000	0.00	0.000
9-A	529	27.2	101	67.0	103	0.350	3.17	-2.52	0.348
18-A	357	27.2	101	0.0	114	0.398	-0.485	3.73	1.16
21-A	41.1	27.2	101	0.0	114	0.398	-0.485	3.73	0.133

- IH powered by hot distillate water from stage 3

Stream	\dot{m} (kg/s)	T (°C)	P (kPa)	w_s (g/kg)	h (kJ/kg)	s (kJ/(kg.K))	e_{ph} (kJ/kg)	e_{ch} (kJ/kg)	E_T (MW)
1	2876	27.2	101	40.0	108	0.376	0.000	0.00	0.000
2	2876	27.3	300	40.0	108	0.376	0.193	0.00	0.556
3	2876	36.2	210	40.0	144	0.493	0.601	0.00	1.73
4	889	36.2	210	40.0	144	0.493	0.601	0.00	0.535
5	889	39.4	5.02	40.0	156	0.534	0.832	0.00	0.740
6	1987	36.2	210	40.0	144	0.493	0.601	0.00	1.19
7	3217	33.7	5.02	67.0	128	0.432	3.31	-2.52	2.56
8	531	33.7	5.02	67.0	128	0.432	3.31	-2.52	0.422
9	531	33.7	240	67.0	128	0.432	3.54	-2.52	0.543
10	2686	33.7	5.02	67.0	128	0.432	3.31	-2.52	2.14
11	3576	35.1	5.02	60.2	135	0.458	2.56	-1.89	2.40
12	3576	35.2	685	60.2	136	0.459	3.23	-1.89	4.77
13	3576	90.7	109	60.2	352	1.105	25.2	-1.89	83.5
14	3576	97.2	88.5	60.2	378	1.174	29.8	-1.89	99.9
15	3256	41.2	7.55	66.2	157	0.526	4.15	-2.44	5.55
16	40.9	111	148	0.00	465	1.430	41.0	3.73	21.662
17	40.9	106	148	0.00	443	1.371	36.2	3.73	1.72
18	40.9	106	1000	0.00	445	1.373	37.2	3.73	1.76
19	255	40.4	7.55	0.00	169	0.578	0.591	3.73	1.10
20	358	32.9	5.02	0.00	138	0.477	-0.360	3.73	1.21
21	358	33.0	200	0.00	138	0.478	-0.161	3.73	1.28
6-A	2876	27.2	101	40.0	108	0.376	0.000	0.00	0.000
9-A	531	27.2	101	67.0	103	0.350	3.17	-2.52	0.349
18-A	358	27.2	101	0.0	114	0.398	-0.485	3.73	1.16
21-A	40.9	27.2	101	0.0	114	0.398	-0.485	3.73	0.133

- IH powered by hot distillate water from stage 4

Stream	\dot{m} (kg/s)	T (°C)	P (kPa)	w_s (g/kg)	h (kJ/kg)	s (kJ/(kg.K))	e_{ph} (kJ/kg)	e_{ch} (kJ/kg)	E_T (MW)
1	2858	27.2	101	40.0	108	0.376	0.000	0.000	0.000
2	2858	27.3	300	40.0	108	0.376	0.193	0.000	0.553
3	2858	36.2	210	40.0	144	0.493	0.601	0.000	1.72
4	892	36.2	210	40.0	144	0.493	0.601	0.000	0.54
5	892	40.2	4.96	40.0	159	0.543	0.948	0.000	0.85
6	1965	36.2	210	40.0	144	0.493	0.601	0.000	1.18
7	3216	33.4	4.96	67.0	127	0.429	3.29	-2.52	2.50
8	533	33.4	4.96	67.0	127	0.429	3.29	-2.52	0.415
9	533	33.5	240	67.0	128	0.429	3.52	-2.52	0.536
10	2684	33.4	4.96	67.0	127	0.429	3.29	-2.52	2.09
11	3576	35.2	4.96	60.2	135	0.458	2.57	-1.89	2.41
12	3576	35.3	685	60.2	136	0.459	3.23	-1.89	4.78
13	3576	90.7	109	60.2	352	1.105	25.3	-1.89	83.6
14	3576	97.2	88.5	60.2	378	1.174	29.8	-1.89	99.9
15	3255	40.9	7.46	66.2	156	0.523	4.11	-2.44	5.43
16	40.6	111	148	0.00	465	1.430	41.0	3.73	21.51
17	40.6	106	148	0.00	443	1.371	36.2	3.73	1.71
18	40.6	106	1000	0.00	445	1.373	37.2	3.73	1.75
19	235	40.2	7.46	0.00	168	0.575	0.552	3.73	1.01
20	359	32.7	4.96	0.00	137	0.474	-0.377	3.73	1.20
21	359	32.8	200	0.00	137	0.475	-0.178	3.73	1.28
6-A	2858	27.2	101	40.0	108	0.376	0.000	0.00	0.000
9-A	533	27.2	101	67.0	103	0.350	3.17	-2.52	0.350
18-A	359	27.2	101	0.0	114	0.398	-0.485	3.73	1.17
21-A	40.6	27.2	101	0.0	114	0.398	-0.485	3.73	0.132

- IH powered by hot distillate water from stage 5

Stream	\dot{m} (kg/s)	T (°C)	P (kPa)	w_s (g/kg)	h (kJ/kg)	s (kJ/(kg.K))	e_{ph} (kJ/kg)	e_{ch} (kJ/kg)	E_T (MW)
1	2839	27.2	101	40.0	108	0.376	0.000	0.000	0.000
2	2839	27.3	300	40.0	108	0.376	0.193	0.000	0.549
3	2839	36.2	210	40.0	144	0.493	0.601	0.000	1.71
4	894	36.2	210	40.0	144	0.493	0.601	0.000	0.538
5	894	40.7	4.92	40.0	161	0.550	1.04	0.000	0.934
6	1945	36.2	210	40.0	144	0.493	0.601	0.000	1.17
7	3216	33.3	4.92	67.0	127	0.427	3.28	-2.52	2.47
8	534	33.3	4.92	67.0	127	0.427	3.28	-2.52	0.410
9	534	33.3	240	67.0	127	0.427	3.51	-2.52	0.531
10	2682	33.3	4.92	67.0	127	0.427	3.28	-2.52	2.06
11	3576	35.2	4.92	60.2	135	0.459	2.56	-1.88	2.41
12	3576	35.3	685	60.2	136	0.460	3.22	-1.88	4.78
13	3576	90.7	109	60.2	352	1.106	25.3	-1.88	83.6
14	3576	97.2	88.5	60.2	378	1.174	29.8	-1.88	99.9
15	3254	40.8	7.40	66.2	156	0.521	4.08	-2.44	5.35
16	40.4	111	148	0.00	465	1.430	41.0	3.73	21.4
17	40.4	106	148	0.00	443	1.371	36.2	3.73	1.70
18	40.4	106	1000	0.00	445	1.373	37.2	3.73	1.74
19	215	40.0	7.40	0.00	168	0.573	0.527	3.73	0.915
20	360	32.6	4.92	0.00	136	0.472	-0.388	3.73	1.20
21	360	32.6	200	0.00	137	0.473	-0.188	3.73	1.28
6-A	2839	27.2	101	40.0	108	0.376	0.000	0.00	0.000
9-A	534	27.2	101	67.0	103	0.350	3.17	-2.52	0.351
18-A	360	27.2	101	0.0	114	0.398	-0.485	3.73	1.17
21-A	40.4	27.2	101	0.0	114	0.398	-0.485	3.73	0.131

- IH powered by hot distillate water from stage 6

Stream	\dot{m} (kg/s)	T (°C)	P (kPa)	w_s (g/kg)	h (kJ/kg)	s (kJ/(kg.K))	e_{ph} (kJ/kg)	e_{ch} (kJ/kg)	E_T (MW)
1	2821	27.2	101	40.0	108	0.376	0.000	0.000	0.000
2	2821	27.3	300	40.0	108	0.376	0.193	0.000	0.546
3	2821	36.2	210	40.0	144	0.493	0.601	0.000	1.70
4	896	36.2	210	40.0	144	0.493	0.601	0.000	0.54
5	896	41.2	4.89	40.0	163	0.556	1.12	0.000	1.00
6	1925	36.2	210	40.0	144	0.493	0.601	0.000	1.16
7	3215	33.2	4.89	67.0	126	0.426	3.28	-2.52	2.44
8	535	33.2	4.89	67.0	126	0.426	3.28	-2.52	0.406
9	535	33.2	240	67.0	127	0.426	3.50	-2.52	0.527
10	2680	33.2	4.89	67.0	126	0.426	3.28	-2.52	2.04
11	3576	35.2	4.89	60.2	136	0.459	2.56	-1.88	2.42
12	3576	35.3	685	60.2	137	0.460	3.22	-1.88	4.79
13	3576	90.8	109	60.2	353	1.106	25.3	-1.88	83.7
14	3576	97.2	88.5	60.2	378	1.174	29.8	-1.88	99.9
15	3254	40.7	7.36	66.2	155	0.520	4.07	-2.44	5.28
16	40.2	111	148	0.00	465	1.430	41.0	3.73	21.3
17	40.2	106	148	0.00	443	1.371	36.2	3.73	1.70
18	40.2	106	1000	0.00	445	1.373	37.2	3.73	1.73
19	195	39.9	7.36	0.00	167	0.572	0.508	3.73	0.825
20	361	32.5	4.89	0.00	136	0.470	-0.396	3.73	1.20
21	361	32.5	200	0.00	136	0.471	-0.196	3.73	1.27
6-A	2821	27.2	101	40.0	108	0.376	0.00	0.00	0.000
9-A	535	27.2	101	67.0	103	0.350	3.17	-2.52	0.351
18-A	361	27.2	101	0.0	114	0.398	-0.485	3.73	1.17
21-A	40.2	27.2	101	0.0	114	0.398	-0.485	3.73	0.130

- IH powered by hot distillate water from stage 7

Stream	\dot{m} (kg/s)	T (°C)	P (kPa)	w_s (g/kg)	h (kJ/kg)	s (kJ/(kg.K))	e_{ph} (kJ/kg)	e_{ch} (kJ/kg)	E_T (MW)
1	2803	27.2	101	40.0	108	0.376	0.000	0.000	0.000
2	2803	27.3	300	40.0	108	0.376	0.193	0.000	0.542
3	2803	36.2	210	40.0	144	0.493	0.601	0.000	1.69
4	896	36.2	210	40.0	144	0.493	0.601	0.000	0.539
5	896	41.4	4.87	40.0	164	0.559	1.17	0.000	1.05
6	1906	36.2	210	40.0	144	0.493	0.601	0.000	1.15
7	3215	33.1	4.87	67.0	126	0.425	3.27	-2.52	2.43
8	535	33.1	4.87	67.0	126	0.425	3.27	-2.52	0.404
9	535	33.1	240	67.0	126	0.425	3.50	-2.52	0.525
10	2679	33.1	4.87	67.0	126	0.425	3.27	-2.52	2.02
11	3576	35.3	4.87	60.2	136	0.459	2.56	-1.88	2.43
12	3576	35.4	685	60.2	137	0.460	3.23	-1.88	4.80
13	3576	90.8	109	60.2	353	1.106	25.3	-1.88	83.8
14	3576	97.2	88.5	60.2	378	1.174	29.8	-1.88	99.9
15	3253	40.6	7.33	66.2	155	0.519	4.06	-2.44	5.25
16	40.0	111	148	0.00	465	1.430	41.0	3.73	21.2
17	40.0	106	148	0.00	443	1.371	36.2	3.73	1.69
18	40.0	106	1000	0.00	445	1.373	37.25	3.73	1.72
19	175	39.9	7.33	0.00	167	0.571	0.498	3.73	0.738
20	361	32.4	4.87	0.00	136	0.470	-0.400	3.73	1.20
21	361	32.4	200	0.00	136	0.470	-0.201	3.73	1.27
6-A	2803	27.2	101	40.0	108	0.376	0.000	0.00	0.000
9-A	535	27.2	101	67.0	103	0.350	3.17	-2.52	0.352
18-A	361	27.2	101	0.0	114	0.398	-0.485	3.73	1.17
21-A	40.0	27.2	101	0.0	114	0.398	-0.485	3.73	0.130

- IH powered by hot distillate water from stage 8

Stream	\dot{m} (kg/s)	T (°C)	P (kPa)	w_s (g/kg)	h (kJ/kg)	s (kJ/(kg.K))	e_{ph} (kJ/kg)	e_{ch} (kJ/kg)	E_T (MW)
1	2785	27.2	101	40.0	108	0.376	0.000	0.000	0.000
2	2785	27.3	300	40.0	108	0.376	0.193	0.000	0.539
3	2785	36.2	210	40.0	144	0.493	0.601	0.000	1.67
4	897	36.2	210	40.0	144	0.493	0.601	0.000	0.539
5	897	41.6	4.86	40.0	165	0.561	1.19	0.000	1.07
6	1888	36.2	210	40.0	144	0.493	0.601	0.000	1.14
7	3215	33.1	4.86	67.0	126	0.425	3.27	-2.52	2.42
8	535	33.1	4.86	67.0	126	0.425	3.27	-2.52	0.403
9	535	33.1	240	67.0	126	0.425	3.50	-2.52	0.525
10	2679	33.1	4.86	67.0	126	0.425	3.27	-2.52	2.02
11	3576	35.3	4.86	60.2	136	0.460	2.56	-1.88	2.44
12	3576	35.4	685	60.2	137	0.461	3.23	-1.88	4.81
13	3576	90.8	109	60.2	353	1.107	25.3	-1.88	83.8
14	3576	97.2	88.5	60.2	378	1.174	29.8	-1.88	99.9
15	3253	40.6	7.33	66.2	155	0.519	4.05	-2.44	5.24
16	39.9	111	148	0.00	465	1.430	41.0	3.73	21.1
17	39.9	106	148	0.00	443	1.371	36.2	3.73	1.68
18	39.9	106	1000	0.00	445	1.373	37.2	3.73	1.72
19	154	39.9	7.33	0.00	167	0.570	0.495	3.73	0.652
20	361	32.4	4.86	0.00	136	0.469	-0.401	3.73	1.20
21	361	32.4	200	0.00	136	0.470	-0.202	3.73	1.27
6-A	2785	27.2	101	40.0	108	0.376	0.000	0.00	0.00
9-A	535	27.2	101	67.0	103	0.350	3.17	-2.52	0.35
18-A	361	27.2	101	0.0	114	0.398	-0.485	3.73	1.171
21-A	39.9	27.2	101	0.0	114	0.398	-0.485	3.73	0.129

Appendix: 8-A

Single effect AC IPSEpro model set/calculated variables

Stream No.	Composition	Flow	Temperature	Pressure	Concentration	Entropy	Enthalpy
1	H ₂ O/LiBr	Cal.	Set	Set	Set	Cal.	Cal.
2	H ₂ O/LiBr	Cal.	Cal.	Set	Cal.	Cal.	Cal.
3	H ₂ O/LiBr	Cal.	Cal.	Cal.	Cal.	Cal.	Cal.
4	H ₂ O/LiBr	Cal.	Cal.	Cal.	Set	Cal.	Cal.
5	H ₂ O/LiBr	Cal.	Cal.	Cal.	Cal.	Cal.	Cal.
6	H ₂ O/LiBr	Cal.	Cal.	Cal.	Cal.	Cal.	Cal.
7	Water	Cal.	Cal.	Cal.	Cal.	Cal.	Cal.
8	Water	Cal.	Cal.	Cal.	-	Cal.	Cal.
9	Water	Cal.	Cal.	Cal.	-	Cal.	Cal.
10	Water	Cal.	Cal.	Cal.	-	Cal.	Cal.
11	Water	Set	Set	Set	-	Cal.	Cal.
12	Water	Cal.	Set	Set	-	Cal.	Cal.
13	Water	Set	Set	Set	-	Cal.	Cal.
14	Water	Cal.	Cal.	Cal.	-	Cal.	Cal.
15	Water	Cal.	Set	Cal.	-	Cal.	Cal.
16	Water	Cal.	Set	Set	-	Cal.	Cal.
17	Water	Cal.	Set	Set	-	Cal.	Cal.

Appendix: 8-B

Single effect AC cycle data per MSF recovered stage.

MSF stages hot water		Single effect AC cycle equilibrium data per recovered stage							
Stage No	\dot{m} (kg/s)	T_{11} (°C)	T_{12} (°C)	X_s (%)	X_w (%)	T_4 (°C)	T_3 (°C)	T_6 (°C)	T_1 (°C)
1	21.3	92.8	87.9	61.0	56.5	84.2	71.3	55.0	46.0
2	42.4	89.4	84.6	59.5	55.0	80.8	68.5	51.5	43.0
3	63.2	85.9	81.2	57.9	53.4	77.4	65.9	47.0	39.5
4	83.8	82.5	77.7	56.2	51.7	73.9	62.6	44.0	36.5
5	104	79.1	74.3	54.6	50.1	70.5	59.4	42.0	34.5
6	124	75.6	70.8	52.8	48.3	67.0	57.5	38.0	32.0
7	144	72.2	67.4	50.9	46.4	63.6	55.0	34.0	29.0

Appendix: 8-C

Single effect AC streams data for recovering hot distillate water from stage 1

Stream No.	\dot{m} (kg/s)	T (°C)	P (kPa)	h (kJ/kg)	s (kJ/(kg.K))	X (%)	e_{cho} (kJ/kg)	e_{chD} (kJ/kg)	e_{ch} (kJ/kg)	e_{ph} (kJ/kg)	E_T (kW)
1	1.95	46.0	1.40	111	0.285	56.5	683	-167	516	2.61	1011
2	1.95	46.0	6.70	111	0.285	56.5	683	-167	516	2.61	1011
3	1.95	71.3	6.70	163	0.437	56.5	683	-167	516	8.55	1023
4	1.81	84.2	6.70	205	0.472	61.0	733	-154	579	11.9	1067
5	1.81	55.1	6.70	150	0.312	61.0	733	-154	579	4.18	1053
6	1.81	55.1	1.40	150	0.312	61.0	733	-154	579	4.18	1053
7	0.144	79.3	6.70	2649	8.53	0.0	50	0	50	111	23.2
8	0.144	38.2	6.70	160	0.549	0.0	50	0	50	1.13	7.35
9	0.144	12.0	1.40	160	0.565	0.0	50	0	50	-3.79	6.65
10	0.144	12.0	1.40	2461	8.64	0.0	50	0	50	-109	8.49
11	21.3	92.8	300	389	1.22	0.0	50	0	50	28.4	1669
12	21.3	87.9	281	368	1.17	0.0	50	0	50	24.7	1591
13	24.4	27.0	160	113	0.396	0.0	50	0	50	0.098	1223
14	24.4	31.0	160	130	0.451	0.0	50	0	50	0.322	1229
15	24.4	34.5	147	145	0.499	0.0	50	0	50	0.695	1238
16	19.7	18.0	238	75.8	0.268	0.0	50	0	50	0.508	992
17	19.7	14.0	140	58.9	0.210	0.0	50	0	50	0.927	1000

Single effect AC streams data for recovering hot distillate water from stage 2

Stream No.	\dot{m} (kg/s)	T (°C)	P (kPa)	h (kJ/kg)	s (kJ/(kg.K))	X (%)	e_{ch0} (kJ/kg)	e_{chD} (kJ/kg)	e_{ch} (kJ/kg)	e_{ph} (kJ/kg)	E_T (kW)
1	3.84	43.0	1.40	99.9	0.275	55.0	666	-170	496	2.09	1914
2	3.84	43.0	6.70	99.9	0.275	55.0	666	-170	496	2.09	1914
3	3.84	68.5	6.70	153	0.433	55.0	666	-170	496	7.80	1936
4	3.55	80.8	6.70	192	0.466	59.5	716	-159	557	11.1	2017
5	3.55	51.5	6.70	135	0.300	59.5	716	-159	557	3.54	1990
6	3.55	51.5	1.40	135	0.300	59.5	716	-159	557	3.54	1990
7	0.290	76.1	6.70	2642	8.51	0.0	49.9	0	49.9	110	46.5
8	0.290	38.2	6.70	160	0.549	0.0	49.9	0	49.9	1.13	14.8
9	0.290	12.0	1.40	160	0.565	0.0	49.9	0	49.9	-3.79	13.4
10	0.290	12.0	1.40	2461	8.64	0.0	49.9	0	49.9	-109	-17.1
11	42.4	89.4	300	375	1.19	0.0	49.9	0	49.9	25.8	3213
12	42.4	84.6	281	354	1.13	0.0	49.9	0	49.9	22.3	3063
13	48.9	27.0	160	113	0.396	0.0	49.9	0	49.9	0.098	2448
14	48.9	31.0	160	130	0.450	0.0	49.9	0	49.9	0.327	2459
15	48.9	34.5	147	144.7	0.499	0.0	49.9	0	49.9	0.695	2477
16	39.7	18.0	238	75.8	0.268	0.0	49.9	0	49.9	0.508	2002
17	39.7	14.0	140	58.9	0.210	0.0	49.9	0	49.9	0.927	2018

Single effect AC streams data for recovering hot distillate water from stage 3

Stream No.	\dot{m} (kg/s)	T (°C)	P (kPa)	h (kJ/kg)	s (kJ/(kg.K))	X (%)	e_{ch0} (kJ/kg)	e_{chD} (kJ/kg)	e_{ch} (kJ/kg)	e_{ph} (kJ/kg)	E_T (kW)
1	5.67	39.5	1.40	87.7	0.263	53.4	648	-172	476	1.52	2708
2	5.67	39.5	6.70	87.7	0.263	53.4	648	-172	476	1.52	2708
3	5.67	65.9	6.70	143	0.432	53.4	648	-172	476	7.06	2740
4	5.23	77.4	6.70	180	0.460	57.9	698	-164	535	10.2	2850
5	5.23	47.0	6.70	119	0.282	57.9	698	-164	535	2.76	2811
6	5.23	47.0	1.40	119	0.282	57.9	698	-164	535	2.76	2811
7	0.441	72.8	6.70	2636	8.49	0	49.9	0	49.9	110	70.3
8	0.441	38.2	6.70	160	0.549	0	49.9	0	49.9	1.13	22.5
9	0.441	12.0	1.40	160	0.565	0	49.9	0	49.9	-3.79	20.4
10	0.441	12.0	1.40	2461	8.64	0	49.9	0	49.9	-109	-26.0
11	63.2	86.0	300	360	1.15	0	49.9	0	49.9	23.4	4633
12	63.2	81.2	281	340	1.09	0	49.9	0	49.9	20.0	4419
13	73.5	27.0	160	113	0.396	0	49.9	0	49.9	0.098	3676
14	73.5	31.0	160	130	0.450	0	49.9	0	49.9	0.328	3693
15	73.5	34.5	147	144.7	0.499	0	49.9	0	49.9	0.695	3720
16	60.2	18.0	238	75.8	0.268	0	49.9	0	49.9	0.508	3038
17	60.2	14.0	140	58.9	0.210	0	49.9	0	49.9	0.927	3063

Single effect AC streams data for recovering hot distillate water from stage 4

Stream No.	\dot{m} (kg/s)	T (°C)	P (kPa)	h (kJ/kg)	s (kJ/(kg.K))	X (%)	e_{cho} (kJ/kg)	e_{chD} (kJ/kg)	e_{ch} (kJ/kg)	e_{ph} (kJ/kg)	E_T (kW)
1	7.40	36.6	1.40	77.5	0.256	51.7	629	-174	455	1.07	3377
2	7.40	36.6	6.70	77.5	0.256	51.7	629	-174	455	1.07	3377
3	7.40	62.6	6.70	133	0.427	51.7	629	-174	455	6.09	3414
4	6.81	73.8	6.70	167	0.454	56.2	679	-168	512	9.31	3546
5	6.81	43.9	6.70	106	0.274	56.2	679	-168	512	2.26	3498
6	6.81	43.9	1.40	106	0.274	56.2	679	-168	512	2.26	3498
7	0.592	69.5	6.70	2630	8.47	0	49.9	0	49.9	109	93.9
8	0.592	38.2	6.70	160	0.549	0	49.9	0	49.9	1.13	30.2
9	0.592	12.0	1.40	160	0.565	0	49.9	0	49.9	-3.79	27.3
10	0.592	12.0	1.40	2461	8.64	0	49.9	0	49.9	-109	-34.9
11	83.8	82.5	300	346	1.10	0	49.9	0	49.9	20.9	5938
12	83.8	77.7	281	325	1.05	0	49.9	0	49.9	17.7	5671
13	98.0	27.0	160	113	0.396	0	49.9	0	49.9	0.098	4902
14	98.0	30.9	160	130	0.450	0	49.9	0	49.9	0.339	4925
15	98.0	34.5	147	144.7	0.499	0	49.9	0	49.9	0.695	4960
16	80.9	18.0	238	75.8	0.268	0	49.9	0	49.9	0.508	4082
17	80.9	14.0	140	58.9	0.210	0	49.9	0	49.9	0.927	4116

Single effect AC streams data for recovering hot distillate water from stage 5

Stream No.	\dot{m} (kg/s)	T (°C)	P (kPa)	h (kJ/kg)	s (kJ/(kg.K))	X (%)	e_{cho} (kJ/kg)	e_{chD} (kJ/kg)	e_{ch} (kJ/kg)	e_{ph} (kJ/kg)	E_T (kW)
1	9.03	34.5	1.40	70.1	0.253	50.1	611	-174	437	0.760	3952
2	9.03	34.5	6.70	70.1	0.253	50.1	611	-174	437	0.761	3952
3	9.03	59.4	6.70	125	0.421	50.1	611	-174	437	5.14	3992
4	8.29	70.6	6.70	156	0.449	54.6	661	-170	491	8.41	4139
5	8.29	42.0	6.70	96.5	0.272	54.6	661	-170	491	1.93	4086
6	8.29	42.0	1.40	96.5	0.272	54.6	661	-170	491	1.93	4086
7	0.744	66.4	6.70	2624	8.45	0	49.9	0	49.9	108	117
8	0.744	38.2	6.70	160	0.549	0	49.9	0	49.9	1.13	38.0
9	0.744	12.0	1.40	160	0.565	0	49.9	0	49.9	-3.79	34.3
10	0.744	12.0	1.40	2461	8.64	0	49.9	0	49.9	-109	-43.9
11	104	79.1	300	331	1.06	0	49.9	0	49.9	18.7	7149
12	104	74.3	281	311	1.01	0	49.9	0	49.9	15.6	6834
13	122	27.0	160	113	0.396	0	49.9	0	49.9	0.098	6122
14	122	30.9	160	130	0.450	0	49.9	0	49.9	0.339	6151
15	122	34.5	147	144.7	0.499	0	49.9	0	49.9	0.695	6195
16	102	18.0	238	75.8	0.268	0	49.9	0	49.9	0.508	5131
17	102	14.0	140	58.9	0.210	0	49.9	0	49.9	0.927	5173

Single effect AC streams data for recovering hot distillate water from stage 6

Stream No.	\dot{m} (kg/s)	T (°C)	P (kPa)	h (kJ/kg)	s (kJ/(kg.K))	X (%)	e_{ch0} (kJ/kg)	e_{chD} (kJ/kg)	e_{ch} (kJ/kg)	e_{ph} (kJ/kg)	E_T (kW)
1	10.7	32.0	1.40	62.5	0.249	48.3	591	-174	417	0.450	4460
2	10.7	32.0	6.70	62.5	0.249	48.3	591	-174	417	0.450	4460
3	10.7	57.4	6.70	119	0.425	48.3	591	-174	417	4.47	4503
4	9.78	67.1	6.70	145	0.445	52.8	641	-173	469	7.38	4657
5	9.78	38.0	6.70	83.0	0.257	52.8	641	-173	469	1.29	4598
6	9.78	38.0	1.40	83.0	0.257	52.8	641	-173	469	1.29	4598
7	0.912	63.2	6.70	2618	8.44	0	49.9	0	49.9	107	143
8	0.912	38.2	6.70	160	0.549	0	49.9	0	49.9	1.13	46.6
9	0.912	12.0	1.40	160	0.565	0	49.9	0	49.9	-3.79	42.1
10	0.912	12.0	1.40	2461	8.64	0	49.9	0	49.9	-109	-53.8
11	124	75.6	300	317	1.02	0	49.9	0	49.9	16.5	8263
12	124	70.8	281	296	0.964	0	49.9	0	49.9	13.6	7907
13	148	27.0	160	113	0.396	0	49.9	0	49.9	0.098	7390
14	148	30.9	160	130	0.449	0	49.9	0	49.9	0.310	7421
15	148	34.5	147	145	0.499	0	49.9	0	49.9	0.695	7478
16	125	18.0	238	75.8	0.268	0	49.9	0	49.9	0.508	6282
17	125	14.0	140	58.9	0.210	0	49.9	0	49.9	0.927	6335

Single effect AC streams data for recovering hot distillate water from stage 7

Stream No.	\dot{m} (kg/s)	T (°C)	P (kPa)	h (kJ/kg)	s (kJ/(kg.K))	X (%)	e_{cho} (kJ/kg)	e_{chD} (kJ/kg)	e_{ch} (kJ/kg)	e_{ph} (kJ/kg)	E_T (kW)
1	12.2	29.0	1.40	54.6	0.242	46.4	570	-173	396	0.183	4823
2	12.2	29.0	6.70	54.6	0.242	46.4	570	-173	396	0.183	4823
3	12.2	54.8	6.70	113	0.427	46.4	570	-173	396	3.69	4866
4	11.1	63.7	6.70	135	0.441	50.9	620	-174	446	6.30	5018
5	11.1	34.1	6.70	70.4	0.244	50.9	620	-174	446	0.74	4957
6	11.1	34.1	1.40	70.4	0.244	50.9	620	-174	446	0.74	4957
7	1.08	60.0	6.70	2612	8.42	0	49.9	0	49.9	107	168
8	1.08	38.2	6.70	160	0.549	0	49.9	0	49.9	1.13	55.0
9	1.08	12.0	1.40	160	0.565	0	49.9	0	49.9	-3.79	49.7
10	1.08	12.0	1.40	2461	8.64	0	49.9	0	49.9	-109	-63.5
11	144	72.2	300	302	0.982	0	49.9	0	49.9	14.5	9274
12	144	67.4	281	282	0.922	0	49.9	0	49.9	11.8	8889
13	172	27.0	160	113	0.396	0	49.9	0	49.9	0.098	8628
14	172	30.9	160	129	0.449	0	49.9	0	49.9	0.331	8668
15	172	34.5	147	145	0.499	0	49.9	0	49.9	0.695	8731
16	147	18.0	238	75.8	0.268	0	49.9	0	49.9	0.508	7416
17	147	14.0	140	58.9	0.210	0	49.9	0	49.9	0.927	7477

Appendix: 8-D

- Exergy destruction of single-effect AC components powered from MSF hot distillate water stage.

Exergy Destruction (kW)							
Powering Stage	1	2	3	4	5	6	7
Generator	10.6	22.7	33.2	41.3	50.2	59.0	64.0
Condenser	6.77	13.7	20.9	28.8	36.0	40.0	50.8
Evaporator	6.90	13.9	21.1	28.3	35.6	43.7	51.6
Absorber	28.2	48.0	59.6	62.7	60.0	52.3	30.0
Heat Exchanger	2.44	4.95	7.72	10.9	14.2	16.6	19.0
Expansion Valve	0.708	1.43	2.17	2.91	3.66	4.49	5.29
Total Destruction	55.6	105	145	175	200	216	221

Appendix: 8-E

– Effect of chilled water temperature (T_{16})

Effect of chilled water inlet temperature on main AC components										
	Unit	14°C	15°C	16°C	17°C	18°C	19°C	20°C	21°C	22°C
\dot{Q}_G	kW	2927	2927	2927	2927	2927	2927	2927	2927	2927
\dot{Q}_E	kW	2377	2397	2418	2438	2459	2480	2500	2521	2541
\dot{Q}_C	kW	2510	2529	2571	2609	2638	2661	2675	2680	2688
\dot{Q}_A	kW	2752	2755	2760	2759	2765	2767	2771	2775	2780
\dot{Q}_{HX}	kW	827.6	817.5	732.2	786.1	714.2	698.1	658.0	621.9	568.0
\dot{m}_1	kg/s	12.4	12.4	12.2	12.4	12.2	12.1	12.0	11.8	11.6
\dot{m}_6	kg/s	11.4	11.4	11.2	11.3	11.1	11.0	10.9	10.8	10.5
\dot{m}_7	kg/s	1.02	1.03	1.05	1.06	1.07	1.08	1.09	1.10	1.11
P_1	kPa	1.1	1.17	1.24	1.32	1.4	1.49	1.59	1.69	1.8
P_2	kPa	6.71	6.71	6.71	6.71	6.71	6.71	6.71	6.71	6.71

Effect of chilled water inlet temperature on AC components exergy destruction										
	Unit	14°C	15°C	16°C	17°C	18°C	19°C	20°C	21°C	22°C
Generator	kW	4.16	20.4	45.0	44.5	64.0	72.2	83.0	89.1	105
Condenser	kW	47.2	49.1	45.7	47.5	50.8	51.2	51.6	50.0	49.0
Evaporator	kW	41.7	46.5	45.0	49.7	51.3	47.5	48.3	52.5	53.6
Absorber	kW	64.2	53.9	38.9	45.1	30.2	30.1	28.1	33.6	29.1
Heat Exchanger	kW	24.4	23.7	22.2	20.6	19.0	17.7	16.5	16.1	13.8
Expansion Valves	kW	6.62	6.21	5.93	5.60	5.26	4.92	4.56	4.17	3.84
Total Destruction	kW	188	200	203	213	221	224	232	245	254
Exergy efficiency	%	24.9	22.8	20.6	18.4	16.3	14.1	12.0	9.80	7.60

– Effect of cooling water temperature (T_{13})

Effect of cooling water temperature on main AC components												
Unit	22 °C	23 °C	24 °C	25 °C	26 °C	27 °C	28 °C	29 °C	30 °C	31 °C	32 °C	33 °C
\dot{Q}_G	kW	2927	2927	2927	2927	2927	2927	2927	2927	2927	2927	2927
\dot{Q}_E	kW	2485	2484	2484	2483	2483	2482	2481	2480	2479	2478	2475
\dot{Q}_C	kW	2645	2644	2643	2642	2641	2640	2638	2637	2636	2635	2633
\dot{Q}_A	kW	2762	2763	2764	2764	2765	2765	2765	2764	2764	2763	2762
\dot{Q}_{HX}	kW	701	703	706	709	712	714	718	723	727	728	735
\dot{m}_1	kg/s	12.15	12.15	12.16	12.17	12.17	12.18	12.18	12.19	12.19	12.20	12.21
\dot{m}_6	kg/s	11.07	11.08	11.08	11.09	11.10	11.10	11.11	11.11	11.12	11.12	11.13
\dot{m}_7	kg/s	1.074	1.075	1.075	1.076	1.076	1.077	1.077	1.078	1.078	1.079	1.080
P_1	kPa	0.90	1.00	1.10	1.20	1.30	1.40	1.50	1.60	1.70	1.80	2.00
P_2	kPa	5.12	5.40	5.70	6.02	6.35	6.69	7.07	7.48	7.90	8.29	9.19

Effect of cooling water temperature on main AC components exergy destruction													
	Unit	22 °C	23 °C	24 °C	25 °C	26 °C	27 °C	28 °C	29 °C	30 °C	31 °C	32 °C	33 °C
Generator	kW	108	100	91.0	81.4	73.0	64.6	55.5	46.5	37.3	29.5	21.4	12.2
Condenser	kW	51.5	51.1	50.7	50.3	49.8	49.4	49.0	48.6	48.2	47.8	47.4	46.9
Evaporator	kW	47.8	48.0	48.2	48.4	48.6	48.8	49.0	49.2	49.4	49.6	49.8	50.0
Absorber	kW	21.7	23.1	24.5	25.9	27.3	28.7	30.1	31.5	32.9	34.3	35.7	37.0
Heat Exchanger	kW	19.1	19.1	19.1	19.0	19.0	18.9	18.9	18.9	18.9	18.9	18.8	18.8
Expansion Valves	kW	6.18	5.99	5.67	5.52	5.36	5.30	5.23	5.20	5.24	5.21	5.24	5.31
Total Destruction	kW	255	247	239	231	223	216	208	200	192	185	178	170
Exergy efficiency	%	30.9	28.3	25.7	23.0	20.4	17.8	15.2	12.6	9.95	7.33	4.71	2.10

Appendix: 9-A

ORC IPSEpro model set/calculated variables

Stream No.	Composition	Flow	Temperature	Pressure	Specific volume	Entropy	Enthalpy
1	Refrigerant	Cal.	Cal.	Set	Cal.	Cal.	Cal.
2	Refrigerant	Cal.	Cal.	Set	Cal.	Cal.	Cal.
3	Refrigerant	Cal.	Cal.	Cal.	Cal.	Cal.	Cal.
4	Refrigerant	Cal.	Cal.	Cal.	Cal.	Cal.	Cal.
A	Water	Set	Set	Set	Cal.	Cal.	Cal.
B	Water	Cal.	Set	Cal.	Cal.	Cal.	Cal.
C	Water	Cal.	Set	Cal.	Cal.	Cal.	Cal.
D	Water	Cal.	Set	Cal.	Cal.	Cal.	Cal.

Appendix: 9-B

- R134a ORC streams data for recovering hot distillate water from stage 1

Stream No.	\dot{m} (kg/s)	T (°C)	P (bar)	h (kJ/kg)	s (kJ/(kg.K))	X (Quality)	E_T (kW)
A	21.3	92.8	1.50	389	1.22	-	602
B	21.3	82.8	1.49	347	1.11	-	446
C	34.1	27.0	1.25	113	0.396	-	1.9
D	34.1	32.6	1.24	137	0.473	-	14.8
1	5.05	84.8	29.1	428	1.68	1.00	353
2	5.05	34.4	8.73	406	1.68	0.935	242
3	5.05	34.4	8.72	248	1.16	0.000	218
4	5.05	36.2	29.1	251	1.17	-0.847	227

- R134a ORC streams data for recovering hot distillate water from stage 2

Stream No.	\dot{m} (kg/s)	T (°C)	P (bar)	h (kJ/kg)	s (kJ/(kg.K))	X (Quality)	E_T (kW)
A	42.4	89.4	1.50	374	1.19	-	1086
B	42.4	79.4	1.49	332	1.07	-	791
C	68.0	27.0	1.25	113	0.40	-	3.70
D	68.0	32.6	1.24	137	0.47	-	29.6
1	10.0	81.4	27.1	429	1.68	1.00	688
2	10.0	34.4	8.73	408	1.68	0.946	479
3	10.0	34.4	8.72	248	1.16	0.00	431
4	10.0	36.0	27.1	250	1.17	-0.721	447

- R134a ORC streams data for recovering hot distillate water from stage 3

Stream No.	\dot{m} (kg/s)	T (°C)	P (bar)	h (kJ/kg)	s (kJ/(kg.K))	X (Quality)	E_T (kW)
A	63.2	85.9	1.5	360	1.15	-	1462
B	63.2	75.9	1.49	318	1.03	-	1043
C	102	27.0	1.25	113	0.396	-	5.60
D	102	32.6	1.24	137	0.473	-	44.4
1	14.8	77.9	25.2	429	1.69	1.00	1007
2	14.8	34.4	8.73	409	1.69	0.954	713
3	14.8	34.4	8.72	248	1.16	0.00	640
4	14.8	35.8	25.2	250	1.17	-0.619	661

- R134a ORC streams data for recovering hot distillate water from stage 4

Stream No.	\dot{m} (kg/s)	T (°C)	P (bar)	h (kJ/kg)	s (kJ/(kg.K))	X (Quality)	E_T (kW)
A	83.8	82.5	1.5	345	1.10	-	1738
B	83.8	72.5	1.49	304	0.985	-	1212
C	136	27.0	1.25	113	0.396	-	7.40
D	136	32.6	1.24	137	0.473	-	59.1
1	19.6	74.5	23.4	429	1.69	1.00	1311
2	19.6	34.4	8.73	410	1.69	0.961	944
3	19.6	34.4	8.72	248	1.16	0	847
4	19.6	35.7	23.4	250	1.17	-0.534	872

- R134a ORC streams data for recovering hot distillate water from stage 5

Stream No.	\dot{m} (kg/s)	T (°C)	P (bar)	h (kJ/kg)	s (kJ/(kg.K))	X (Quality)	E_T (kW)
A	104	79.1	1.50	331	1.06	-	1924
B	104	69.1	1.49	289	0.943	-	1307
C	170	27.0	1.25	113	0.396	-	9.30
D	170	32.6	1.24	137	0.473	-	74.0
1	24.4	71.1	21.7	429	1.69	1.00	1600
2	24.4	34.4	8.73	411	1.69	0.97	1174
3	24.4	34.4	8.72	248	1.16	0.000	1052
4	24.4	35.5	21.7	250	1.17	-0.461	1080

- R134a ORC streams data for recovering hot distillate water from stage 6

Stream No.	\dot{m} (kg/s)	T (°C)	P (bar)	h (kJ/kg)	s (kJ/(kg.K))	X (Quality)	E_T (kW)
A	124	75.6	1.50	317	1.02	-	2029
B	124	65.6	1.49	275	0.901	-	1337
C	204	27.0	1.25	113	0.396	-	11.2
D	204	32.6	1.24	137	0.473	-	88.8
1	29.1	67.6	20.1	428	1.70	1.00	1874
2	29.1	34.4	8.73	412	1.70	0.972	1404
3	29.1	34.4	8.72	248	1.16	0.00	1257
4	29.1	35.4	20.1	249	1.17	-0.396	1286

- R134a ORC streams data for recovering hot distillate water from stage 7

Stream No.	\dot{m} (kg/s)	T (°C)	P (bar)	h (kJ/kg)	s (kJ/(kg.K))	X (Quality)	E_T (kW)
A	144	72.2	1.50	302	0.981	-	2062
B	144	62.2	1.49	260	0.859	-	1311
C	238	27.0	1.25	113	0.396	-	13.0
D	238	32.6	1.24	137	0.473	-	103.8
1	33.9	64.2	18.5	428	1.70	1.00	2133
2	33.9	34.4	8.73	413	1.70	0.976	1633
3	33.9	34.4	8.72	248	1.16	0	1462
4	33.9	35.2	18.6	249	1.17	-0.339	1491

- R134a ORC streams data for recovering hot distillate water from stage 8

Stream No.	\dot{m} (kg/s)	T (°C)	P (bar)	h (kJ/kg)	s (kJ/(kg.K))	X (Quality)	E_T (kW)
A	164	68.7	1.5	288	0.940	-	2030
B	164	58.7	1.49	246	0.815	-	1238
C	273	27.0	1.25	113	0.396	-	14.9
D	273	32.6	1.24	137	0.4727	-	119
1	38.6	60.7	17.1	427	1.70	1.00	2376
2	38.6	34.4	8.73	414	1.70	0.980	1863
3	38.6	34.4	8.72	248	1.16	0	1668
4	38.6	35.1	17.1	249	1.17	-0.287	1696

- R245fa ORC streams data for recovering hot distillate water from stage 1

Stream No.	\dot{m} (kg/s)	T (°C)	P (bar)	h (kJ/kg)	s (kJ/(kg.K))	X (Quality)	E_T (kW)
A	21.3	92.8	1.50	389	1.22	-	602
B	21.3	82.8	1.49	347	1.11	-	446
C	33.7	27.0	1.25	113	0.396	-	1.8
D	33.7	32.6	1.24	137	0.473	-	14.7
1	4.02	84.8	8.87	470	1.80	1.00	162
2	4.02	46.0	2.09	443	1.80	1.06	53.6
3	4.02	34.3	2.08	246	1.16	0.000	28.5
4	4.02	34.7	8.88	247	1.16	-0.493	30.6

- R245fa ORC streams data for recovering hot distillate water from stage 2

Stream No.	\dot{m} (kg/s)	T (°C)	P (bar)	h (kJ/kg)	s (kJ/(kg.K))	X (Quality)	E_T (kW)
A	42.4	89.4	1.50	374	1.19	-	1086
B	42.4	79.4	1.49	332	1.07	-	791
C	67.5	27.0	1.25	113	0.3955	-	3.70
D	67.5	32.6	1.24	137	0.4727	-	29.4
1	8.07	81.4	8.16	467	1.79	1.00	311
2	8.07	45.2	2.09	442	1.79	1.06	107
3	8.07	34.3	2.08	246	1.16	0	57.3
4	8.07	34.7	8.17	247	1.16	-0.449	61.1

- R245fa ORC streams data for recovering hot distillate water from stage 3

Stream No.	\dot{m} (kg/s)	T (°C)	P (bar)	h (kJ/kg)	s (kJ/(kg.K))	X (Quality)	E_T (kW)
A	63.2	85.9	1.50	360	1.15	-	1462
B	63.2	75.9	1.49	318	1.03	-	1043
C	101	27.0	1.25	113	0.396	-	5.5
D	101	32.6	1.24	137	0.473	-	44.1
1	12.2	77.9	7.49	465	1.79	1.00	448
2	12.2	44.3	2.09	441	1.79	1.0517	161
3	12.2	34.3	2.08	246	1.16	0.000	86.4
4	12.2	34.6	7.50	247	1.16	-0.407	91.5

- R245fa ORC streams data for recovering hot distillate water from stage 4

Stream No.	\dot{m} (kg/s)	T (°C)	P (bar)	h (kJ/kg)	s (kJ/(kg.K))	X (Quality)	E_T (kW)
A	83.8	82.5	1.50	345	1.10	-	1738
B	83.8	72.5	1.49	304	0.985	-	1212
C	135	27.0	1.25	113	0.396	-	7.40
D	135	32.6	1.24	137	0.473	-	58.8
1	16.3	74.5	6.86	462	1.79	1.00	573
2	16.3	43.4	2.09	440	1.79	1.05	215
3	16.3	34.3	2.08	246	1.16	0	116
4	16.3	34.6	6.87	247	1.16	-0.367	122

- R245fa ORC streams data for recovering hot distillate water from stage 5

Stream No.	\dot{m} (kg/s)	T (°C)	P (bar)	h (kJ/kg)	s (kJ/(kg.K))	X (Quality)	E_T (kW)
A	104	79.1	1.50	331	1.06	-	1924
B	104	69.1	1.49	289	0.943	-	1307
C	169	27.0	1.25	113	0.396	-	9.2
D	169	32.6	1.24	137	0.473	-	73.6
1	20.5	71.1	6.27	459	1.79	1.00	684
2	20.5	42.5	2.09	439	1.79	1.04	269
3	20.5	34.3	2.08	246	1.16	0	146
4	20.5	34.6	6.28	246	1.16	-0.329	152

- R245fa ORC streams data for recovering hot distillate water from stage 6

Stream No.	\dot{m} (kg/s)	T (°C)	P (bar)	h (kJ/kg)	s (kJ/(kg.K))	X (Quality)	E_T (kW)
A	124	75.6	1.50	317	1.02	-	2029
B	124	65.6	1.49	275	0.901	-	1337
C	203	27.0	1.25	113	0.396	-	11.1
D	203	32.6	1.24	137	0.473	-	88.5
1	24.7	67.6	5.72	457	1.78	1.00	781
2	24.7	41.7	2.09	438	1.78	1.04	324
3	24.7	34.3	2.08	246	1.16	0.000	176
4	24.7	34.5	5.73	246	1.16	-0.293	183

- R245fa ORC streams data for recovering hot distillate water from stage 7

Stream No.	\dot{m} (kg/s)	T (°C)	P (bar)	h (kJ/kg)	s (kJ/(kg.K))	X (Quality)	E_T (kW)
A	144	72.2	1.50	302	0.981	-	2062
B	144	62.2	1.49	260	0.859	-	1311
C	238	27.0	1.25	113	0.396	-	13
D	238	32.6	1.24	137	0.473	-	104
1	29.1	64.2	5.21	454	1.78	1.00	865
2	29.1	40.8	2.09	438	1.78	1.03	379
3	29.1	34.3	2.08	246	1.16	0.000	206
4	29.1	34.5	5.22	246	1.16	-0.258	213

- R245fa ORC streams data for recovering hot distillate water from stage 8

Stream No.	\dot{m} (kg/s)	T (°C)	P (bar)	h (kJ/kg)	s (kJ/(kg.K))	X (Quality)	E_T (kW)
A	164	68.7	1.50	288	0.940	-	2031
B	164	58.7	1.49	246	0.815	-	1239
C	272	27.0	1.25	113	0.396	-	14.9
D	272	32.6	1.24	137	0.473	-	119
1	33.4	60.7	4.73	452	1.78	1.00	933
2	33.4	40.0	2.09	437	1.78	1.03	435
3	33.4	34.3	2.08	246	1.16	0.000	237
4	33.4	34.5	4.74	246	1.16	-0.224	244

Appendix: 9-C

- Effect of evaporator temperature on exergy efficiency (%) and exergy destruction ratio (%) of the R134a ORC components.

Exergy Efficiency							
ORC Component	Evaporator temperature (°C)						
	58	59	60	61	62	63	64
Evaporator	80.9	82.8	84.6	86.5	88.3	90.1	91.8
Turbine	76.0	76.0	76.0	76.0	76.0	76.0	76.0
Condenser	53.1	53.1	53.1	53.1	53.1	53.1	53.1
Pump	97.3	97.1	97.0	96.9	96.7	96.6	96.4

Exergy Destruction Ratio							
ORC Component	Evaporator temperature (°C)						
	58	59	60	61	62	63	64
Evaporator	37.5	34.6	31.6	28.4	25.1	21.7	18.3
Turbine	27.7	29.4	31.1	32.8	34.6	36.4	38.3
Condenser	22.8	23.3	23.8	24.3	24.7	25.2	25.7
Pump	11.8	12.7	13.6	14.6	15.6	16.6	17.8

- Effect of evaporator temperature on exergy efficiency (%) and exergy destruction ratio (%) of the R245fa ORC components.

Exergy Efficiency							
ORC Component	Evaporator temperature (°C)						
	58	59	60	61	62	63	64
Evaporator	81.6	83.6	85.6	87.5	89.4	91.3	93.1
Turbine	76.0	76.0	76.0	76.0	76.0	76.1	76.1
Condenser	53.1	53.1	53.1	53.1	53.1	53.1	53.1
Pump	95.5	95.3	95.0	94.8	94.5	94.3	94.0

Exergy Destruction Ratio							
ORC Component	Evaporator temperature (°C)						
	58	59	60	61	62	63	64
Evaporator	40.4	37.2	33.9	30.3	26.6	22.7	18.4
Turbine	30.2	32.3	34.6	36.8	39.3	41.9	44.6
Condenser	26.1	26.9	27.8	28.7	29.6	30.7	31.7
Pump	3.22	3.50	3.80	4.13	4.46	4.82	5.22

- Effect of cooling water temperature on exergy efficiency (%) and exergy destruction ratio (%) of the R143a ORC components.

Exergy Efficiency												
ORC Component	Cooling water temperature (°C)											
	22	23	24	25	26	27	28	29	30	31	32	33
Evaporator	83.5	84.0	84.5	85.0	85.5	85.9	86.4	86.9	87.3	87.7	88.1	88.5
Turbine	76.0	76.0	76.0	76.0	76.0	76.0	76.0	76.0	76.0	76.0	76.0	76.0
Condenser	29.0	32.4	30.3	40.4	47.6	53.7	58.3	62.2	65.4	68.1	70.4	72.7
Pump	96.5	96.6	96.7	96.7	96.8	96.9	97.0	97.1	97.1	97.2	97.3	97.4

Exergy Destruction Ratio												
ORC Component	Cooling water temperature (°C)											
	22	23	24	25	26	27	28	29	30	31	32	33
Evaporator	30.6	30.4	30.1	29.9	29.6	29.4	29.1	28.9	28.6	28.5	28.2	28.2
Turbine	33.6	33.5	33.3	33.1	32.8	32.6	32.2	31.9	31.5	31.1	30.7	30.3
Condenser	22.2	22.3	22.5	22.9	23.4	23.6	24.2	24.7	25.2	25.8	26.4	26.8
Pump	13.7	13.9	14.0	14.2	14.3	14.4	14.5	14.5	14.6	14.6	14.7	14.7

- Effect of cooling water temperature on exergy efficiency (%) and exergy destruction ratio (%) of the R245fa ORC components.

Exergy Efficiency												
ORC Component	Cooling water temperature (°C)											
	22	23	24	25	26	27	28	29	30	31	32	33
Evaporator	84.8	85.3	85.7	86.2	86.6	87.0	87.4	87.8	88.2	88.5	88.9	89.2
Turbine	76.1	76.1	76.1	76.1	76.0	76.0	76.0	76.0	76.0	76.0	76.0	76.0
Condenser	2.90	16.0	29.3	39.3	46.6	52.5	57.3	61.3	64.6	67.4	69.8	72.0
Pump	94.2	94.3	94.4	94.5	94.7	94.8	95.0	95.2	95.3	95.5	95.7	95.8

Exergy Destruction Ratio												
ORC Component	Cooling water temperature (°C)											
	22	23	24	25	26	27	28	29	30	31	32	33
Evaporator	32.3	32.1	31.8	31.7	31.5	31.2	31.1	30.9	30.8	30.6	30.5	30.4
Turbine	37.6	37.4	37.1	36.9	36.6	36.3	35.9	35.5	35.1	34.6	34.1	33.5
Condenser	26.2	26.7	27.1	27.4	28.0	28.5	28.9	29.5	30.1	30.6	31.3	32.0
Pump	3.87	3.91	3.95	3.99	4.00	4.04	4.05	4.09	4.10	4.11	4.12	4.13

Appendix: 10-A

- SED IPSEpro model set/calculated variables

Stream	Composition	Flow	Temperature	Pressure	Salinity	Entropy	Enthalpy
1	Seawater	Cal.	Set	Set	Set	Cal.	Cal.
2	Seawater	Cal.	Set	Cal.	Cal.	Cal.	Cal.
3	Seawater	Cal.	Cal.	Cal.	Cal.	Cal.	Cal.
4	Seawater	Cal.	Cal.	Cal.	Cal.	Cal.	Cal.
5	Seawater	Cal.	Cal.	Cal.	Cal.	Cal.	Cal.
6	Seawater	Cal.	Cal.	Cal.	Cal.	Cal.	Cal.
7	Seawater	Cal.	Cal.	Set	Cal.	Cal.	Cal.
8	Water	Set	Set	Cal.	-	Cal.	Cal.
9	Water	Cal.	Set	Cal.	-	Cal.	Cal.
10	Water	Cal.	Cal.	Cal.	-	Cal.	Cal.
11	Water	Cal.	Cal.	Cal.	-	Cal.	Cal.
12	Water	Cal.	Cal.	Cal.	-	Cal.	Cal.
13	Water	Cal.	Cal.	Set	-	Cal.	Cal.

Appendix: 10-B

- Hot distillate waster from MSF stage 1 powering SED

Stream No.	\dot{m} (kg/s)	T (°C)	P (kPa)	ws (g/kg)	h (kJ/kg)	s (kJ/(kg.K))	e_{ch} (kJ/kg)	e_{ph} (kJ/kg)	E_T (MW)
1	24.2	27.2	101	0.04	108	0.376	0.000	0.000	0.000
2	24.2	27.2	150	0.04	108	0.376	0.047	0.000	0.001
3	24.2	34.5	150	0.04	137	0.471	0.366	0.000	0.009
4	23.1	34.5	150	0.04	137	0.471	0.366	0.000	0.008
5	1.06	34.5	150	0.04	137	0.471	0.366	0.000	0.000
6	0.760	81.3	48.3	0.056	317	1.01	18.7	-1.49	0.013
7	0.760	81.3	200	0.056	317	1.01	18.9	-1.49	0.013
8	21.3	92.8	78.0	0	389	1.23	25.6	3.73	0.625
9	21.3	82.8	53.1	0	347	1.11	18.6	3.73	0.475
10	0.300	81.3	48.3	0	340	1.09	17.6	3.73	0.115
11	0.300	80.5	48.3	0	337	1.08	17.1	3.73	0.006
12	0.300	80.5	13.4	0	337	1.08	17.0	3.73	0.006
13	0.300	80.5	200	0	337	1.08	17.2	3.73	0.006

- Hot distillate waster from MSF stage 2 powering SED

Stream No.	\dot{m} (kg/s)	T (°C)	P (kPa)	ws (g/kg)	h (kJ/kg)	s (kJ/(kg.K))	e_{ch} (kJ/kg)	e_{ph} (kJ/kg)	E_T (MW)
1	48.9	27.2	101	0.04	108	0.376	0.000	0.000	0.000
2	48.9	27.2	150	0.04	108	0.376	0.047	0.000	0.002
3	48.9	34.5	150	0.04	137	0.471	0.366	0.000	0.018
4	46.8	34.5	150	0.04	137	0.471	0.366	0.000	0.017
5	2.13	34.5	150	0.04	137	0.471	0.366	0.000	0.001
6	1.52	77.9	42.0	0.056	304	0.972	16.8	-1.49	0.023
7	1.52	77.9	200	0.056	304	0.972	16.9	-1.49	0.023
8	42.4	89.4	68.5	0	374	1.19	23.1	3.73	1.14
9	42.4	79.4	46.2	0	332	1.07	16.4	3.73	0.852
10	0.610	77.9	42.0	0	326	1.05	15.5	3.73	0.215
11	0.610	77.0	42.0	0	322	1.04	15.0	3.73	0.011
12	0.610	77.0	13.4	0	322	1.04	15.0	3.73	0.011
13	0.610	77.0	200	0	323	1.04	15.1	3.73	0.012

- Hot distillate waster from MSF stage 3 powering SED

Stream No.	\dot{m} (kg/s)	T (°C)	P (kPa)	ws (g/kg)	h (kJ/kg)	s (kJ/(kg.K))	e_{ch} (kJ/kg)	e_{ph} (kJ/kg)	E_T (MW)
1	74.2	27.2	101	0.04	108	0.376	0.000	0.000	0.000
2	74.2	27.2	150	0.04	108	0.376	0.047	0.000	0.004
3	74.2	34.5	150	0.04	137	0.471	0.366	0.000	0.027
4	71.0	34.5	150	0.04	137	0.471	0.366	0.000	0.026
5	3.22	34.5	150	0.04	137	0.471	0.366	0.000	0.001
6	2.30	74.4	36.4	0.056	290	0.933	14.9	-1.49	0.031
7	2.30	74.4	200	0.056	290	0.933	15.0	-1.49	0.031
8	63.2	85.9	60.0	0	360	1.15	20.7	3.73	1.542
9	63.2	75.9	40.1	0	318	1.03	14.3	3.73	1.141
10	0.920	74.4	36.4	0	311	1.01	13.5	3.73	0.304
11	0.920	73.6	36.4	0	308	0.999	13.0	3.73	0.015
12	0.920	73.6	13.4	0	308	0.999	13.0	3.73	0.015
13	0.920	73.6	200	0	308	0.999	13.2	3.73	0.016

- Hot distillate waster from MSF stage 4 powering SED

Stream No.	\dot{m} (kg/s)	T (°C)	P (kPa)	ws (g/kg)	h (kJ/kg)	s (kJ/(kg.K))	e_{ch} (kJ/kg)	e_{ph} (kJ/kg)	E_T (MW)
1	100	27.2	101	0.04	108	0.376	0.000	0.000	0.000
2	100	27.2	150	0.04	108	0.376	0.047	0.000	0.005
3	100	34.5	150	0.04	137	0.471	0.366	0.000	0.037
4	95.7	34.5	150	0.04	137	0.471	0.366	0.000	0.035
5	4.33	34.5	150	0.04	137	0.471	0.366	0.000	0.002
6	3.09	71.0	31.5	0.056	277	0.894	13.1	-1.49	0.036
7	3.09	71.0	200	0.056	277	0.894	13.3	-1.49	0.036
8	83.8	82.5	52.4	0	345	1.10	18.4	3.74	1.853
9	83.8	72.5	34.7	0	303	0.985	12.4	3.73	1.350
10	1.24	71.0	31.5	0	297	0.967	11.6	3.73	0.381
11	1.24	70.2	31.5	0	294	0.958	11.2	3.73	0.018
12	1.24	70.2	13.4	0	294	0.958	11.1	3.73	0.018
13	1.24	70.2	200	0	294	0.958	11.3	3.73	0.019

- Hot distillate waster from MSF stage 5 powering SED

Stream No.	\dot{m} (kg/s)	T (°C)	P (kPa)	ws (g/kg)	h (kJ/kg)	s (kJ/(kg.K))	e_{ch} (kJ/kg)	e_{ph} (kJ/kg)	E_T (MW)
1	127	27.2	101	0.04	108	0.376	0.000	0.000	0.000
2	127	27.2	150	0.04	108	0.376	0.047	0.000	0.006
3	127	34.5	150	0.04	137	0.471	0.366	0.000	0.046
4	121	34.5	150	0.04	137	0.471	0.366	0.000	0.044
5	5.46	34.5	150	0.04	137	0.471	0.366	0.000	0.002
6	3.90	67.6	27.1	0.056	263	0.855	11.4	-1.49	0.039
7	3.90	67.6	200	0.056	263	0.855	11.6	-1.49	0.039
8	104	79.1	45.6	0	331	1.06	16.2	3.73	2.08
9	104	69.1	30.0	0	289	0.943	10.6	3.73	1.49
10	1.56	67.6	27.1	0	283	0.925	9.80	3.73	0.446
11	1.56	66.8	27.1	0	280	0.916	9.43	3.73	0.021
12	1.56	66.8	13.4	0	280	0.916	9.42	3.73	0.021
13	1.56	66.8	200	0	280	0.916	9.61	3.73	0.021

- Hot distillate waster from MSF stage 6 powering SED

Stream No.	\dot{m} (kg/s)	T (°C)	P (kPa)	ws (g/kg)	h (kJ/kg)	s (kJ/(kg.K))	e_{ch} (kJ/kg)	e_{ph} (kJ/kg)	E_T (MW)
1	154	27.2	101	0.04	108	0.376	0.000	0.000	0.000
2	154	27.2	150	0.04	108	0.376	0.047	0.000	0.007
3	154	34.5	150	0.04	137	0.471	0.366	0.000	0.056
4	147	34.5	150	0.04	137	0.471	0.366	0.000	0.054
5	6.60	34.5	150	0.04	137	0.471	0.366	0.000	0.002
6	4.72	64.1	23.3	0.056	250	0.815	9.88	-1.49	0.040
7	4.72	64.1	200	0.056	250	0.815	10.1	-1.49	0.040
8	124	75.6	39.6	0	317	1.02	14.1	3.73	2.22
9	124	65.6	25.8	0	275	0.901	8.87	3.73	1.57
10	1.89	64.1	23.3	0	268	0.882	8.17	3.73	0.498
11	1.89	63.4	23.3	0	265	0.873	7.83	3.73	0.022
12	1.89	63.4	13.4	0	265	0.873	7.82	3.73	0.022
13	1.89	63.4	200	0	265	0.873	8.01	3.73	0.022

- Hot distillate waster from MSF stage 7 powering SED

Stream No.	\dot{m} (kg/s)	T (°C)	P (kPa)	ws (g/kg)	h (kJ/kg)	s (kJ/(kg.K))	e_{ch} (kJ/kg)	e_{ph} (kJ/kg)	E_T (MW)
1	181	27.2	101	0.04	108	0.376	0.000	0.00	0.000
2	181	27.2	150	0.04	108	0.376	0.047	0.00	0.009
3	181	34.5	150	0.04	137	0.471	0.366	0.00	0.066
4	174	34.5	150	0.04	137	0.471	0.366	0.00	0.064
5	7.77	34.5	150	0.04	137	0.471	0.366	0.00	0.003
6	5.55	60.7	19.9	0.056	236	0.774	8.45	-1.49	0.039
7	5.55	60.7	200	0.056	236	0.775	8.64	-1.49	0.040
8	144	72.2	34.3	0	302	0.982	12.2	3.73	2.30
9	144	62.2	22.1	0	260	0.858	7.31	3.73	1.59
10	2.22	60.7	19.9	0	254	0.839	6.66	3.73	0.540
11	2.22	59.9	19.9	0	251	0.830	6.36	3.73	0.022
12	2.22	59.9	13.4	0	251	0.830	6.35	3.73	0.022
13	2.22	59.9	200	0	251	0.830	6.54	3.73	0.023

- Hot distillate waster from MSF stage 8 powering SED

Stream No.	\dot{m} (kg/s)	T (°C)	P (kPa)	ws (g/kg)	h (kJ/kg)	s (kJ/(kg.K))	e_{ch} (kJ/kg)	e_{ph} (kJ/kg)	E_T (MW)
1	210	27.2	101.3	0.04	108	0.376	0.000	0.000	0.000
2	210	27.2	150	0.04	108	0.376	0.047	0.000	0.010
3	210	34.5	150	0.04	137	0.471	0.366	0.000	0.077
4	201	34.5	150	0.04	137	0.471	0.366	0.000	0.073
5	8.96	34.5	150	0.04	137	0.471	0.366	0.000	0.003
6	6.40	57.2	17	0.056	223	0.734	7.16	-1.49	0.036
7	6.40	57.3	200	0.056	223	0.734	7.34	-1.49	0.037
8	164	68.7	29.5	0	288	0.940	10.4	3.73	2.32
9	164	58.7	18.8	0	246	0.815	5.87	3.73	1.58
10	2.56	57.2	17	0	240	0.796	5.29	3.73	0.560
11	2.56	56.5	17	0	237	0.787	5.03	3.73	0.022
12	2.56	56.5	13.4	0	237	0.787	5.02	3.73	0.022
13	2.56	56.5	200	0	237	0.787	5.21	3.73	0.023